Machinability and microstructural studies on phase transformations in Austempered Ductile Iron

Ashwin Polishetty

A thesis submitted to Auckland University of Technology in fulfilment of the requirements for the degree of Doctor of Philosophy (PhD)

2011

School of Engineering

AUT
AUCKLAND UNIVERSITY OF TECHNOLOGY
TE WĀNANGA ARONUI O TAMAKI MAKAU RAU

Abstract

Austempered Ductile Iron (ADI) is a type of nodular, ductile cast iron subjected to heat treatments - austenitising and austempering. The heat treatment gives ADI its unique ausferrite microstructure through which ADI gets its advantageous material properties. Possibly the most significant hurdle for the engineering community to overcome, to fully realise the potential of ADI, is in its successful machining. Whilst machining is conducted prior to heat treatment and offers no significant difficulty, machining post heat treatment is demanding and often avoided. Phase transformation of retained austenite to martensite leading to poor machinability characteristics is a common problem experienced during machining.

This research was divided into two categories: characterisation of ADI and study of phase transformations. Machinability of grades 900, 1050, 1200 and 1400 was evaluated using surface texture, microhardness, chip morphology and metallography analysis. The assessment was conducted on a cross-sectioned hole surface obtained from drilling at a pre-defined set of cutting parameters - cutting speeds (rpm) of 697 and 929, feed rates (mm/rev) of 0.1 and 0.2, coolant on/off and hole depth, 25mm. Grade 1200 was the best rank grade exhibiting good machinability characteristics.

Study of phase transformations was an investigative study on the factors - plastic strain (ε_p) and thermal energy (Q) which effect phase transformations during machining. The experimental design consists of face milling grade 1200 at variable Depth of Cut (DoC) range from 1 to 4 mm, coolant on/off, at constant speed, 1992 rpm and feed rate, 0.1 mm/tooth. Plastic strain (ε_p) and martensite content (M) at fracture point for each grade was evaluated by tensile testing. The effect of thermal energy (Q) on phase transformations was also verified through temperature measurements at DoC-3 and 1 mm using thermocouples embedded into the workpiece. Finally, the amount of plastic strain (ε_p) and thermal energy (Q) responsible for a given martensite increase (M) during milling was related and calculated using a mathematical function, $M = f(\varepsilon_p, Q)$.

Future work considers an in-depth study on the tool materials, geometry and wear; microstructural displacement during phase transformations using quick-stop (chip freezing), evaluating ADI compatibility for high speed machining and extending the experimental trials to grades 900, 1050 and 1400.

Contents

List of Figures

List of Tables

Acknowledgements

This thesis is dedicated to my loving wife, Shailaja and my parents, Polishetty Shyam Mohan and Jagadamba, for their constant support and encouragement throughout the project. My special thanks to family, friends and well-wishers for their support throughout the thesis.

I am grateful to my supervisor Dr. Timotius Pasang for the support and co-operation in the hours of need and for his expert metallurgical advices on phase transformations.

I offer my profuse thanks with humble reverence to Prof. Guy Littlefair for his invaluable guidance and support. He was a beacon light, whose constant efforts and encouragement proved to be a parallel stimulus in completing this project successfully. I would like to thank Dr. Moshe Goldberg, ISCAR for his kind gesture in sponsoring the tools. I would also like to thank Doug Maxwell, Steele & Lincoln Foundry for sponsoring the material, ADI. I extend my thanks to Ian Langley from SECO Tools NZ.

I am grateful to AUT University for providing me this opportunity and the support provided in terms of funding and resources. I extend my thanks to the faculty of mechanical engineering especially ex-supervisor, Dr. Sarat Singamneni and technicians, Bradley, Ross and Mark. I offer my sincere thanks to the School manager, Kath Mills.

"Every dark cloud has a silver lining"

Declaration

I hereby declare that this submission is my own work and that to the best of my knowledge and belief, it contains no material previously published or written by another person (except where explicit has been defined in the acknowledgements), nor material which to a substantial extent has been submitted for the award of any other degree or diploma of a university or other institution of higher learning.

Name: Ashwin Polishetty

Sign:

Date:

1 Research on machining Austempered Ductile Iron

Machining has been a prominent part of manufacturing till date. According to available research data on machining, more than 70% of the products manufactured has got machining involved in it. The knowledge base of machining is expanding due to regular contributions from researchers involved in making it efficient and worthy. Researchers due to their efforts have provided machinist with innovative techniques to machine any hardest possible material with ease, safety and productivity. Some of the results focus on machining materials at micro-level as the nano concepts overlap into manufacturing sector. The potential in solving such issues are highly valuable and bring in major changes in the field of manufacturing technology. With the introduction of new materials, there arises a need to machine these materials effectively and efficiently. The success of using these new materials in design application is very much related to the science of machining these materials. The question to be answered before applying these materials to a design application is:

Are these materials machinable?

The answer to this question is still unexplored. This unexplored opportunity gives rise to a need to research the possibilities to machine them effectively and efficiently. One of such opportunities has led to initiation of this research on machining Austempered Ductile Iron, from now on referred as “ADI”. The research consists of ADI machinability studies; study on phase transformations due to machining and identifying factors responsible for phase transformations. ADI belongs to the family of nodularised ductile cast iron. Recent trends in the heat treatment technology have given rise to this new variety of light weight iron known as ADI. ADI is produced by a two-staged heat treatment process of austenitising and austempering. The emergence of ADI is proven to be a key to manufacture product demanding high quality and low manufacturing costs. The dilemma associated with the modern day engineering artefacts is that they have to pass through a thin line of freedom against regulations framed to support ethical issues such as environmental impacts. e.g. environment regulations on CO_2 emissions in automobiles. Situations like these have made the manufacturers of automotive engines and ancillaries to shift from the traditional, age-old, heavy, grey cast iron to a light-weight, high strength ADI.

"Lower the automotive weight, less is the fuel required to run the automotive and lower are the emissions"

The other reason for the rising popularity of ADI is the strong and healthy competitive markets, which demand high quality products at lower costs and in quick time. The low cost of production is achieved, provided the manufacturers use materials having high strength to weight ratio such as ADI. ADI has been a good replacement for steel and aluminium in certain design application as it leads to reduced material usage and costs. The benefits resulting from such replacements are passed on to the end user. As mentioned earlier, the versatile nature of ADI can only be used effectively unless a suitable or viable technique is developed to machine the potential material. As witnessed by science, a positive effect has a drawback associated with it; similar is the case with ADI. The material looks attractive but machining ADI is problematic.

ADI has a unique ausferrite microstructure, which consists of ferrite needles against austenite background and spheriodal graphite nodules. The unique microstructure is advantageous in providing better mechanical properties, when compared to Aluminium and Steel. Contrary, the microstructure is disadvantageous, in case of machining as the retained austenite present in it undergoes phase transformation to a hard and difficult to machine, martensite. Although numerous technical publications have been made on commercial use of the material and its material properties, very little research work exists on machinability of ADI especially in the post heat treatment stage. Hence, manufacturers are uncertain in using ADI due to the inadequate knowledge which exists on machining ADI.

1.1 Research aim

The primary purpose of conducting this research work on ADI machining is to understand the phase transformational behaviour during machining. The experimental design mainly focuses on phase transformational causes and its effects on machining. The research aim is to investigate the new possibilities involved in machining of Austempered Ductile Iron (ADI). During the machining of ADI, the microstructure is rapidly changed from ausferrite to martensite due to high rate of plastic deformation and heat or combination of both.

Therefore, the key to the machinability of ADI is either to machine despite the formation of martensite - i.e. use ultra-hard cutting tools and low cutting speeds with elevated penetration (feed) rates; or to use different approaches to minimise, or even completely eradicate, the production of martensite by not allowing strain hardening to commence.

The specific aims of the investigation are three fold:

- to establish the relationship between subsurface microstructural changes brought about by machining post-heat treatment
- to determine if it is possible to adopt an approach where the toughest grades of ADI can be successfully machined
- to generate data for the machinability community to enable the growth of ADI to continue into new application bases currently not accessible due to the belief that it has relatively poor machining characteristics

1.2 Research methodology

Engineers are known for exploring, depicting and explaining practical occurrence through models built and tested by applying scientific methods. Research methodology is primarily divided into two sections: quantitative and qualitative. The present research uses principles of quantitative methodology; which involves formation of a hypothesis, gathering of necessary infrastructure - machine tool, material, instruments; design of experiments – variability and model creation; data gathering, modelling, analysis and evaluation. This research study is based on experimental type of quantitative research. On considering previous research works on machining ADI and its phase transformations during machining, the research forms a hypothesis, as said below:

"The phase transformation is due to either of the reasons or combination of high rate of plastic deformation and heat generated during machining"

The research is unique on its own as very few researchers in the history of machining have tried to study and give a statistical data of phase transformation and plastic deformation during machining of ADI.

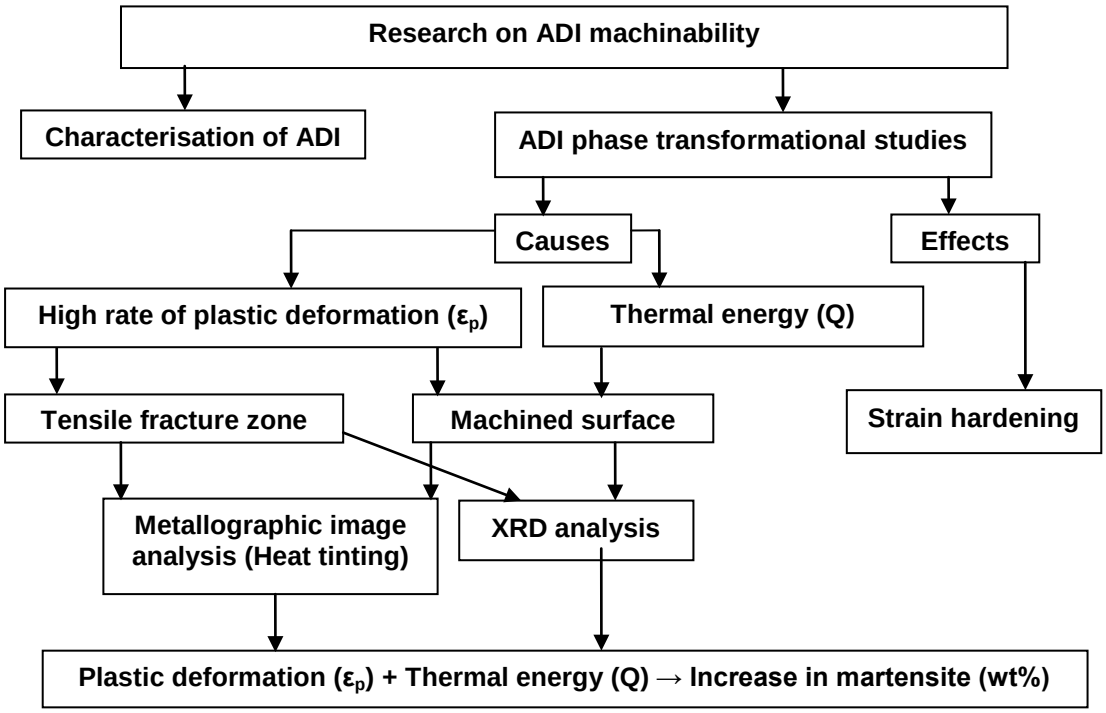

Figure 1: Research approach

The research work is novel regards to the simplified approach used to study the phase transformational behaviour during machining of ADI. The approach connects: theory behind microstructural phase (martensite) evolution, plastic deformation during tensile testing and machining, in order to develop a prediction model for determining the amount of phase transformation (increase in weight fraction of martensite) for a range of plastic deformation. The innovative approach adapted in this research, opens new avenue of opportunities and supports phase transformational studies on other similar materials. The research approach modelled taking into account the various factors influencing ADI machining is shown in Figure 1.

1.3 Research limitations

The material property associated with machining of ADI is the high hardness of the materials before strain hardening. Some of grades such as grade 1200 and 1400 used in this research are on an average having hardness, 40 R_C on a Rockwell scale. Because of the high hardness, limitations arise in selecting the appropriate cutting parameters and tools. As the research hypothesis revolves around phase transformational studies of ADI during machining, machining ADI slightly away from the safe zone is considered to be the best way to encourage occurrence of phase transformation. This approach involves considerable amount of risk connected to it.

The research did experience setbacks in the form of cutting tool failures as the tool was not able to withstand the high forces and temperature in the cutting zone. Hence, the parameters were selected with caution at a range slightly higher than the tool supplier recommendation.

1.4 Strategic importance

The research generates data to machine ADI successfully across a range of heat treated grades. The approach is to analyse the subsurface condition after a machining operation. This allows formulating a model to predict the most suitable machining parameters to adopt for a particular grade/component feature/application. The machining approach discovered from the research has to support and justify the fact that it is viable and economical to machine ADI. It is expected that the outcome from this research could contribute to the global machinability community. Furthermore, engaging in machinability research does support and compliment the other material processing research currently being undertaken in the School of Engineering through Engineering Research and Innovation Cluster (ERIC).

1.5 Thesis structure

The report narrates the scientific investigation undertaken as part of this research work on ADI phase transformational studies. The report has been divided into nine chapters elucidating the different stages of the research. Chapter one includes introductory comments on research involving ADI machining. Chapter two introduces the material used in the research, Austempered Ductile Iron (ADI) and involves production, microstructural significance, engineering applications and problems associated with ADI machining. Chapter three consists of introduction to machining and machinability, ductile cast iron machining, machinability factors and assessment techniques. Chapter four introduces microstructural phase transformations, its causes, effects and types. Chapter five explains the experimental design of the research. Chapter six presents the results and the analysed data. Chapter seven involves discussion. Chapter eight is the conclusion part of the research and summarises the whole research. Chapter nine explains the future work of the research.

2 Introduction to Austempered Ductile Iron

Austempered Ductile Iron (ADI) is a modified Ductile Cast Iron (DCI) produced by heat treatment processes - austenitising and austempering. ADI on subjected to heat treatment produces a uniform microstructure of acicular ferrite and austenite (known as "Ausferrite" or "Bainite" in steels) with graphite nodules. In recent times, ADI has been a material with great potential, fast replacing the metals such as Steel, Aluminium and other light weight alloys. During the twentieth century, researchers have conducted experiments exploring the nature of the material. As a result a number of technical papers and journals have been published on ADI describing the metal and its advantageous properties. The latest survey on American market distribution of ADI applications in various fields of engineering is shown in Figure 2 [1].

2.1 History of ADI

ADI market had begun to rapidly increase from a modest beginning in the early 1970's to an estimated worldwide production level of 125,000 tons annually. The use of austempering heat treatment and its effects to produce a material with desirable properties were confined to research experiments, till the first commercial production of a small crankshaft for a hermetically sealed refrigerator compressor by Wagner Castings Co. for Tecumseh products in 1972 [2].

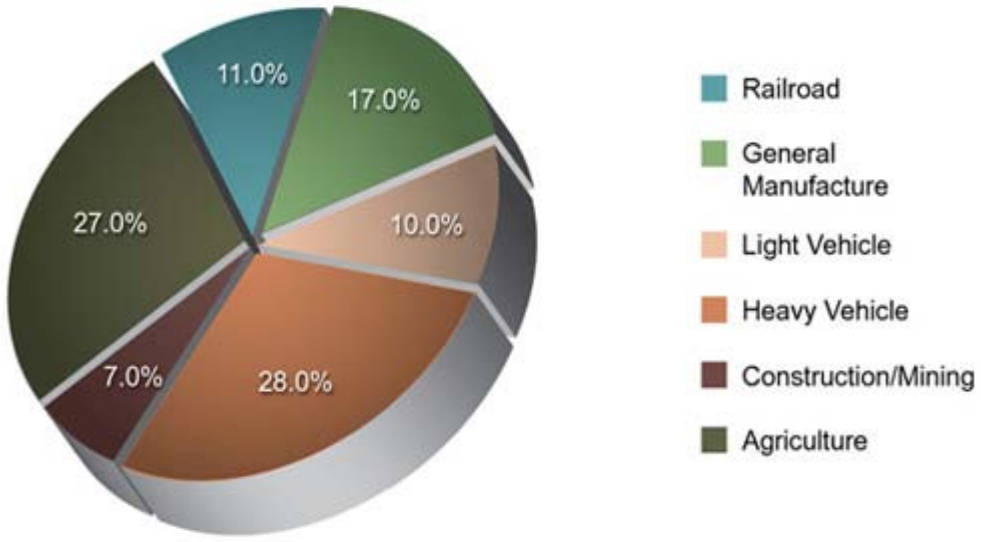

Figure 2: ADI - American market distribution - year 2008 [1]

In 1977, General Motors used ADI as replacement material for steel, ring gear and pinion for use in Pontiac rear-drive automobiles [2]. In 1983, Cummins Engine Co. used ADI timing gears in its B and C series diesel engines. In 1971, ADI was developed in Czechoslovakia and widely used in the automobile, tractor and mechanical industries owing to its excellent damping capacity, high wear resistance and low fabrication cost [3]. The new environment legislations on CO2 and other harmful emissions are encouraging automobile manufacturers to shift to higher strength to weight materials in their engines.

2.2 ADI standards

The acceptable standards of ADI was first published in 1990 by ASTM 897M-90 which was later revised in 2002. In 2003, SAE J2477 standards of ADI has been approved and published. The ISO/CD 17804 was also published in the same year. The comparison of the ISO, SAE and ASTM standards for ADI are shown in Table 1. The ISO designations in Table 1 are applicable for sections less than 30mm. The convention used in Table 1 below is: tensile strength (MPa) - yield strength (MPa) - elongation (%) [4]. A comparison of the Brinell hardness numbers for the various grades of ADI is shown in Table 2.

Table 1: Comparison of ISO, ASTM and SAE standards [5]

ISO/CD 17804	SAE J2477	ASTM A897/A 897M
800-50-10		
		850-550-10
900-600-08	900-650-09	
1050-700-06	1050-750-07	1050-700-07
1200-850-03	1200-850-04	1200-850-04
1400-1100-01	1400-1100-02	1400-1100-01
	1600-1300-01	1600-1300-00

Table 2: Comparison of Brinell hardness numbers [5]

Grade (TS MPa)	ISO/CD 17804	SAE J2477	ASTM A897/A897M
800	250-310		
850			269-321
900	280-340	269-341	
1050	320-380	302-375	302-363
1200	340-420	341-444	341-444
1400	380-480	388-477	388-477
1600		402-512	444-512

2.3 Production of ADI

The production of ADI is a two-stage heat treatment process involving decomposition of austenite to ferrite and enriched austenite in the first stage and further in the second stage involves decomposition of enriched austenite to ferrite and carbide. The heat treatment procedure is shown in Figure 3. If the casting is held too long at the austempering temperature, an alloy accumulates large amount of carbide and this makes the materials very brittle which is undesirable in ADI, to get the best combination of mechanical properties, the heat treatment parameters should be optimised after the completion of first reaction (AB) known as austenitisation at temperatures of 1550 ^{o}F - 1750 ^{o}F (840 ^{o}C - 950 ^{o}C) and at the onset of the second reaction (DE) known as austempering at temperatures of 450 ^{o}F - 750 ^{o}F (230 ^{o}C - 400 ^{o}C). The time lag between the two reactions is defined as process window (CD or the quenching phase) and a wider process window is always desirable for commercial applications. The size of the process window determines the technical feasibility of successfully producing ADI. For avoiding pearlite formation the cooling rate should be high and desired austempering temperature should be reached in the casting prior to the nucleation of ferrite. In ADI, the matrix is altered to give a structure known as ausferrite which consists of ferrite needles in retained austenite. Factors effecting austempering process and microstructure are austempering time and temperature, austenitising time and temperature, alloy segregation, chemical composition and alloying elements, casting quality and section size of the castings [6].

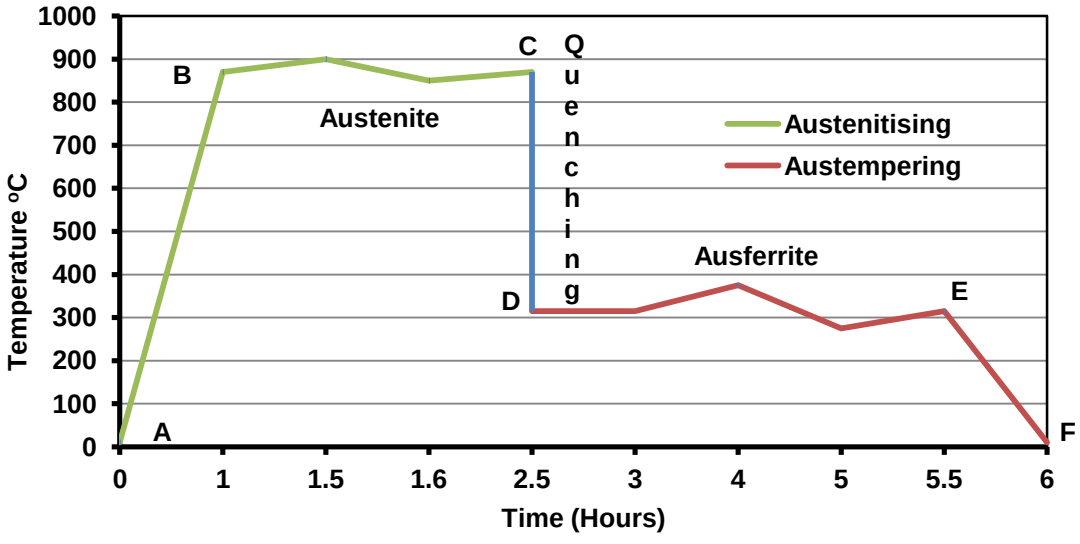

Figure 3: ADI Heat treatment diagram [2]

The effect of carbon and different alloying elements used in iron is expressed in terms of a value (wt%) known as Carbon Equivalent (C.E), which is calculated using the formula given in equation 2-1. Material properties such as hardenability, toughness are varied to a desired value suitable for an application using C.E (wt%).

$$\text{C.E (wt\%)} = \text{C} + \frac{1}{3} \times (\text{Si} + \text{P}) \quad \text{----------} \quad \text{2-1}$$

C.E is an important factor in deciding if a cast iron is eutectic (equals to 4.3%), hypo eutectic (less than 4.3%) and hyper eutectic (greater than 4.3%). For ADI carbon content is in the form of spheriodal graphite nodules. At eutectoid temperature (2066 ^{o}F) the maximum carbon austenite can dissolve is 2.1%. For ADI to reach that point takes up to 4 hours if austenitising temperature is around 871 ^{o}C [6]. It takes less time if the austenitising temperature is increased to 927 ^{o}C with same austempering temperature. Mechanical Properties like fatigue and tensile strength depend on carbon content in the transformed austenite.

A few elements that may have significant effect in ADI are Si, Cu, Mg, S, Mn, Ni, Mo, P, Cr, V and Ti. Silicon is used to delay the austempering reaction in order to allow a carbide free structure of bainite and austenite to occur. Silicon prevents precipitation of carbon. The delay in the austempering due to the effect of silicon is from 70 minutes to 4.5 hours. The preferred silicon content is 1-3%. If the silicon content is increased beyond 3.2%, it enhances the performance of ductile iron at elevated temperatures by stabilising the ferrite matrix and forming a silicon rich surface which inhibits oxidation. Copper increase the hardenability of ADI and the maximum added is 0.8%. Copper stabilises austenite by acting as a barrier to carbon diffusion at the austenite-graphite interface and widens the austenite zone of the phase diagram increasing both the transformation rate and the carbon content in the matrix during austenitising and restrains carbide formation during austempering [7].

Manganese acts as carbide stabiliser and is considered to be much less potent than sulphur. Hence, in commercial practice, it is best to use manganese than sulphur. Bainitic reaction slows down because of slower diffusion rate of carbon due to manganese content. More than 5% of manganese causes brittleness by restricting ferrite transformation and segregation with carbon leading to low fracture toughness.

Most commercial cast iron contains sulphur in the range 0.06-0.12%. The higher the sulphur content, greater is the amount of combined carbon and produces a hard and brittle white iron. The effect of sulphur on iron is vice versa to the effect of silicon. Nickel along with copper is used to improve austemperability of thick castings. Fatigue and toughness is improved by approximately 2% of nickel. Molybdenum and Nickel delay the time period for the austempering reaction and hence, creating a larger process window. Molybdenum is strong carbide former and hence, it segregates the cell boundaries to form carbides. Molybdenum carbide is hard to dissolve in carbon during austenitisation and results in formation of martensite. Hence, molybdenum should be used in limited quantities. Phosphorous (0.1-0.9%) increases fluidity. Chromium, Vanadium, Titanium, Cerium and Antimony have tendency to form carbides at cell boundaries and have less effect on mechanical properties [6].

An increase in austenitising temperature causes an increase of dissolved carbon, austenite grain size and reduction in the rate of austenitising. As the austenitising time is increased, there is an increase in dissolved carbon which leads to high hardness and strength. The structure is more likely to be upper bainitic with an increased elongation and impact strength. The final microstructure of ADI is greatly affected by austempering temperature and time. At lower austempering temperatures, due to lack of complete stabilisation these structures contain up to 12% martensite leading to an increase in hardness. At higher austempering temperature relatively coarse and distinct bainitic ferrite needles are produced. The higher austempering temperatures is considered as the upper bainite transformation range, leading to more ductility and smaller increase in strength and hardness than at lower bainite transformation [8].

$$\gamma(\text{Austenite}) \rightarrow \alpha(\text{Ferrite}) + \gamma_{hc}(\text{enriched Austenite}) \quad \text{----------} \quad 2\text{-}2$$

$$\gamma_{hc} \rightarrow a(Ferrite) + \epsilon\,(Carbide) \quad \text{----------} \quad 2\text{-}3$$

Austempering time is critical because the bainitic ferrite-austenite structure is produced by the austenitising, while the second reaction (equation 2-3) is undesirable because it reduces the ductility and toughness. Shorter austempering time leads to poor mechanical properties. If austempering time is too long, the second reaction (equation 2-3) occurs where austenite is decomposed to ferrite and carbide which leads to reduction in ductility values.

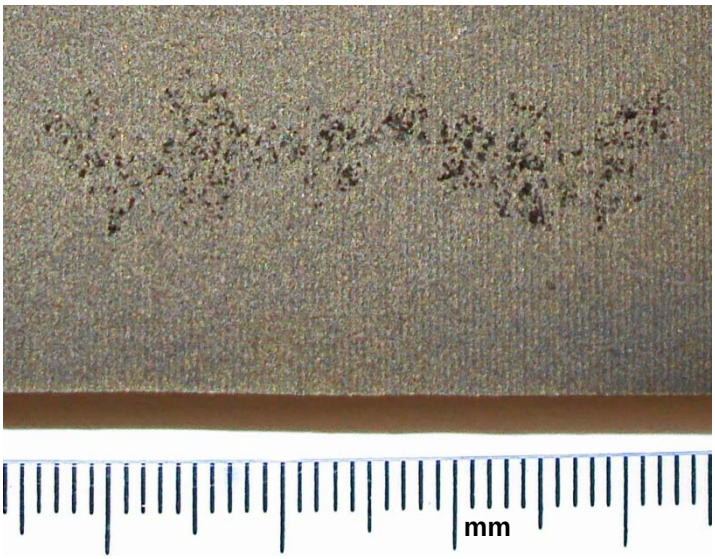

Figure 4: Porosity - common defect in ADI

Casting quality factors like poor nodularity and low nodule count detoriate ADI properties. Porosity or carbides which are not dissolved does show more effect on the properties. Nodularity is defined as:

$$Nodularity\ (N) = 100 \times \frac{D}{d} \quad \text{----------} \qquad 2\text{-}4$$

Where D is the diameter of major axis of the nodule and d is the diameter of the minor axis of nodule. The number of graphite nodules per unit area is known as nodule count. Tensile and impact properties decrease with decrease in nodularity [6]. The critical characteristics for getting a good quality ADI are consistent chemical analysis, 100 nodules/mm^2, minimum of 90% nodularity, maximum of 0.5% carbides and inclusions, maximum of 1% micro shrinkage and consistent austenite and ferrite ratio. Porosity which is a common defect for a cast and heat treated material like ADI is shown in Figure 4. Variations in chemical analysis can affect the heat treatment times and temperature and hardenability of iron. High nodule count is required to increase toughness, strength and machinability of ADI by reducing the micro segregations, micro shrinkage and cell boundary carbides. A consistent austenite/ferrite ratio minimises the variations in mean volumetric expansion during austempering. Addition of copper (0.6%), increases the strength and the number of graphite nodules [9]. Improper heat treatment procedures during production of ADI, lead to incomplete transformation of enriched austenite to ausferrite and leave behind a fraction of unreacted or retained austenite.

2.4 Material properties of ADI

The material properties of ADI are high strength-weight ratio, ductility and toughness, good fatigue strength, damping properties and wear resistance. ADI can retain a high proportion of its room temperature toughness even at low temperatures [10]. It is an important material in light weight design considerations where strength and toughness along with design flexibility and density matters. The fatigue strength of ADI is greatly increased by mechanical working of the surface layers through processes such as fillet rolling or shot peening [11].

The wear resistance of ADI is increased significantly by introducing carbides into the ausferrite matrix producing a new variety of ADI known as Carbide Austempered Ductile Iron (CADI). CADI is produced by reducing the graphitising elements such as silicon or to alloy the melt with a carbide stabilising element such as chromium, molybdenum or titanium or by under cooling using a chill in the mould [12]. The wear resistance and hardness of ADI can also be increased by alloying with elements such as chromium and molybdenum by using surface alloying and surface melting techniques [13]. ADI exhibits good fatigue life when subject to cyclic loads and experimental results have shown that specimen preparation such as grinding and polishing can affect the endurance life time of ADI. Poor grinding or polishing leads to lower endurance strength [14].

Elongation, strength and impact energy strongly depend on the amount of retained austenite and ferrite present in the microstructure [7].When austempering is done in the range of 350-400 ^{o}C, ADI has high ductility, yield strength in the range of 500 MPa, good fatigue strength and impact strength and when lower austempering temperatures are used ADI has very high yield strength, high hardness, excellent wear resistance and contact fatigue strength [15]. The austempering time should be chosen to optimise properties through the formation of a stable microstructure of ausferrite. At shorter austempering times, there is not enough time for carbon to stabilise the austenite and results in martensitic microstructure having high hardness and low ductility [15].

2.5 Applications of ADI

The application of ADI differs on considering different grades of ADI. The grade 900 and grade 1050 are considered to be structural grades of ADI, used in suspension components and many other dynamic applications because of their ductile nature; grade 1200 and grade 1400 are wear grades because of their high hardness, used in applications where wear resistance is the primary criteria for material selection [16]. ADI provides a unique combination of high strength and toughness combined with design flexibility for chassis application [11]. In Australian truck industry, hauling freights over rough and isolated distances is an interesting challenge for independent trailer suspension bracket as it provides an increased space and ability to withstand the fatigue. ADI is proven to be a good material for making independent trailer suspension bracket [10]. ADI is used in the making of crankshafts for TVR Tuscan inline six cylinder engine because of its low production costs and weight saving [17].

ADI is good choice for rail wheels where the primary properties under consideration are damping capacity and lubrication. ADI is used in making lock cases as it can resist penetration because of its strain hardening property under severe conditions [10]. ADI is used as a gear material with respect to the bending strength, surface durability and the pitting strength of the gear [18]. ADI gears are used in diesel engine applications for their strength, noise reduction and ease of manufacture. Wheel axles are converted from a steel assembly to a single piece ADI casting for agricultural purposes [10]. The current application of ADI include ground engagement components-digger bucket teeth and dozer blades, truck suspension brackets, differential spiders, tow hooks, cylinder liners, engine con rods and crank shafts [10]. ADI is an attractive alternative to steel, with 10% less dense than steel, weighs less and cost less. The machinability of softer grades of ADI is equal to or superior to that of steel with equivalent strength [15]. ADI is easily deformed into various shapes which is advantageous for thin products which generally cannot be fabricated using conventional casting techniques and also for products which are used under severe conditions [18].

The energy requirement for production of ADI is less than that required to produce steel castings and forgings. Hence, there is reduced manufacturing cost and these cost savings are passed on to the consumer [19]. The substantial increase in strength and wear resistance of ADI could offer some machining problems [15].

Gear hobbing of ADI is difficult because of the occurrence of tool failure in a short time [18]. The acceptance of ADI in high volume automotive applications is limited because of machining difficulties and inconsistent performance [20]. The properties that make ADI appealing also create a major challenge in machining due to their hardness and strength [21].

3 Introduction to machining and machinability

Machining is defined as a production process in which a harder metal cuts a softer metal and the metal is removed in the form of chips (swarf) by a plastic deformation process. The deformation temperature and the force significantly contribute to the quality of the process. Temperature affects the cutting tool material and the forces effect the power and strength needed to perform the process [22]. There are two general ways to machine described so far by researchers - orthogonal and oblique cutting. Orthogonal cutting has cutting edge perpendicular to the direction of cut and oblique cutting involves cutting edge at an angle to the feed direction. Orthogonal cutting represents a two-dimensional type of cutting. The general principle in orthogonal cutting is the sum of rake angle, clearance angler and wedge angle is a right angle. In orthogonal cutting, the resultant force is normal to the machined surface of the workpiece. Shaping is a machining operation which is used to generate flat surfaces on the workpiece by reciprocating motion of the tool against a securely mounted workpiece. Shaping is a perfect example of orthogonal cutting [23].

3.1 Machining Ductile Cast Iron

Cast iron machining has been noteworthy in establishing metal cutting theories by eminent researchers such as G. Boothroyd, M.C. Shaw, E. J. A. Armarego and R. H. Brown. The history of cast iron machining has been long and extensive with significant gains during the industrial revolution. Grey cast iron is widely used in the automotive industry for many years in manufacturing automotive components such as engine blocks, cylinder heads, differential housings, shafts, flywheels, brake drums and disks [24]. The development of cast iron machining is associated with advancement in tooling and machinery. With the introduction of new cutting tool materials such as Polycrystalline Cubic Boron Nitride (PCBN), Ceramics and other metal matrix composites, the cutting tools are able to survive in adverse cutting conditions. The machinery has advanced significantly offering wide range of speeds, array of spindle options and multiple axis machining. The demand for higher productivity, lower manufacturing costs and better quality of products has lead to development of high speed machining in cast iron. Cast iron is an alloyed material where ferrous (iron) and carbon are the main elements which affect the material property of iron. Cast iron also has higher amounts of silicon. The fraction of carbon decides the hardness levels in iron.

According to the Fe-C phase diagram, Fe-C alloy having less than 2% carbon is classified as steel and more than 2% as cast iron. The rising demand for materials having high strength-weight ratio and customised material properties has led to evolution of new variety of iron such as Ductile Cast Iron (DCI) and Austempered Ductile Iron (ADI) [25]. As the name suggests, DCI and ADI have better ductility, higher modulus of elasticity and improved material properties when compared to age old grey cast iron [24].

The common observation in DCI and ADI is the carbon which exists in its allotropic form “graphite” and is nodular shaped. Graphite exists as flakes in gray cast iron. Silicon is used to control the size and shape of graphite in DCI and cast iron. Due to the presence of higher amount of carbon in DCI and ADI, these materials have an advantage in lubrication and heat dissipation during machining compared to normal cast iron. Graphite present in cast iron helps to dispose heat from the tool/workpiece interface and reduces the friction on the chip/tool interface during machining [26]. The common challenges faced in DCI machining are rapid wear out of the cutting tool insert as DCI has higher amount of silicon which increases the abrasiveness. The presence of carbon in DCI and ADI is also disadvantages in certain machining circumstances as it causes hindrance in predicting the tool behaviour and surface quality. Although PCBN cutting tools are popular and extensively used for grey cast iron machining, the use of PCBN for DCI especially for high speed machining is problematic as the reaction between the high ferrite content and PCBN due to chemical dissolution at high temperatures leads to rapid wear of the cutting tool [24].

There exists different grades of DCI based on combinations of proportion of ferrite and pearlite i.e. all ferrite, all pearlite and ratios of ferrite and pearlite matrix. The higher the amount of pearlite, the better is mechanical properties such as strength and hardness, elongation but machinability is reduced drastically. There are noticeable variations in machinability of DCI and grey cast iron. Machinability of iron depends on factors such as graphite size and distribution, composition, ferrite/pearlite ratio, cooling rate from eutectic through eutectoid temperatures and presence of external and internal inclusions [27]. Research studies on gray cast iron machining by Griffin et al. reveals that higher tool wear rates are associated with lower free carbon concentrations and higher combined carbon, higher manganese and tin content; and higher concentration of hard inclusions.

There is no correlation between the wear rates and graphite structure in case of cast iron machining [27]. Work done by Bhattacharyya et al. on cast iron machining state that there is no effect of coolant on cast iron machining as the flake shaped graphite present in the iron, lowers the shear strength and assists in lubricating the tool/workpiece interface producing discontinuous chips. Powder metal residue along with the discontinuous chip is common during cast iron machining. The use of cutting fluids in cast iron machining leads to thermal cracking of the tool, especially for ceramic tools, as the sudden cooling of the tool from high temperatures during machining leads to thermal cracks and breakage of the cutting edge [28]. Ductile cast iron produces a continuous chip during machining. Continuous chip with built-up edge is quite common in ductile cast iron during the final stages of machining. The chip formation undergoes a process known as adiabatic shear which was explored further through extensive research by Komanduri on high speed machining [29]. In an adiabatic shearing process, chip is produced as a result of thermal softening of the shear plane zone. According to Recht and Komanduri, initiation of cut takes place in a material at the onset of plastic deformation reaching a certain limit. If the rate of plastic deformation is low, then the potential for strain hardening along the shear zone is low and vice-versa at increased speeds. The strain hardening effect causes localised heat in the shear zone and contributes to the thermal softening of the workpiece in the shear zone and thus causes the chip to slip rather than shear along the shear plane [29, 30].

Based on the works of Nakayama, chip formation does not start from the tool/workpiece interface but initiates at the free surface of the workpiece material. Nakayama also suggests the build up of the stress normal to the rake face and crack formation which propagates along the shear plane reaching the tip of the tool [31]. Shaw termed such cracks as “gross cracks”. For a ductile material, micro cracks are developed around the tool/chip interface and these micro cracks initiate the process of strain hardening that leads to adiabatic shearing process which has been discussed by Komanduri in his research. As a result of strain hardening the gross crack extends from the free surface to a point in the shear plane where the rate of strain hardening is greater than crack propagation and leads to arrest of the crack formation process [32]. Strain hardening through plastic deformation is a common phenomenon in DCI and ADI. During machining, plastic deformation results in cold working of the surface layer. The depth of cold worked layer depends on the ductility of the material [33].

Lattice crystal defects such as dislocations which are irreversible deformation caused on a microscopic scale effect strain hardening. Variations in local stress fields cause dislocations leading to rearrangement of the lattice structure as the dislocations propagate [34]. As a result of increase in dislocation density of the material, strain hardening occurs in order to prevent nucleation of new dislocations. This resistance to dislocation can also be considered as resistance to plastic deformation. Plastic deformation is due to the work done on a material or energy imparted to the material. In case of machining, the energy applied is of high magnitude and in quick time which not only moves the existing dislocations but also encourages new dislocation by jarring and working the material sufficiently enough [34]. Ghani et al. studies on machining DCI using ceramics say that the surface finish of the workpiece is not influenced by the tool wear but speed, feed and depth of cut play an important role to influence the surface finish [35].

Most of ADI machining is done under dry conditions because of the graphite in ADI with its small coefficient of friction acts as a good lubricant and hence, increasing the tool life and reducing the tool wear [18]. According to Okazaki et al. the γ-pool (the massive austenite which exists on the boundary of the eutectic cell) average area in ADI structure, as a factor which affects the tool wear in drilling. The flank wear of the drill decreases with the decreases in γ pool average area and hence, it is important to decrease the γ-pool in order to improve the machinability. ADI tool wear phenomenon is characterised by extreme crater wear located very close to the cutting edge which destabilises the cutting edge and leads to fracture of the crater lip. The unusual combination of abrasive and adhesive wear mechanisms is due the special ausferrite microstructure of ADI [36].

3.2 Machinability factors

It is considered that the word machinability was first used in the 1920 referred to the speed/tool life relationship. Although extensive research was carried out on machining, researchers are still elusive about an assignable material property to judge machinability [37]. Machinability of a material is defined as the ability of a material, to allow machining efficiently consuming less power, producing good surface texture and without excessive tool wear or failures. Machinability of a material depends not only on its material properties and microstructure but also on proper selection and control of process variables [38].

Machinability factors play an important role in effective and efficient running of the metal cutting operation. Machinability factors include machining conditions such as cutting parameters - speed, feed and depth of cut; cutting tool material properties and wear, material properties of workpiece, cutting fluids, surface texture, chip formation, rigidity of the machine tool, Metal Removal Rate (MMR) - power required to machine, manufacturing cost and productivity. There are four factors which determine the machinability of a material i.e. surface texture and integrity of the machined part, tool life, force and power requirements and chip control [38].

3.2.1 Cutting forces

Cutting forces play an important role in machining as they initiate the process of chip formation and control the flow of chip and thermal gradient involved in machining. The role of cutting forces is explained using a Hooke's law, where stress is directly proportional to strain. The stress-strain curve (as shown in Figure 5) indicates that up to a certain limit of stress the material is elastic and obeys proportionality. On increasing the stress, the material loses its elasticity and slips into the plastic zone undergoing plastic deformation and breaks away from the parent material. Similar is the case with chip formation, the cutting forces should reach a specific level to initiate the chip formation and the minimum force where the plastic deformation starts is known as the specific cutting force. The cutting forces acting along the direction of tool travel (F_c) and thrust force (F_t) are measured using a dynamometer supported by charged amplifier.

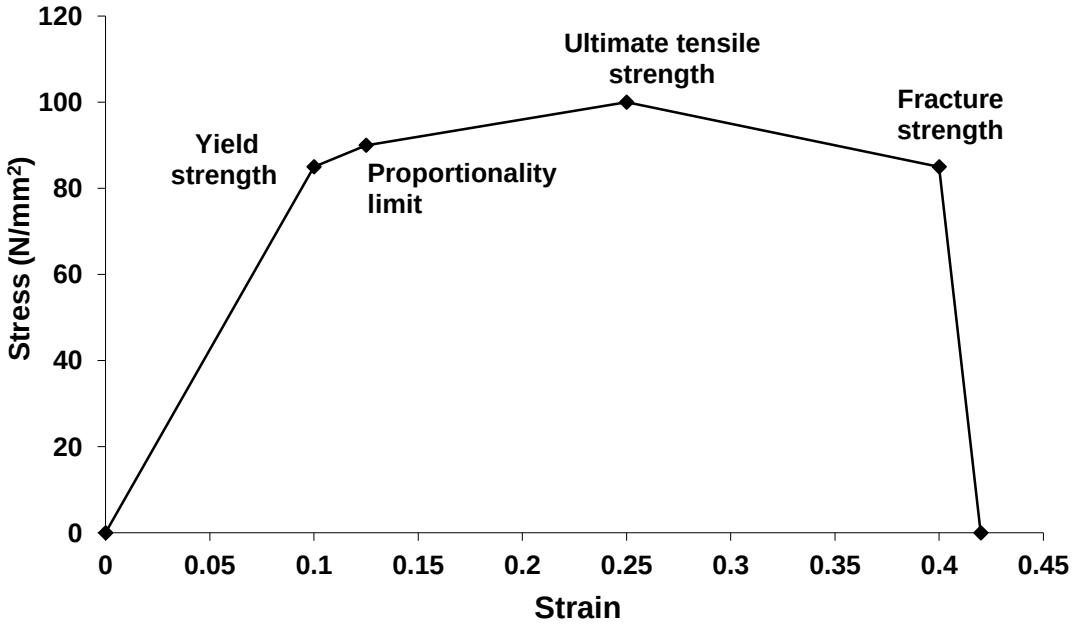

Figure 5: Stress - Strain curve

In any machining operation, the shear strength and cutting forces are related as

$$F_c = t \times S_o \times \tau_s \times f \quad \text{----------} \quad 3\text{-}1$$

$$f = \zeta - \tan(\gamma_o) + 1 \quad \text{----------} \quad 3\text{-}2$$

where t is depth of cut in mm; S_o is the feed in mm and f is form factor, which is a constant. Form factor (f) is determined from the tool geometry and chip thickness using equation 3-2, where ζ is the chip reduction coefficient and γ_o is the orthogonal rake angle [39]. Cutting force analysis for a specific machining operation is required in order to have a balanced and positive cutting action with respect to the cutting edge strength and action [23]. The cutting force mainly consist of shear force (F_s), axial cutting force (F_c) and frictional force (F_f). The equilibrium in the cutting forces is explained using Merchant's circle in Figure 6. The cutting forces are mostly compressive and shear in nature and depend on the rake angle, cutting fluids, tool and workpiece material, cutting geometry and area of contact between the chip and rake face. Specific cutting force is the initial force required by the tool to initiate plastic deformation or chip formation [22]. High cutting speeds generates high temperatures in the flow zone which leads to lower values of specific cutting force.

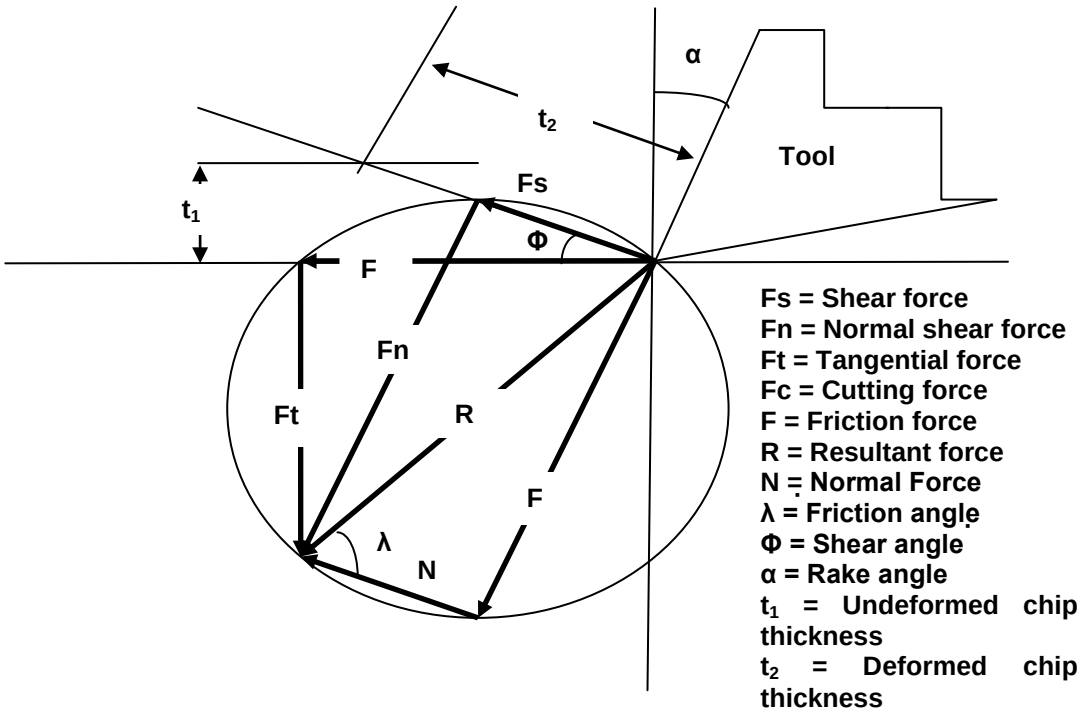

Figure 6: Merchant circle - cutting force diagram

Positive rake angles also reduce specific cutting force. The parameters associated with cutting forces in drilling are the feed force, torque and power and the cutting forces generated in drilling are effective on the lips, the chisel edge and the chip surfaces [22]. The thrust force and the torque are important to calculate the efficiency of a drilling operation [37]. The axial cutting force or along the direction of feed is an important factor in drilling. The diameter of the drill influences the axial cutting force. The relationship between the cutting forces significantly affects the stability of the machining operation as improper balance of cutting forces leads to vibrations, deflections and BUE. The radial cutting force or force acting perpendicular to the axial cutting force is effective in machining operation like drilling and boring and depends on the entering angle [22].

3.2.2 Cutting speed

The cutting speed to be chosen depends on factors such as machine tool used, stiffness, precision, damping capacity, numerical control response, contouring capabilities at high feed rates, chip disposal, coolant flow, dynamic balance in case of rotating cutters, part requirements, number of parts, type of machining operation, ratio of non-cutting time to cutting time, safety and economics [22]. Figure 7 below shows the relationship between cutting speed, feed rate and too life for machining at constant depth of cut (DoC) [40]. From Figure 7, for constant DoC, longer tool life is obtained for the best possible combination of low feed rate and low speed.

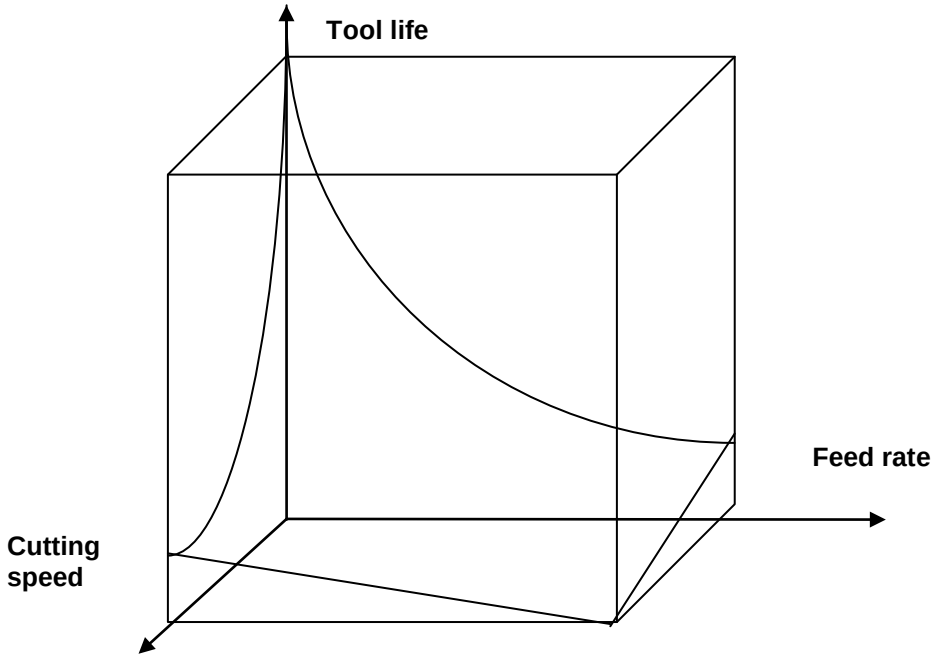

Figure 7: Relationship between feed rate, cutting speed and tool life at constant depth of cut

3.2.3 Tool wear

There are two basic forms of tool wear: flank wear and crater wear. Flank wear is most common in machining hard and difficult to machine materials. Tool wear can also exist in different categories such as abrasion, adhesion, diffusion, fatigue, oxidation, deformation, creep and chemical wear.

During the chip flow, the deformed chip material gets welded to the tip of the cutting edge due to the high temperature and pressure involved at the cutting edge. The phenomenon generates an additional edge at the tip which is known as Built-Up Edge (BUE) [22]. For a Body Centered Cubic (BCC) structure such as ductile material, the formation of BUE is a result of high plasticity region in front of the tool rake face within the contact length. According to Astakhov, a BUE is avoided by allowing the cutting process to take place at optimum temperature [33]. BUE in most of the cases is considered to be a negative factor in machining as it changes the tool geometry - rake angle, reduces the cutting edge strength and leads to inefficient cutting. BUE formation indicates the possibility of more tool wear and therefore, less machinability.

Heavy built-up edges leads to excessive heat generation and high frictional force against the flow of chip along the chip-tool interface resulting in high cutting force [23]. Another way, in which BUE is detrimental to tool life, occurs during the cooling of the tool tip at the end of the cut. As the coefficient of linear expansion of steel is approximately twice that of a carbide tool material, cracks may be introduced in the tip where the attached portion of built-up edge has contracted, during cooling, by a greater amount than the carbide [37].

Work hardening in some materials reduces the tendency for BUE. The strength of BUE decreases with increase in temperature. BUE is more prone to rounded cutting edges and is avoided by using positive rake angles. During drilling, apart from BUE, flank wear occurs on the clearance side of the cutting edge and crater wear which arises on the chip face [22]. Larger rake angle leads to less chip curls through a large radius and lower cutting forces. Negative rake angles are favourable for cutting materials which are hard and to act as chip breakers at low feed rates [22].

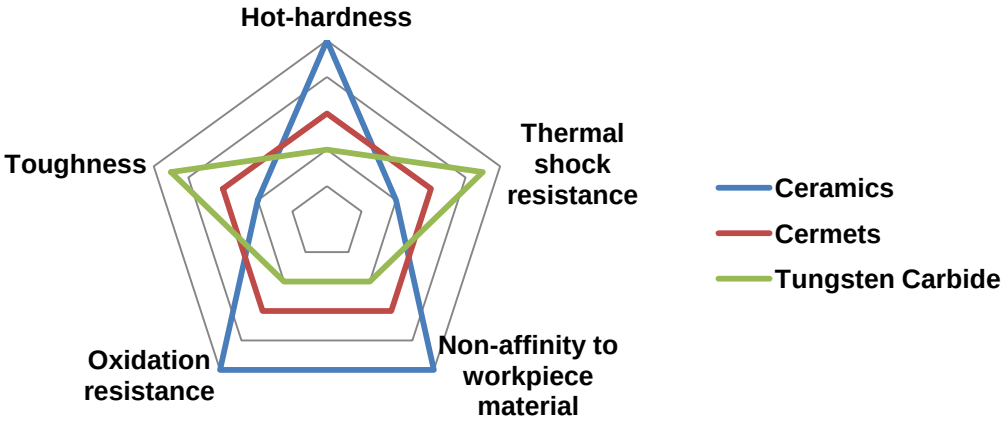

Figure 8: Cutting tool material characteristics for efficiency

Figure 8 shows the qualities of a cutting tool material for effective and efficient metal cutting operation [40]. From Figure 8, Cermets are known to have optimum properties required for a cutting tool. Tungsten carbide tools are known for their toughness and thermal shock resistance; and ceramics for their hot hardness.

Surface integrity of the materials worsens as the flank wear on the tool increases. Flank wear is smaller for finishing operations and higher for roughing operations [41]. The high demand of using ADI in design considerations has initiated researchers to find an appropriate cutting tool for machining. According to the research conducted by N. Pretorius et.al, the cutting tool materials suitable for machining ADI are Poly Crystalline Diamond (PCD), Polycrystalline Cubic Boron Nitride (PCBN), Ceramics, Cermets and Coated Carbides. PCD and PCBN tools are good for high speed machining and ceramics, cermets and coated carbides for low speed machining. PCD is the best tool material for machining ADI as it considerably increases tool life and gives good surface finish quality [42]. Machining ADI involves cutting tools having good thermal conductivity to dissipate the heat generated during machining and high toughness to withstand the tool wear at high cutting speeds [19].

3.2.4 Chip formation

The initiation of shear or chip formation or metal removal in metals depends on the manner in which the atoms are arranged in the lattice. Generally, there are two common types of arrangements: FCC and BCC.

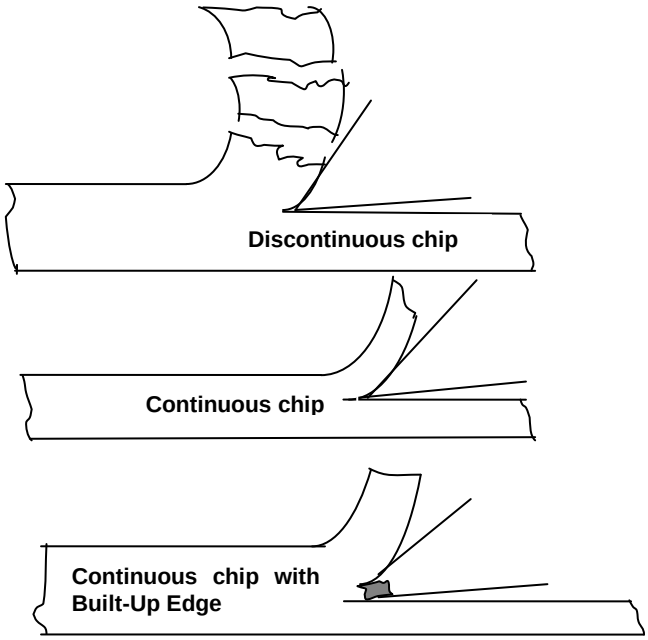

Figure 9: Chip formation types

Further studies, at atomic level show that shearing process in a metal is caused by dislocations, slips and fractures taking place in an atomic structure. The phenomenon of work-hardening has been explained with respect to BCC and FCC structures, as increase in the internal stress cause locking of dislocations at the grain boundaries of crystals or inhomogeneity within grains, so that further slip is produced by an increase in the external loads. Hexagonal crystal structure have less tendency to work hardened than cubic crystal such as BCC which harden easily [37].

Continuous chips are a regular feature for materials having extensive slip system (BCC or FCC structures), ductile, good thermal conductivity, hardness and discontinuous chip formation – occurs in material having limited slip system, high hardness, poor thermal conductivity. In case of a continuous chip, strain hardening always predominates over thermal softening.

The phenomena of strain hardening means the stress should rise in order to continue deforming the material in the plastic region [37]. The chips formed during a machining operation are of three types-discontinuous chips or segmented chips, continuous chips and continuous chips with built-up edge formation. The last two varieties of chip formation are problematic due to constant clogging of the drill area and decrease in drilling efficiency. To overcome clogging, the point of the drill is grounded at certain angles on sides to form chip breakers which restrict the chip to small size.

There are two mechanisms of surface fracture known so far i.e. brittle and ductile fracture. Both involve formation of small cracks and propagation. An analogy is made between the principles of surface fracture and chip formation. In case of ductile materials, the propagation is a plastic flow process and brittle fracture has very little plastic flow. According to Griffith's Theory, for any applied load, a crack does not spread until it is of sufficient length for its stress concentration effect to provide the energy needed to create two new surfaces.

$$S_n = \gamma \frac{E}{2C} \qquad \text{----------} \qquad 3\text{-}3$$

where S_n is the minimum tensile strength for crack propagation and γ is the specific surface energy, E - Young's Modulus and C is the length of the crack [37].

For some materials, notably the ferrous alloys, a sharp yield point exits followed by a drop in stress as plastic flow commences which indicates that for these materials the initiation of dislocation movement is more difficult than its continuation. The conditions in metal cutting are more extreme than in the other deformation processes. The distinguishing features of the metals cutting process are:

- It is a plastic flow process with an exceptional large strain. There is high compressive stress acting on the plastic zone and this prevents rapture from occurring until the strain is well above the rupture value.
- The deformation is localised to an extremely small plastic zone and has high strain rates.
- The chip material rubbing over the tool face which has been freshly formed and is chemically clean causes adhesion and high fracture force [37].

When the shear stress is zero, the normal stress is known as the principal stress. At a certain critical speed, the nature of deformation is altered giving a decrease in forces and temperature with further increase in speed is known as adiabatic shear [22]. At any point in a stressed body, the stress may be resolved into nine components acting on the face of an imaginary infinitesimal cube represented as σ_{11}, σ_{22}, and σ_{33} are normal stress and τ_{12}, τ_{23}, τ_{31}, τ_{21}, τ_{32} and τ_{13} are the shear stress.

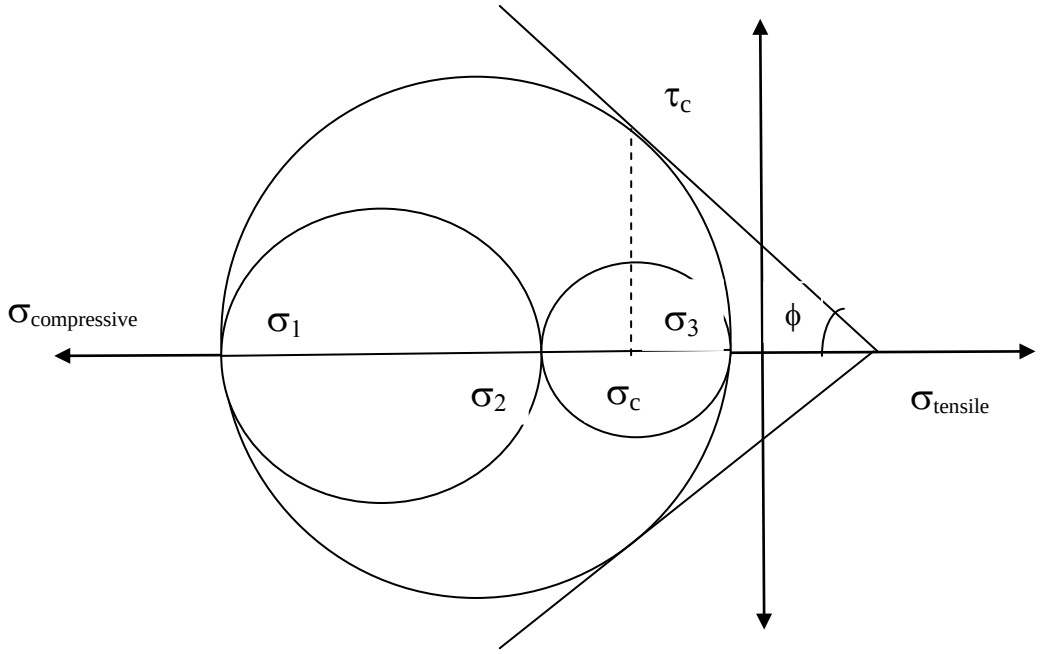

Figure 10: Mohr's circle diagram

The circle drawn with centres on a direct stress axis and the shear stress is plotted on perpendicular axis is called Mohr's circle (as shown in Figure 10). It is always desirable to have lesser chip thickness for better machinability. The chip takes the largest portion of the heat generated and increases with cutting speed and feed within the tested range of conditions [23].

Chip reduction coefficient (ζ) is defined as the ratio of deformed chip thickness (a_2) and uncut chip thickness (a_1). Chip reduction coefficient (ζ) and the shear strength (τ_s) play an important role in machining. The chip reduction coefficient is related to the main cutting edge angle (Φ) and the chip thickness by the relationship as shown in equation 3-4.

$$\zeta = \frac{a_2}{a_1} = \frac{a_2}{s_o} \times sin\Phi \quad \text{----------} \quad 3\text{-}4$$

In orthogonal cutting, main cutting edge angle (Φ) is 45^o. The shear strength (τ_s) is given as in equation 3-5.

$$\tau_s = \frac{F_c}{t\left(\sqrt{2} \times a_2 + s_o\right)} \quad \text{----------} \quad 3\text{-}5$$

The chip formation is a two stage process - the first stage involves plastic instability and strain localisation in a narrow band of primary shear zone leading to a shear separation along a surface which originates from the tool tip almost parallel to the cutting velocity vector and gradually curves concavely upward until it meets the free surface. The second stage involves gradual build up of the segment with negligible deformation by the upsetting of the wedge shaped work material ahead of the advancing tool [29]. The entering angle of the tool affects the chip formation. The width of the chip is increased and the thickness is reduced with a smaller entering angle. The shape and direction of the chip change with the nose the radius on the cutting edge.

Study on chip cross-section reveals that chips with square cross-section mean that the chips are hard and compressed and characterised by a small chip curve and larger thickness. Chips of comma shaped cross-section are generated at small cutting depths and smaller entering angles. Larger depth of cuts leads to spiral shaped chip formation in the outward direction and has more influence on the entering angle.

Figure 11 shows the relationship between shear stress and work hardening for a range of metals such as - Aluminium(Al), Copper(Cu), Nickel (Ni), Ferrous(body centered and face centered cubic) crystals, ADI and Titanium (Ti) [43].

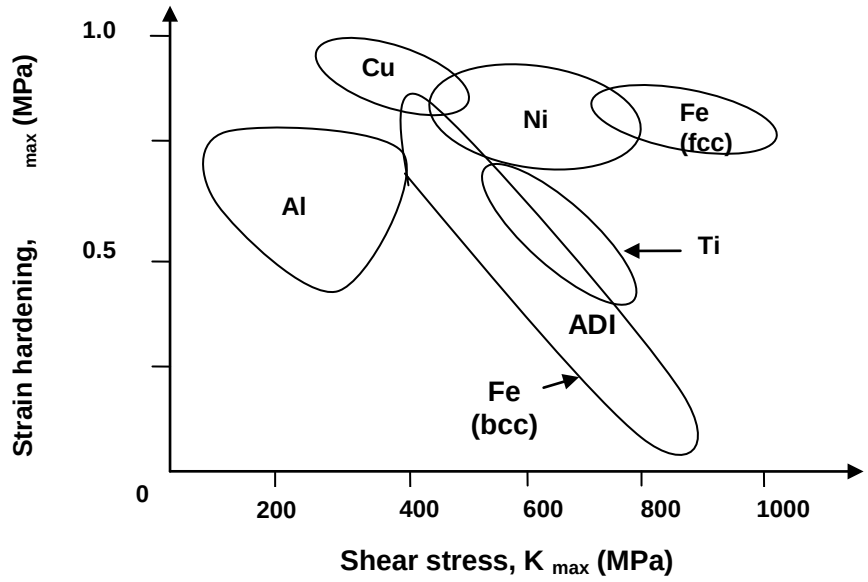

Figure 11: Relationship between work hardening and shear stress for Al, Cu, Ni, Fe (BCC & FCC) and Ti

The different ways to break a chip are self-breaking, breaking when stopped by tool and breaking when stopped by workpiece. The control of chip flow is an important factor in high speed machining process like drilling. Congestion of chips in the flutes can lead to the tool breakage and abrupt cutting. The chip formation depends on material properties of workpiece, cutting tool, cutting fluids, nature of cut, machine tool, cutting edge geometry and cutting parameters. The benefits of machining ADI are the discontinuous chip formation which are easy to handle and recycle; and does not clog the equipment in case of automated machines [16]. Shear stress (K_{max}) and strain hardening in the primary shear zone ($\Delta K/K_{max}$) act as indicators for material machinability. Strain hardening is a negative factor in chip formation as more energy is required for chip formation.

Chip morphology

The transition of the chip from a semi-continuous (segmented) to a completely discontinuous chip is taken as a sign for a work hardened material due to Strain Induced Transformation (SIT). Generally, a material with high ductility produces a continuous chip and as the ductility decreases, the chip becomes discontinuous. Similar observations were seen in drilling of grades 900, 1050, 1200 and 1400. Chip morphology varies for different cutting speeds due to the changes in crack initiation and propagation and flow localisation in the cutting zone [44]. Cooks research relates chip morphology with the cutting speed in machining of titanium. Based on his research, higher cutting speed generates high temperature in the primary deformation zone which leads to thermal softening. The chip produced is serrated if the thermal softening effect is stronger than the strain hardening effect [45].

As explained in section 3.1, Komanduri et al. in their research on high speed machining talk about catastrophic shear chip (serrated chip), while conducting chip morphology study on Ti-6Al-4V using a high speed camera and an explosive quick-stop device [29, 46]. According to Seah and Li, effect of coolant on cutting tool performance; at higher cutting speeds, the temperature at the tool chip interface increases leading to thermal softening of the workpiece material leading to a bigger chip curl. The radius of the chip curl signifies the cutting parameters [47]. Cutting parameters such as feed rate, speed and coolant condition do impact the size and shape of chip especially in drilling [48]. Through chip morphology study, a meaningful conclusion is drawn on the cutting process and the resulting surface texture.

Efficient evacuation of the chip through the flutes depends on the size and shape of the chip. For high metal removal rates, the chip size increases and hence, the torque requirement increases for efficient chip removal through the flutes [48]. The surface texture of the machined surface does depend on the efficient evacuation of the chip [49]. Rough surface texture is expected out of a drill where the flutes are clogged with large size chips and worst case might result in tool failure. According to the research work on chip morphology in drilling by Stephen et.al, feed rate significantly influences the chip size and shape; the effect of coolant on chip size is negligible. Small size chips have no significant impact on the surface texture of the hole where as larger size chips produce consistently a rougher surface texture [50].

Shear plane principle

The boundary line between the chip and the workpiece which separates the deformed and undeformed metal is called shear plane (OA). The angle between the shear plane and workpiece is called shear plane angle (Φ). The metal to the right of shear plane is the deformed chip thickness (t) and the metal left to the shear plane is an undeformed chip thickness. The thickness of the undeformed chip depends on the rake angle (α) and workpiece mechanical properties. Figure 12 shows the shear zone diagram, where a chip of thickness (t) is formed from an undeformed layer of workpiece, feed (f) by a tool of rake angle (α). The contact length (l) with the tool is given by the line (OB) and the chip radius (r). Primary and secondary shear zones define the plastic flow regions. The primary deformation zone exists around the line (OA) and strain increments are regularly detectable next to the rake face, in the secondary shear zone which might still be in a plastic state [43].

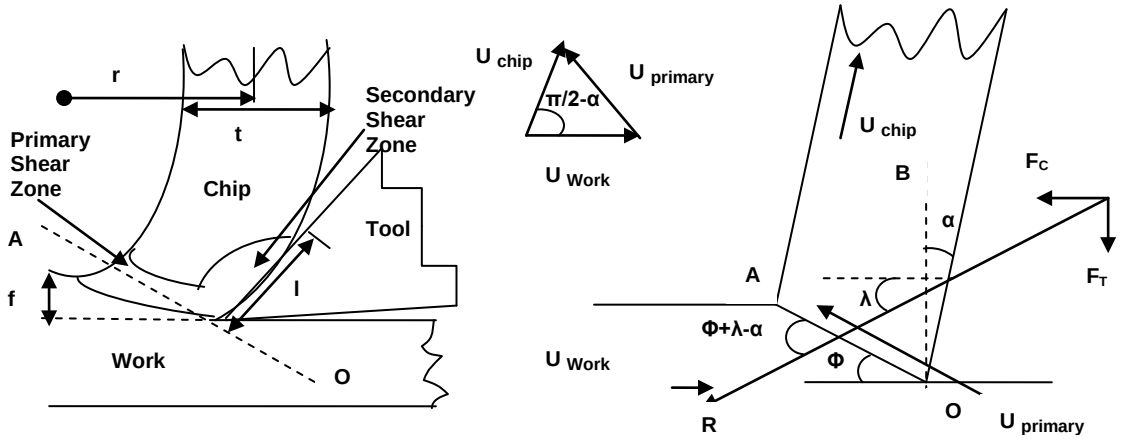

Figure 12: Shear zone diagram

Length (L) of the shear plane OA is given by equation 3-6.

$$L = \frac{f}{\sin \Phi} = \frac{t}{\cos(\Phi - \alpha)} \quad \text{----------} \quad 3\text{-}6$$

$$\frac{t}{f} = \frac{\cos(\Phi - \alpha)}{\sin \Phi} \quad \text{----------} \quad 3\text{-}7$$

The shear angle (Φ) is given by equation 3-8.

$$\Phi = \frac{\pi}{4} - \frac{(\lambda - \alpha)}{2} \quad \text{----------} \quad 3\text{-}8$$

Figure 12 also identifies the velocity change, $U_{Primary}$ that occurs on the primary shear plane and converts U_{Work} to U_{Chip}. The resultant force(R) is inclined at an angle (λ) to the rake face normal, which is known as friction angle and the coefficient of friction (μ) is given by μ= tan (λ). The angle between the resultant and the shear plane is (Φ+λ-α).

$$\frac{U_{Primary}}{\cos \alpha} = \frac{U_{Chip}}{\sin \Phi} = \frac{U_{Work}}{\cos(\Phi - \alpha)} \quad \text{----------} \quad 3\text{-}9$$

The shear strain (γ) responsible for chip formation is the ratio of the primary shear velocity to the component of the work velocity normal to the shear plane [43].

$$\gamma = \frac{U_{Primary}}{U_{Work} \sin \Phi} \quad \text{----------} \quad 3\text{-}10$$

$$\epsilon = \frac{\gamma}{\sqrt{3}} = \frac{cos\alpha}{\sqrt{3} Sin\Phi \cos(\Phi - \alpha)} = \frac{cos\alpha \times t}{\sqrt{3} \cos^2(\Phi - \alpha) \times f} \quad \text{----------} \quad 3\text{-}11$$

Total strain (Є) is approximately (0.5 to 0.75) (t/f). In metal cutting, low friction coefficients and chip equivalent strains are 0.25 to 0.5 and 1 to 3 respectively. For high friction coefficients and strains the range is from 0.5 to 1 and up to 5. High strain hardening rates experimentally lead to high chip thickness ratio. It is difficult to vary strain hardening without varying friction coefficient [43]. The measure of strain hardening is done by the ratio of increase in equivalent stress (σ_{max} - σ_o) to the maximum equivalent stress (σ_{max}) caused by machining. Thicker chips are the sign of increased strain hardening and friction coefficient has similar influence on chip thickness ratio.

The shear stress (k) on the shear plane is expected to be that of the fully work hardened material. Strain hardening increases the cutting force, reduces shear angle with a thicker chip flowing harder over the rake face. Shearing angle is inversely proportional to shear force [22]. The main factors affecting the chip flow are the rake angle, the friction between tool and the chip and the strain hardening of the work material. Metal cutting means considerable plastic deformation at the shear plane, responsible for strain hardening of the chip and the workpiece cut surface. For a given depth of cut (d), the resultant force (R) and cutting force (Fc) and the thrust force (F_t) are given by equations below

$$R = \frac{Kfd}{Sin\Phi \cos(\Phi + \lambda - \alpha)} \quad \text{----------} \quad 3\text{-}12$$

$$F_c = \frac{kfdcos(\lambda - \alpha)}{Sin\Phi \cos(\Phi + \lambda - \alpha)} \quad \text{----------} \quad 3\text{-}13$$

$$F_t = \frac{kfdsin(\lambda - \alpha)}{Sin\Phi \cos(\Phi + \lambda - \alpha)} \quad \text{----------} \quad 3\text{-}14$$

$$kfd = (F_c cos\Phi - F_t sin\Phi)sin\Phi \quad \text{----------} \quad 3\text{-}15$$

For a typical work hardened material such as iron, aluminium and cooper, the contact pressure is not uniform along the primary shear plane (OA), varies from a lower value of zero at point O to maximum value at point A as shown in Figure 13.

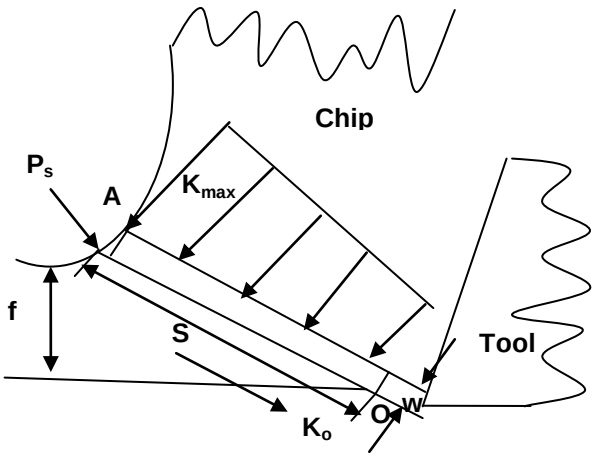

Figure 13: Contact pressure during machining

If w and s are the width and length of the shear zone, strain hardening results in maximum stress (K_{max}) at exit and minimum stress (K_o). As the material work hardens, angle ($\Phi+\lambda-\alpha$) decreases [43]. For a given contact pressure (P_s), the difference in stress (ΔK) due to strain hardening is given by

$$\Delta k = k_{\max} - k_o \quad \text{----------} \quad 3\text{-}16$$

$$Tan(\emptyset + \lambda - \alpha) = \frac{P_s}{k_{\max}} - \frac{1}{2}\frac{s}{w}\frac{\Delta k}{k_{\max}} \quad \text{----------} \quad 3\text{-}17$$

Moment (M) about point 'O' is expressed as

$$M = \frac{1}{3} + \frac{1}{6}\frac{\frac{P_s}{k_{max}}}{Tan(\emptyset + \lambda - \alpha)} \quad \text{----------} \quad 3\text{-}18$$

From section 3.2.1, merchant circle is further extended to the specific wok in metal cutting. Specific work is defined as the work done per unit machined volume (F_c/kfd). Specific work is a dimensionless quantity. Accordingly, the specific work is the total of work done in the primary deformation zone and frictional work between the rake face and the chip. The specific primary shear work (U_p), is the product of shear force (kfd/sinΦ) and velocity.

$$\frac{U_p}{kfd} = \frac{cos\alpha}{Sin\Phi \cos(\Phi - \alpha)} \quad \text{----------} \quad 3\text{-}19$$

Heat (q) generated during machining and its distribution - chip and workpiece is shown in Figure 14.

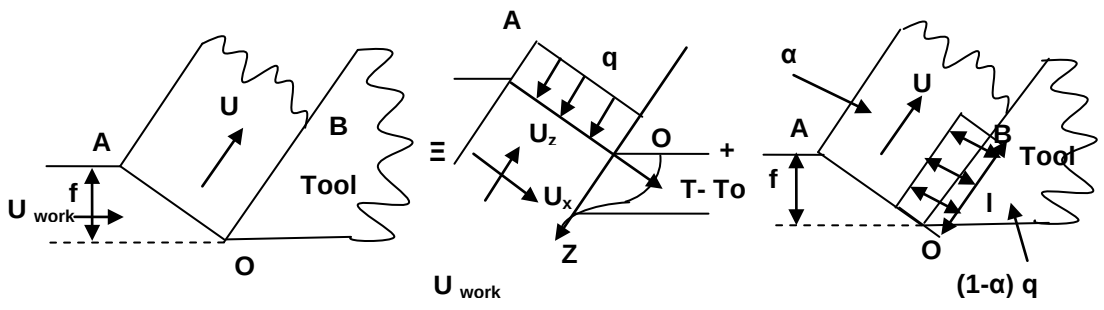

Figure 14: Heat generation and distribution during machining

Based on the assumption, the total primary shear work is converted into heat and the heat transferred to chip. The mean temperature (ΔT) rise in the chip is given by

$$\Delta T = \frac{k}{\rho c}\frac{cos\alpha}{sin\Phi \cos(\Phi - \alpha)} \quad \text{----------} \quad 3\text{-}20$$

Where, ρc is the heat capacity of the chip.

3.2.5 Surface integrity

Surface integrity is defined as the set of properties of an engineering surface that affect the performance of the component in service. The set of properties include surface finish, texture and profile; fatigue, corrosion and wear resistance; adhesion and diffusion properties and also in service properties such as frictional resistance, strain resistance, thermal emissivity, surface tension, optical properties etc. [41].

Surface integrity plays an important role in the performance, reliability and longevity of a machined component when subjected to stress and temperature, in service [51]. Surface integrity involves study and control of two factors, surface roughness and surface metallurgy. The surface metallurgy entails investigation of the possible alteration in the surface layers after machining such as plastic deformation and residual stress distribution which are mainly generated in the final stages of machining. Workpiece microstructure has significant effect on the surface quality of the machined surface. The grain size and its orientation influence surface roughness. Finer grains are always desirable [22]. The surface integrity produced by different machining operations can significantly affect machinability. According to the work done by Bhattacharyya et al. on cast iron machining using ceramic cutting inserts, almost similar to ADI machining, the surface texture improves with an increase in cutting speeds and depends on contact between the tool and workpiece.

At high cutting speed, sufficient heat is generated in the shear zone leading to thermal softening of the workpiece which increases the tool/workpiece contact resulting in reduced friction at the tool/workpiece interface. Hence, better surface finish exists on the machined surface at higher cutting speeds. At lower cutting speeds, there is an intermittent contact between the tool and the workpiece leading to trapping of hard abrasive particles at the tool/workpiece interface, which at a later stage rub against the fresh machined surface [28].

Surface alterations such as plastic deformation, microcracking, phase transformations, microhardness tears and laps related to built-up edge formation, residual stress distribution provide detail description of measuring methods available for surface integrity [41]. Microcracking is a common surface defects while machining brittle materials where as for ductile materials the high temperature and pressure during machining causes healing of these cracks. Material removal process causes structural changes to the workpiece surface in the form of plastic deformation due to the action of cutting forces and friction of tool flank [33]. Built-up edge on the tool is the primary cause of poor surface finish on the machined surface especially for a ductile material.

3.2.6 Cutting fluid

The main functions of a cutting fluid are cooling at high cutting speeds and lubrication at low cutting speeds. Generally, cutting fluid should have high specific heat (absorb more heat quickly for small temperature rise) as the temperature rise during machining is rapid and maximum temperature is located at the middle of tool-chip interface. In drilling, the process of chip removal is through the flutes of the drill and cutting fluid is important to flush the chips out of the cutting area by forcing the chips to flow through the flutes rather than clogging which is disastrous. The other functions of the cutting fluid is to lubricate the drill, workpiece and the chip to reduce the friction between each other, to improve the surface finish, and to absorb and dissipate the heat at the same rate as it is generated during cutting. Certain drills are specially designed to carry cutting fluid through them by means of oil holes drilled or oil tube passing through them.

There should be a suitable mechanism for disposal of the chip as it carries the major portion of the heat generated during the cutting process [23]. During a metal cutting operation most of the mechanical energy consumed is transformed to heat. Therefore, heat generation and dissipation from the cutting zone plays an important role in machining [22]. Excessive heat generation is always a disadvantageous factor which should be avoided as it affects the tool life and limits the cutting speed. The three principle zones of heat during a machining operation are the shear zone, the rake face and the clearance side of the cutting edge. Small shear angles and rake angles can raise the heat flow into the workpiece. The various ways to measure the cutting temperatures is using infra-red photography, thermo couple technique, calorimetric technique, radiation pyrometers and temperature sensitive chemicals [23].

3.3 Introduction to drilling

Drilling is defined as a machining operation to make cylindrical holes in a workpiece using a cutting tool which removes metal in the form of chips. The cutting action is due to the tool (drill) revolving at n, rpm and penetration into a fixed workpiece at a penetration rate of f, mm/min. Drilling is the oldest and common form of machining operation existing in manufacturing engineering. The technology transfer is best described by the transformation from carpenters using a hand rotated brace drill to the machinist using a latest electric motor driven, variable speed and multi functional, electronic controlled drilling machine. Broaching, reaming, boring and counter boring all come under the same category of drilling. The cutting action involved in drilling is described as a rotating cutting edge combined with a linear feed into the workpiece.

In drilling, the machinability of ADI is poor because of the transformation of retained austenite into martensite which is hard and difficult to machine. The increase in number of graphite particles decreases the amount of retained austenite. Kita has emphasised that in case of drilling the enhancement of machinability makes the distance between the graphite particles shorter and decreases the retained austenite [18]. The process of chip formation and removal becomes complicated as the hole depth increases. There is a well defined criterion to determine the hole depth; for a hole diameter less than 30mm, the depth of drilling is 5 to 6 times the diameter of the hole. For hole diameter greater than 30mm, the depth of the drill is 2.5 times the diameter. A pre-drilled hole can cause deflection of the drill when tools with asymmetrical geometry are used [22].

3.3.1 Nomenclature of a drill

A drill is defined as a rotary end cutting tool having one or multiple cutting edges and one or more helical or straight flutes cut around, to carry and dispose chips and coolants. The typical design parameters in a drill which effect the cutting forces and drilled hole qualities are flutes, point angle, chisel edge angle, length of chisel edge, cutting lip length and helix angle (rake angle) [52]. The drill consists of two cutting edges, main cutting edge or lips and minor cutting edge or chisel edge. Lips do the major part of the cutting action efficiently and the chisel edge plays a less part in cutting and often seen as inefficient leading to geometrical errors in drilling and high thrust loads [19, 22].

In a drill, the rake angle varies along the cutting edge from positive at the outer radius to negative near the center of rotation and the cutting speed varies from a maximum at the outer radius to zero at the center [23]. The margin of the drill which is located at the extreme diameter is subjected to the greatest cutting velocity. During hole formation, the lips are subjected to flank wear similar to that experienced in a single point cutting tool [19]. Lip clearance is the relief given to the cutting edge to penetrate into the workpiece. Lip clearance should be maintained at an optimum angle between 7-10^{o}. Higher lip clearance reduces the strength of the cutting edge and lower clearance reduces the space between the tool and surface to be cut and resulting in spinning and rubbing action rather than penetrating and cutting the material. The flutes of the drill are the twisted helical or straight groves running around the drill and are carriers of swarf out of the drill area and supply of coolant into the drill area. The drill flutes are designed to give the cutting edges straightness at the point of the drill [53].

Most of the short hole drills have two chip channels or flutes and two cutting edges. The chips are evacuated via flutes. Modern drill tools have holes or flutes cut through them for supply of the cutting fluid. The undeformed chip thickness increases with the increasing point angle and feed per edge. With an increase in feed rate, the feed angle increases and clearance decreases. The clearance angle should increase from the periphery towards the centre in order to avoid abrasion between the tool and the walls of the hole.

Lip angle is defined as the angle between the cutting edge (lip) and the axis of the drill. The point angle is the sum of the lip angles made by each edge with the drill axis in a double edged drill. The optimum lip angle is 59^{o}, higher lip angle makes the cutting edge concave and lower lip angle makes the cutting edge convex. The condition for a drill to avoid either of the cutting edges doing more work than the other, resulting in over sized holes, imbalanced forces, is that the lip angles should be equal on either side of the drill axis.

Cutting lip length should also be equal to avoid the point of the drill not to be in the same line as the axis of the drill which leads to heavy wear and breakage of the drill. The cutting edges should be rounded in order to strengthen the edges and to avoid breaking on applying heavy thrusts. While drilling harder materials using a straight cutting edge, the chips produced, resemble a corkscrew and are long.

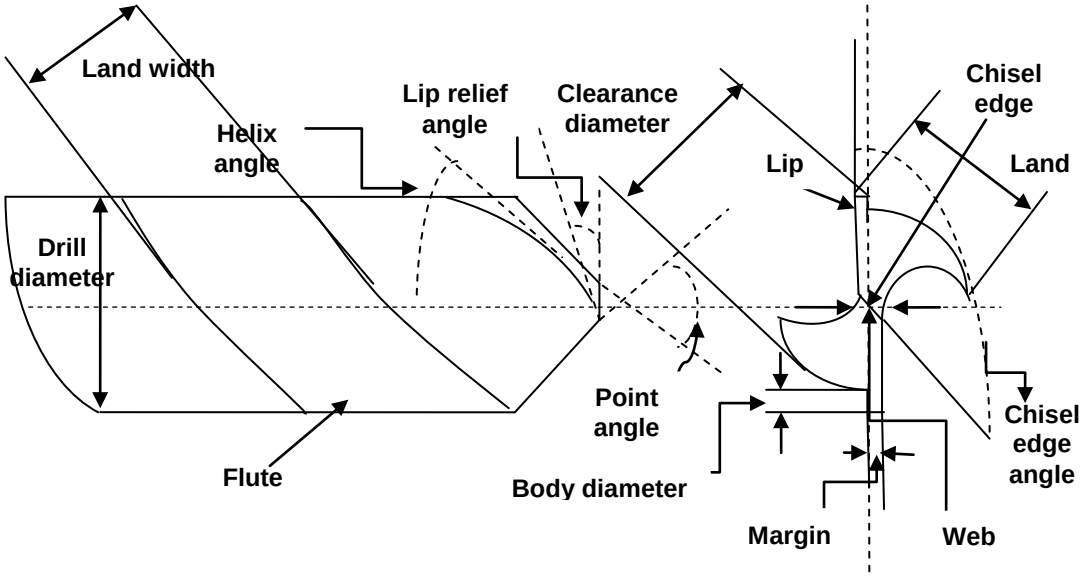

Figure 15: Twist drill terminology [54]

Concave cutting edges results in moving the chip particles towards the center and inside particles towards the periphery which results in broken chip and vice versa follows in case of convex edges, also resulting in broken chips but not as quick as in a concave cutting edge [53]. The point of the drill is grounded to form a minor cutting edge called the chisel edge. Chisel edge is an important part of the drill as any improper changes in its dimensions changes the results to a large effect. The point angle is defined as the angle between the two main cutting edges (lips) of the drill. The optimum point angle of 118^o is good for drilling. Higher point angle creates centering problems, lower point angle results in weakening the point and also increase of power to drive the drill due to the increase in length of cutting edges. The point controls the formation of the chip, the size and shape of the chip, the flow of chips along the flutes, increases the strength of the cutting lip, reduces the rate of cutting lip wear, reduces the drilling thrust required, controls the drilled hole size, quality and straightness, reduces heat generated and permits greater variation of speeds and feeds for more efficient drilling.

For drilling harder and tough materials, flat angle point drills (135^o-140^o) are used. Long angle point drills (60^o-90^o) are used to drill soft materials such as plastics. The double angled point is used for hard cast iron and abrasive materials as it acts as a chip breaker, increases the cutting lip length and lip corner angle, and reduces the wear of the corner. Split point drills (135^o) are used in deep hole drilling as in the case of drilling oil holes in crankshaft [53]. The portion joining the two lands of a drill is known as web. The length of the chisel edge is known as web thickness.

The web is generally subjected to thinning for efficiency in drilling and reduces the pressure required to penetrate into the material. The angle between the tangent of the main cutting edge and the axis of the drill is known as rake angle or helix angle. Higher rakes weaken the cutting edge and require high power to cut but increase the helix angle which necessary for rapid removal of the chips. The lower rake angle increases the lip relief angle and the amount of rake to be used depends upon the toughness of the material to be drilled.

The clearances given to the drill for easy centering and cutting action are the body diameter clearance and margin [53]. The shank and socket of the drill should be cleaned and free from chips and any swarf to avoid production of lateral stress and wobbling while machining [55]. The factors affecting the economy of drill usage are proper application of drill, proper condition of drilling machine, proper holding of drill, proper condition of material being drilled, proper reconditioning program and proper care of drills. The reconditioning program consists of removal of the worn part and web thinning [53].

3.4 Introduction to milling

Milling is a metal removal process where a rotating tool having multiple cutting edges removes material by moving along the axis of the workpiece. The speciality with a milling cutter is that it produces multiple chips in one revolution of the tool depending on the number of cutting edges on the tool. Popular milling approach include: face milling and end milling. Face milling is employed in the second part of this research on ADI machinability involving study on phase transformations.

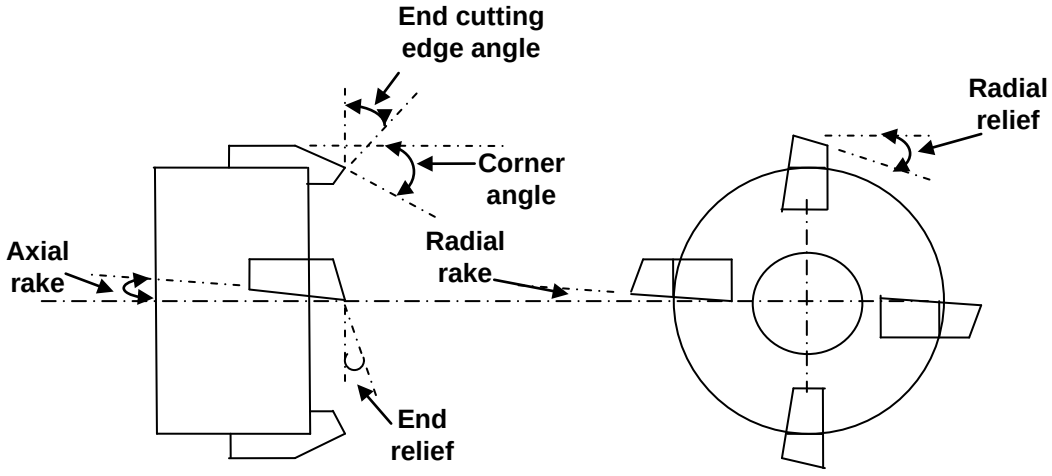

Figure 16: Terminology for a face milling cutter

Climb milling is avoided in the experiments as ADI being a cast material has a hard and abrasive top layer which, result in excessive tool wear and also tool failure. In face milling, the cutter is mounted on the machine spindle in such a way that the axis of rotation of the cutter is perpendicular to the workpiece surface [38]. The cutting action is due to combination of rotation of the tool at n, rpm and movement of the workpiece along a straight path at a linear speed (υ), m/min.

Milling is an intermittent cutting process where each tooth produces a chip of variable thickness. In case of face milling, the undeformed chip thickness increases to the maximum value at the center of the travel and decreases towards the end of the tooth engagement. The initial and final size of the undeformed chip depends on the width of the workpiece with respect to the cutter diameter and symmetry of the cutter axis with the workpiece [37]. In milling, the torque and power are not limited by the workpiece strength rather it is the strength of the cutter spindle which is important. For a milling cutter of diameter (D), the torque (T) varies by D^3. If the length of the spindle is proportional to the diameter (D), cutting forces and machine power varies by D^2 [43].

3.5 Earlier studies on ADI machinability

Machining ADI using machining techniques applicable to an as-cast or ductile cast iron, leads to failures in machining. A proper study into the material properties and metal matrix of ADI leads to conclusions of successfully machining ADI. There has been no comprehensive reasoning on machining ADI suggesting that it can only exhibit good machinability properties prior to the heat treatment. Machining post heat treatment leads to SIT caused by strain and thermal energy generated in the shear zone due to the cutting action. This phenomenon is a consequence of rapid change in microstructure from acicular ferrite to a completely difficult to machine microstructure, martensite. The fear of the material getting work hardened has made the machinist cut the material to complex, deep and long cuts prior to austempering. Some of the solution applicable to the above problem is to machine the material despite the formation of hard martensite by using an ultra hard cutting tool at low cutting speeds and increases feed rates or using different machining approaches or completely remove martensite from the material by heat treatment process or prevent the commencement of martensite formation.

Recently, a new variant of ADI is introduced known as Machinable Austempered Ductile Iron (MADI), which has high strength compared to ductile iron and better fatigue properties compared to ADI (grade 900). MADI has unique properties exhibiting lower machining forces than ductile iron and ADI [20]. Alloying elements also play a significant role in machinability of ADI. Carbide forming elements such as Molybdenum and Manganese significantly reduce tool life as the carbides hinder the machining process. Prior research in machining recommends using molybdenum as low as possible in the presence of higher levels of manganese [16].

When ADI is subjected to machining operations like drilling, turning and milling, the high normal loads acting at the periphery of the cut lead to localised phase transformations at the surface layer, in advance of the tool. The ductile and tough austenite undergoes a phase transformation forming martensite which relatively hard, brittle and difficult to cut. When machining ADI, the graphite particles determine the cutting forces and surface roughness and the microstructure determines the tool life. When machining ADI with high ferrite content, the machinability is reduced as the ferrite sticks to the clearance face of the tool and causes poor surface finish [9].

Variation in the microstructure of workpiece material due to cutting action has considerable effect on the machinability of the material and tool wear. Machinability definitions are connected to the factors effecting machining like the metallurgy, chemistry, heat treatments, additives, inclusions, surface skin, cutting edge, tool holding, operation and machining conditions [23, 56]. Macro inclusions are undesirable as they are abrasive and hard and lead to tool damage. Micro inclusions like FeO and MnO are also undesirable as they cause deflections. Silicates are desirable inclusion as they are softer at high temperatures and form a protective layer and retard tool wear. Sulphur is added to improve machinability as it increases the shear angle and chip curl, reduces the chip thickness and acts as a lubricant on the interface. Lead is also a good additive [57].

3.6 Machining mathematics

The cutting speed (V_c) for a drill of diameter (d) and rotational speed (n) rpm is given by equation 3-21.

$$V_c = \frac{d \times \pi \times n}{1000}, m/min \quad \text{----------} \quad 3\text{-}21$$

The feed speed or penetration rate V_f (mm/min) is the feed of the tool in relation to the workpiece. For a feed rate (f) in mm/rev, which expresses the movement of the tool in one revolution, V_f is given by equation 3-22.

$$V_f = f \times n \quad \text{----------} \quad 3\text{-}22$$

The cutting width or radial cutting depth (a_p) is the part of the workpiece surface which the tool covers and is measured as for turning on half the diameter

$$a_p = \frac{D\text{-}d}{2} \quad \text{----------} \quad 3\text{-}23$$

As the drilling tool is equipped with several cutting edges, the feed per edge in mm/edge, where z = number of cutting edges.

$$f_z = \frac{f}{z} \quad \text{----------} \quad 3\text{-}24$$

The chip area (A) in mm^2 which is the area of the material removed in one cut

$$A = a_p \times f_z \quad \text{----------} \quad 3\text{-}25$$

The material removal rate (V) is the volume of the material removed per unit of time.

$$V = A \times V_c \times 1000 \ mm^3/min \quad \text{----------} \quad 3\text{-}26$$

By stipulating the length feed (L + h) in mm and dividing it by the feed speed, the effective drilling time (T in min)

$$T = \frac{L + h}{V_f} \quad \text{----------} \quad 3\text{-}27$$

$$h = \frac{D}{d} \times \cot\left(\frac{\Phi}{2}\right) \quad \text{----------} \quad 3\text{-}28$$

The specific cutting force (K_c) N/mm^2 is required to calculate feed force, torque and power. The specific cutting force is defined as the tangential force required cutting a chip with a cross-section of one square millimetre or the effective cutting force divided by the theoretical area. The cutting force is divided into three components, radial, axial and tangential cutting force. The axial cutting force gives rise to feed force or drilling pressure, where K_r is the entering angle.

$$F_p = 0.5 \times K_c \times a_p \times f_z \times \sin(K_r) \quad \text{----------} \quad 3\text{-}29$$

The total tangential force (F_t) is the main cutting force gives rise to torque (M) in N-m

$$F_t = K_c \times a_p \times f_z \quad \text{----------} \quad 3\text{-}30$$

The torque (M) is the sum of the moment on each cutting edge which is the product of the tangential cutting force and the radius to the centre point of the chip area (r_A), hole diameter (D) and the core diameter (d) in mm. For a feed in mm/rev, the product shown in equation 3-31 is divided by 1000 for torque to be expressed in N-m.

$$M = F_c \times r_A \quad \text{----------} \quad 3\text{-}31$$

$$r_A = \frac{d}{2} + \frac{a_p}{2} = \frac{D + d}{4} \quad \text{----------} \quad 3\text{-}32$$

The drilling power (P_c) in Kilowatt is the product of drill turning moment and its angular speed (ω) with uniform movement. The angular speed is 2π times the spindle speed, since the power is expressed in kilowatt (1000 N-m/sec) and if the moment is given in N-m, the result should be divided by 1000. If the spindle speed is given in rpm, the result should be additionally divided by 60 to convert into seconds.

The final formula for power is given by equation 3-33.

$$P_c = K_c \times f \times V_c(D^2\text{-}d^2)/D\times 240000 \text{ KW} \quad \text{----------} \quad 3\text{-}33$$

The primary shear stress (k) in machining is given by equation 3-34.

$$k = \frac{(F_c Cos\emptyset - F_t Sin\emptyset)Sin\emptyset}{fd} \quad \text{----------} \quad 3\text{-}34$$

For milling, the cutting speed (V) is the peripheral speed of the cutter and is expressed as in equation 3-35.

$$V = \pi D N \quad \text{----------} \quad 3\text{-}35$$

where D is the cutter diameter and N is the rotational speed of the cutter. The linear speed or feed rate (υ), mm/min of the workpiece is given by equation 3-36.

$$\upsilon = f n N \quad \text{----------} \quad 3\text{-}36$$

where n is the number of teeth on the cutter periphery and f is feed per tooth in mm/tooth. The cutting time (t) is given by equation 3-37.

$$t = \frac{l + l_c}{\upsilon} \quad \text{----------} \quad 3\text{-}37$$

where l is the length of the workpiece and l_C is the initial contact length between the cutter and the workpiece. Metal Removal Rate (MMR) is given by equation 3-38.

$$MMR = \frac{lwd}{t} \quad \text{----------} \quad 3\text{-}38$$

where w is the width of the cut and d is the depth of cut.

4 Introduction to phase transformations

The following study on phase transformation deals with the changes that occur within a given system. e.g. ADI microstructural phase change from austenite to martensite due to machining. The microstructural phase is defined as a portion of the system having homogenous composition and material properties and which is physically different from other phases in the system. The term phase composition refers to the relative amounts of each phase present in the system [58].

4.1 Gibbs free energy equation

The constitution of an alloy is described in three ways: the phases, the weight fraction of each phase and the composition of each phase. An alloy is said to be in equilibrium, if it is stable and resist further change at constant temperature and pressure (thermal equilibrium). For a given alloy composition, equilibrium is always expressed at constant temperature and pressure. At constant temperature and pressure, the relative stability of the system during transformations is determined by Gibbs free energy equation 4-1.

$$G = H - TS \qquad \text{----------} \qquad 4\text{-}1$$

G - Free energy, H - Enthalpy, T - Absolute Temperature and S - Entropy of the system. Enthalpy of the system is given by equation 4-2.

$$H = E + PV \qquad \text{----------} \qquad 4\text{-}2$$

E - Internal (kinetic + potential) energy of the system, P - Pressure and V - Volume (refer glossary for definitions)

During a transformation, heat evolved or absorbed is determined by the change in internal energy of the system, which depends on the volume changes. At constant pressure, the heat evolved or absorbed is determined by change in enthalpy. As in solids, the atoms are closely packed and the internal energy of the system is almost equal to the enthalpy of the system (the term ‘PV’ is too small to be considered).

According to classical laws of thermodynamics, a closed system (fixed mass and composition) is stable at constant temperature and pressure, if the change in Gibb's free energy is minimum (dG=0). Therefore, the criterion for a phase transformation to occur is given by equation 4-3:

$$\Delta G = G_2 - G_1 \leq 0 \qquad \text{----------} \qquad 4\text{-}3$$

G_1 and G_2 are the initial and final states of the system respectively. In a multi-phase system, the fundamental process that controls the rate at which many transformations occur is the diffusion of atoms. Diffusion occurs in a system in order to lower its Gibbs free energy (G).

4.2 Role of physical metallurgy

Principles of physical metallurgy play an important role in phase transformations of metals: movement of dislocations, determining the Gibbs free energy level, chemical potential and equilibrium of a system. Microstructure plays an important role in determining the material properties through the phase composition and its content. The other factors affecting material properties are the internal microstructural behaviour such as the dislocation movement and transformation reactions. The basic composition of steel consists of components - Carbon(C) and Iron (Fe) distributed in the matrix at definite proportions which give rise to phases such as austenite, ferrite, martensite and cementite (high carbon materials). The microstructure in an alloy exists in different forms such as a single solid solution, two separated pure components, two separated solid solutions and a chemical compound together with a solid solution [59]. An engineering product undergoes various manufacturing operations in order to be transformed into a finished product having desired material properties.

Diffusion in a system is defined as the movement of atoms from one system to another or within the system in order to attain stability. The driving force for diffusion is also expressed in terms of chemical potential gradient. Diffusion ceases when the chemical potential of the atoms is constant in all directions and the system is in equilibrium. The two common mechanisms through which diffusion takes place in solids are through substitutional diffusion and interstitial diffusion [58, 60].

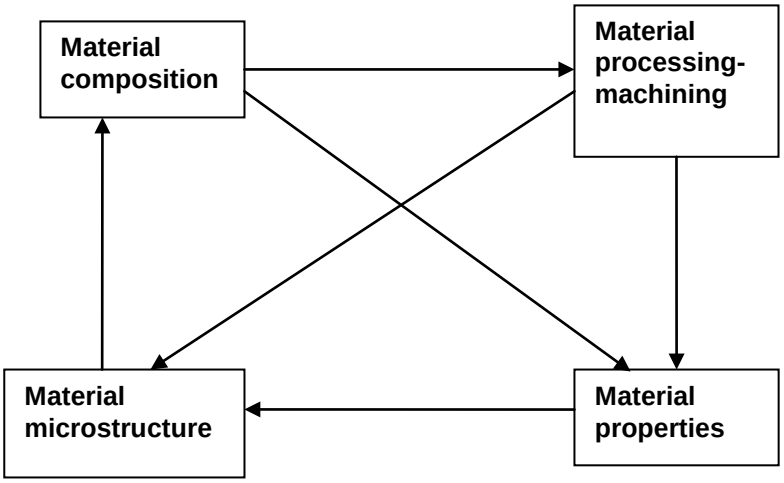

Figure 17: Microstructure, composition, properties and machining dependency diagram [38, 40]

Apart from the design, the material properties are a requisite for proper functioning of the product without a failure. Manufacturing operation such as machining does influence the material properties as there is a high magnitude of heat and forces in the cutting zone. Strain hardening and thermal softening are typical cases of changing material properties during machining. Figure 17 explains the relationship between composition, machining, properties and microstructure of the material. In ADI, wear resistance and fatigue strength is enhanced due to the microstructural phase transformation of retained austenite converted to a harder phase - martensite. Hence, it becomes relevant to understand the complex relationship between microstructure and material properties during machining. An engineering component is made to pass through commercial heat treatment techniques in order to improve the material properties which aim to refine the size, shape and spacing of the phase particles in the microstructure. The nature and spacing of the phase particles affects the amount of force required to push the dislocations through the particle gaps. Properties such as yield strength and toughness depend on microstructure. The microstructure and properties do not remain constant throughout a product life cycle but may evolve (change) during the service life of the component [59].

4.2.1 Iron-Carbon equilibrium diagram

Phase diagram provides a fundamental understanding of the stability of a phase as a function of temperature and composition. An alloy is defined as a mixture of two or more metallic or non-metallic elements [59].

The different elements in an alloy are known as components of an alloy or system. e.g. Brass is an alloy made up of components - Copper and Zinc. Steel is an alloy of ferrous and carbon mixed in proportion as per the material property requirement. The general rule in case of steel: higher the carbon (%), the greater the hardness level. The components of a system are defined in term of Weight (%) or Atomic (%). If an alloy consists of components A and B, the weight (%) of A is given by equation 4-4.

$$W_{\mathrm{A}} = \frac{\text{Weight of component A}}{\sum \text{Weight of all components(A\&B)}} \times 100 \quad \text{----------} \quad 4\text{-}4$$

The independent state variables controlling the equilibrium in a phase diagram are temperature, pressure and composition. In materials (solid state), pressure has almost no influence on the equilibrium condition For a binary system (two components) such as Iron-Carbon alloys, the equilibrium diagram is shown in Figure 18 [61]. Hence, equilibrium state is described using a graph, by plotting temperature (T) against the phase composition (X).

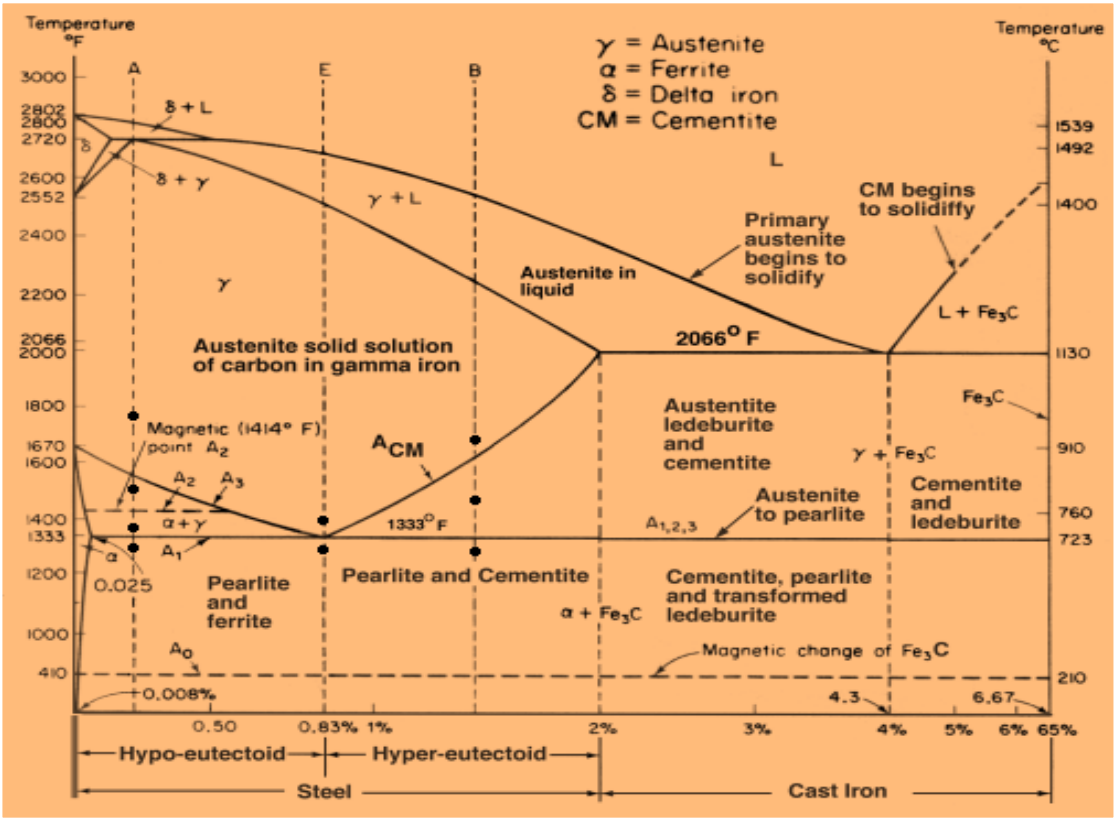

Figure 18: Iron-Carbon equilibrium diagram [62]

4.3 Study of martensite formation

Generally, martensite formation is a diffusionless transformation mechanism. If Steel/Iron-Carbon alloy is subjected to high rate of cooling/ heating, there is insufficient time for eutectoidal diffusion controlled transformation to occur and the austenite present transforms into martensite (or) martensite with few amount of retained austenite. Martensite production is a regimented transformation in which from start to completion, individual atomic movements are less than one inter atomic spacing. The martensitic phase is in the shape of a lens and spans an entire grain diameter. The elevated speed at which martensite forms, makes it difficult to study experimentally the process of nucleation and grain growth. The first plate of martensite forms at the Martensite start temperature (M_s). This temperature is associated with a certain driving force for the diffusionless transformation. In low Carbon Steels, M_s is approximately 500^o C and decreases with an increase in carbon (%).The driving force (Gibb's free energy, $\Delta G^{\gamma \rightarrow M}$) responsible for phase transformation varies with fixed carbon (%) and temperature, as shown in Figure 19. Martensite finish temperature (M_f) signifies the temperature below which further cooling does not increase the amount of martensite. M_f does not correspond to 100% martensite transformation and some retained austenite is left even below M_f. The retention of austenite in such cases may be due to the high elastic stress between the last martensite plates to form which tend to suppress further growth or thickening of existing plates [58]. The driving force for nucleation of martensite at M_s temperature is given by equation 4-5.

$$\Delta G^{\gamma \rightarrow M} = \Delta H^{\gamma \rightarrow M} \frac{(T_o - M_s)}{T_o} \quad \text{----------} \quad 4\text{-}5$$

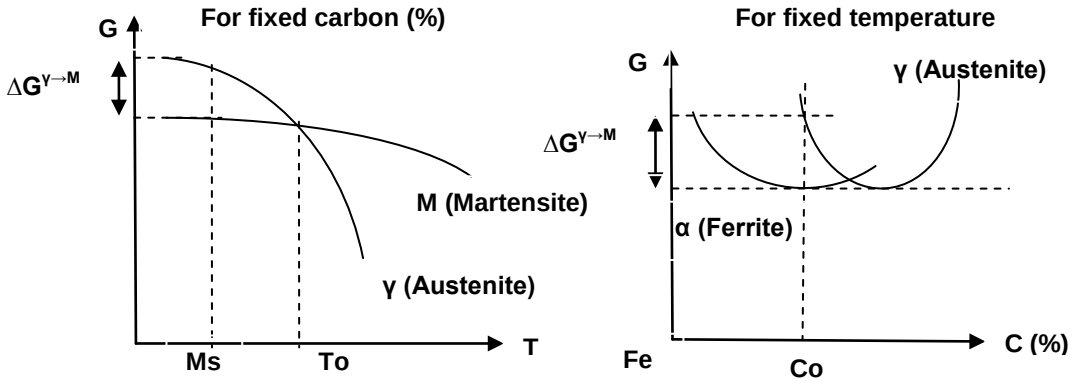

Figure 19: Driving force for phase transformation for fixed carbon (%) and temperature [58]

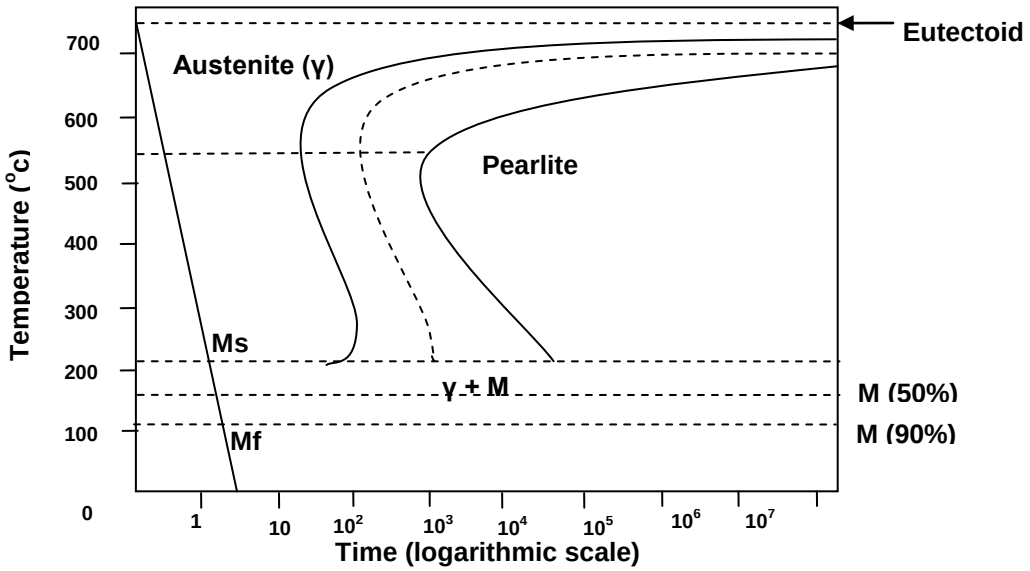

Figure 20: TTT diagram for martensite formation [59]

The TTT diagram shown in Figure 20 conveys information on martensite formation upon fast cooling from austenite temperature with respect to temperature and time.

4.3.1 Martensite crystallography

The irrational nature of the growth planes of high carbon martensite has been subject of discussion. If martensite is able to grow at speeds approaching the speed of sound, then there is some sort of highly mobile dislocation plane (habit plane) or interface required. The growth or habit plane of martensite is defined a plane common to both austenite and martensite where distortions or angular separations in all directions of the plane remain unchanged during the transformation. The martensite habit plane is macroscopically undistorted as shown in Figure 21. The absence of plastic deformation in the form of discontinuity at the surface shows that the shape strain does not cause any significant rotation of the habit plane. If the habit plane has been rotated then it becomes necessary for plastic deformation to occur in order to maintain coherence between the martensite and parent austenite.

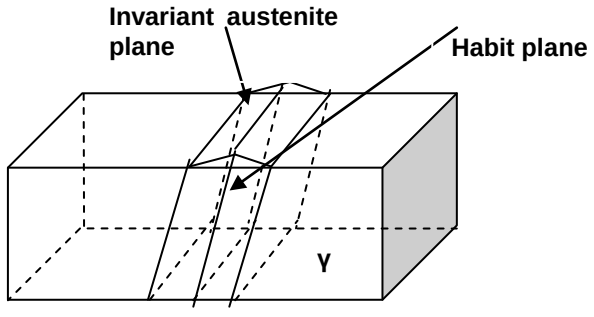

Figure 21: Martensite crystallography [58]

As austenite to martensite transformation (γ→M) is associated with approximately 4% expansion, the dilatation should take place normal to the habit plane. The macroscopic shape change in the formation of a martensite plate is a twining shear occurring parallel to the habit plane and a simple uniaxial tensile dilatation perpendicular to habit plane (invariant plane strain) [58].

The Bain model of the Face Center Cubic (FCC) to Body Center Tetragonal (BCT) transformation

Bain's model explains the austenite to martensite phase transformation reaction as shown in Figure 22. Bain successfully demonstrated the transformation of FCC austenite to BCT martensite with minimum atomic movement and strain in the parent lattice. The transformation to a BCT crystal lattice is explained by expanding the cell 20% along the z-axis and contracting the cell 12% along the x and y-axis. Bain deformation involves the absolute minimum atomic movement in generating BCT from the FCC lattice. In some cases, Bain transformation does not fulfil the requirements of brining about a transformation with an undistorted plane [58]. The high hardness and strength of martensite is due to the effectiveness of the interstitial carbon atoms hindering the dislocation movement and relatively few slip systems for a BCT structure.

4.3.2 Effect of alloying elements

The proportion of carbon and other elements in ADI play an important role in both inhibiting and promoting the SIT. The percentage of carbon and other alloying elements recommended for ADI is given in Table 3 [63]. Alloying elements such as Chromium (Cr), Nickel (Ni), Tungsten (W) and Sulphur (S) aid martensite formation at relatively low cooling rates. When Carbon (%) is less than 0.25, a very high cooling rate is required to produce 100% martensite.

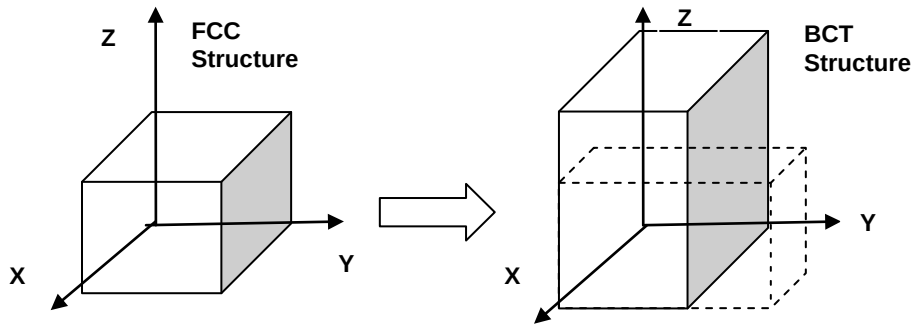

Figure 22: Bain model of FCC→BCT transformation [58]

Table 3 Effects of carbon, silicon and the major alloying elements [6]

Element	Required (%)	Effect on SIT in ADI
Carbon	3.6 to 3.8	Beyond 4% increases the hardness largely and makes it prone to SIT
Silicon	2.4 to 2.8	Silicon promotes graphite nodule formation and decreases the solubility of carbon in austenite. Using silicon outside the recommended range leads to increase in percentage of retained austenite and the casting easily undergoes SIT because of retained unstable austenite
Manganese	Less than 0.3	Increases hardenability and forms carbides at cell boundaries during solidification process of the castings and retards austempering reaction. These segregations increase the amount of retained and unstable austenite at the cell boundaries along with the carbides
Copper	Up to 0.8	Copper increase ductility in ADI and softens the material and the effect of copper on SIT is negligible
Nickel	Up to 2	Nickel increase the hardenability and high proportion promote SIT
Molybdenum	Not more than 0.2	Molybdenum is the potential hardening agent and is a good promoter of SIT. It affects the material properties by segregating at the cell boundaries and forming carbides. Hence, it should only be used in heavier castings for prevention of pearlite formation

4.3.3 Effect of plastic deformation

Plastic deformation plays an important in atomic movements and has a major influence on dislocations in the crystal lattice. Dislocation strain energy assisted transformation reduces the nucleation barrier to form coherent nuclei of martensite. ΔG_d represents the dislocation interaction energy which reduces the nucleation energy barrier.

$$\Delta G_d = 2\mu S\pi acb \qquad \text{----------} \qquad 4\text{-}6$$

S - Shear strain of the nucleus, b - Burger's vector of dislocations, a - Diameter of the martensite nucleus, c - Thickness of the martensite nuclei and μ - Shear modulus of austenite. Grain size, external stress and phenomenon of stabilization are some additional factors which affect the growth of martensite. Plastic deformation aids both nucleation and growth of martensite, excess deformation suppresses the transformation. Dislocation density increases as a result of increase in the number of potential nuclei due to deformation. During machining, Strain Induced Transformation (SIT) occurs when the surface of the component is subjected to a high rate of plastic deformation.

The other reason is the inertia of the unstable retained austenite to transforms into martensite under the action of high cutting forces in order to attain stability. The probability of SIT is high in ADI having higher percentage of retained austenite. In most of the cases, austenite in ADI is a thermodynamically stable phase even at subzero temperatures and is often misunderstood with the retained and unstable austenite as in a heat treated steel [63].

In some cases, enriched austenite is advantageous as it transforms to harder martensite phase due to SIT, enhancing its wear resistance and prevents crack propagation in a fatigue cycle. SIT depends on factors such as grain size, stress intensity, annealing temperature, alloying elements and heat treatment history [64]. SIT is characterised by localized increase in volume and high compressive forces in the transformed area. Higher austempering temperature produces ADI with high ductility, yield strength, good fatigue, impact strength and the probability of SIT increases in ADI having high ductility and fatigue strength.

4.3.4 Effect of residual stress

A residual stress is defined as static triaxial stress that is in equilibrium without the action of external forces and moments. The occurrence of residual stress is always related to plastic deformation of microscopic area of a multiphase material by external and internal forces. Residual stress in machining is associated with incompatibilities of strain in the cutting zone [65]. As explained earlier, machining is a non-linear deformation process where a material undergoes both elastic and plastic deformations. For purely elastic deformation, the stress involved is released once the cutting forces are removed. As machining also involves plastic deformation, there is a certain amount of stress induced into the workpiece even after the removal of cutting forces. This type of stress is termed as residual stress which determines the fatigue and wears characteristics of the material. Residual stress can be tensile or compressive in nature. A tensile residual stress is disadvantageous and should be avoided where as a compressive residual stress is beneficial as it inhibits the fatigue crack growth. During machining, compressive residual stress are induced in the material.

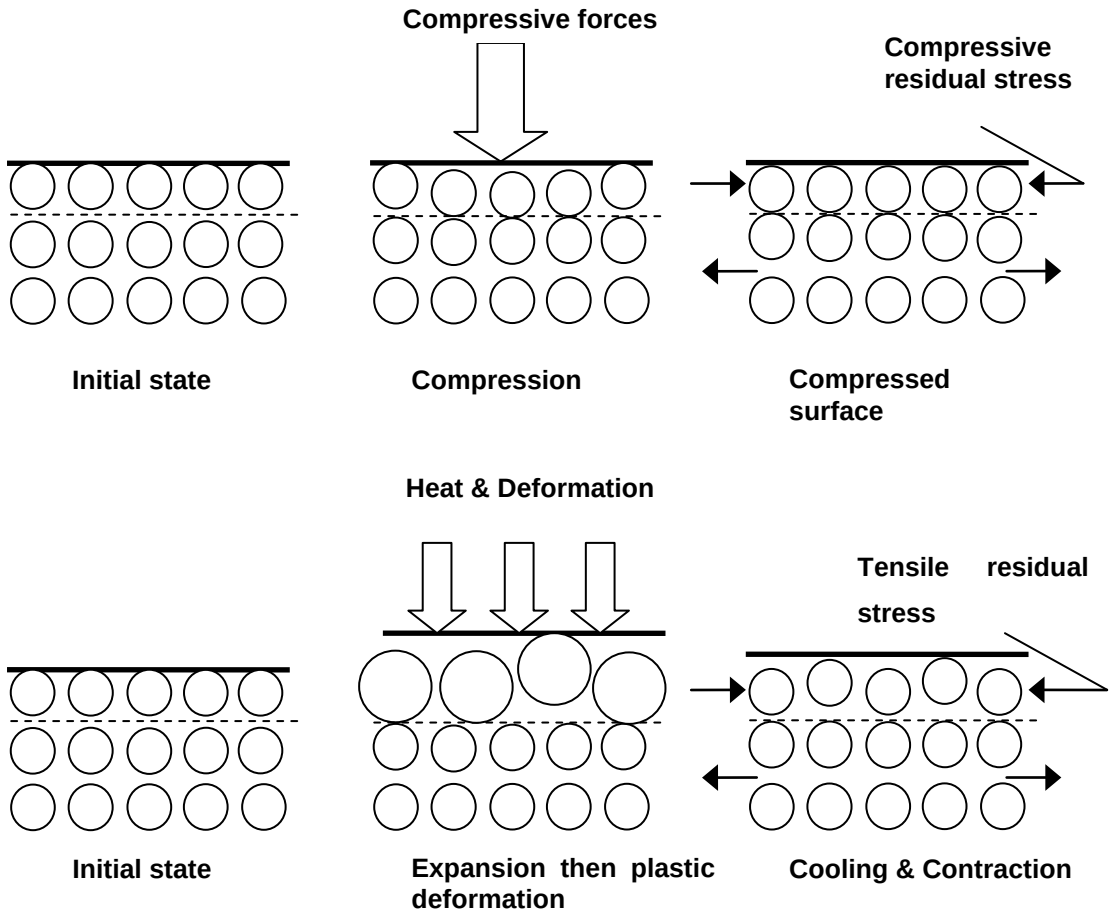

Figure 23: Effect of the mechanical deformation upon residual stress [66]

The reason for formation of residual stress is due to thermal deformation, mechanical deformation; and combination of thermal and plastic deformation [66]. Figure 23 explains the formation of compressive and tensile residual stress. In case of thermal deformation, on heating, there is a change in volume of surface layer of the component. When accompanied by a phase change the surface layers tend to contract, where the bulk of material resists contraction and causes the surface layer to go into tension (tensile residual stress) and vice-versa for a compressive residual stress.

Shot peening is the best example for residual stress induced through mechanical deformation. Stress from machining represent the third case of residual stress induced by combination of thermal and plastic deformation. The heat generated during machining expands the surface layer and further, the plastic flow involved relieves this expansion. On removal of heat, the surface layer contracts resulting in tensile residual stress at the workpiece surface. It is proven fact that growth of martensite depends on dislocation nucleation.

Application of external stress (residual) assists nucleation of dislocations by lowering the nucleation barrier. Bain strain is the minimum amount of strain required for the commencement of phase transformation from austenite to martensite. External stress also aid martensite formation by local elastic strain contributing to the bain strain. The martensite start (M_s) temperature is limited to an upper value (M_d) as a result of plastic deformation. On compression, the M_s is suppressed to a low temperature. On increasing the pressure, the austenite phase with smaller atomic volume and closely packed atomic structure stabilises, thereby lowering the driving force (ΔG_v) for martensite transformation.

4.3.5 Role of grain size

Grain size is an important factor affecting the final martensite plate size. The size of the grain is directly proportional to the final martensite plate size. The number of martensite nuclei in a given volume is independent of the grain size. Another important feature of the grain size is its influence on residual stress. In large sized grain materials, the dilatational strain associated with the transformation causes large residual stress to be built up between adjacent grains and this can even lead to grain boundary rupture and increase dislocation density in the martensite [58, 67].

4.3.6 Effect of thermal energy

Temperature in the cutting zone effects the phase transformation by acting as a catalyst to SIT. High cutting temperature leads to increase in atomic energy levels, making it easier for the dislocations to cross the grain boundaries and leads to decrease in dislocation density. The temperature in the cutting zone affects the machinability of the workpiece as the shear plane aligns against each other in a parallel pattern due to the excitation of the atoms on absorption of energy. Thermal softening of the workpiece by the tool is also due to the effect of temperature in the cutting zone. Temperature affects the cutting tool material and the forces effect the power and strength needed to perform the process [22]. ADI is a heat treated material with an adequate amount of compressive residual stress due to austempering. The high temperature in the cutting zone acts as a residual stress reliever and speeds up the SIT reaction by transforming the unstable retained austenite to a stable martensite phase. The same reason is attributed for the material to work harden at a fast rate as the dislocation density is decreased. These factors support the idea of machining ADI under dry conditions.

During a metal cutting operation most of the mechanical energy consumed is transformed to heat. Therefore, heat generation and dissipation from the cutting zone plays an important role in machining [22]. The three principle zones of heat during a machining operation are the shear zone, the rake face and the clearance side of the cutting edge. Small shear angles and rake angles can raise the heat flow into the workpiece. The various ways to measure the cutting temperatures is using infra-red photography, thermo couple technique, calorimetric technique, radiation pyrometers and temperature sensitive chemicals [23]. Excessive heat generation is always a disadvantageous factor, which should be avoided as it affects the tool life and limits the cutting speed. The chip takes the largest portion of the heat generated and increases with cutting speed and feed within the tested range of conditions [23].

When a hardened material is machined, the surface of the workpiece is modified due to rapid thermal working resulting in phase transformations. The machined surface is quite different in microstructure compared to the bulk of the material [41]. According to the research on high speed machining of Titanium by Hua and Shivpuri, the effect of thermal energy in the deformation zone on phase transformation is explained using a mathematical model [44]. Assuming the heat generated in the deformation zone is due to plastic deformation and friction between the tool and workpiece. The heat generated and transfer is given by equation 4-7.

$$k_1 T + r - \rho c \Delta T = 0 \qquad \text{----------} \qquad \text{4-7}$$

Where T and ΔT represent temperature and temperature variation, $k_1 T$ represen the heat transfer rate, r is the mechanical energy (plastic deformation energy) and $\rho c \Delta T$ is the internal energy rate.

The plastic deformation energy (r) is given by equation 4-8

$$r = \kappa \sigma \varepsilon \qquad \text{----------} \qquad \text{4-8}$$

Where σ and ε represent the shear stress and strain in the deformation zone, κ is the fraction of mechanical energy transformed into heat and is assumed to be 0.9.

The rest of the energy (1-κ) is responsible for changes in dislocation density, grain boundaries and phases [44]. The energy balance equation in the deformation zone is written as shown in equation 4-9.

$$\int_V k_1 T \delta T \, dV + \int_V \rho c \Delta T \delta T \, dV - \int_V \kappa \sigma \epsilon T_1 \delta T \, dV - \int_{S_q} q_n \delta T \, dS = 0 \quad - \qquad 4\text{-}9$$

Where q_n represents heat flux across boundary surface S_q and $q_n = k_q T_n$;

δT - arbitrary perturbation.

5 Experimental design

The main objective of the experiments is to study and understand ADI phase transformational behaviour during machining and assess the machinability of grades 900, 1050, 1200 and 1400. A complete overview of the microstructural phase reactions is achieved by conducting drilling and milling trials across a range of machining parameters. This chapter describes the experiments undertaken as part of ADI machinability studies. The description includes the machining centre operational data, the cutting tools used, machining parameters - speed, feed rate and depth of cut; use of coolant and overall, aim of the experiments. This chapter also describes operational conditions of the various instruments used to obtain and analyse the data obtained from bulk hardness test, cutting force analysis, surface texture analysis, microhardness and tensile tests. The experimental design for the research work is divided into two sections

- Characterisation of ADI
- Study of phase transformations

Grades 900, 1050, 1200 and 1400 used in this research were supplied post heat treatment and categorised accordingly. The supplied ADI blocks were of two different sizes – 300x150x50 mm^3 and 300x150x25 mm^3. Smaller blocks of size 300x150x25 mm^3 were used to conduct experiments on characterisation of ADI and large blocks of size 300x150x50 mm^3 were used for drilling and milling trials.

The role of statistics in experimental design, data collection, data analysis and data interpretation has been exemplary. Statistical method such as factorial design was used in the experimental design. Factorial design gives a control approach and variability to the experimentation by allowing unique set of combinations for each of the experiments using the available set of independent variables – cutting speed, feed rate, coolant [68]. In order to ensure accuracy and efficient data capturing, the error (%) is reduced by proper calibration of instruments and repetitive experimentation. Computer modelling and simulations of tensile test were done using ANSYS, in order to generate theoretical support based on Finite Element Methods (FEM).

Implementation of standards during experimentation was given a top priority in order to abide by international standards such as ATSM A897-03 for material properties of ADI and E8-96 for preparation of tensile specimens. The results obtained from experiments are tabulated and discussed using graphs and tables in chapter 6.

5.1 Characterisation of ADI

Characterisation of ADI was done in order to understand the fundamentals of physical metallurgical behaviour in terms of the microstructural constituents. The characterisation includes determining chemical composition of ADI, material properties of grades 900, 1050, 1200 and 1400; quantify the microstructural phases - retained austenite, ferrite and martensite. The characterisation of ADI was done using small size blocks - 300x150x25 mm^3. Grades are designated according to their minimum tensile strength such as grade 900 denotes the minimum tensile strength of the material is 900 MPa. Accordingly, lower grades such as 900 and 1050 of ADI have low tensile strength and high ductility. Higher grades such 1200 and 1400 have higher tensile strength, hardness and good wear resistance. The difference in heat treatment range for different grades is explained in section 2.4. Lower austempering temperature and time leads to higher grades of ADI and vice-versa.

5.1.1 Chemical composition of ADI

The chemical composition of ADI used in this research, in terms of weight (%) is given in Table 4. The chemical composition of ADI was determined using spectrometry. ADI being a heat treated ductile cast iron, higher amount of carbon - 3.6% denote the presence of nodular graphite (carbon allotrope) dispersed in the ADI matrix. As expected, ADI contains nodulisers agents, Magnesium (Mg) - 0.5%; carbide stabilisers such as Copper (Cu) - 0.68% and Manganese (Mn) - 2.7%. The significance of each alloying element used in ADI production has been explained in section 2.3.

5.1.2 Bulk hardness testing

Bulk hardness is defined as resistance of the specimen against plastic deformation on application of load. It is hardness of the material at macroscopic level.

Table 4: Chemical composition of ADI

Element	C	Mn	Si	S	P	Ni	Cr	Mo	Cu	Mg
Wt%	3.6	2.7	2.5	.04	.01	.27	.02	.01	.68	0.5

Some of the common bulk hardness tests available are Rockwell hardness, Vickers hardness and Brinell hardness test. In this research, Rockwell hardness test is used to evaluate the hardness of the material before machining. Bulk hardness test are conducted on grades 900, 1050, 1200 and 1400 using a Rockwell hardness testing machine with a load of 150 Kg for 20 sec. The samples for the test are cut to size - 25x25x25 mm^3 from the small size blocks of grades 900, 1050, 1200 and 1400; and checked for porosity and defects.

ADI blocks with good quality and no defect were grinded and polished in order to have a flat surface. The specimens for the test were cut using spark erosion or Electro Discharge Machining (EDM) in order to minimise the effect of heat on ADI microstructure. Coolant/lubricant was used in grinding and polishing the top and bottom surfaces of the specimen. Flat surface enables the specimen base to remain aligned to the instrument base without any tilt during application of load and also helps the indentation process on the top surface. The result from the test is explained in section 6.1

5.1.3 Metallographic analysis

Metallography is an important tool in physical metallurgy as it is used to study microstructural phases which constitute a metal or an alloy and their composition by generating the microstructural images of the phases. As the present research on ADI machining involves studying the phase transformation, use of metallographic techniques becomes a major part of the research. Metallography consists of preparation of specimen, grinding, polishing, etching and analysing the microstructure at microscopic level. There were two type of metallographic techniques used in this research - conventional and heat tinted (colour) metallography. The advantage of heat tinted metallography over conventional is the colour coded representation of each microstructural phase.

Conventional metallography

Conventional metallography consists of specimen preparation - cutting to size and shape, hot mounting of the specimen using Bakelite resin, polishing of the specimen to one micron using SiC grit papers and polishing cloth plus diamond paste. The next step of metallography consists of etching the polished specimen surface using Nital.

Nital is a chemical solution, which contains 2-4% alcoholic (ethanol) solution of nitric acid used at room temperature. The sample was dipped in Nital and held for 10-15 seconds, after which the etched surface was washed with water in order to stop the etching reaction. Over etching of the surface is not permitted as it darkens the surface. The purpose of etching is to reveal the microstructure as the etchant reacts with the surface of the specimen (oxidation process) and the marks the grain boundaries. The result from the conventional metallography is explained in detail in section 6.2.

Heat tinted metallography or colour metallography

With the advances in technology and storage in digital format, it has become easier to generate and reproduce a colour microstructure wherever necessary [69]. Colour metallography becomes advantageous in examining a metal or an alloy having multi-grain microstructure as the different phases or grains which constitute the system are shown in contrasting colours. Colour metallography has been of limited use due to the difficulty and cost involved in capturing and reproducing the microstructural image. The use of colour metallography on a multi-phase ADI microstructure has become popular after the publication of works done by eminent researcher on ADI, Kovacs [70]. A sample heat tinted microstructure of grade 900 is shown in Figure 24. The colour code representing the microstructural phase is given in Table 5.

Table 5: Colour code representing each microstructural phase

Microstructure	Retained austenite	Austenite	Ferrite needles	Graphite nodules	Martensite
Colour	Light blue	Purple	Black	Beige	Dark Blue

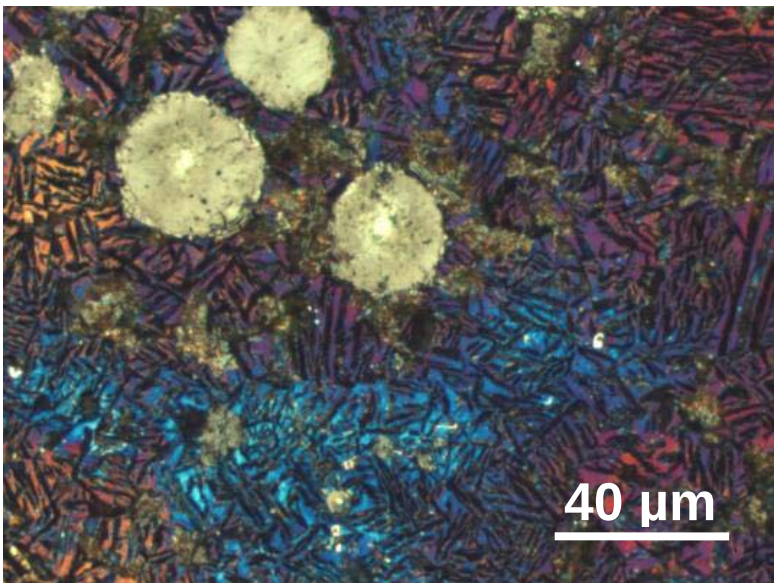

Figure 24: Heat tinted grade 900 microstructure - Kovacs method

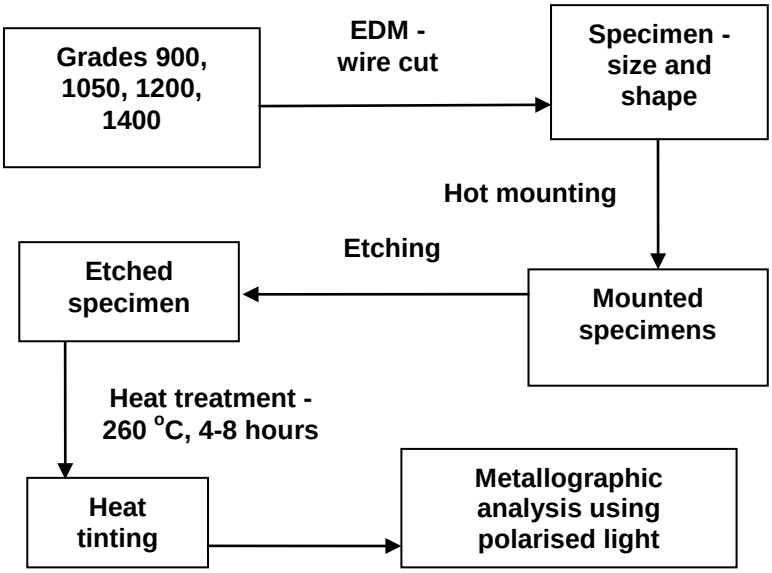

Figure 25: Heat tinting procedure

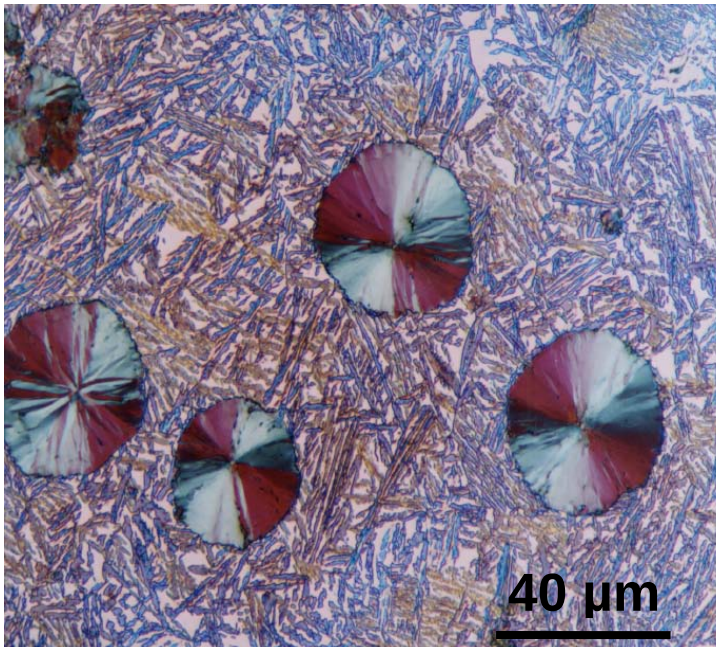

Figure 26: Heat tinted ADI - Vander Voort method [69]

The procedure for heat tinting using Kovacs method is shown in Figure 25. Some recent works on application of colour metallography on ADI by George Vander Voort, suggest application of etchant - Beraha's CdS reagent, heat tint and viewing under a polarised light. In case of Vander Voort method, the colour codes representing the microstructural phase are ausferrite-blue and brown and retained austenite-white [69]. Heat tinted microstructure of ADI using Vander Voort method is shown in Figure 26.

On comparison, heat-tinting has been done using Kovacs method due to its easy and inexpensive process. The latest techniques in etching have introduced new etchants used to generate colour microstructure such as Beraha-Martensite (B-M) etchant. The chemical composition of B-M etchant is 2 grams of potassium meta bi sulphate ($K_2S_2O_5$) and 2 grams of ammonium acid fluoride ($NH_4F.HF$), 100 millilitres of BWI: five volume parts of distilled water, one volume part of Hydrochloric acid. On using B-M etchant, the ferrite needles are tinted light brown and rarely blue. Martensite needles are tinted blue and dark brown, austenite remains colourless [71]. The result from heat tinting on grades 900, 1050, 1200 and 1400 is shown and explained in section 6.3.

5.2 Machinability analysis

Machinability of grades 900, 1050, 1200 and 1400 is evaluated in terms of cutting force analysis, surface texture analysis, microhardness analysis, chip morphology and metallographic analysis. The samples used for machinability analysis were cut to size from the available ADI blocks using spark erosion (EDM) in order to minimise the effect of heat on ADI microstructure. The process diagram for the machinability analysis is shown in Figure 27.

5.2.1 Dynamometer consistency tests

The objective of conducting dynamometer consistency test was to check the calibration of the instrument as it has been inoperative for a long duration. The dynamometers available and under check were the Kistler dynamometer, turning type-9257B and drilling type-9272. Dynamometer works on the principle of peizo-electricity and has quartz crystals which act as sensors and are placed at four corners of the dynamometer. Quartz crystals are known for their peizo-electric property i.e. they generate a charge on application of force under static/dynamic conditions.

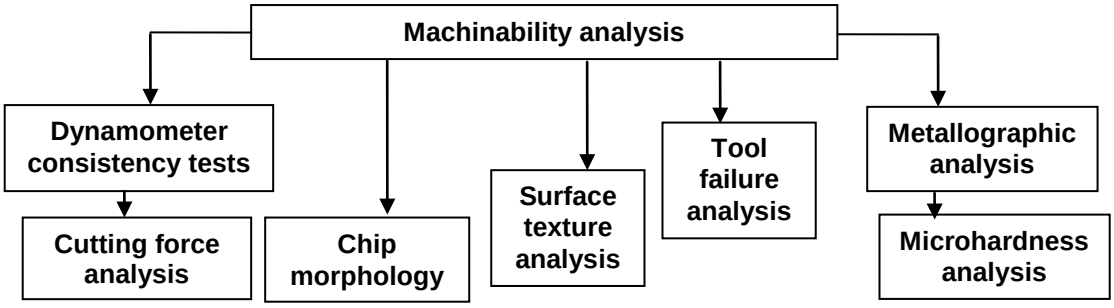

Figure 27: Process diagram for machinability evaluation

Figure 28: Kistler Dynamometer 9257B and 9272

Figure 28 shows the dynamometer-9257B and 9272. The dynamometer correspondingly measures forces along the X, Y and Z-directions using the charge generated by the quartz crystals. The charge generated was received by the Kistler charge amplifier type 5070, which converts the charge into analogue signal and gives the output (force) correspondingly using the data acquisition card installed in the computer. The data generated was subjected to refinement and displayed in the tabular and graphical format using customised Kistler DynoWare software. The dynamometer was also calibrated using known weights under static conditions. For example, place a weight of 1kg on the dynamometer and check for corresponding 9.8N force from the instrument.

Dynamometer consistency test consist of conducting drilling trials using cutting parameters - velocity (V_c = 35m/min, n = 1250 rpm), drilling depth (a_p = 10mm), feed (f = 0.1 mm/rev) and without coolant; as mentioned in the manual for dynamometer type-9272. The drilling trials were conducted using a High Speed Steel (HSS) drill of 10 mm diameter and the material being mild steel 1020 (USt37-2). Cutting forces were measured using dynamometer type-9272, type 9257B and validated with the data given in the manual 9272). On comparison of the results and due to superior results, dynamometer type-9257B is selected and used to measure the cutting force for all the machining trials in this research. The working process of measuring cutting force using dynamometer is shown in Figure 29. The results from these tests are explained in detail in section 6.4.1.

5.2.2 Cutting force analysis

The effect of cutting parameters - feed rate, speed, depth of cut and coolant, on cutting force and moment for grades 900, 1050, 1200 and 1400 was determined using cutting force analysis.

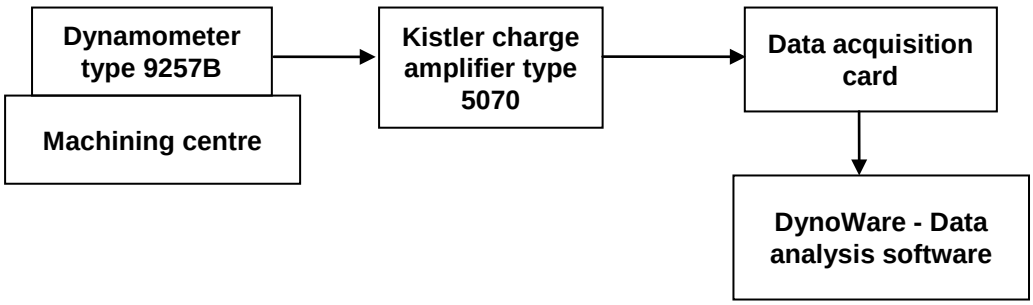

Figure 29: Working procedure for cutting force measurements

The working procedure for the cutting force analysis is shown in Figure 29. The experimental design consists of conducting drilling trials on grade 900, 1050, 1200, and 1400 at constant depth of cut, 25mm; speed, 697 rpm; feed rates, 0.1 mm/rev and using coolant. Kistler cutting force dynamometer of type 9257B was used to measure the cutting forces, F_X, F_Y and F_Z; and moment, M_Z. As the cutting forces, F_X and F_Y are balancing forces; these forces were not taken into consideration in evaluating the machinability of the material. The cutting tool used for the trials was an insert type drill made and supplied by ISCAR; diameter-13.7 mm, tool holder: DSM 130-039-16A-3D and insert: IDK137. Drilling trials were carried out on a machining centre, Leadwell MCV-0. Images shown in Figure 30 represent the experimental set up. The specimen for the analysis were cut to half size-150x150x50 mm^3 from the large blocks of ADI using spark erosion (EDM) machine and holes were drilled in order to fix it firmly on top of the dynamometer as seen in Figure 30.

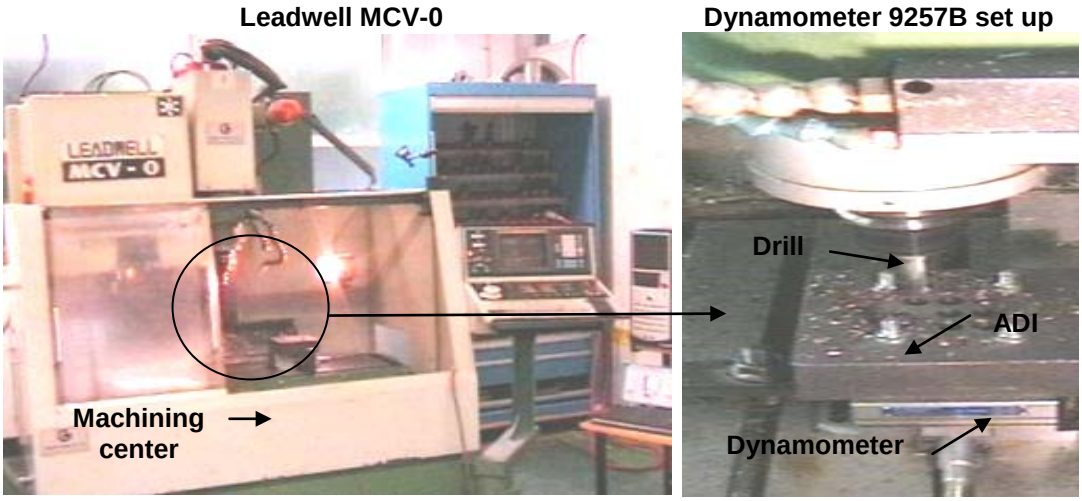

Figure 30: Machining centre and dynamometer set up

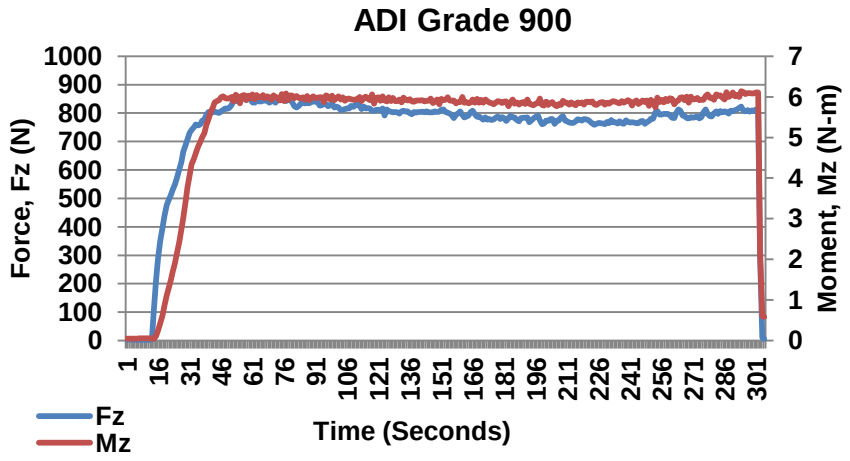

Figure 31: Comparison of thrust force, F_Z (N) and moment, M_Z (N-m)

ADI microstructure being heat sensitive utmost care was taken in selecting the cutting parameters and priority was given to operate within the safe limits of the tool, machining centre and material. A sample graph comparing the thrust force, F_Z and moment, M_Z for grade 900 is shown in Figure 31. The drilling trials performed as part of the cutting force analysis were the initial machining trials conducted using the dynamometer. Hence, these trials provide information on the behaviour of the cutting tool, workpiece, cutting parameters, dynoware software settings and failure information (if any), which can be taken into consideration while designing machining trials in the later part of the research. The results from the drilling trials are explained in detail in section 6.4.2.

Effect of feed on cutting force

The effect of feed on the cutting force and moment for grades 1200 and 1400 was determined by cutting force analysis using the combination of cutting parameters tabulated in Table 6.

Table 6: Cutting parameters - effect of feed rate on cutting force

Grade	Speed, rpm	Depth of Cut, mm	Coolant	Feed, mm/rev
1200 & 1400	1150	25	Off	0.200
1200 & 1400	1150	25	Off	0.225
1200 & 1400	1150	25	Off	0.250
1200 & 1400	1150	25	Off	0.275
1200 & 1400	1150	25	Off	0.300
1200 & 1400	1150	25	Off	0.325
1200 & 1400	1150	25	Off	0.350

The experimental design consists of conducting drilling trials on grade 1200 and 1400 at constant depth of cut, 25mm; constant speed, 45m/min; no coolant and variable feed rates from 0.2 to 0.35 mm/rev (as shown in Table 6). Kistler cutting force dynamometer of type 9257B was used to measure the cutting forces, F_X, F_Y and F_Z; and moment, Mz. As the cutting forces, F_X and F_Y are balancing forces; these forces were not taken into consideration in evaluating the machinability of the material. The cutting tool used for the trials was an insert type drill made and supplied by ISCAR; diameter-13.7 mm, tool holder, DSM 130-039-16A-3D and insert IDK137. The objective of the analysis was to understand the relationship between the feed and machinability.

5.2.3 Surface texture analysis

A completely new experimental design was adopted for surface texture analysis, microhardness analysis, metallographic analysis and chip morphology. The experimental work was designed using three independent variables: cutting speed, feed and use of coolant, on grades 900, 1050, 1200 and 1400. The cutting parameters selected include cutting speeds (rpm) of 697 and 929; feed rates (mm/rev) of 0.1 and 0.2. The hole depth, 25 mm remains constant for all trials. The cutting tool used for the trials was an insert type drill made and supplied by ISCAR (tool holder, DSM 130-039-16A-3D and insert IDK137). A new insert (TiAlN coated) was selected for each grade of ADI. The drilling trials were carried out on a machining centre, Leadwell MCV-0. The specimen for the analysis was cut to half size - 300x75x25 mm^3 from the small size blocks using spark erosion (EDM). Figure 32 shows cutting of ADI samples using EDM.

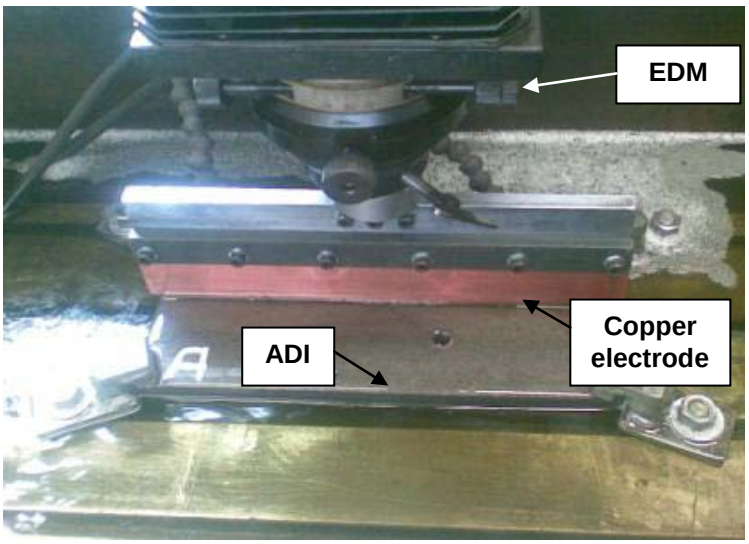

Figure 32: Cutting ADI blocks using EDM

Table 7: Factorial design of experiments for grade 900, 1050, 1200 and 1400

Grade 900	Cutting speed (rpm)	Feed rate (mm/rev)	Coolant	Grade 1050	Cutting speed (rpm)	Feed rate (mm/rev)	Coolant
A1	697	0.1	on	E1	697	0.1	on
A3	697	0.2	on	E3	697	0.2	on
A7	929	0.1	on	E7	929	0.1	on
A9	929	0.2	on	E9	929	0.2	on
C1	697	0.1	off	G1	697	0.1	off
C3	697	0.2	off	G3	697	0.2	off
C7	929	0.1	off	G7	929	0.1	off
C9	929	0.2	off	G9	929	0.2	off
Grade 1200	**Cutting speed (rpm)**	**Feed rate (mm/rev)**	**Coolant**	**Grade 1400**	**Cutting speed (rpm)**	**Feed rate (mm/rev)**	**Coolant**
J1	697	0.1	on	N1	697	0.1	on
J3	697	0.2	on	N3	697	0.2	on
J7	929	0.1	on	N7	929	0.1	on
J9	929	0.2	on	N9	929	0.2	on
L1	697	0.1	off	Q1	697	0.1	off
L3	697	0.2	off	Q3	697	0.2	off
L7	929	0.1	off	Q7	929	0.1	off
L9	929	0.2	off	Q9	929	0.2	off

Factorial design ensures delivery of quality data using fewest possible experimental runs and optimises the experimental process by efficient utilisations of the available resources [72].

The cutting parameters selected for drilling represent machining under extreme and moderate conditions. The permutations and combinations of the drilling trials using the three independent variables (factors): speed, feed and coolant and two levels for each factor; on grades 900, 1050, 1200 and 1400 is shown in Table 7. The number of combinations for each grade using the three factors and each factor having two levels is eight (2^3), given by the formula, n^m, where m is the number of factors and n is the number of levels for each factor [72]. This research employs surface texture (roughness, R_a) and microhardness (H_k) analysis in order to demonstrate the surface integrity effect on machinability. The role of surface texture in determining the machinability of a material is explained in section 3.2.5.

A normal surface on machining undergoes deviations such as roughness, waviness and form errors - flatness, roundness and cylindricity etc. As surface roughness is a dominant characteristic related to machinability, the machinability of ADI was assessed with respect to the surface roughness.

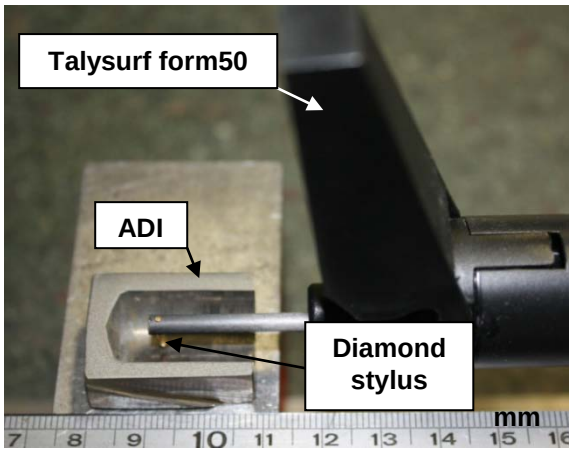

Figure 33: Cross-section of a hole cut in half using EDM

There are numerous arithmetic parameters available to evaluate roughness such as R_a - center line average, R_t - maximum peak to valley, R_z - average peak to valley etc. In this research, the center line average technique (R_a) was used to measure roughness because of the ease to use and define the limits.

The drilled holes are subjected to surface texture analysis in order to derive a relation between the hardness values and the surface texture of hole. A sample cross-section of a bisected hole is shown in Figure 33. The result from the surface texture analysis is explained in detail in section 6.4.3. Each hole was cut in half using spark erosion in order to minimise the affect of heat on the microstructure. The surface texture tests were conducted using instrument, Taylor Hobson's - Talysurf form50 and analysed using the Taylor Hobson software-µltra. Considering the range of surface roughness (R_a) values for drilling according to the manuals, the Ra value lies between 1.6 to 3.3 µm [51]. The cut-off (L_c) and data length selected for the analysis are 2.5 mm and 12.5 mm. The effect of tool retraction on the R_a values has been ignored, as it remains constant for all the holes. The instrument- Talysurf was calibrated using a standard calibration ball (radius-12.5342 mm) prior to the actual use of the instrument in surface texture analysis.

5.2.4 Microhardness analysis

The objective of the microhardness analysis was to generate microhardness profiles moving away from the hole edge and along the hole depth for all the grades. Drilling trials were conducted according to the experimental design as explained in section 5.2.3. Microhardness analysis was used to determine the machinability of grades 900, 1050, 1200 and 1400.

The drilled holes were later on subjected to microhardness analysis in order to identify the occurrence of phase transformation during drilling. As martensite is a harder phase of iron and end product of a phase transformation in ADI machining. An increase in microhardness value closer to the hole edge on comparison with bulk of material is taken as one of the criterion for occurrence of phase transformation. Knoop microhardness tests were used in this present research. Knoop microhardness test has been developed by National Bureau of Standards, USA. Knoop microhardness number is defined as the applied load divided by the unrecovered projected area of the indentation [24]. The formula shown in equation 5-1 is used to calculate Knoop microhardness (H_k).

$$H_k = \frac{P}{A_p} = \frac{P}{L^2 C} \qquad \text{----------} \qquad 5\text{-}1$$

Where P = applied load (Kg), A_p = unrecovered projected area of indentation (mm^2), L = length of the long diagonal (mm) and C = manufacturer supplied constant for each indentor. Figure 34 shows a sample Knoop indentation on grade 900. Microhardness test has been conducted on grade 900 1050, 1200 and 1400 using a Knoop indenter. The process consists of preparation of specimen, grinding, polishing, and indenting the microstructure using Knoop indentor for 20 seconds using load of 500 grams. A total of six locations were selected and at each location the hardness test were conducted three times and mean value of the three readings represents the Knoop microhardness at the location. The tests were conducted under magnification-55X. By using image measurement software and mathematical calculations, the scale for the tests is roughly one millimeter equals one micrometer.

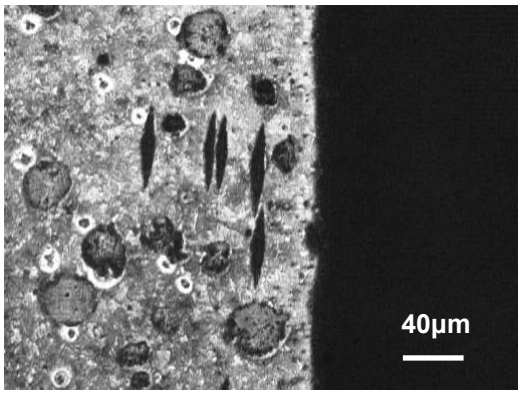

Figure 34: Knoop indentation on grade 900

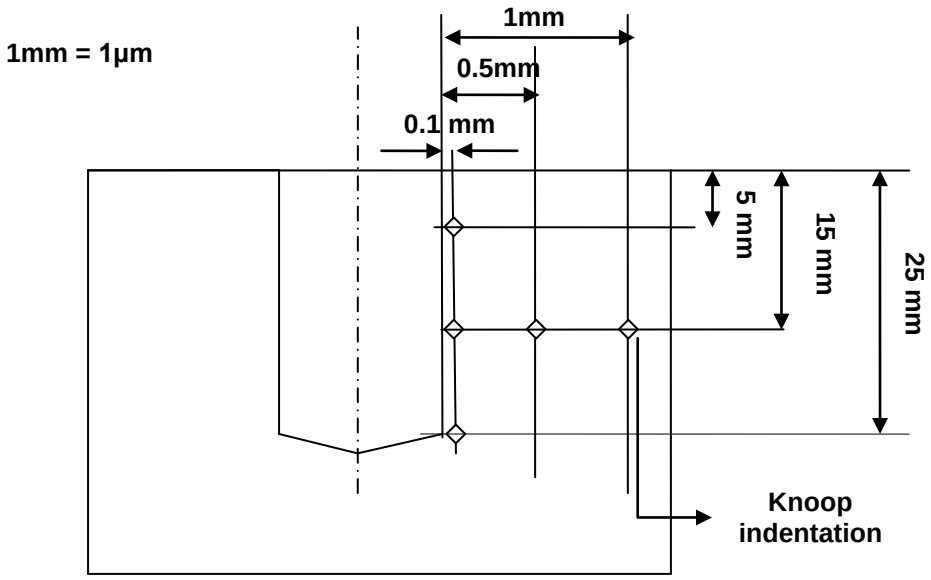

Figure 35: Indentation locations on a hole cross-section

The distance between the locations along X and Y axis are measured using the screw gauges attached to the instrument having least count of 0.01 mm. Figure 35 shows the locations of the microhardness test indentation in order obtain a hardness profile along the edge and away from the edge. In order to provide consistency and reliability in the readings, standard error (%) has been calculated and shown in the form of error bars in the graphical format as shown in Figure 36. The graph demonstrate three categories of hardness profile: microhardness of as received ADI termed as "base", microhardness along the hole depth and microhardness away from the hole edge.

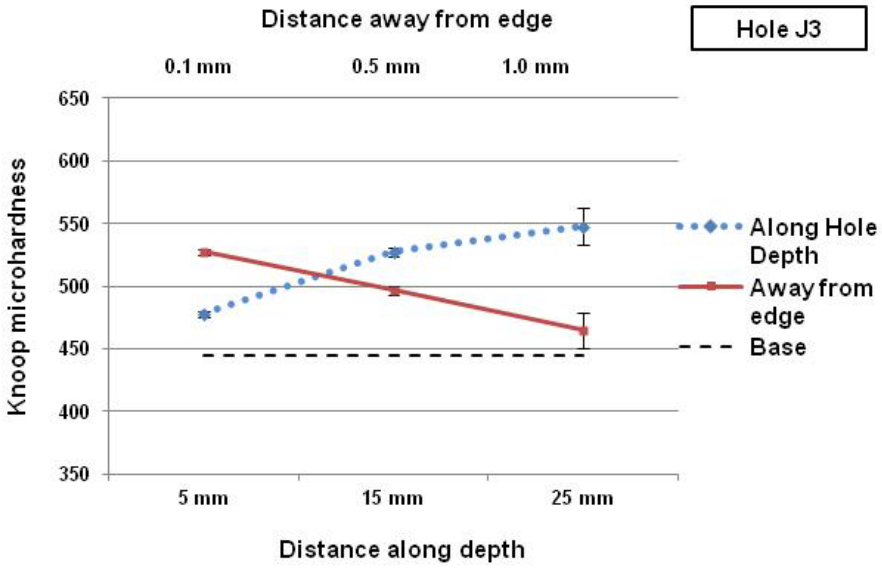

Figure 36: Microhardness along depth and away from edge for hole J3 - grade 1200

In order to introduce 'taper sectioning' in sectioning of the holes using EDM or spark erosion, a small taper was applied to all the samples while cutting. Taper sectioning is advantageous in interrogation of subsurface features such as phase transformations, plastic flow zones and localised cracking. Taper sectioning overcomes the limitations of perpendicular sectioning by modifying the magnitude of the subsurface features without undue distortion to the transversely cut surface topography [51]. Few precautions were followed while conducting microhardness test especially for a material such as ADI having graphite: avoid indentation on slippery graphite as it might give misleading results; make sure the base of the sample is parallel and grounded to the indentation surface in order to avoid tilt while indenting and which would rather result in out of focus, unequal lengths on either side of the indentation diagonals; and best to conduct test on a polished and non-etched sample as this makes indentation clearly visible rather than searching among the densely populated different phases in ADI (ferrite needles and graphite). The result from the microhardness analysis is explained in detail in section 6.4.4.

5.2.5 Chip morphology

Chip morphology is a study of chip or metal residue from machining and characterisation based on physical appearance of the chip – size and form (continuous or discontinuous) of the chip. Machinability characteristics of a material was determined using chip morphology as it gives information on the tool, workpiece material properties, use of coolant, machining dynamics, chip formation and material flow in the shear zone. It is an important tool in developing new cutting process for difficult to machine materials like ADI as it gives an in-depth information on the thermo-mechanical behaviour at tool/workpiece interface [44]. The use of chip morphology in the current thesis was warranted as it gives information on the chip formation and phase transformational reactions which take place in the shear zone, leading to work hardening.

The different types of chip as defined in the literature for ADI includes needle shaped chips e.g: sample A1 and C9, chisel edge chips e.g: sample L7, fan shaped chips e.g: sample Q1 and amorphous chips or flower shaped chips e.g: sample Q7, L9 and G7 [49, 50]. Chip morphology study consists of observing the form - shape and size of the chips generated while drilling ADI at combinations of cutting parameters given in Table 7. The experimental process consists of collecting chips after each drilling trial.

5.2.6 Metallographic analysis

Metallographic analysis was used to evaluate the machinability of grade 900, 1050, 1200 and 1400 by examining the occurrence of phase transformation during machining. The pictorial representation is advantageous in comparison of the microstructure before and after machining. For ferrous alloys such as steel and iron, formation of martensite is associated with a term 'White Layer'. White layer is an age old metallographic identification sign for martensite formation in steel and iron. White layer confirms the presence of martensite formed due to phase transformation encouraged by factors such as plastic strain, strain rate, heating rate, cooling rate and local environment operating conditions [33].

Metallographic analysis was performed on all the grades of ADI and checked for martensite formation or any microstructural changes (as shown in Figure 37). The microstructure observed after drilling was compared against the original microstructure of ADI before drilling. The comparison was a foremost step in setting up criteria and develops an understanding to confirm the microstructural transformations of retained austenite to martensite during machining. The analysis was performed with special emphasis on microstructural observation along the hole boundaries by cross-sectioning the hole along the hole depth.

The microstructural images shown in Figure 37 represents white layering along the hole edge and bottom region of the hole. Correspondingly, high plastic strain along the hole edge and extrusion (cold work) by the chisel edge at the bottom of the hole play a major role in the formation of white layer. Microscopic lens of magnification 40X was used to generate the microstructural images shown in Figure 37.

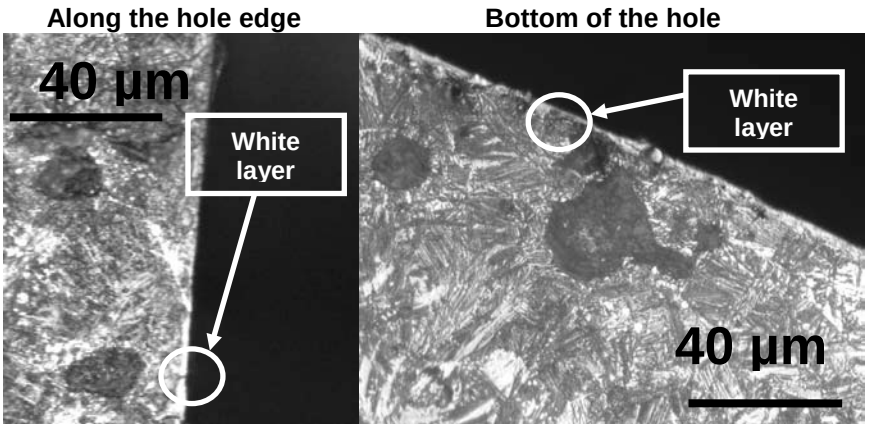

Figure 37: White layer assessment

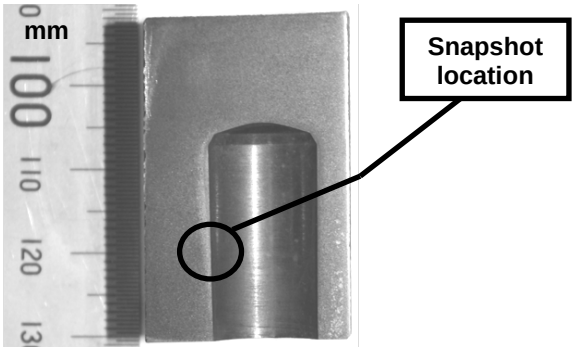

Figure 38: Snapshot location for microstructural images

As said earlier, the hole edge was the point of focus during metallographic examination in order to look out for phase transformations or white layer formation. As the surface near to the edge was curvy, lower magnification was used in order to avoid focus problems (blur images). Consistency was maintained in selecting the location for taking the snapshot of the microstructure for all samples as shown in Figure 38. The results from metallographic analysis were considered as data in support of other related analysis undertaken to assess the machinability of grades 900, 1050, 1200 and 1400. The results from metallographic analysis are explained in detail in section 6.4.6.

5.2.7 Tool failure analysis

Unexpected failure of the tool while drilling grade 1200 at cutting speed 65 m/min, feed rate, 755 mm/min and without coolant; was used to study the reasons for tool failure with respect to the workpiece microstructure and material properties. Tool failure analysis was a type of machinability analysis undertaken on grade 1200 at combinations of speed and feeds in the extreme range, without coolant and tool failure being the end condition for the process. The damaged tool is shown in Figure 39. The purpose of tool failure analysis was to establish relationship between the martensite content leading to hardening of the material due to SIT and failure of the tool. The semi drilled portion of the workpiece (as shown in Figure 39) was subjected to metallography analysis and XRD in order to check for work hardening due to SIT.

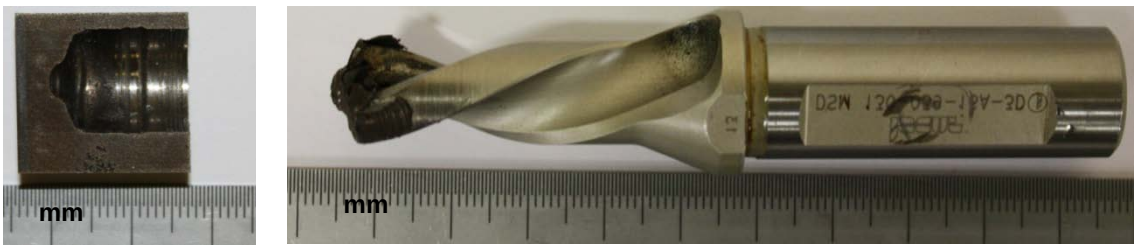

Figure 39: Tool failure while drilling grade1200

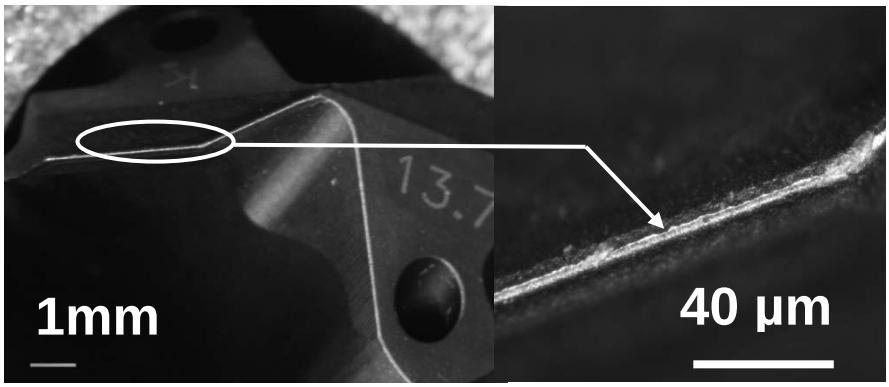

Figure 40: Drilling inserts-tool wear

Initial verification for the occurrence of SIT and increase in martensite content was done using colour metallography (heat tinting) and on confirmation, microstructural phases such as martensite was quantified using XRD analysis. The results from tool failure analysis focussing on SIT using supportive analysis such as XRD and metallographic analysis is given in section 6.4.7. Tool wear experienced by the drilling insert is shown in Figure 40.

5.3 Study of phase transformations

An investigation into the factors effecting phase transformation in ADI during machining and their influence on the machinability is described in this section. Study of phase transformations was considered to be the second and final part of the research work on ADI machinability. The experimental design mainly focuses on studying the effect of plastic deformation on the microstructure using tensile testing and similar study on effect of plastic deformation on microstructure during machining. Even tough, the plastic deformation rate in case of machining is reported to be very high compared to that in case of tensile testing. Keeping in mind the available resources and instrumentation, tensile testing was selected as the best possible way to study effect of plastic deformation on microstructure because of its ease and non complex nature. Machining history does confirm trials for measurement of plastic deformation during machining e.g. machining research by Komanduri [29].

Taking into consideration the results from the first part of the thesis-machinability evaluation of ADI, this part of thesis was designed to have an in-depth investigation of the trends or phenomenon seen in the first part. The purpose of this study of phase transformations was to develop an in-depth understanding on the thermo-mechanical reactions which lead to phase transformation (retained austenite to martensite) during machining of ADI.

Hence, the main focus was to have a corroborative study between the SIT due to machining and tensile testing. The experimental design for study of phase transformations was divided into two sections based on the source of plastic deformation: tensile testing-standard and tapered samples; milling trials-dry and wet machining. Supportive analysis such as metallography and XRD analysis was used for microstructural phase identification and quantification. Colour metallographic technique heat tinting was also used for microstructural phase identification.

5.3.1 Milling trials

The second part of this study on ADI phase transformation during machining consists of establishing a relationship between the factors such as plastic deformation and thermal energy; and SIT. To achieve the rationale behind this study, milling trials on grade 1200 at variable Depth of Cut (DoC) under dry (no coolant) and wet (coolant) machining were conducted in order to verify the effect of thermal and plastic deformation energy on phase transformations. ADI samples used in this trial were cut from the large size blocks-300x150x50 mm^3. The process diagram for the milling trial is given in Figure 41.

The experimental design consists of face milling grade 1200 at variable DoC range from 1 to 4 mm, variable coolant condition-dry and wet, at constant speed of 1992 rpm and feed rate of 0.1 mm/tooth. The machine tool used for the purpose of milling was HASS Super VF-3 model having maximum spindle speed of 12,000 rpm.

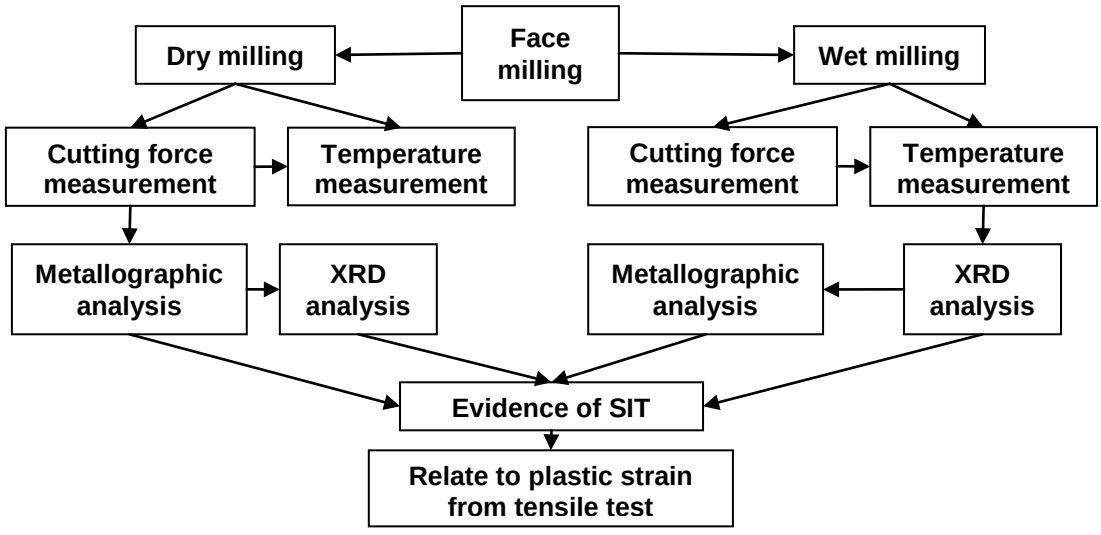

Figure 41: Experimental design – milling trials

The milling cutter used in the trials was insert type milling cutter manufactured by SECO having tool holder-R220.70-0080-09-6 (diameter-80mm) and six slots (tooth) to position round mill inserts (CBN300, diameter-9mm). The milling inserts (CBN300) were made out of Polycrystalline Cubic Boron Nitride (PCBN) which are well known for their toughness and thermal conductivity. For wet milling, the coolant used for the purpose was water soluble oil containing nearly 2.8% phenol mixed with water in the ratio of 1: 10. Analysis such as cutting force, metallography and XRD analysis helpful in evidencing the occurrence of phase transformation during milling was conducted.

Figure 42 shows the experimental set up consisting of workpiece fixed to the dynamometer and thermocouples inserted into the pre-drilled holes. The influence of thermal energy on phase transformation leading to martensite formation was also studied with the help of temperature measurements using thermocouple at chosen locations. The result obtained from the milling trials was used to relate the plastic strain obtained from tensile testing. Overall, a function governing the relationship between plastic strain and SIT was established through these trials.

Cutting force analysis

During milling, cutting force and moment was recorded using dynamometer-9257B following similar procedures as explained in earlier sections involving cutting force measurements.

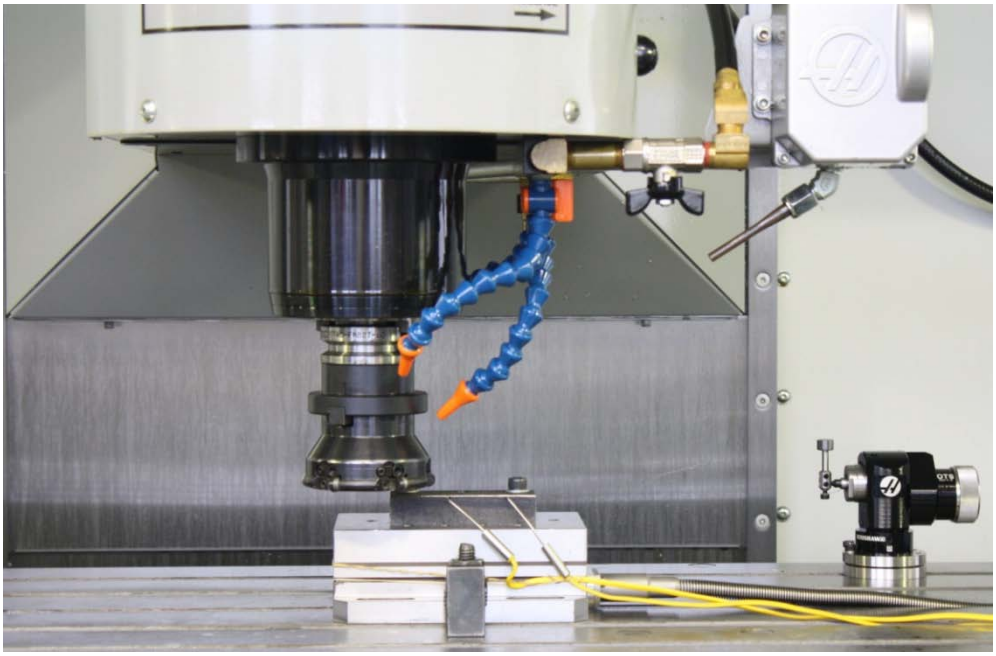

Figure 42: Experimental set-up milling trials - grade 1200

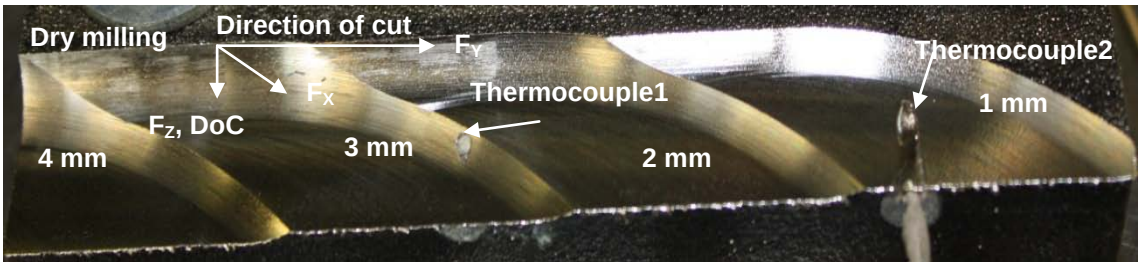

Figure 43: Machined sample under dry milling for variable DoC - grade 1200

Figure 43 shows a machined sample under dry milling, the forces and direction of cut for the grade1200. The important parameters under consideration for the milling trials are the thrust force, (F_Z) and feed force, (F_Y) and moment (M_Z). A comparative study was conducted between the thrust force, (F_Z) and feed force, (F_Y) and moment (M_Z) for milling under dry and wet machining. The effect of depth of cut on SIT was verified through these trials by observing any sudden changes in cutting force and moment. The results from the cutting force analysis both for dry and wet machining is given in section 6.5.1.

Metallographic analysis-heat tinting

Metallographic examination of the machined samples was conducted to check for martensite formation due to SIT. For dry and wet milling, each sample representing a DoC was selected and subjected to metallographic analysis. The sample preparation and experimental procedure was similar to the metallographic analysis shown in Figure 25. Specialised metallographic technique such as heat tinting is useful for easy identification of the microstructure. Microscopic lens of magnification-40X was used to capture the microstructural images. The evidence of martensite formation due to SIT was further verified and quantified using XRD analysis. Any increase in martensite (wt%) was related to the plastic strain obtained from tensile testing-standard specimen. The results from the metallographic analysis are given in section 6.5.1.

XRD analysis

XRD is an age old technique used to identify and quantify the microstructural phases in a material using the atomic structure of the material. The technique works by analysing the pattern of reflected X-ray (in terms of intensity or wavelength), reflected after striking the atomic or crystal structure of the material.

XRD is based on a law proposed by its inventor i.e. Braggs Law (equation 5-2)

$$n\lambda = 2d\ sin\theta \quad \text{----------} \quad 5\text{-}2$$

where λ is the wavelength of the reflecting X-ray, d is the spacing between the reflecting planes and θ is the angle of reflection.

Sample preparation for the XRD analysis consists of cutting the samples to size-25x25x2.5 (mm) and polishing the surface using silicon carbide papers and diamond paste up to one micron. Polishing was done to remove any irregularities and to have an ideal flat surface for the x-rays to hit the target. Prepared sample was then subjected to XRD analysis on a Siemens Kristalloflex Difrraktometer D5000 having CuKα radiation (λ=0.15406, 40 KV, 30 mA), graphite mono chromator with an angle of 24^o and goniometer radius of 217.5 mm. The prepared samples for XRD were placed and subjected to analysis on the machine using Bragg-Brentano geometry with a step mode collection. The measurements were done in the angle (2θ) range between 20^o to 104.92^o at the rate of 5 seconds/step. The data obtained from the XRD machine is in the form of a graph with angle of reflection (2θ) on x-axis and intensity of the x-ray on y-axis. Although numerous traditional XRD phase quantification methods using mathematical functions are available, the reliable Reitveld method was selected to refine the crystal structure data in this research. Reitveld method was selected as it takes into consideration correction factors such as the refinement of scale factors, lattice parameters and atomic site occupancy of the individual phase in the sample. The data obtained was sorted by Reitveld method using MAUD software, which is customised microstructural phase quantification software. MAUD is a java based, free to use specialised XRD software available online. The software automatically does the background subtraction and peak fitting of the XRD data against the peak data for selected microstructural phases (space groups) such as Graphite (P63/mmc), Austenite (Fm3m), Ferrite (Im3m) and Martensite (I4/mmm).

Overall, the method used was considered to be a semi-quantitative analysis for quantification of the microstructural phases with an error (±1%). The microstructural phase quantification data was done in terms of weight (%). A sample graph is shown in Figure 44 displays the XRD peaks and quantification data in terms of weight (%) for a basic sample of grade 900.

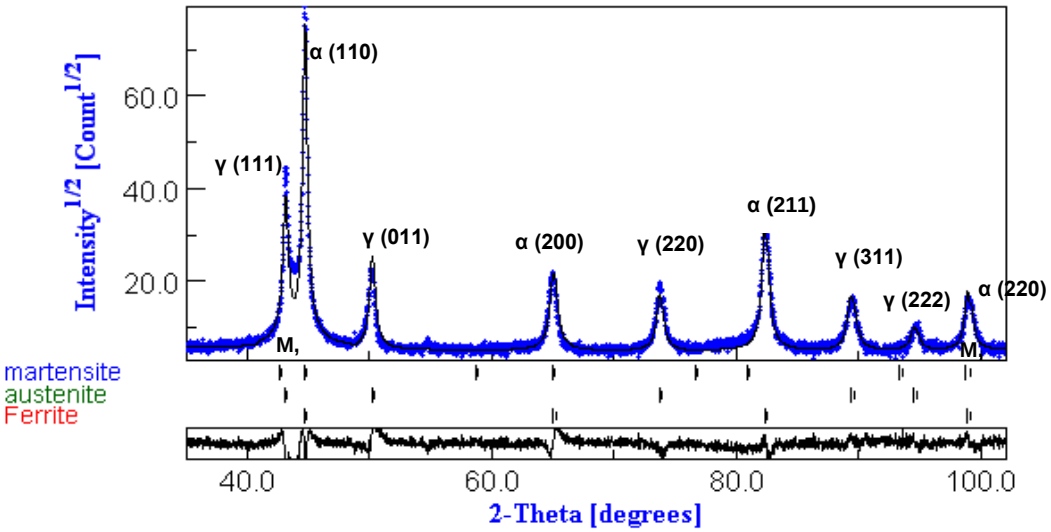

Microstructural phase Weight (%)	Austenite(γ)	Ferrite(α)	Martensite(M)
	30.4 ± 0.5	69.3 ± 0.8	0.4 ± 0.3

Figure 44: XRD analysis - grade 900 – basic

The graphite content was assumed to be constant for all the samples. The XRD data under consideration by MAUD lies between angle (2θ) 30^o to 105^o. As shown in Figure 44, the XRD peaks represent austenite (γ), ferrite (α) and martensite (M) at various unit cells in the crystal structure. The reason for unseen martensite peak between the angle (2θ) 40^o to 50^o and at other locations, was due to overlapping with the wider ferrite peak and also due to tetragonal nature of the martensite crystal structure. The same has been reported by J.L. Garin and R.L Mannheim in their research paper on strain induced martensite in ADI alloys [73].

On initial confirmation of presence of martensite on samples mill at variable DoC using metallographic analysis-heat tinting. Microstructural phases present in the samples were further verified and quantified using XRD analysis. A comparative analysis was conducted between the amount of martensite formed from retained austenite due to SIT for dry and wet milling at variable DoC. The initial martensite content for grade 1200 was obtained from the XRD analysis of basic samples and the increase in martensite content was evaluated in order to confirm an occurrence of SIT. The results from the XRD analysis for dry and wet milling at variable DoC are displayed in section 6.5.1.

Temperature measurement

The effect of thermal energy on phase transformation was verified by measuring temperature during milling under dry and wet conditions at variable DoC. Temperature measurement during milling was done using thermocouples placed at locations along the direction of cut (as shown in Figure 43 & Figure 45). The change in temperature was used to calculate the amount of thermal energy involved. As explained in section 4.3.6, thermal energy plays an important role in transformation of retained austenite to martensite by lowering the energy barrier. The experimental design consists of recording the time-temperature data which was passed on by the thermocouple placed at different location along the direction of cut. Thermocouples were connected to a system through the data logger which receives and process the data. PDAQ software on the system, sorts the data to generate time-temperature graphs. K-type thermocouple was used for temperature measurements having SS tip of diameter-1.5 mm and length of 60 mm. K-type thermocouple has a measurement range of 200 ^{o}C to 1350 ^{o}C. The length and diameter of the sensor tip plays an important role in temperature ratings.

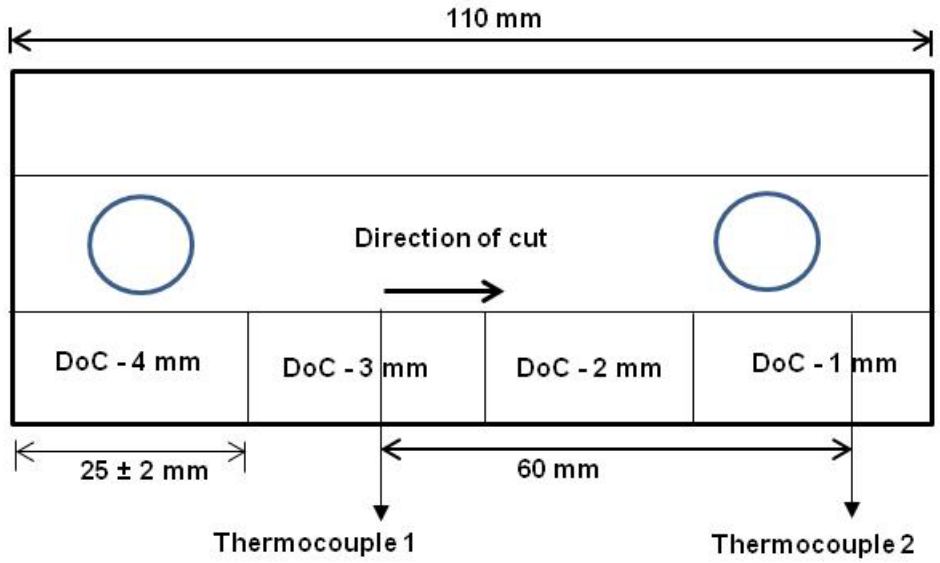

Figure 45: Thermocouple locations for dry and wet milling - grade 1200

The thermocouples were placed at location intersecting the cutter path for DoC-3 and 1 mm (as seen in Figure 45). The readings from the thermocouple were ignored after it was sheared or cut-off by the tool. As the trials were conducted under room temperature, the initial or reference temperature before milling was taken as 25 ^{o}C. Temperature measurements for dry and wet milling at variable DoC is shown and discussed in section 6.5.1.

5.3.2 Tensile testing - standard specimen

This work was an experimental study on effect of microstructural change due to Strain Induced Transformation (SIT) of Austempered Ductile Iron (ADI) and corroborates the result with SIT related to machining of ADI. On machining ADI, the microstructure changes rapidly from austenite to martensite due to SIT. The analogy between SIT and machining was addressed in this section. Evaluation to quantify the likely extent of SIT during machining of grades 900, 1050, 1200 and 1400 via heat tinting of plastically deformed samples has been conducted.

Tensile testing of grades 900, 1050, 1200 and 1400 consists of specimen preparation and tensile testing the specimen till fracture. The tensile testing instrument used for the test was Tinus Olson-H50KS, having a maximum load capacity of 50 KN. The specimen used for tensile testing was a flat, rectangular specimen as shown in Figure 46. The tensile specimens are sized and shaped based on the ASTM standard (E8-96). Due to the sensitive nature of ADI microstructure, the specimens are cut from each grade using EDM-wire cutting machine. For each grade, the tensile specimen was cut from small size blocks-300x150x25 (mm). Five specimens are cut for each grade of ADI having a thickness of 2 mm. Further, the specimens are subjected to grinding and polishing sequentially, to remove the micro cracks and other casting defects around the gauge section [74].

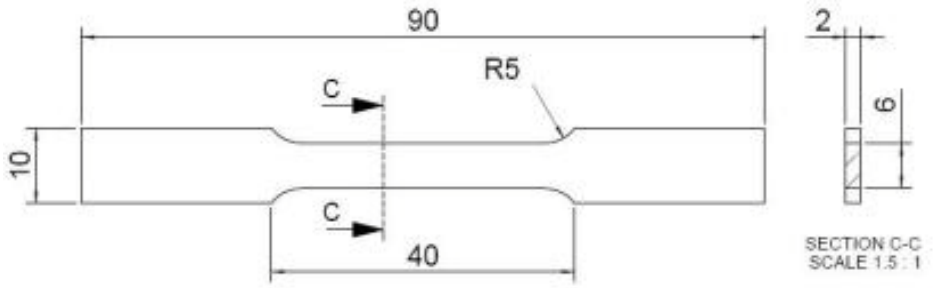

Figure 46: Tensile testing specimen (in mm)

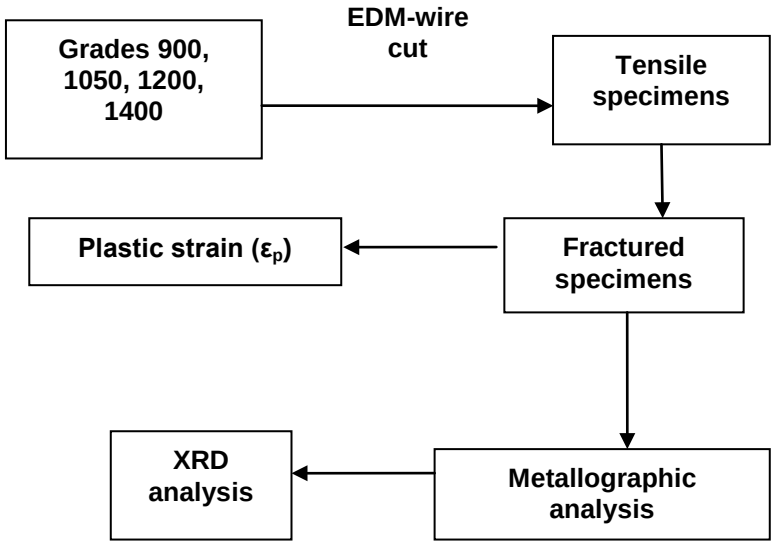

Figure 47: Process diagram for tensile test

This process helps to reduce the premature failure of the specimen due to the tensile forces and thereby, giving accurate results. After specimen preparation, the specimen ends were held using collets connected to a stationary and moving crosshead of the machine. The specimen was given a pre-tension load (300 N) by upward movement of the crosshead in order to remove the slack and to hold the specimen rigidly.

The gauge length for the specimens was 40 mm. The process diagram for the experiments is shown in Figure 47. The machine was programmed to pull the firmly held specimen by upward displacement of the moving crosshead at a constant rate of 3 mm/min till fracture. ADI being a harder material (40 R_c), holding the specimen for higher grades was problematic and therefore, a slow rate of crosshead movement was selected in order to avoid the specimen slip. The ends of the specimen are roughened using sand paper in order to develop friction between the specimen and the collet jaw for firm grip.

The tensile load and elongation data during the test was recorded and saved on a PC using the Tinus Olson software, supplied with the machine. Upon fracture, the data obtained from the tests consists of the maximum load and extension at fracture; and tensile load-elongation curve. This data was later used to calculate the other important points on the curve such as yield strength, Ultimate Tensile Strength (UTS) and strain hardening exponent (n).

The data obtained directly from tests was also used to calculate the engineering stress and strain; and true stress and strain. Ultimate Tensile Strength (UTS) and elongation (%) were used as benchmarks for evaluating the tensile properties of ADI. A comparative assessment was made between the tensile test results and the ASTM A897-03 standard. Strain hardening exponent was used to establish the relationship between plastic deformation and SIT. The results from the tensile tests are given in section 6.5.2.

Strain hardening exponent

Strain hardening exponent (n) is a hardening factor associated with non linear, plasticity region of the stress-strain curve. The machinability of a material is determined using the strain hardening exponent as it decides the work hardening capability of a material. Generally, a material with low strain hardening exponent is considered to be having good machinability. The strain hardening exponent is related to the number of dislocations and their entanglement in the material atomic structure. The results for the strain hardening exponent (n) are given in section 6.5.2. According to the research paper on plastic behaviour of ADI published by Jakob et.al, plastic behaviour is highly dependent on combination of austempering temperature and austempering time [75]. For calculating the strain hardening exponent, international standard, ISO10275:1993 (E) was used. For a uniaxial tensile test, strain hardening exponent (n) is defined as the exponent of true strain (Є) in the mathematical equation 5-3 relating to true stress (σ) [76].

$$\sigma = K\epsilon^{n} \quad \text{----------} \quad 5\text{-}3$$

and expressed logarithmically as

$$ln\sigma = lnK + nln\epsilon \quad \text{----------} \quad 5\text{-}4$$

where K - Strength Coefficient. Strain hardening exponent (n) can also be defined as the gradient (α) of the straight line (σ versus Є).

$$n = tan\alpha \quad \text{----------} \quad 5\text{-}5$$

The strain hardening exponent (n) was calculated using the plastic strain region of the stress- strain curve when subjected to a uniaxial loading. Considering five random points (N = 5) on the plastic region of the stress strain curve, strain hardening exponent was calculated using the mathematical formula (equation 5-6) given below

$$n = \frac{N\sum_{i=1}^{N} x_i y_i - \sum_{i=1}^{N} x_i \sum_{i=1}^{N} y_i}{N\sum_{i=1}^{N} x_i^2 - (\sum_{i=1}^{N} x_i)^2} \quad \text{----------} \quad 5\text{-}6$$

Where y=ln (σ), x=ln (Є)

Metallographic analysis - heat tinting

Metallographic analysis using heat tinting was conducted on fractured tensile samples in order to identify the microstructural phases and check for increase martensite content. As shown in Figure 25, heat tinting is a metallographic technique leading to coloration of different phases in ADI. The purpose of conducting metallographic analysis was to check the occurrence of SIT as ADI having higher amount of retained austenite (light blue) has greater probability of SIT during machining. The different colours representing each microstructural phase makes it easier to identify the transformation of retained austenite to martensite i.e. light blue getting transformed to dark blue.

The smaller fractured sample was mounted and polished. They are then etched and heat treated as part of heat tinting process. Nital containing 2-4% alcoholic solution of nitric acid at room temperature was used as an etchant. The etched sample was subject to heat treatment in a furnace maintained at 260^{o} C for 4-8 hours and cooled down to room temperature in a natural way using air. The colour microstructure obtained due to heat tinting was observed using optical microscope and 40X magnification lens. For initial microstructural identification and quantification, the tensile samples are subjected to metallography and XRD analysis. Metallography examination does reveal the presence of martensite even at the initial stage and the same has been confirmed using a XRD analysis. Generally, improper casting and heat treatment techniques used in the making of ADI lead to the formation of martensite. On final identification and quantification of the microstructural phases using the fractured sample, a comparative assessment was done between the microstructural phase before and after tensile testing. The results from metallographic analysis using heat tinting are shown in section 6.5.2.

XRD analysis

XRD analysis was used to quantify a microstructural phase. The sample preparation and experimental procedure was similar to the procedures used in XRD analysis in section 5.3.1. The microstructural phase quantification data was calculated in terms of weight (%). The microstructural phases in the fractured sample after identification were subjected to XRD analysis for quantification of the individual phase present in the sample. XRD analysis was conducted on basic, non-tensile tested sample in order to quantify the microstructural phases present in the material before tensile testing. A comparative study between the microstructural phases before and after tensile testing was done. Consequently, the change in microstructural phase quantity was related to the plastic strain associated with the tensile fractured sample. The results from the XRD analysis on samples before and after tensile test are presented elaborately in section 6.5.2.

5.3.3 Tensile testing - tapered specimen

After observing initial results using a standard tensile specimen (E8 standard), tensile testing using a non standard and tapered specimen were conducted on grades 1200 and 1400. Three samples representing each grade were cut using EDM and subjected to tensile testing. As tapered samples (as shown in Figure 48) were used for tensile testing, variable strain was obtained along the gauge length due to varying cross-sectional area. Three regions-small, medium and large were selected along the gauge length based on the cross-sectional area. For each region, reference lines at a distance of 10mm were marked (initial) and after tensile testing, the distance between the lines increased (final) due to tensile load. As expected, on tensile loading, the specimen did break in the region of small cross-sectional area. The expected trend of having large elongation (%) for smaller cross-sectional area was observed. The purpose of conducting tensile test using a tapered specimen was to obtain high value of plastic deformation at the fracture region i.e. small, due to reduced cross-sectional area and to develop a relationship between the plastic deformation and SIT. The results obtained represent the average elongation (%) values of three samples along with the standard error. A similar experimental design as described in section 5.3.2 for a standard specimen was used in this section except XRD analysis.

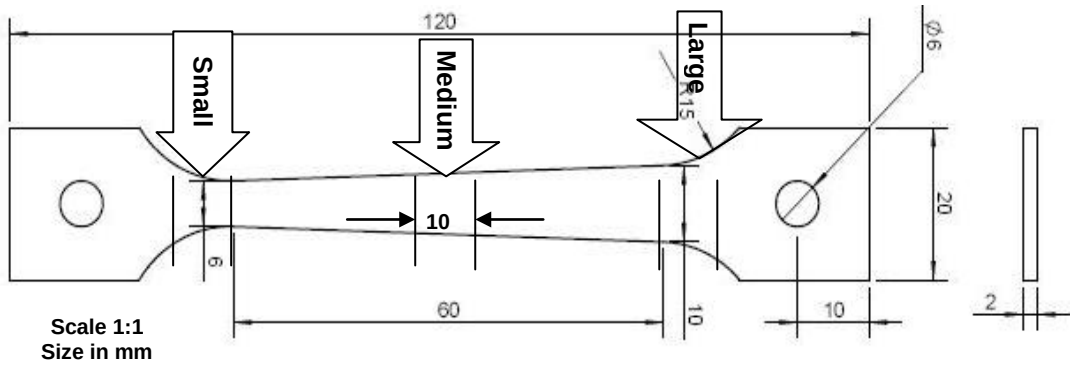

Figure 48: Tensile testing - tapered specimen

The fractured region was subjected to metallographic analysis and microhardness testing. The purpose of metallographic and microhardness testing was to identify the occurrence of phase transformation near to the fractured region. The results from the tensile testing of tapered specimen are given in section 6.5.3.

Metallographic analysis - tapered specimen

The fractured samples obtained from the tensile testing using tapered samples for grade 1200 and 1400 were subjected to metallographic analysis. The objective of this analysis was to check for SIT near to fracture region. The results from this analysis are explained and given in section 6.5.3.

Microhardness analysis - tapered specimen

The fractured samples obtained from the tensile testing using tapered specimen for grade 1200 and 1400 were subjected to microhardness analysis. Knoop microhardness was used to measure the microhardness levels in the direction moving away from the fracture zone. The objective of this analysis was to check for SIT near to fracture region by interpreting high microhardness near to the fractured region and gradual decrease in microhardness on moving away from the fracture zone.

5.3.4 Modelling of tensile data using ANSYS

The results from tensile testing using standard and tapered specimen were validated using Finite Element Method (FEM). FEM is a powerful tool extensively used to analyse, simulate and validate wide range of engineering processes. The tensile sample under consideration was divided into elements where the material properties and governing relationships such as tensile loads and constraints were attached to these elements. As a result of this process, a set of equations were generated and solution to these equations gives us the approximate tensile behaviour of the sample.

FEM process consists of a pre-processing and post-processing stage. The pre-processing stage consists of modelling the tensile sample, assigning material properties such as young's modulus and poisson's ratio to the model, applying loads and constraints in order to achieve selected degree of freedom and finally, submit the model for analysis. The post-processing stage consists of equation solving and solution generation in required graphical and tabular format. Experimental tensile test setup for a standard and tapered specimen was simulated using ANSYS for all grades. This section further discusses the relationship between the plastic strain and SIT.

The comparative analysis was done between the tensile stress-strain data obtained experimentally and using FEM for all grades. The tensile sample modelling was done on 3D-CAD solidworks and later transferred into ANSYS. The experimental elastic and plastic data obtained from the stress-strain graph for each grade was used to assign the material properties. Finally, the prepared sample was subjected to non-linear, implicit steady state analysis which takes into consideration plasticity of the material and involves an incremental application of the displacement similar to the upper crosshead movement of the tensile testing machine. The results from tensile test using ANSYS consisting of the validation data between the experimental and ANSYS generated solution is given in section 6.5.4.

6 Results

This chapter presents the results from the experiments conducted as part of machinability studies on ADI. As said in chapter 5, experimental results are divided into two parts: first part consists of the results from experimentation done to characterise and confirm the material properties of grade 900, 1050, 1200 and 1400; second part consists of the results from experimentation done to study the phase transformations in ADI due to machining. This chapter also explains various reasons leading to any deviations from the regular trend.

6.1 Rockwell hardness test (R_C)

The results from the bulk hardness test conducted on grades 900, 1050, 1200 and 1400 are given in Table 8. As mentioned in section 5.1.2, tests were conducted on a Rockwell (R_C) scale and converted to Brinell Hardness Number (BHN) as the ASTM standards specify the bulk hardness for grades in terms of BHN. Table 8 also shows equivalent value in BHN. Grade 1200 has the highest bulk hardness, 441 BHN and grade 900 has the lowest value, 262 BHN. Bulk hardness test was useful in validating the hardness data obtained from the test with the ASTM standard data in order to confirm the grade. A deviation such as lower, out of range hardness for grade 900 was attributed to the localised defects in the castings such as porosity. The bulk hardness for rest of the grades was within the ASTM standards. An increasing trend in hardness was observed for an increase in grades from 900 to 1400. The overlapping of ASTM bulk hardness range was clearly seen in case grades 1200 and 1400, which justifies common bulk hardness values, can exist between different grades.

Table 8: Rockwell hardness test on ADI

	Grade900 R_C (BHN)	Grade1050 R_C (BHN)	Grade1200 R_C (BHN)	Grade1400 R_C (BHN)
Reading1	**26 (258)**	**41 (381)**	**47 (443)**	**45 (421)**
Reading2	**26 (258)**	**38 (353)**	**48 (455)**	**46 (432)**
Reading3	**28 (271)**	**39 (362)**	**46 (432)**	**44 (409)**
Reading4	**26 (258)**	**39 (362)**	**47 (443)**	**45 (421)**
Reading5	**27 (264)**	**39 (362)**	**47 (443)**	**45 (421)**
Reading6	**27 (264)**	**41 (381)**	**46 (432)**	**45 (421)**
Average reading	**26 (262)**	**39 (366)**	**46 (441)**	**45 (420)**
ASTM-A897-03 Range in BHN	**269-341**	**302-375**	**341-444**	**388-477**

6.2 Conventional metallography

The results for the metallographic analysis conducted on grades 900, 1050, 1200 and 1400 are given in Figure 49. Nital (4%) was used as an etchant and the samples were etched at room temperature. The typical microstructure of ADI also known as ausferrite consists of ferrite needles and graphite nodules distributed in the austenite phase. In Figure 49, white background represents the austenite phase, dark needle like structures constitute the ferrite and spherical nodules represent the graphite.

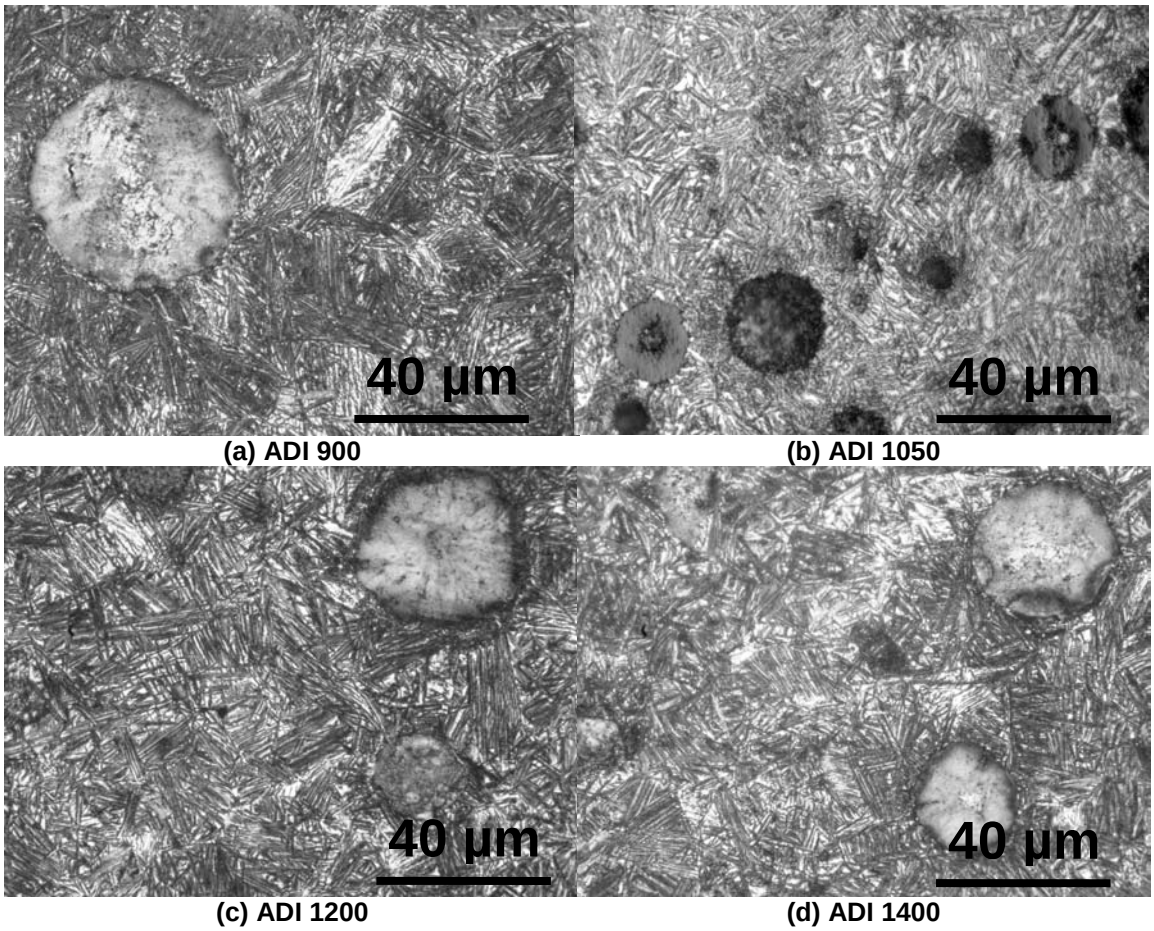

Figure 49: ADI microstructure using conventional metallography (a) Grade 900, (b) Grade 1050, (c) Grade 1200 and (d) Grade 1400

6.3 Heat tinted metallography

Heat tinted metallography is a modified version of conventional metallography where the etchant, nital forms an interference film on heating and produces colours representing each microstructural phase, when viewed under a polarised light. Heat tinting is a kind of an etching technique, leading to coloration of different phases in ADI.

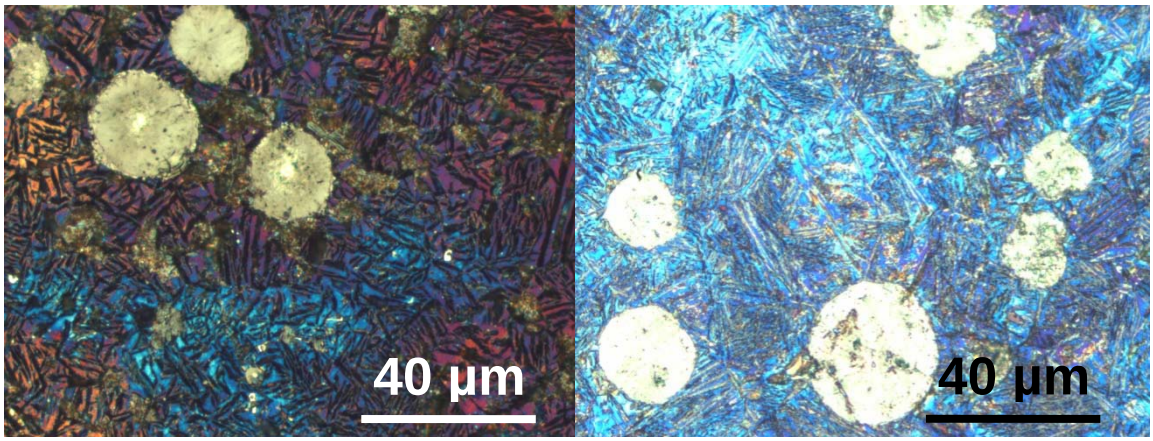

(a) ADI 900 (b) ADI 1050

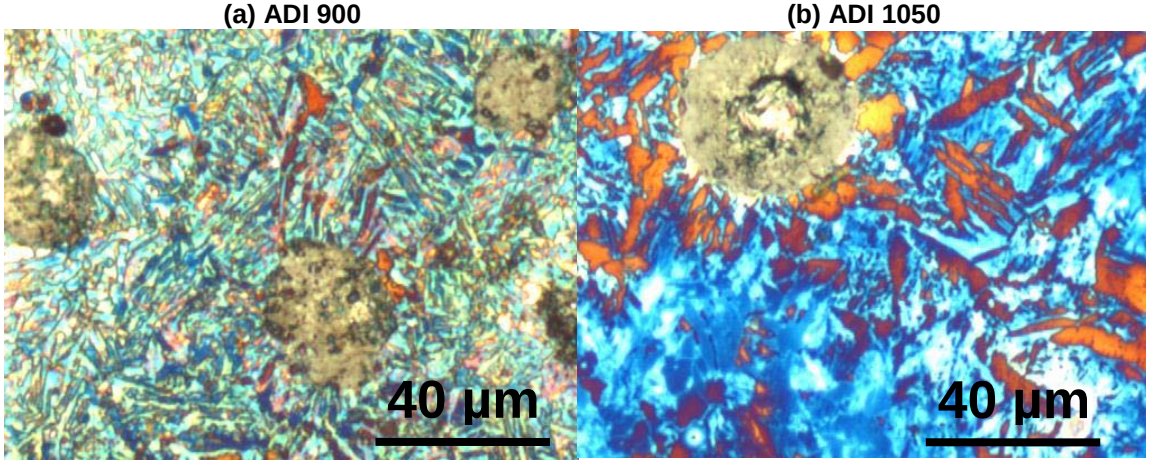

(c) ADI 1200 (d) ADI 1400

Microstructure	Retained austenite	Austenite	Ferrite needles	Graphite nodules	Martensite
Colour	Light blue	Purple	Black	Beige	Dark Blue

Figure 50: ADI microstructure using Kovacs Method (a) Grade 900, (b) Grade 1050, (c) Grade 1200 and (d) Grade 1400

The colour code representing the ADI microstructural phases is given in the table below Figure 50 which also shows the ADI microstructure obtained as result of heat tinting metallography.

6.4 Machinability analysis

The results from the machining trials conducted on grades 900, 1050, 1200 and 1400 are discussed in this section. Machinability was evaluated in terms of cutting force analysis, chip morphology, surface texture analysis, microhardness analysis and metallographic analysis. This section also explains preparatory trials such as dynamometer consistency tests.

6.4.1 Dynamometer consistency tests

Dynamometer consistency tests were helpful in finding out the working conditions of the dynamometer type 9272 and 9257B. The test make use of the data provided in the manual for the dynamometer – 9272 regards to the cutting parameters used and cutting forces obtained. The experimental results, cutting force (F_Z) and moment (M_Z) obtained through drilling trials using dynamometer type 9272 and 9257B were validated against the data provided in the manual. On validation, the cutting force (F_Z) and Moment (M_Z) were nearly similar for dynamometer type 9272 and 9257B and lower cutting forces in comparison to the manual data. The lower value was justified because of the different machining environments and the different material used for the tests i.e. mild steel 1020(experiments) and steel USt-37-2(Kistler 9272 manual). Finally, the working condition of dynamometer type 9272 and 9257B was evaluated. Due to better performance and ease to operate, the dynamometer, 9257B was selected to measure the cutting force during all the trials in this research. The comparative graph based on the mean value of the cutting force and moments is shown in Figure 51.

6.4.2 Cutting force analysis

As described in section 5.2.2, the data obtained from cutting force analysis consists of the cutting forces; F_X, F_Y, F_Z and moment M_Z. F_X and F_Y were not taken into consideration as these represent the balancing forces. The outputs under consideration are thrust force, F_Z (N) and moment M_Z (N-m).

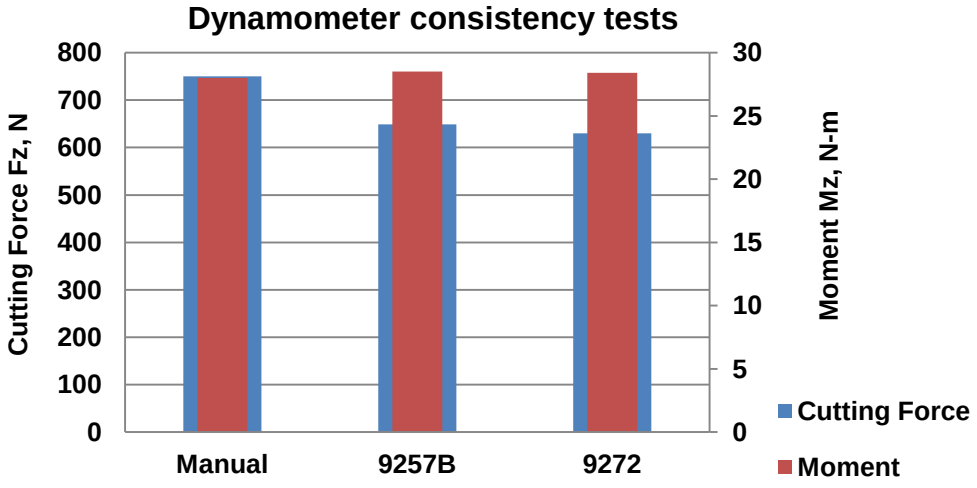

Figure 51: Dynamometer consistency tests - type9257B and 9272

Table 9: Comparison of thrust force and moment

	ADI 900	ADI 1050	ADI 1200	ADI 1400
Thrust Force (F_Z), N	785	773	782	810
Moment (M_Z), N-m	5.9	5.75	5.8	6.1

The mean values of thrust force (F_Z) and moment (M_Z) for grades 900, 1050, 1200 and 1400, machined at 693 rpm and 0.1 mm/rev are tabulated in Table 9. There was no significant variation in the thrust force, F_Z (N) between the grades 900, 1050, 1200 and 1400. The moment, M_Z (N-m) was almost constant between the grades 900, 1050, 1200 and 1400. Figure 52 shows the comparison graphs for thrust force (F_Z) and moment (M_Z) for the grades 900, 1050, 1200 and 1400. The result from the trials confirms comment from previous researchers, the golden rule, i.e. the use of low feed and high speed to machine ADI irrelevant of the hardness or the grade.

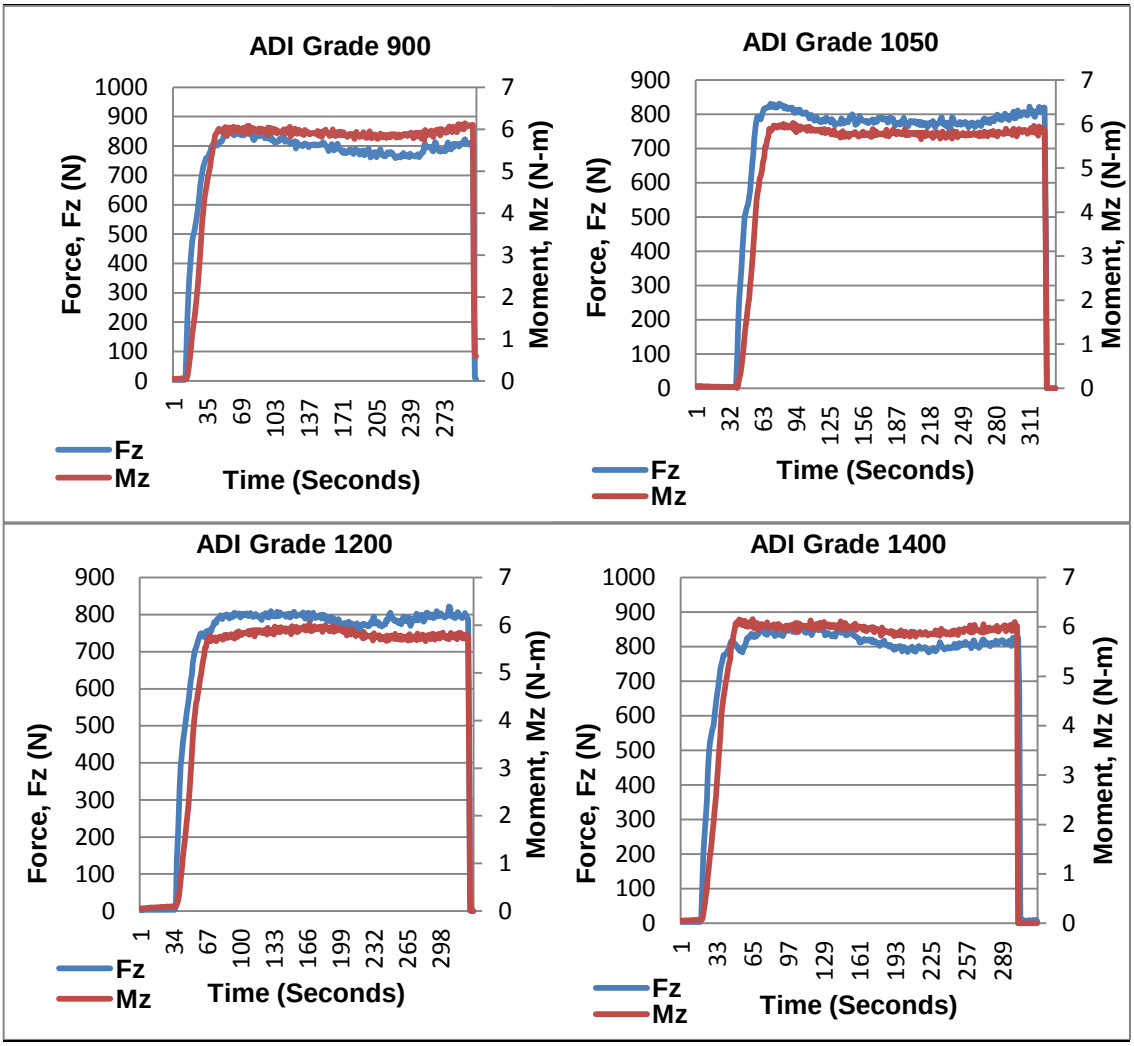

Figure 52: Comparison of thrust force, F_Z (N) and moment, M_Z (N-m) for grade 900, 1050, 1200 and 1400

At certain locations, abrupt rise in the thrust force was observed during drilling because of the cutting edge encountering hard spots. The conclusion made by previous researchers that ADI microstructure is sensitive to changes in cutting forces during machining was corroborated to some extent.

Effect of feed rate on cutting force

The cutting force data obtained from the drilling trials for grade 1200 and 1400 is tabulated in Table 10 and displayed in the form of graphs in Figure 53. As explained in 5.2.2, the purpose of conducting these trials was to understand the effect of feed rate on the cutting forces and moment. Phase transformation during machining being one of the objectives of the research, drilling without coolant and selecting higher grades such as 1200 and 1400 was considered to be the hypothetical factors encouraging phase transformation. The trials also give an insight into the effect of feed rate on phase transformations. As shown in Table 10, the cutting parameters such as speed, Depth of Cut (DoC) and without coolant were kept constant for a given grade and feed rate varied from 0.2 to 0.35 mm/rev.

The result obtained for grade 1200 and 1400 shows that for initial and final feed rates, 0.2 to 0. 25 mm/rev and 0.3 to 0.35 mm/rev respectively, the cutting force and moment increase with an increase in feed rate. For the middle portion of the curve i.e. feed rate, 0.25 to 0.3 mm/rev, the force and moment almost remain constant.

Table 10: Effect of feed rate on cutting force and moment

Grade	Speed, rpm	Depth of Cut, mm	Coolant	Feed, mm/rev	M_Z, N-m	F_Z, N
1200	1150	25	Off	0.200	23.77	3018.04
1200	1150	25	Off	0.225	26.54	3318.33
1200	1150	25	Off	0.250	30.97	3857.48
1200	1150	25	Off	0.275	32.55	3632.2
1200	1150	25	Off	0.300	41.31	4074.86
1200	1150	25	Off	0.325	42.77	4841
1200	1150	25	Off	0.350	64.95	5579.07
1400	1150	25	Off	0.200	25.59	3242.49
1400	1150	25	Off	0.225	30.24	3573
1400	1150	25	Off	0.250	40.27	4432.68
1400	1150	25	Off	0.275	45.71	4094.39
1400	1150	25	Off	0.300	42.87	4886.63
1400	1150	25	Off	0.325	53.32	6136.47
1400	1150	25	Off	0.350	61.09	5948.33

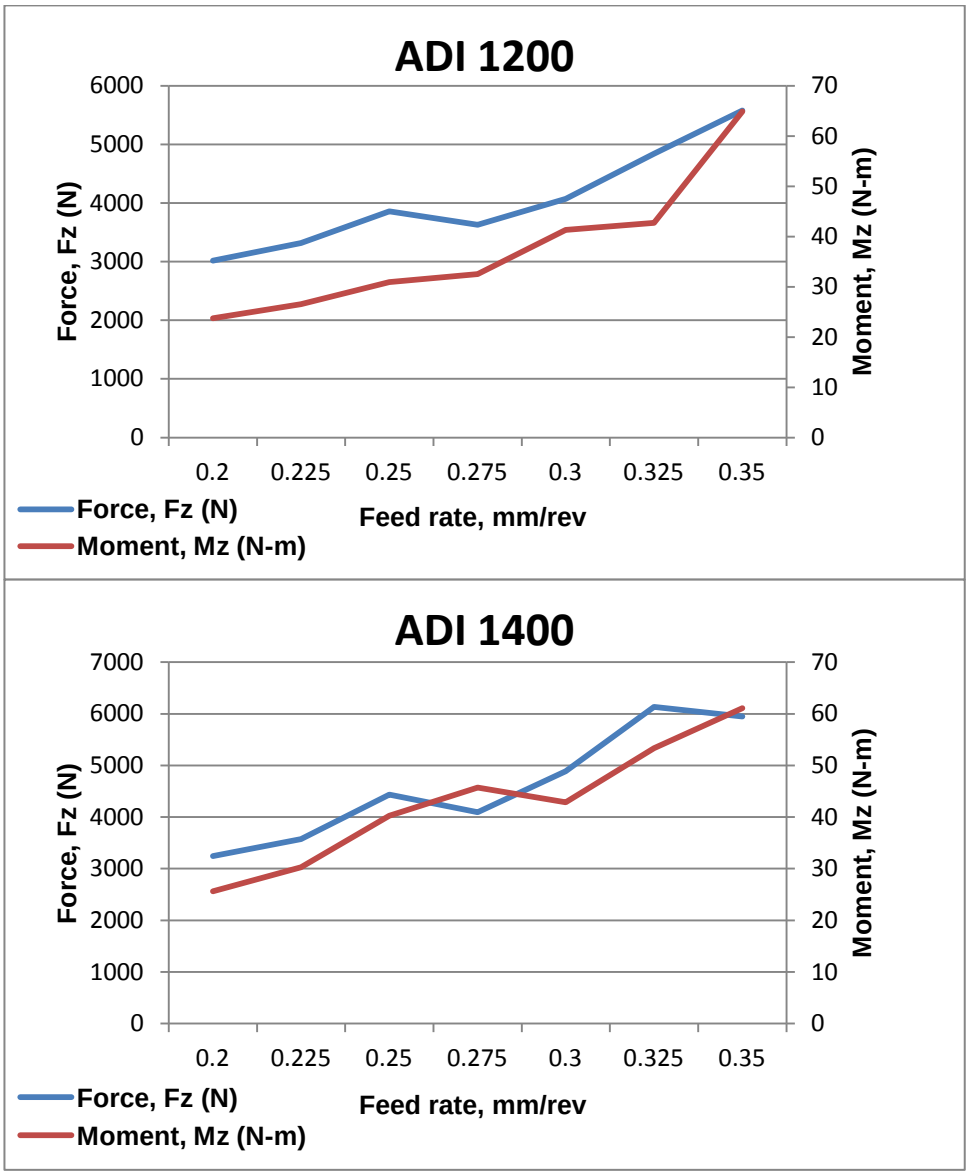

Figure 53: Effect of feed rate on force, F_Z (N) and moment, M_Z (N-m) - grade 1200 and 1400

An abrupt increase in cutting force and moment was considered to be the sign of cutting tool encountering hardened spots due to SIT. Thrust force (F_Z) and moment (M_Z) were considered for the analysis (as shown in Figure 53). The effect of feed rate on phase transformations and machinability is further discussed in chapter 7.

6.4.3 Surface texture analysis

Surface texture is an important factor to determine the machinability of a material. In post-machining stage, the lower surface roughness (R_a) for a machined surface means the material is having better machinability [51]. The data obtained from the surface roughness test conducted on grades 900, 1050, 1200 and 1400 is shown in Figure 54.

The test procedure is explained in section 5.2.3. Three readings were taken for each sample and mean value of the readings were considered for the analysis. A standard error was calculated using the standard deviation principle and any deviation from the mean value was represented in the form of error bars as shown in Figure 54. The effect of common defects such as porosity was observed in case of holes C1, C7, Q7, Q9, G9 and G7 (refer Table 7 for hole representation) as they produced a higher surface roughness (R_a). The effect of tool retraction on surface roughness was ignored as it remains constant for all the samples. The analysis also facilitates to establish a relationship between the hardness values (bulk and microhardness) and the surface texture of the hole. From the graph shown in Figure 54, sample L7 (grade 1200) has a best surface finish with a lower surface roughness (R_a) value of 0.730 µm. Sample C3 has a highest surface roughness (R_a) due to the excess porosity present in the material. For all samples drilled without coolant, the surface roughness (R_a) was high compared to the sample drilled with coolant except grade 1200. On comparison, grades 900 and 1050 have high surface roughness (R_a) than grades 1200 and 1400. Grade 1200 has shown better machinability performance when compared to rest of grades as the surface roughness (R_a) values were low and optimised.

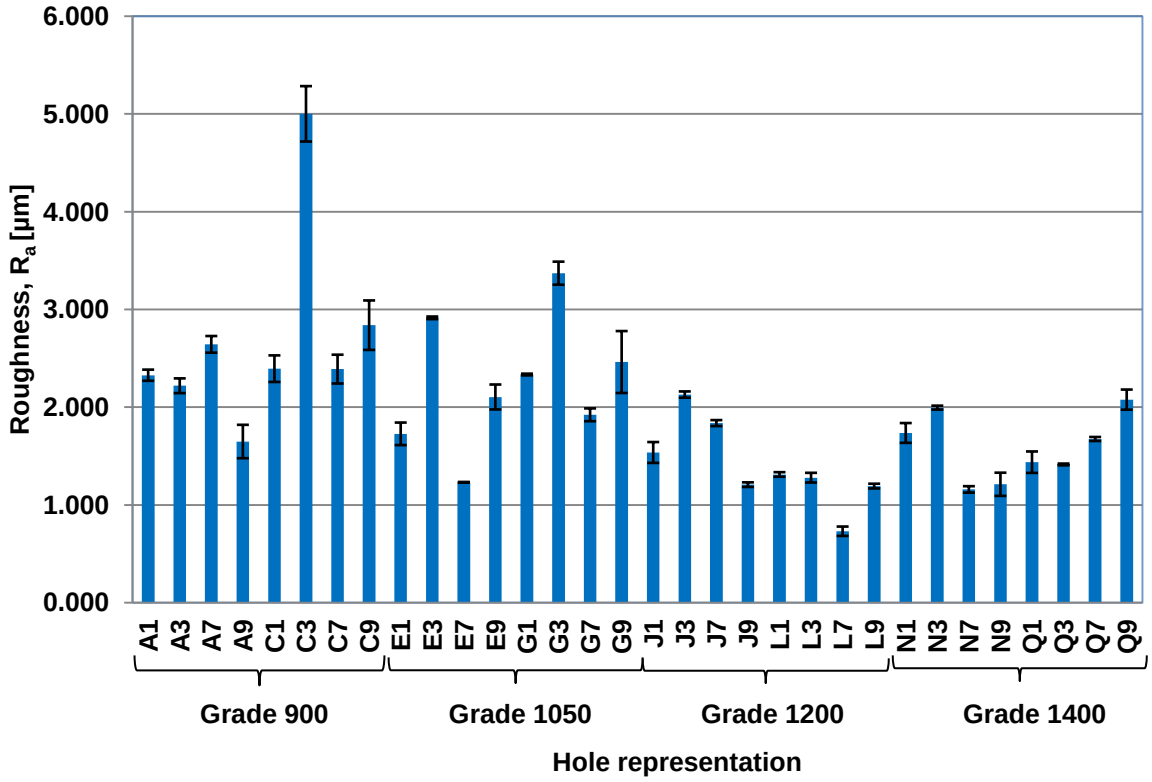

Figure 54: Surface roughness (R_a) graph for grades 900, 1050, 1200 and 1400. [Refer Table 7 for x-axis label definition]

Samples drilled at high feed rate and without coolant have a rough finish (high surface roughness (R_a)) as seen in case of samples G3, G9, Q3 and Q9. The sample L7 which was drilled at high speed, low feed and without coolant has the top finish (low surface roughness (R_a)) among all the samples. Similar trend was reported through the research paper on drilling performance of ADI by Anil and El Mansori [49]. The temperature generated in the shear zone plays an important role in determining the surface quality of machined surface.

6.4.4 Microhardness analysis

Phase transformational studies being major part of this research work on ADI machinability, microhardness test play an important role in estimating the occurrence of SIT due to machining. The data obtained from the microhardness analysis conducted on grades 900, 1050, 1200 and 1400 is presented in this section. As explained in section 5.2.4, an increase in the microhardness near to the hole edge was considered as a sign of SIT. The machined surface of each sample drilled using the combinations of cutting parameter as given in Table 7, was subjected to microhardness test. The variations of microhardness data with respect to cutting speed, feed rate, coolant on/off and grade was verified. The variations in "base" initial microhardness values or microhardness for as-received grades 900, 1050, 1200 and 1400 is shown in Figure 55.

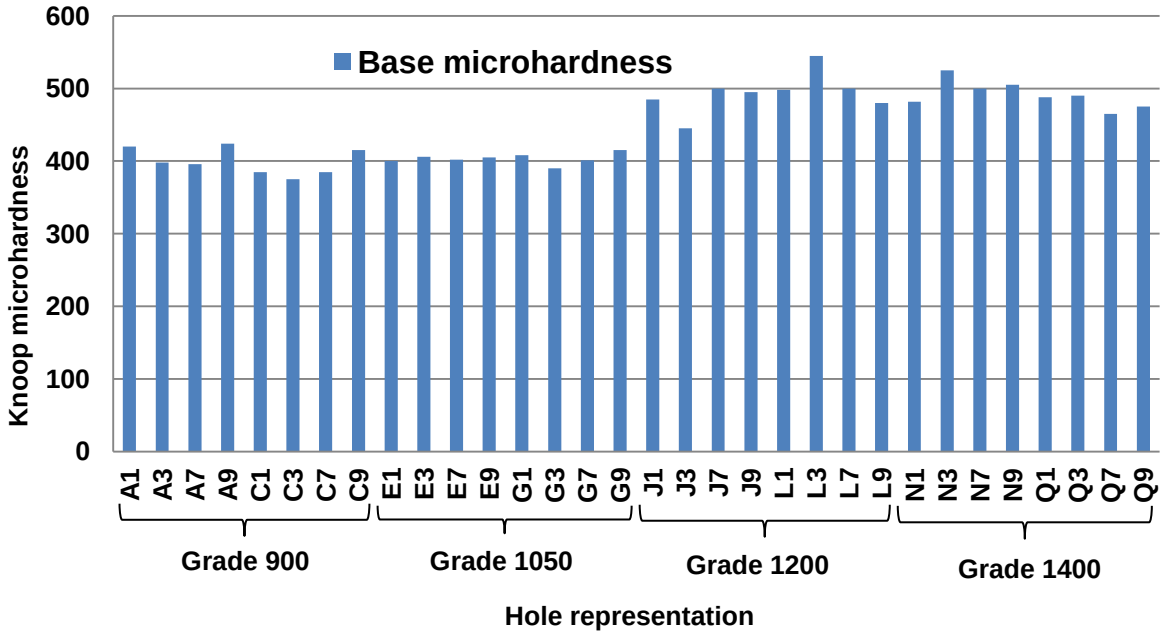

Figure 55: Knoop microhardness variations for grades 900, 1050, 1200 and 1400 - as-received condition. [Refer Table 7 for x-axis label definition]

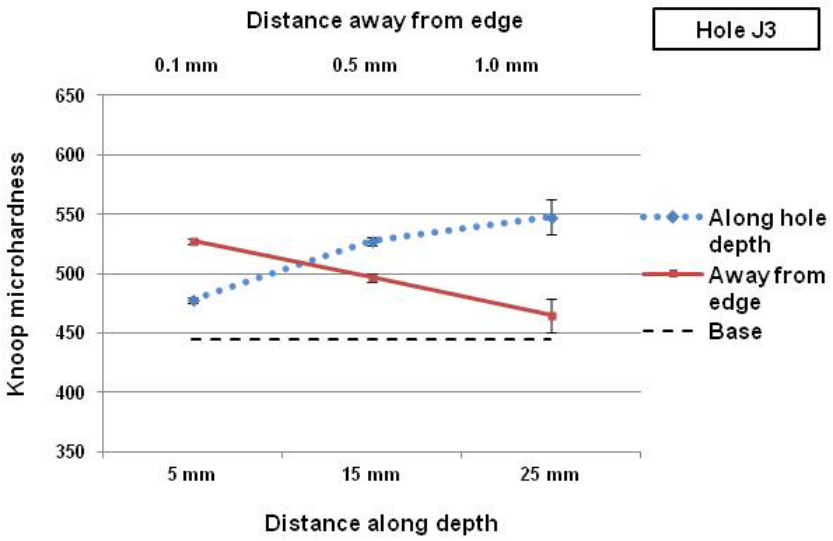

Figure 56: Knoop microhardness variations along depth and away from edge for sample J3 - grade 1200

The effect of tool retraction was ignored as it remains constant for all samples. The variations observed in the surface roughness (R_a) values tally with those observed in microhardness analysis. The data obtained from the microhardness test was divided into three categories which were useful in generating hardness profiles along the hole depth (direction of cut), away from the hole edge and initial microhardness of as received ADI termed as "base". The base microhardness increases as grades increase from 900 to 1400. A sample graph shown in Figure 56 displays the variations in Knoop microhardness values along the hole depth and away from the hole edge for sample J3-grade 1200, having cutting parameters, speed - 697 rpm, feed rate 0.2mm/rev and using coolant.

The microhardness variations for all samples belonging to grade 1200 is shown in the form of microhardness profiles - away from the edge and along the hole depth in Figure 57. Deviation from the regular trend was observed in case of samples having porosity and heat treatment defects. A sudden surge in microhardness was also observed in certain samples, which probably indicate the occurrence of hardening of the material due to SIT. The black broken line indicates the base or initial microhardness of the as-received ADI and was considered as microhardness before drilling. Generally, there is an increase in the microhardness value after drilling; the same was reported for almost all samples as the microhardness profiles generated were close to, below or above the "base" line.

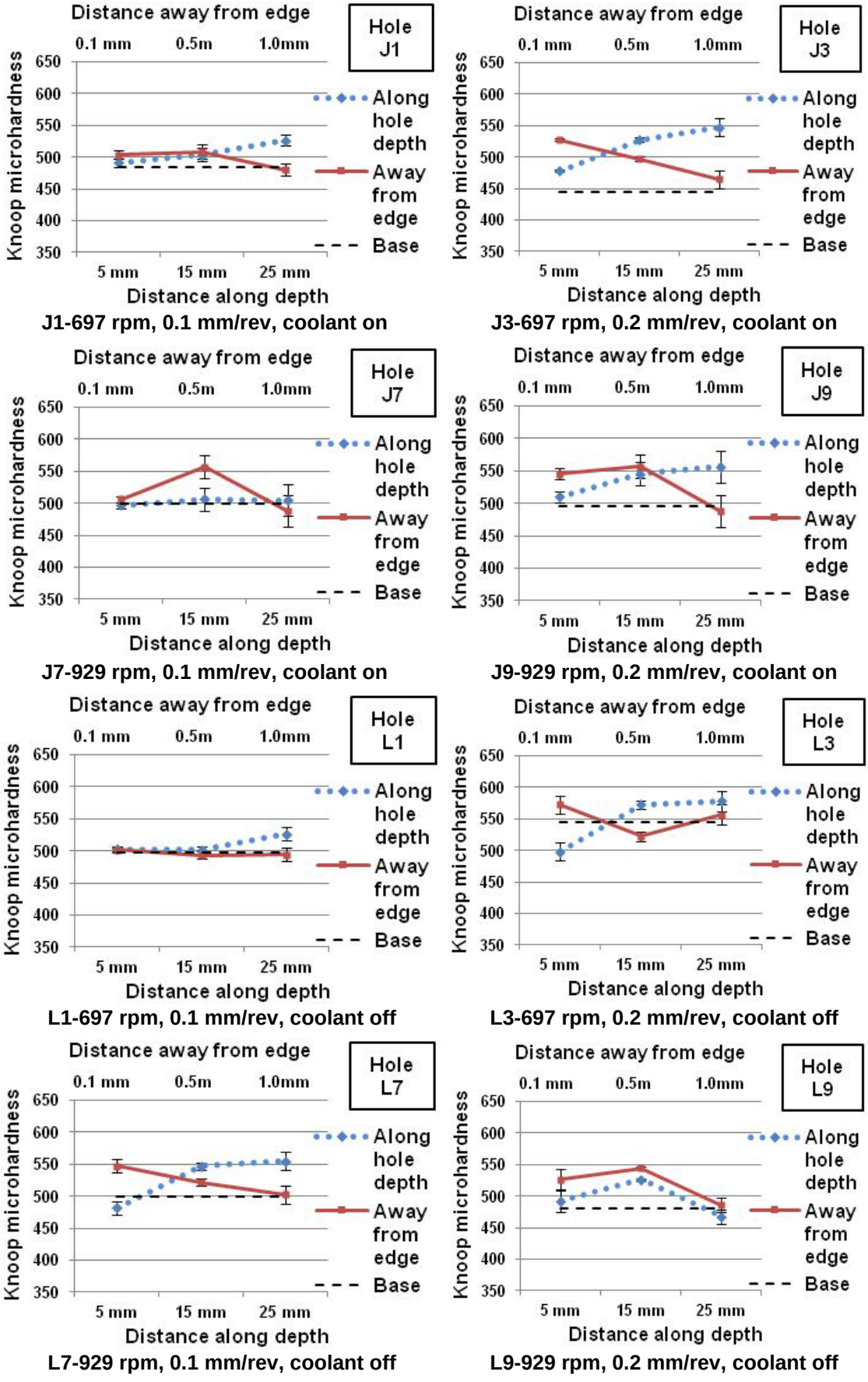

Figure 57: Knoop microhardness variations along depth and away from edge for grade 1200

From Figure 57 and microhardness variations for rest of grades, it was observed that the microhardness value increases as the cutting speeds increases irrespective of the feed rate, grade and coolant condition. Similar trend was reported through the research paper on drilling performance of ADI by Anil and El Mansori [49].

As mentioned in section 3.3, the majority of the cutting during drilling is performed by the lips or the main cutting edge and chisel edge at the bottom of the tool is responsible for extruding the material. High value of microhardness was reported in the locations near to the chisel edge which shows that the cold work by the chisel edge also plays an important role in phase transformation apart from SIT due to machining. Based on earlier results from cutting force analysis, surface texture analysis and metallographic analysis, grade 1200 was considered to have optimum values. Due to limited reporting space available, microhardness variations for rest of grades 900, 1050 and 1400 is given under - Appendix: Microhardness analysis.

The common observation for almost all samples of grades 900, 1050, 1200 and 1400 was that the microhardness has a lower value for a location away from the hole edge and the microhardness has a high value for a location along the hole depth or direction of cut. Overall, the analysis infers the microhardness values were higher for dry machining for any grade. The microhardness values followed an increasing trend from grade 900 to grade 1050, optimised from grade 1050 to grade 1200 and reduced from grade 1200 to grade 1400. The results obtained from microhardness analysis were corroborative with the results from surface roughness and metallography analysis.

6.4.5 Chip morphology

As explained in section 5.2.5, the purpose of chip morphology analysis was to study the effect of cutting parameters – feed rate, speed and coolant on chip form - size and shape. As chip morphology gives a picture of the chip formation process and the thermo-mechanical reaction taking place in the shear zone, it was considered to be a reference criterion to evaluate the machinability of ADI. The results from this analysis also explain the effect of chip size on evacuation of the chip through the drill flutes and its effect on the surface texture of the machined surface. Hence, the results from the chip morphology analysis corroborate the trends observed in other machinability evaluations such as microhardness and surface texture analysis

The different types of chips collected after drilling grades 900, 1050, 1200 and 1400 using the combination of cutting parameters given in Table 7 is shown in Figure 58.

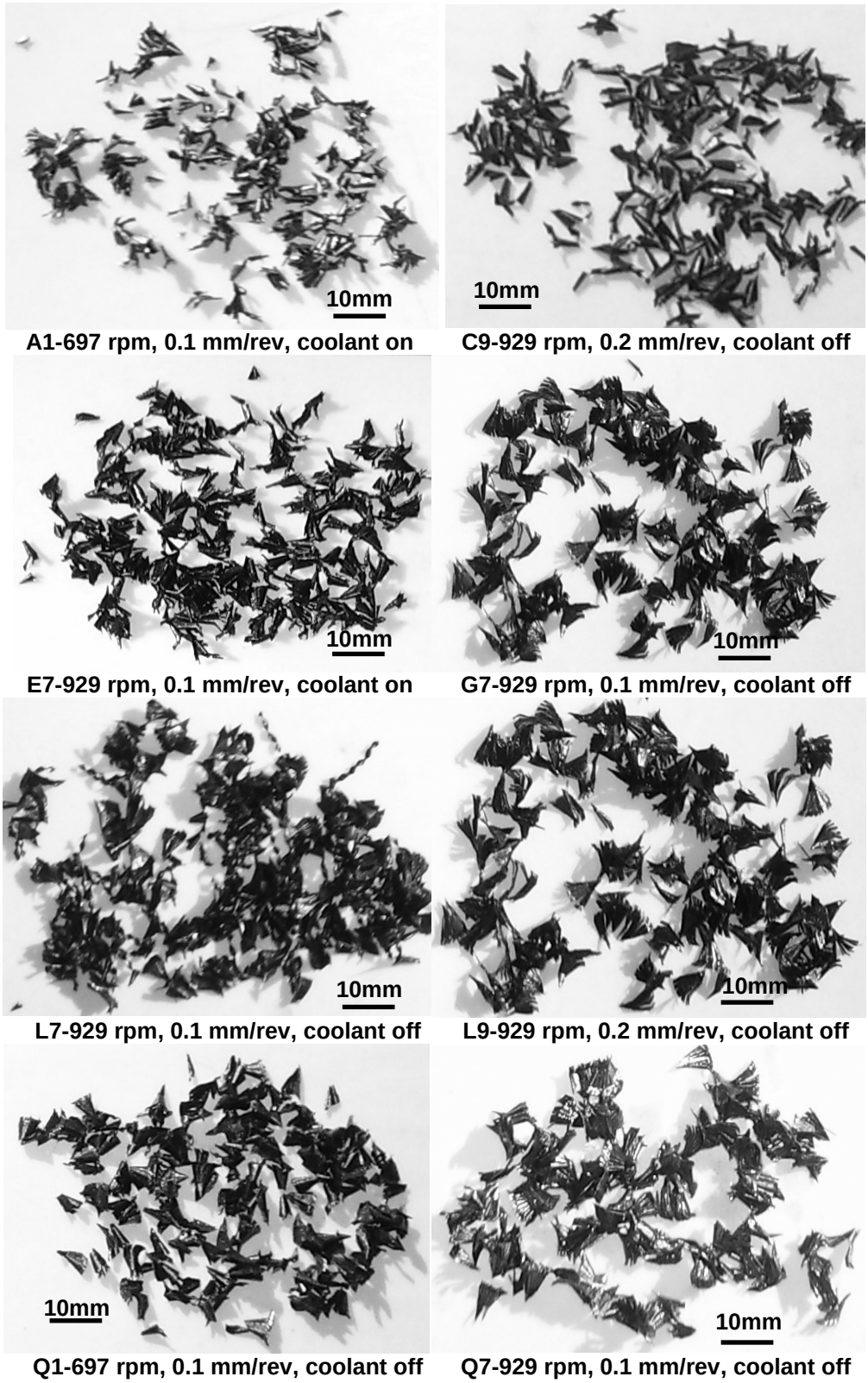

Figure 58: Chip morphology analysis for grades 900, 1050, 1200 and 1400

Some of the common observation during drilling, the effect of BUE formation on work hardening due to SIT and rough surface texture due to clogging of the drill flutes is explained through this study. For almost all samples, the type of chips produced while drilling ADI was classified as discontinuous chips except one or two samples having semi-continuous chips. In Figure 58, for each grade, two samples having variations in chip size and shape are selected. The different types of chip as shown in Figure 58 is classified as needle shaped chips e.g: sample A1 and C9, chisel edge chips e.g: sample L7, fan shaped chips e.g: sample Q1 and amorphous chips or flower shaped chips e.g: sample Q7, L9 and G7 [49, 50]. For lower grades 900 and 1050, at low feed rates and speeds, the chip produced was smaller in size on comparison with the chip produced for high feed rate and speed. As the grade increases from 900 to 1400, the hardness levels in the material increase and this leads to increase in the size of the chip and hence, an increase in cutting force and torque to evacuate the large chips was justified.

According to Nakayama, needle shaped chips e.g: sample A1 and C9 indicate the formation of BUE where the strain hardened workpiece material welds itself to the rake face of the tool [77]. The chisel edge chips for sample L7 was due to the formation of the chip by the chisel edge which extrudes the material to produce long and narrow chips. Feed rate and grade does influence the chip as large chips where observed for samples with high feed rate. There was no significant effect of coolant on the chip size and shape. Similar observation has been reported by other researchers working on ADI and chip morphology [49, 50]. Due to limitations in including chip morphology for all the samples, the chip morphology for rest of the samples is shown under Appendix: chip morphology analysis.

6.4.6 Metallographic analysis

The results from the metallographic examinations of the holes drilled using the combination of cutting parameters given in Table 7 is presented in this section. The verification for phase transformation was accomplished by taking pictures along the hole boundaries. The analysis examines the relationship between ADI microstructure and machinability. According to the Matsuoka et al., the occurrence of SIT is lower in ADI having high nodule count of graphite nodules as there is less amount of retained austenite present, to be transformed to martensite [18]. Moreover, graphite nodule serves the purpose of lubrication and heat dissipation during the machining process.

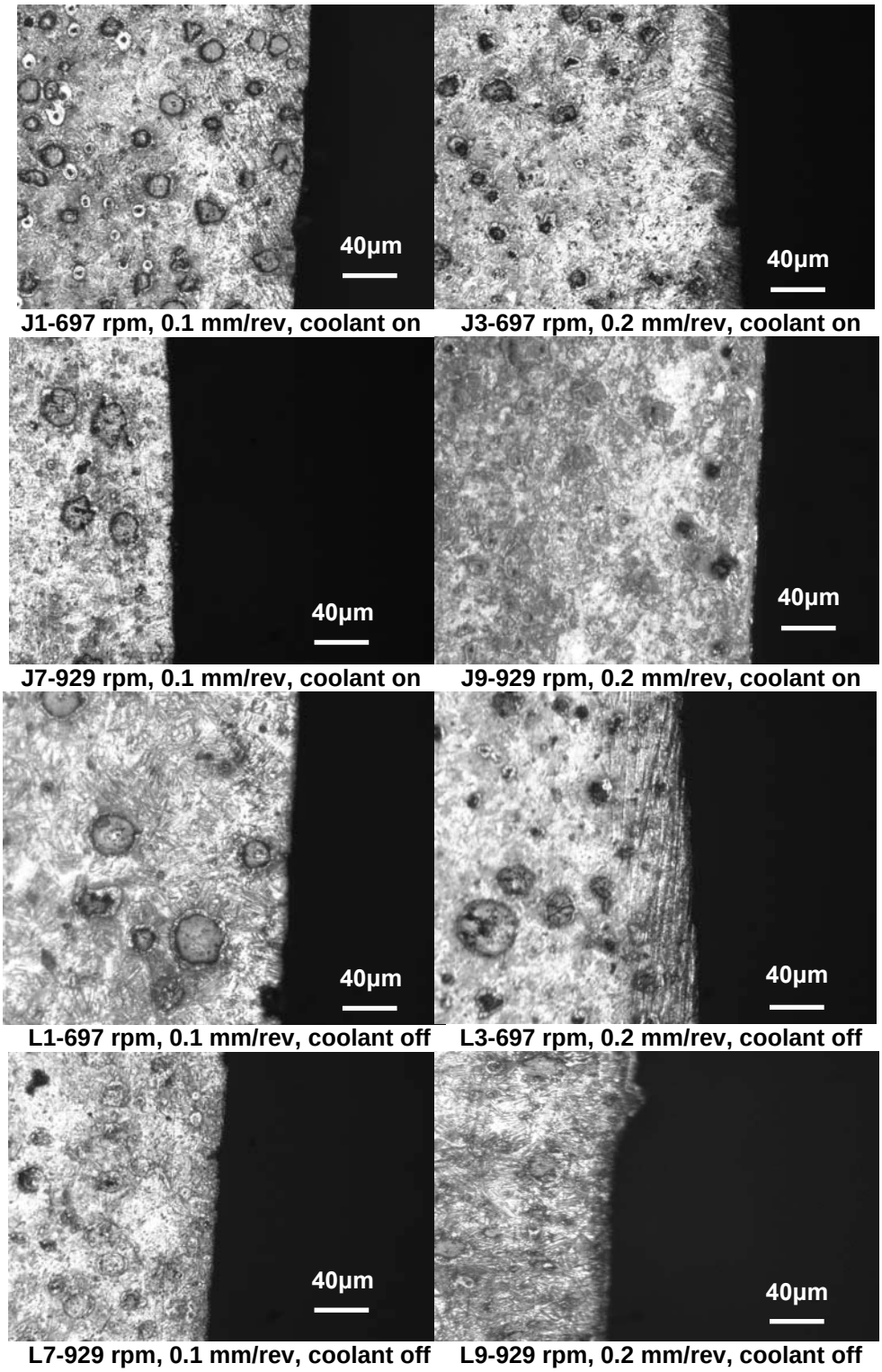

Figure 59: Metallography analysis - grade 1200

Figure 59 shows metallographic images obtained for grade 1200. Metallographic analysis reveals that lower grades of 900 and 1050 have high nodularity which indicates the possibility of occurrence of SIT in these grades was quite low. Grade 1200 was selected as the best grade to examine for phase transformation because of the increased affinity of higher grades towards SIT.

The chosen speeds and feed rate were in ineffective in triggering phase transformation due to SIT for almost all the samples except in few samples for grade 1200 and 1400. The same has been reported in technical conferences-industrial tooling ’08 and MSEC2008. Further study on phase transformations and white layer formations along the hole boundaries was undertaken.

The metallographic results confirm that feed rate plays an important role in determining the extent of SIT during machining. Samples drilled at low feed rate irrespective of the cutting speed and coolant, for any grade of ADI did not show any sign of SIT where as sample drilled at high feed rate did reveal at certain location along the hole boundary, the occurrence of SIT e.g. sample J9 as shown in Figure 59. The effect of feed rate was also confirmed through the Tool failure analysis in section 6.4.7 where, drilling at high feed rate has led to the failure of the tool. The white layer formation along the hole boundaries warrant the need for further study to identify the microstructural phases and quantify if necessary.

As metallography analysis was the final stage of first segment of the research, the machinability assessment of grades 900, 1050, 1200 and 1400, the data obtained was used in selection of grade, cutting parameters and experimental design for the next segment of the research - study on phase transformations. The results from metallography analysis for rest of grades 900, 1050 and 1400 is given under Appendix: Metallography analysis.

6.4.7 Tool failure analysis

The result from the tool failure analysis undertaken on grade 1200 at cutting speed 65m/min, feed rate 755 mm/min and without coolant is given in this section. The result from the analysis is made up of metallography - heat tinting images and microstructural quantification data from the XRD analysis. Thermo-mechanical reaction takes place when a combination of strain and thermal energy is applied to ADI i.e. the retained austenite transforms to hard and brittle martensite. Thermo-mechanical reaction occurs ahead of the tool causing lot of wear and eventually results in tool failure. The importance of using the golden rule of machining ADI-using low feed and high speed is evident. High feed leads to high plastic strain, triggering SIT to occur ahead of the tool and hence, the workpiece material is hardened resulting in rapid tool wear and in extreme situations leading to tool failure.

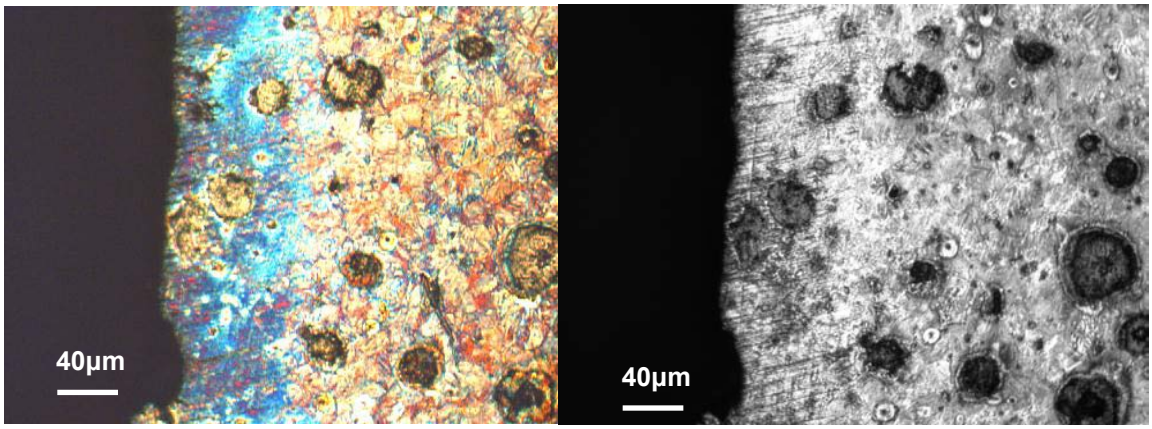

Grade 1200 - tool failure sample Grade 1200 - tool failure sample

Figure 60: Metallography analysis - grade 1200 - tool failure sample

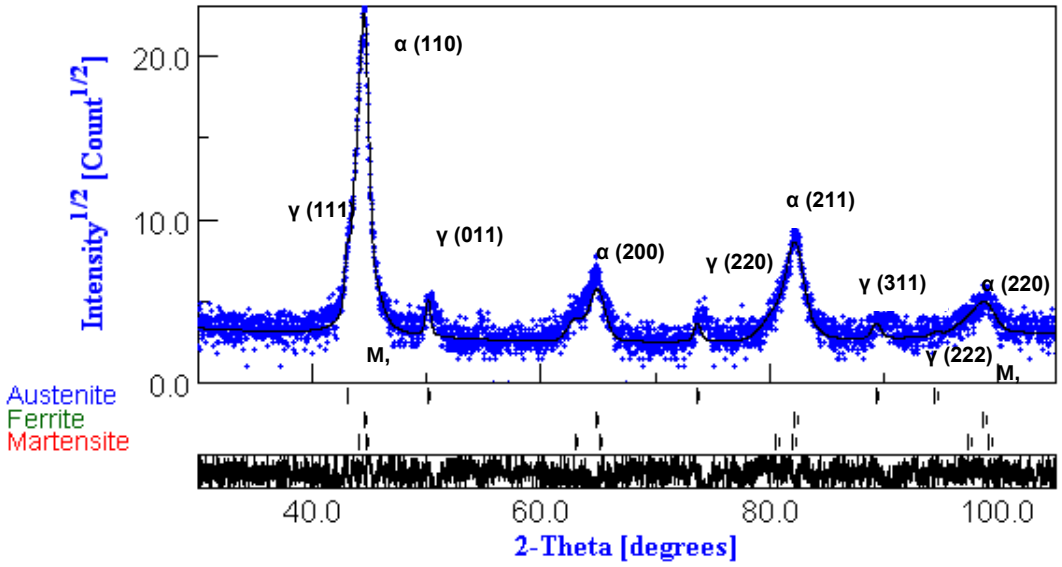

Microstructural phase	Austenite(γ)	Ferrite(α)	Martensite(M)
Weight (%)	5.2 ± 0.2	49.7 ± 3	45.1 ± 3

Figure 61: XRD analysis - grade 1200 - tool failure sample

The metallographic images, both colour and normal for grade 1200 - tool failure is shown in Figure 60. Figure 61 shows the microstructural phase quantification through the XRD peaks obtained for grade 1200 - tool failure using “MAUD” XRD analysis software. Earlier assumption on the probability of occurrence of phase transformation, for a tool failure sample was true, as supportive analysis such as metallography and XRD have shown enough evidence to confirm SIT. The analysis serves to establish a criterion for the minimum amount of martensite required for hardening the material and indirectly leading to tool failure during machining.

6.5 Study on phase transformations

The results from the experiments carried out to establish the relationship between plastic deformation and phase transformation is described here. As explained in section 5.3 the experimentation is mainly divided in two segments: milling trials - plastic strain and temperature effect on microstructure and tensile testing - plastic deformation effect on ADI microstructure. Supportive analysis such as metallography - heat tinting and XRD analysis was used to identify and quantify the microstructural phases.

6.5.1 Milling trials

Milling trials at variable depth of cut on grades 1200 were conducted in order to verify the effect of thermal and plastic deformation energy on phase transformations. The results from the milling trials are presented in this section, which includes effect of plastic deformation on phase transformations using evaluation techniques such as cutting force, metallographic, microhardness and XRD analysis. Temperature measurement was also done in order to understand the effect of thermal energy on phase transformations. As explained in section 5.3.1., the experimental design for milling trials consists of face milling grade 1200 at variable DoC range from 1 to 4 mm, variable coolant condition - dry and wet, at constant speed of 1992 rpm and feed rate of 0.1 mm/tooth. The trials seek to establish a relationship between plastic strain obtained from tensile testing and increase in martensite (%) due to SIT during milling.

Cutting force analysis

As explained earlier in literature review on machinability factors, cutting force is an important factor to judge the likely occurrence of SIT due to machining by giving an in-depth information on the thermo-mechanical reaction taking place in the shear zone. Cutting force analysis was conducted in order to estimate the effect of plastic deformation on phase transformation during milling. For milling, the important parameters under consideration were the forces: thrust force (F_Z) and feed force (F_Y); and moment (M_Z). A comparative analysis was made between dry and wet milling for each DoC. The effect of depth of cut on SIT was verified through these trials by observing any sudden changes in cutting force and moment. Table 11 tabulates the thrust force (F_Z), feed force (F_Y) and moment (M_Z) comparison for wet and dry milling. Results from cutting force analysis were further checked and quantified using metallography and XRD analysis respectively.

Table 11: Thrust (F_Z), Feed force (F_Y) and moment (M_Z) for wet and dry milling - grade 1200

	Dry Machining				Wet Machining			
DoC (mm)	DoC-4	DoC-3	DoC-2	DoC-1	DoC-4	DoC-3	DoC-2	DoC-1
M_z (N-m)	49.09	68.03	36.77	15.61	81.1	97.38	37.37	9.85
F_z (N)	672.77	990.26	838.7	643.22	733.51	1124.51	784.08	531.91
F_y (N)	1018.9	1288.47	959.94	721.30	1254.87	1416.11	914.72	376.52
F_x (N)	362.23	608.92	290.87	143.98	307.2	502.6	285.63	84.75

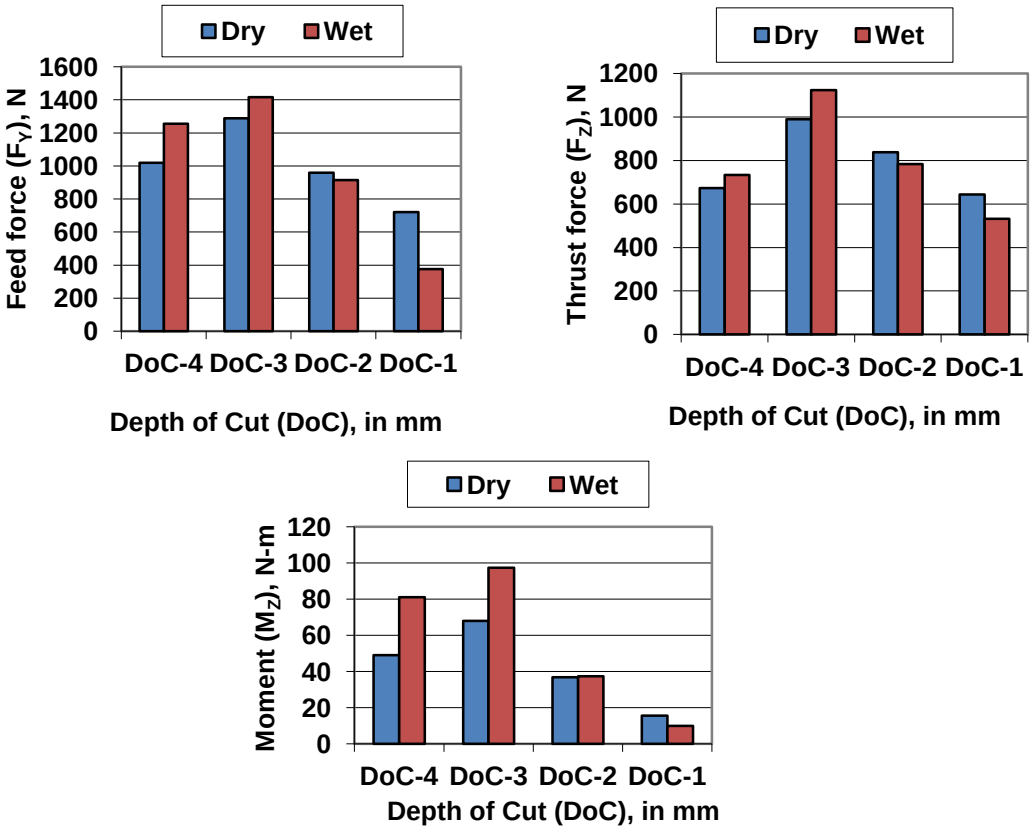

Figure 62: Thrust (F_Z), feed force (F_Y) and moment (M_Z) comparison for wet and dry milling - grade 1200

The thrust force (F_Z), feed force (F_Y) and moment (M_Z) variations for variable DoC under wet and dry milling is shown in Figure 62. It was observed that DoC-3 mm has the highest thrust force (F_Z), feed force (F_Y) and moment (M_Z) for both dry and wet milling. The other significant observation was that the thrust force (F_Z), feed force (F_Y) and moment (M_Z) obtained for wet milling was higher than dry milling. One of the reasons may be due to the effect of tool, as PCBN tool generate high cutting force when a coolant is used. The other reason regards to workpiece material i.e. ADI, was studied using analysis such as metallography and XRD in order to verify the extent of SIT for wet and dry milling.

Metallographic analysis – heat tinting

The samples obtained from the milling trial at variable DoC under dry and wet milling were subjected to identification of microstructural phase using metallography. For easy differentiation of the microstructural phase, colour metallography using heat tinting was selected. Figure 63 and Figure 64 show the metallographic images of the sample subjected to milling at variable DoC under dry and wet machining. The purpose of conducting metallographic analysis was to examine the formation of martensite due to SIT during milling. The heat tinted metallography images shown in Figure 63 and Figure 64 indicates the presence of martensite (dark blue), retained austenite (light blue) and ferrite needle.

Colour metallographic images confirm martensite formation (dark blue) for higher DoC-4 and 3 mm. Retained austenite (light blue) was seen to maximum extent in DoC-1 and 2 mm, which implies that the machining forces were insufficient for SIT to occur leading to martensite formation. From previous observation of heat tinting trials, it was confirmed that all grades of ADI used in the experiments contain some amount of retained austenite due to improper heat treatment techniques and defects. Hence, unstable retained austenite was seen on all grades of ADI.

The heat tinted images corroborates with cutting force results as DoC-3 and 4 mm generate higher cutting force than DoC-1 and 2 mm. On comparison of the heat tinted images for wet and dry milling under variable DoC, it was observed that the transformation of retained austenite to martensite due to SIT was high in case of wet milling. The microstructural phases identified are quantified using XRD analysis.

XRD analysis

Machined (milling) sample obtained from the milling trial at variable DoC under dry and wet milling were subjected to quantification of microstructural phase using XRD. A similar quantification technique as explained in section 5.3.2 was used to quantify the microstructural phases. Table 12 tabulates microstructural phase quantification data for wet and dry milling. A comparative analysis was done between the martensite content before and after milling. The reason for experiencing high cutting forces for wet milling was also investigated using XRD.

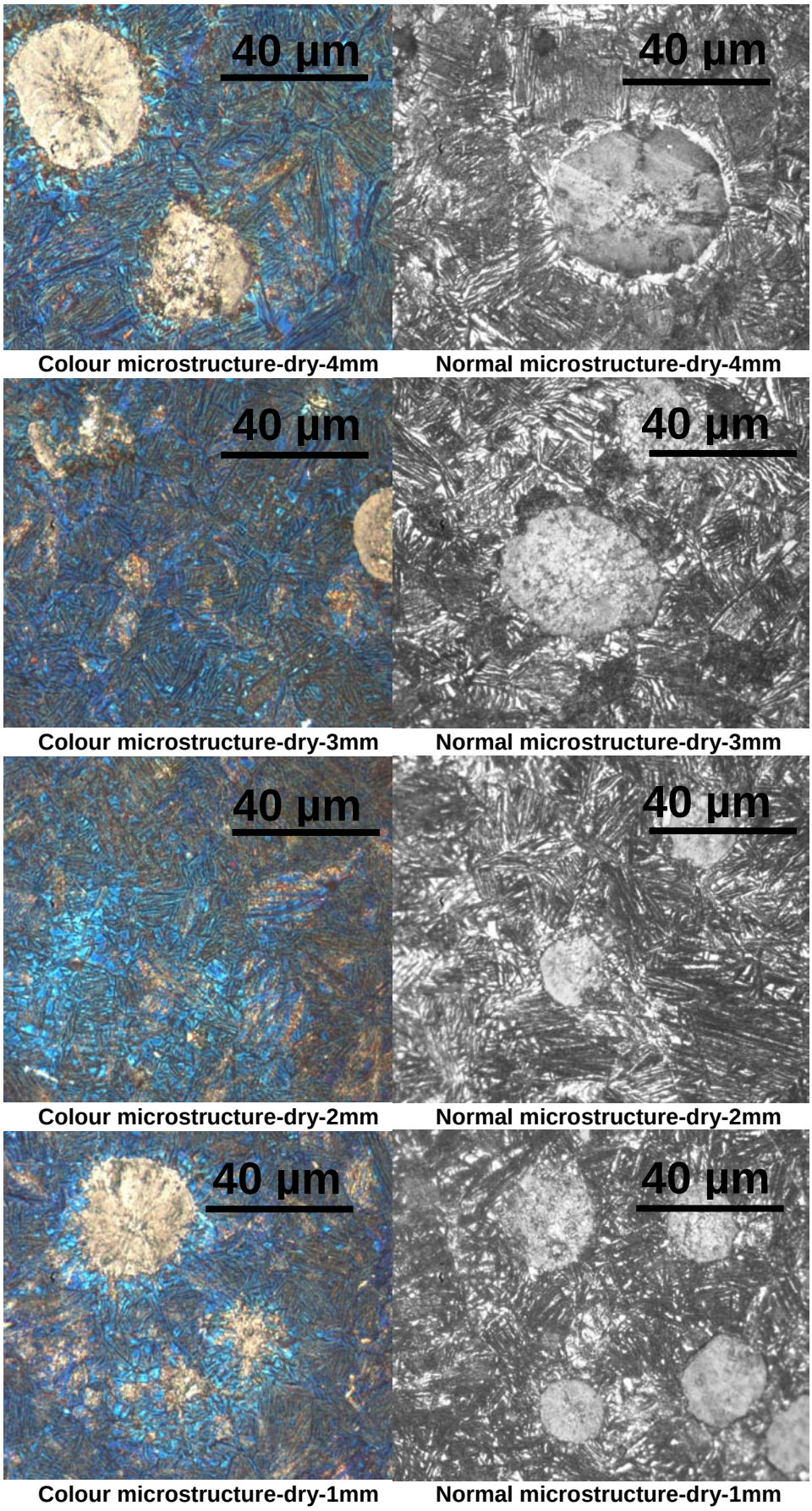

Figure 63: Metallography for DoC (in mm) - 4, 3, 2 and 1 for dry milling - grade 1200

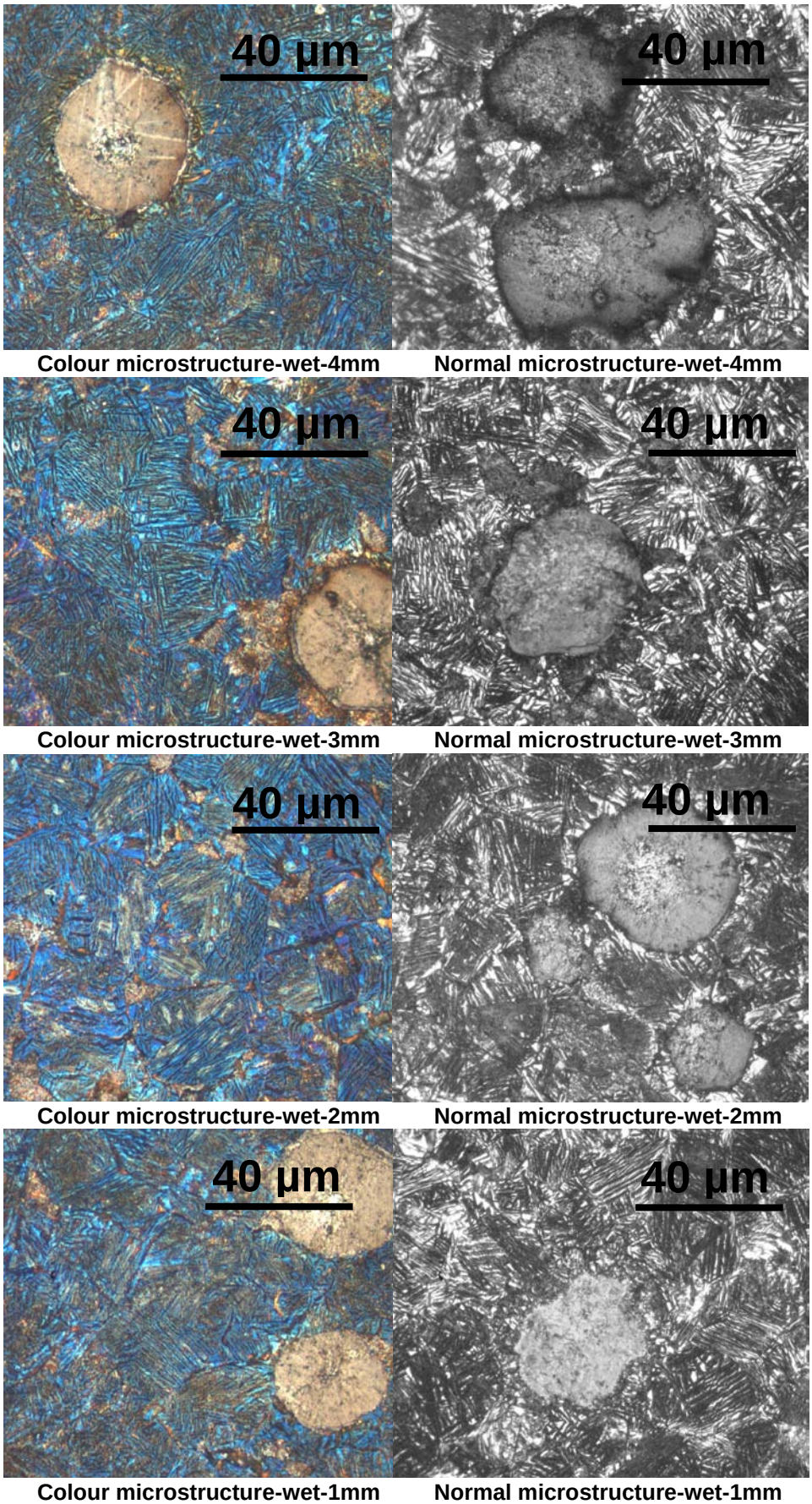

Figure 64: Metallography for DoC (in mm) - 4, 3, 2 and 1 for wet milling - grade 1200

Table 12: Microstructural phase quantification data for wet and dry milling - grade 1200

	Wet milling			Dry Milling		
	Martensite (wt%)		Increase in Martensite (wt%)	Martensite (wt%)		Increase in Martensite (wt%)
DoC (mm)	Before	After		Before	After	
4	0.2	22.1	21.9	0.2	17.5	17.3
3	0.2	25	24.8	0.2	24.6	24.4
2	0.2	17	16.8	0.2	19.4	19.2
1	0.2	12	11.8	0.2	17.6	17.4

The initial martensite content for grade 1200 was obtained from the XRD analysis of basic samples and the increase in martensite content was evaluated in order to confirm an occurrence of SIT. It was observed that high martensite content obtained for DoC-3 mm under wet and dry milling corroborate high cutting forces for DoC-3 mm under wet and dry milling. The amount of martensite formed during wet milling justifies the fact that higher forces were obtained for wet milling in addition to the effect of using PCBN tools. The increase in martensite (wt%) was calculated for each DoC as shown in Table 12. The highest martensite (25 wt%) increase was for DoC-3 mm under wet milling and the least (12 wt%) was for DoC-1 mm under wet milling.

The quantification data obtained corroborates with the results from metallographic analysis. Hence, the effect of plastic strain on SIT during milling was confirmed by relating the microstructural quantification data and the plastic strain from tensile tests. XRD data for DoC-4 and 3 mm for wet and dry milling is shown in Figure 65 and Figure 66 respectively. Due to limitation in reporting, XRD data for rest of the samples is given under appendix. The main microstructural constituents; austenite, ferrite and martensite were quantified as shown in Figure 65 and Figure 66. It should be noted that the phase quantification of XRD data using MAUD is a semi–quantitative process.

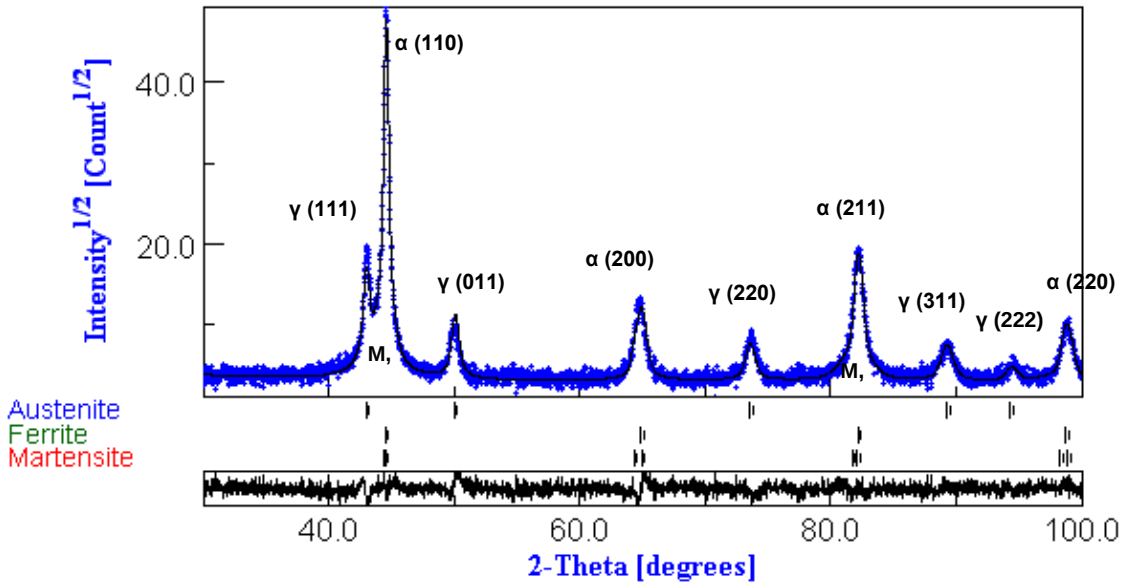

Microstructural phase	Austenite(γ)	Ferrite(α)	Martensite(M)
Weight (%)	18 ± 0.3	60 ± 1	22.1 ± 0.85

DoC-4 mm

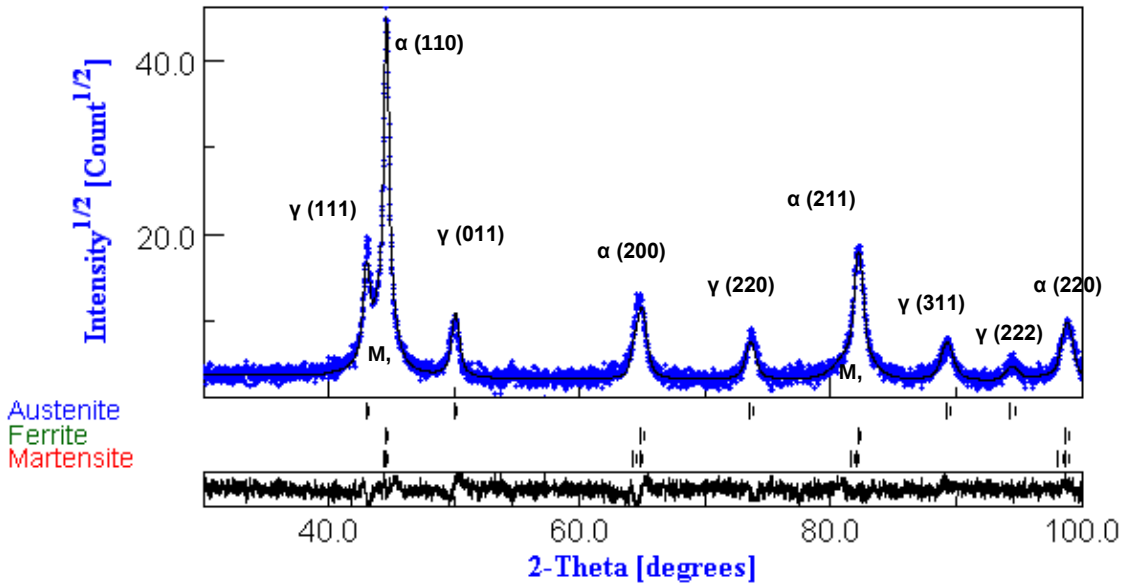

Microstructural phase	Austenite(γ)	Ferrite(α)	Martensite(M)
Weight (%)	18.2 ± 0.3	57 ± 1.2	25 ± 1

DoC-3 mm

Figure 65: XRD data for DoC-4 and 3 mm for wet milling

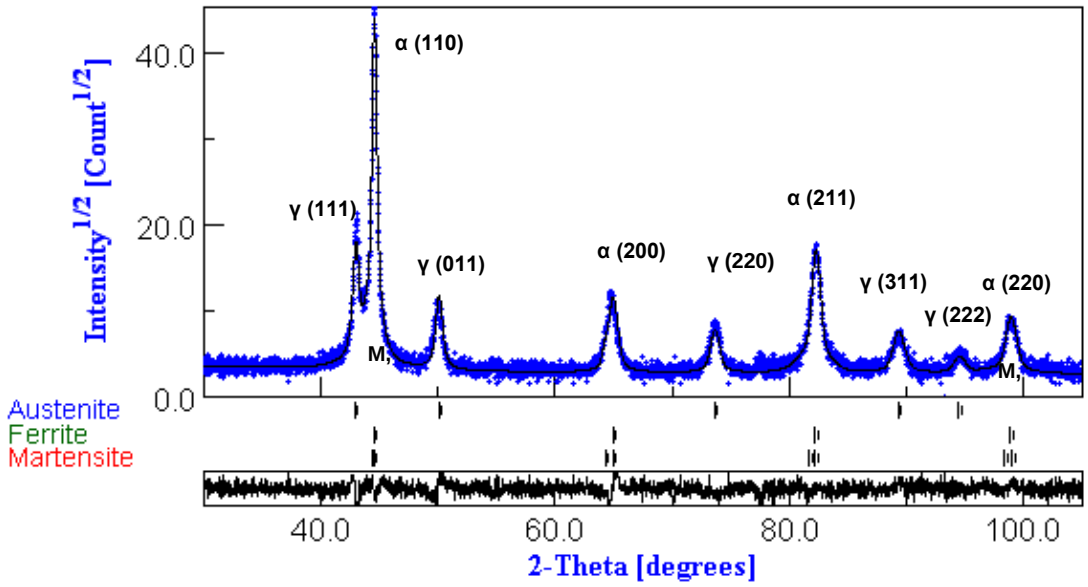

Microstructural phase	Austenite(γ)	Ferrite(α)	Martensite(M)
Weight (%)	21.4 ± 0.3	61.1 ± 1.4	17.5 ± 1.2

DoC-4 mm

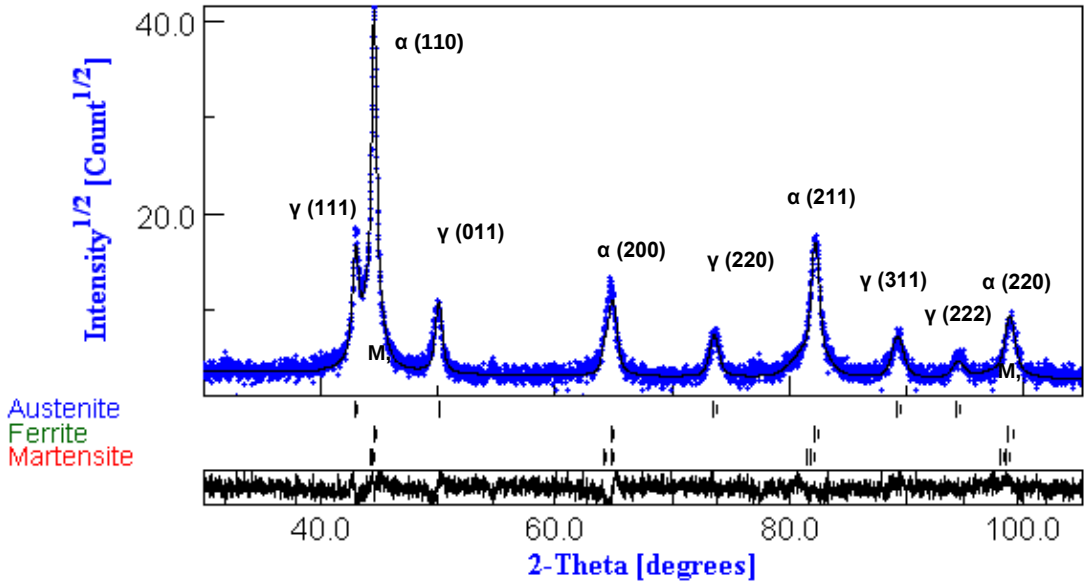

Microstructural phase	Austenite(γ)	Ferrite(α)	Martensite(M)
Weight (%)	19.3 ± 0.3	56 ± 1.3	24.6 ± 1.1

DoC-3 mm

Figure 66: XRD data for DoC-4 and 3 mm for dry milling

Temperature measurement

The effect of thermal energy on martensite formation due to phase transformation during milling under wet and dry milling at variable DoC was investigated using the temperature measurements.

The thermocouple readings taken during milling were used to evaluate the amount of thermal energy involved during milling. As explained in section 5.3.1, temperature measurements were done for DoC-3 and 1 mm by placing thermocouple along the path of the cutter. The effect of coolant on cutting action of the tool and thermal energy generated in the cutting zone was evaluated using temperature measurements. It was confirmed that ADI is a good thermal conductor due to the presence of graphite. Hence, the effect of ADI material properties during dry milling was also investigated. Figure 67 and Figure 68 shows the time-temperature graph for DoC-3 and 1 mm under dry and wet milling respectively.

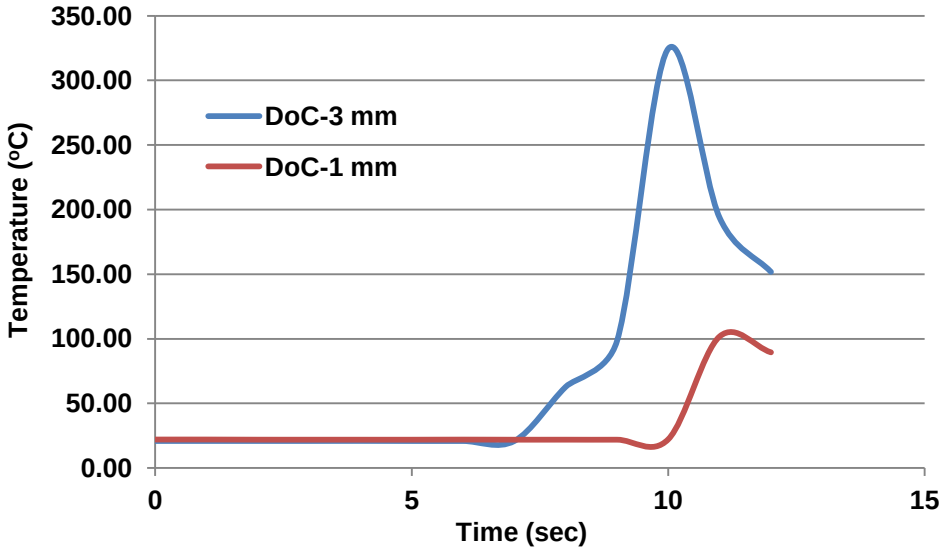

Figure 67: Time-Temperature graph for DoC-3 and 1 mm - dry milling - grade 1200

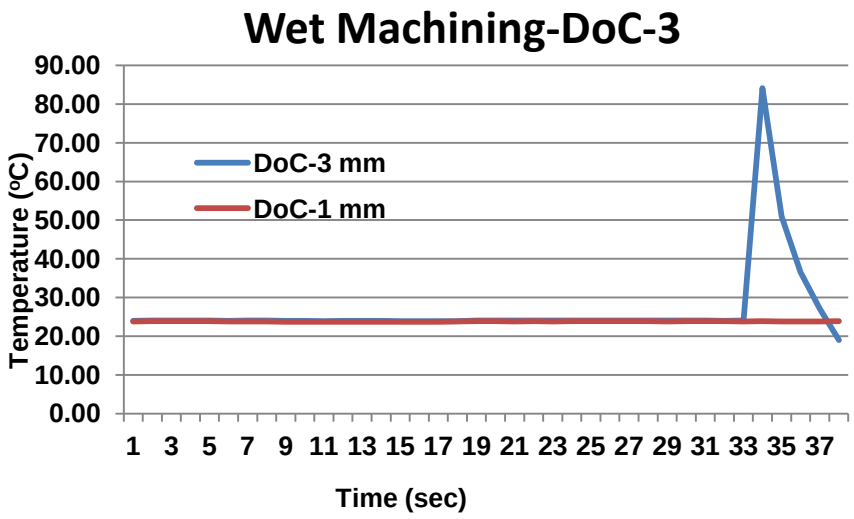

Figure 68: Time-Temperature graph for DoC-3 and 1 mm - wet milling - grade 1200

Table 13: Thermal energy for DoC-3 and 1 mm - wet and dry milling - grade 1200

	Dry milling		Wet milling	
DoC (mm)	Temperature rise (K)	Thermal energy (J/sec)	Temperature rise (K)	Thermal energy (J/sec)
3	576	12319.5	333	7159.5
1	348	7482	0	0

Thermal energy generated in the shear zone was calculated for DoC-3 and 1 mm under dry and wet milling and tabulated in Table 13. As the process of temperature measurement involves heat loss and instrumentation error due to time lag, the measurement technique was considered to be a semi-quantitative technique with considerable error. Some consideration should also be given to the shorter cutting time as the cut lasted roughly about 2-4 sec, as the cutter had to cover roughly 25mm (out of 110mm) for each DoC. An extensive study was required to study the various techniques for efficient temperature measurements. The temperature rise for DoC-1 mm under wet milling was too small and hence, the thermal energy was assumed to be zero. The results attempt to establish a relationship between the thermal energy in the shear zone and the martensite formation due to SIT. Thermal energy (J/sec or watt) involved during milling was calculated using equation 4-7 given in section 4.3.6, where thermal conductivity of grade 1200 was taken as 21.2 W/m-K, according to ASTM-897 standards.

6.5.2 Tensile testing - standard specimen

The purpose of conducting tensile test on grades 900, 1050, 1200 and 1400 was to establish the relationship between the microstructural phase change and plastic deformation. The data obtained from the tensile test conducted on tensile samples made out of grades 900, 1050, 1200 and 1400 is presented in this section. The output data consists of a graph between the tensile load (y-axis) and elongation (x-axis). Using the cross-section area of the sample and considering the 0.2% proof load (N), the value of yield stress, UTS and elongation (%) was calculated. Hardening factor known as strain hardening exponent was also calculated using the tensile test data. UTS and elongation (%) were used as benchmark to analyse the tensile data. A comparative study was conducted between the tensile test results and ASTM897-06A standards. The purpose of this comparative study was to check for any deviations from the regular range mentioned in the standards. Any abnormality was picked up as a sign for phase transformation. Indeed, abnormality was observed in UTS values for grade 1400.

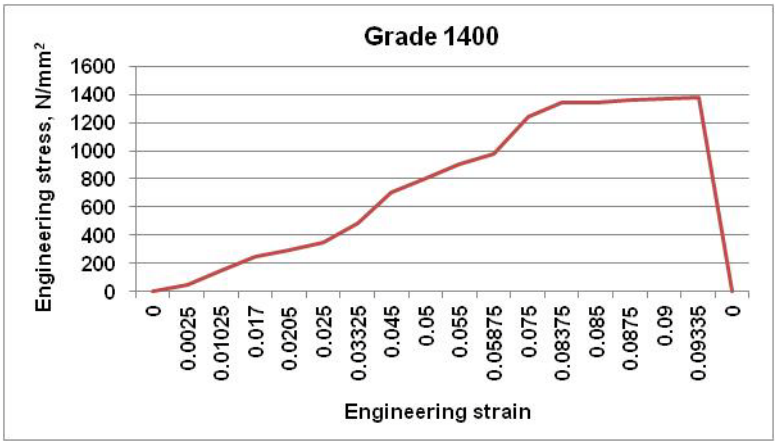

Figure 69: Engineering stress-strain curve for grade 1400

Table 14: Comparison between ASTM897-06M and tensile test results for Ultimate Tensile Strength (UTS) and Elongation (%)

	Grade 900	Grade 1050	Grade 1200	Grade 1400
Ultimate Tensile Strength (UTS), MPa, minimum ASTM 897-06	900	1050	1200	1400
Experimental UTS, MPa,	1130	1097	1373	1337
Elongation(%),minimum ASTM 897-06	9	7	4	2
Experimental Elongation (%)	12	14	11	9

A sample stress strain curve for grade 1400 is shown in Figure 69. The comparison between the standard, ASTM 897M-06 values and the tensile test results for grades 900, 1050, 1200 and 1400 are shown in Table 14. The elongation (%) and UTS values (displayed in Figure 69 and Table 14) represents the average values of the five tensile tested samples. The ASTM 897M-06 standard values of elongation (%) and UTS used represent the minimum value for each grade.

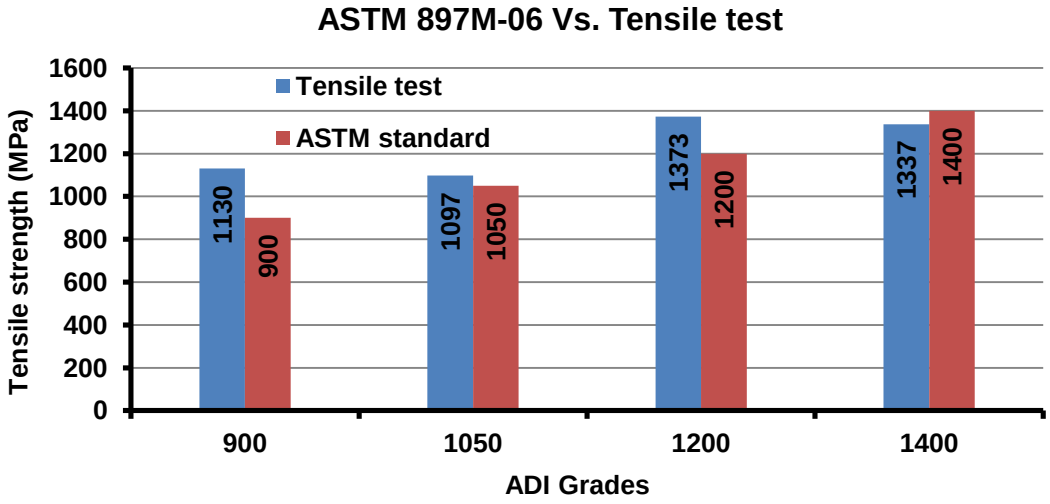

Figure 70: Comparison of UTS between the ASTM-897M-06 and experimental results

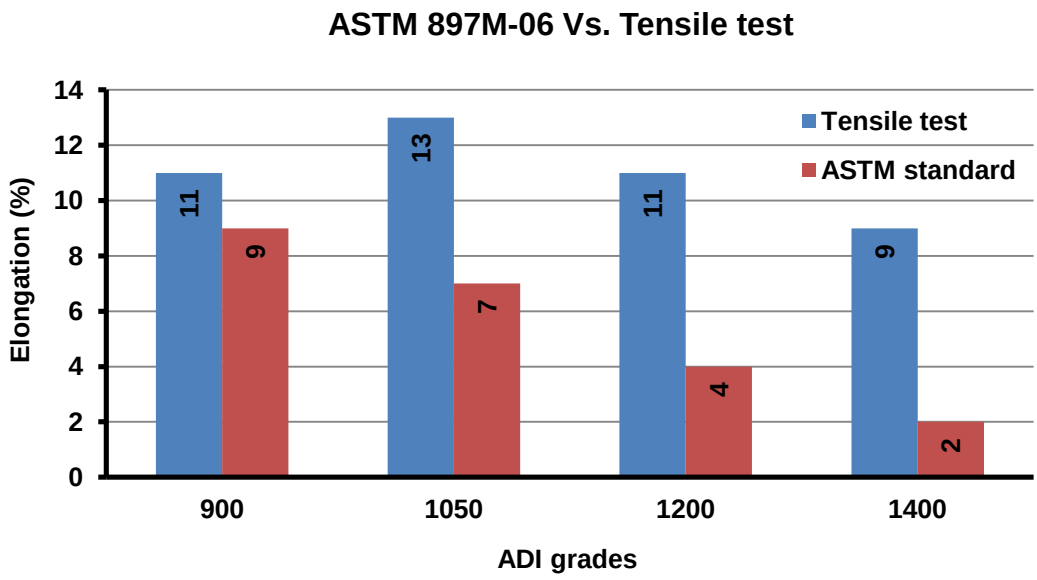

Figure 71: Comparison of elongation (%) between the ASTM-897M-06 and experimental results

Figure 70 and Figure 71 shows the graph comparing the UTS and elongation (%), according to ASTM 897M-06 standards and the tensile test results. The tensile test results imply that the UTS and elongation (%) were consistent with the ASTM standards except for grade1400. Grade 1050 has the maximum elongation-13% and grade 1200 was the best grade showing optimum values of elongation-11% and UTS-1373 MPa. Tensile test modelling using ANSYS was also done to validate the experimental data.

Strain hardening exponent

Strain hardening exponent (n) is an important factor in evaluating the chances of work hardening due to SIT in ADI. Strain hardening exponent conveys the plastic behaviour of a material during machining. A material with higher 'n' value has greater tendency for work hardening due to SIT. Ideally, for most materials, the value of 'n' lies between zero and one. The range of strain hardening exponent represents a true plastic or a linearly elastic material. e.g. n=0, for a true plastic material and n=1 for an elastic linear material. According to the ASTM A897-03 standard, the value of 'n' is from 0.133 to 0.160 for grades 900 to 1400 respectively. According to the paper published by Jakob et al. on plastic behaviour of ADI, the range of 'n' is found to be from 0.05 to 0.3 [75]. Any material with lower 'n' value is said to be having good machinability characteristics and less tendency to work harden due to SIT during machining.

Estimation of strain hardening exponent for ADI was justified as major part of this research deals with phase transformations in ADI due to SIT during machining. The tensile test data of grades 900, 1050, 1200 and 1400 was used to calculate the engineering stress and strain. The engineering strain data from the tests represents the sum of elastic and plastic strain. Within an elastic limit, there exists a linear relationship between the stress-strain and non-linear for a plastic zone. On substituting these values as shown in Table 14, in equation 6-1, the value of strain hardening exponent (n) obtained for grade 1200 was 0.178, which was nearly equal to the strain hardening exponent (n), 0.143 according to the standard, ASTM A897-03.

Table 15: Stress -strain data from plastic region of the curve

Grade 900						
	True Stress(σ)	True Strain(Є)	y	x	xy	x^2
1	952.666	0.069526	6.859264	-2.66605	-18.2872	7.107842
2	983.4892	0.072321	6.891107	-2.62665	-18.1005	6.899266
3	1007.951	0.074644	6.915675	-2.59503	-17.9464	6.734187
4	1137.044	0.09531	7.036187	-2.35062	-16.5394	5.525408
5	1189.817	0.110109	7.081555	-2.20628	-15.6239	4.867682
		Summation(Σ)	34.78379	-12.4446	-86.4974	31.13439
Grade 1050						
1	1006.436	0.060154	6.914171	-2.81085	-19.4347	7.90087
2	1056.269	0.067659	6.962498	-2.69328	-18.752	7.253758
3	1066.51	0.072321	6.972147	-2.62665	-18.3134	6.899266
4	1146.693	0.09531	7.044637	-2.35062	-16.5593	5.525408
5	1241.793	0.128723	7.124312	-2.05009	-14.6055	4.20288
		Summation(Σ)	35.01777	-12.5315	-87.6648	31.78218
Grade 1200						
1	1414.474	0.072321	7.254513	-2.62665	-19.055	6.899266
2	1498.197	0.079273	7.312018	-2.53486	-18.5349	6.425492
3	1540.448	0.086178	7.339829	-2.45134	-17.9924	6.009087
4	1581.384	0.09531	7.366056	-2.35062	-17.3148	5.525408
5	1613.851	0.107463	7.386379	-2.23061	-16.4761	4.975602
		Summation(Σ)	36.65879	-12.1941	-89.3733	29.83486
Grade 1400						
1	1452.394	0.080427	7.280969	-2.5204	-18.351	6.352427
2	1459.357	0.08158	7.285751	-2.50617	-18.2593	6.280895
3	1483.918	0.083881	7.302441	-2.47835	-18.098	6.142221
4	1495.297	0.086178	7.31008	-2.45134	-17.9195	6.009087
5	1504.155	0.089246	7.315987	-2.41635	-17.678	5.838769
		Summation(Σ)	36.49523	-12.3726	-90.3059	30.6234

$$n = \frac{N\sum_{i=1}^{N} x_i y_i - \sum_{i=1}^{N} x_i \sum_{i=1}^{N} y_i}{N\sum_{i=1}^{N} x_i^2 - (\sum_{i=1}^{N} x_i)^2} \quad \text{----------} \quad 6\text{-}1$$

To consider the effect of plastic strain and also to calculate the value of 'n', the engineering stress and strain directly obtained from the tensile test was converted into true stress and strain, i.e. representation of stress-strain curve on a logarithmic scale. Hence, true plastic strain from the test was separated from the total strain and was used to calculate strain hardening exponent (n). Strain hardening exponent (n) was calculated using the formula given in equation 6-1. Using equations given in section 5.3.2, the values of logarithmic stress(y) and strain(x) were calculated.

Similar observation was reported by Jakob et al. in the research papers related to effect of austempering temperature and time on plastic behaviour of ADI [75]. Figure 72 shows the graph representing the comparison of strain hardening exponent between the ASTM 897-03 standards and experimental results. According to the graph shown in Figure 72, grade 1200 and 1400 were the results having the value of strain hardening exponent close to the ASTM-A897 standards. A large deviation from the standards was observed in case of grade 900 and 1050 may be due to the material defects. Overall, the strain hardening exponent for grade 1200 and 1400 does imply the ability of the material to undergo SIT during machining and the same was observed from the first segment of the thesis – evaluating ADI machinability.

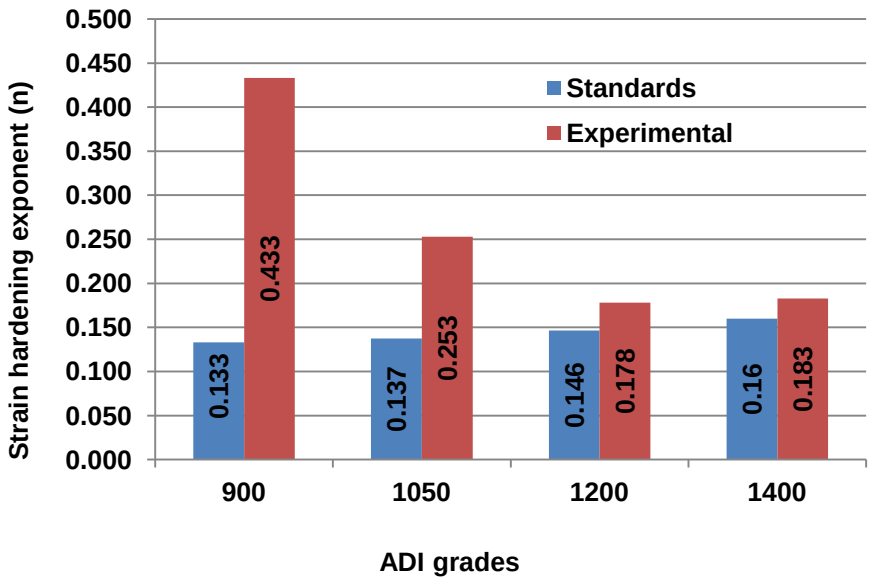

Figure 72: Comparison of strain hardening exponent

Metallographic analysis - heat tinting

A comparative evaluation of the microstructural phases, before and after tensile testing for grades 900, 1050, 1200 and 1400 is given in Figure 73.

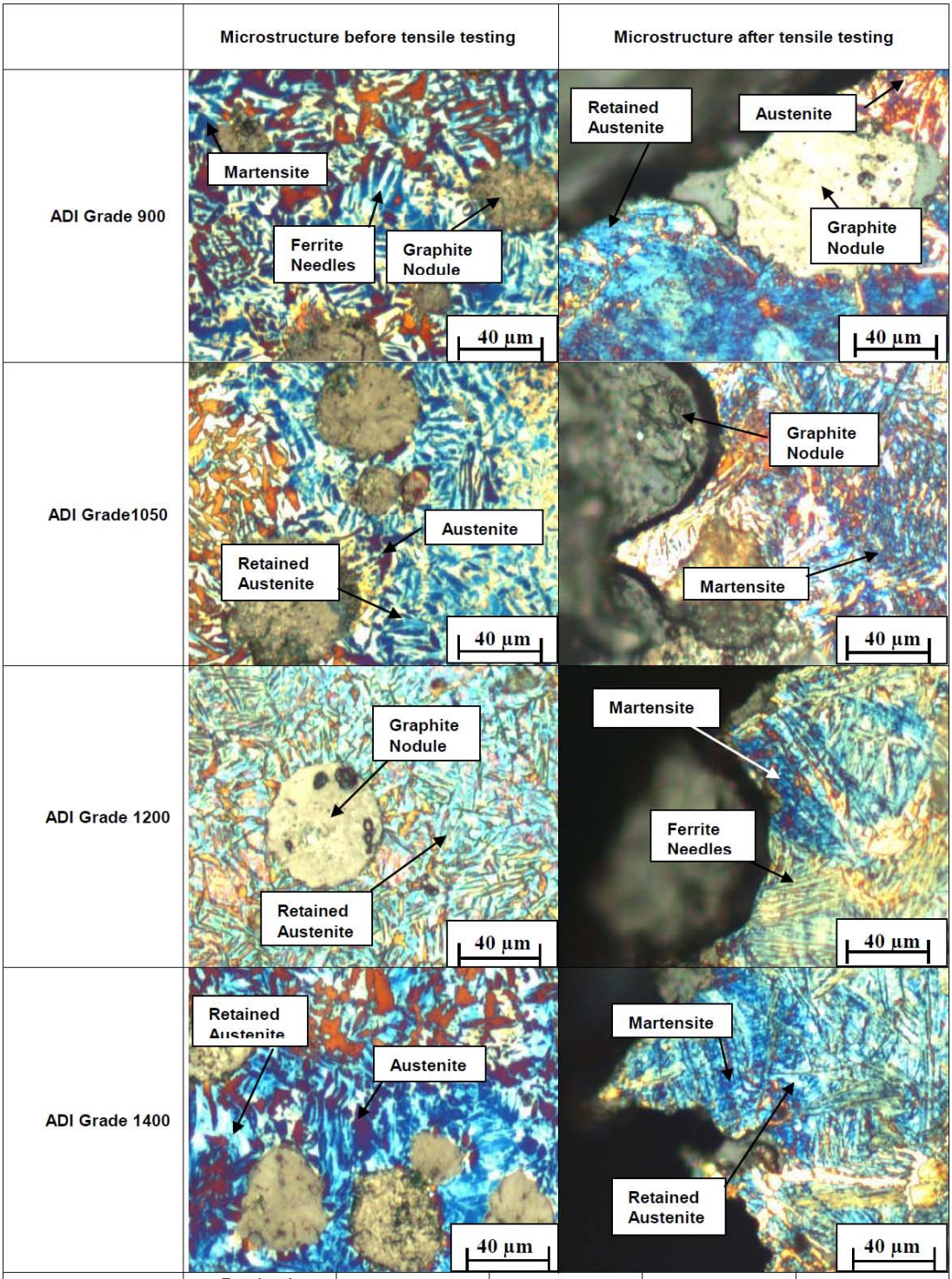

Figure 73: Comparison of microstructure before and after tensile test

The initial results appear to indicate the occurrence of SIT on all grades of ADI. SIT was excessively seen on grade 1200 and 1400, which needs further verification. Generally, improper casting and heat treatment techniques lead to increase in percentage of retained austenite in ADI. Hence, ADI with higher amount of retained austenite has greater tendency for SIT during machining. Further, SIT leads to hardening of the material due the transformation of retained austenite to martensite on increase in machining parameters (strain rate). Similar analogy was applied to the microstructure after tensile testing where the regions marked martensite (dark blue) are randomly distributed, near to the fractured surface. On comparing the microstructure after the test for grade 900, 1050, 1200 and 1400, the percentage of dark blue region was increasing steadily. It is a common observation that for a Fe-C alloy containing more martensite, its mechanical properties such as hardness are considerably higher.

Figure 73 shows that retained austenite (light blue) is the most dominant microstructural phase before tensile testing on all grades of ADI. The tensile test results in Table 14 and metallographic results in Figure 73 indicate the trend, higher the grade, larger the UTS values with lower elongation (%). The reason for the low experimental UTS values of grade 1400 was explained using the separation shown in Figure 74. The specimen (grade 1400) was having higher proportion of retained austenite and considerable amount of martensite before tensile test due to improper casting and heat treatment techniques, in addition to the martensite formed from SIT. Hence, the specimen was expected to fracture at lower UTS. The above reasoning has been confirmed using heat tinting as shown in Figure 74.

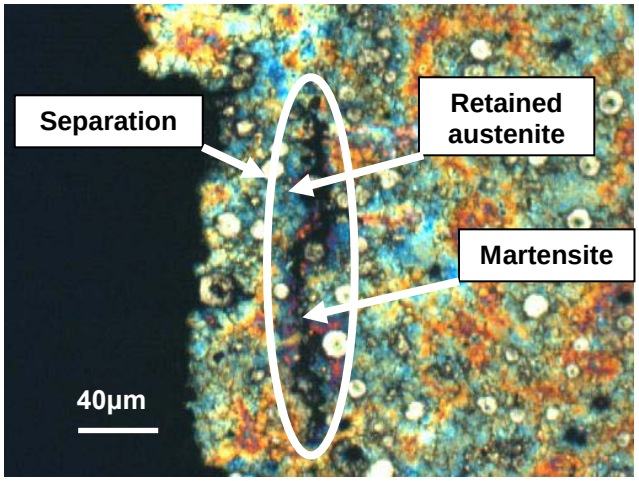

Figure 74: Phase transformation around separation close to fracture region of grade 1400

XRD analysis

The fracture samples obtained from the tensile test using standard specimen were subjected to XRD analysis in order to quantify the microstructural phase. As explained in section 5.3.1, basic samples of grade 900, 1050, 1200 and 1400 (before tensile test) and corresponding fracture samples (after tensile test) were subjected to XRD analysis. XRD analysis was mainly focused on quantification of the three important microstructural phases i.e. austenite, ferrite and martensite. The increase in martensite content on comparison with the martensite content for a basic sample was taken as evidence for SIT, where retained austenite transforms to martensite. The results from the XRD analysis were corroborated with the metallographic examination results of the fractured samples. The objective behind XRD analysis was to establish a relationship between the increase in martensite content and corresponding plastic strain.

As explained in section 5.3.1 on XRD, MAUD software was used to quantify the microstructural phase using the XRD data. XRD results after quantification using XRD software "MAUD" represent the weight (%) of the microstructural phase. Figure 75 and Figure 76 shows the corresponding XRD data for a grade 900-basic and tensile fractured sample.

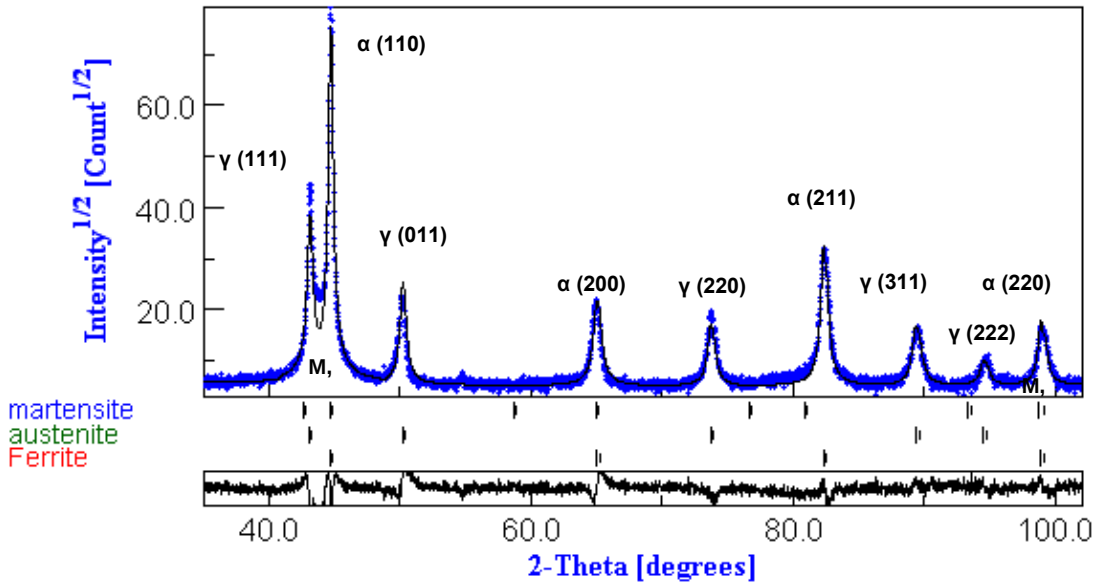

Microstructural phase	Austenite(γ)	Ferrite(α)	Martensite(M)
Weight (%)	30.4 ± 0.5	69.3 ± 0.8	0.4 ± 0.3

Figure 75: XRD analysis - grade 900 - basic

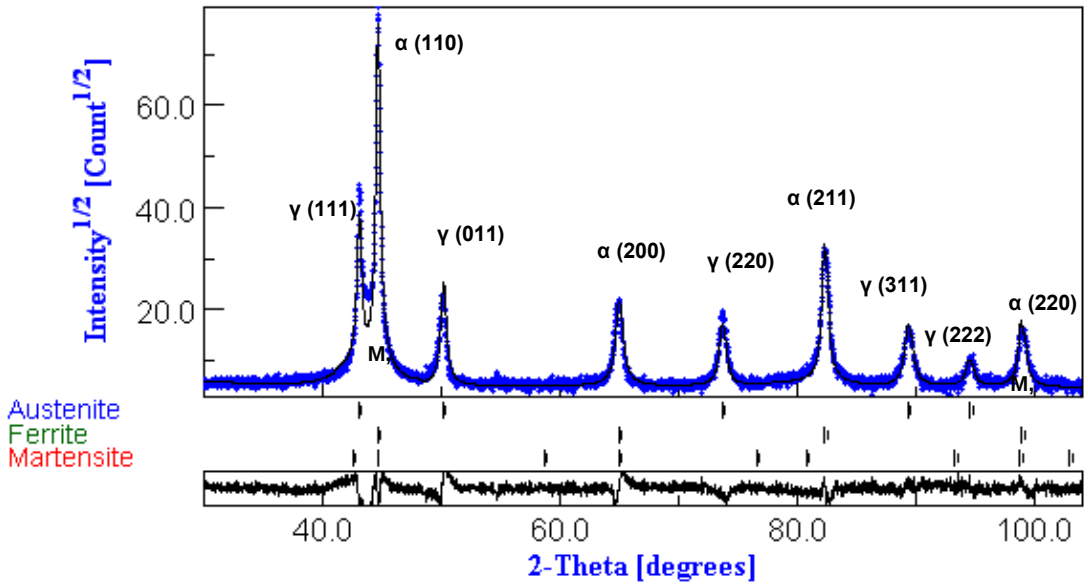

Microstructural phase	Austenite(γ)	Ferrite(α)	Martensite(M)
Weight (%)	28.7 ± 0.3	66.5 ± 0.5	4.9 ± 0.3

Figure 76: XRD analysis - grade 900 - tensile standard specimen

The quantification data related to the microstructural phases is given below each figure. On comparison of the martensite (wt%), it was clearly evident that for grade 900, there was an increase in martensite after tensile testing due to SIT. Considering the tensile test results for grade 900, a relationship was established between the plastic strain (0.1) and strain hardening exponent (0.433) for percentage increase in martensite. Table 16 shows the plastic strain data, strain hardening exponent and corresponding final martensite content for grades 900, 1050, 1200 and 1400. It was assumed that the weight (%) of graphite remains constant for all the samples. The XRD peaks and quantification data for grades 1050, 1200 and 1400, for a basic and tensile standard specimen is found under appendix.

Table 16: Plastic strain - final martensite (wt%) data for grades 900, 1050, 1200 and 1400

	Plastic strain (ε_p)	Strain hardening exponent (n)	Martensite (wt%)	
			Initial	Final
Grade 900	0.11	0.433	0.4	4.9
Grade 1050	0.13	0.253	1.8	4.5
Grade 1200	0.11	0.178	0.2	3.1
Grade 1400	0.01	0.183	0.1	1.2

6.5.3 Tensile testing - tapered specimen

The results from tensile testing using a tapered specimen for grade 1200 and 1400 is displayed in this section. Tapered specimens were considered in order to have a variable cross-sectional area and corresponding variable strain along the gauge length. As explained in section 5.3.3, cross-sectional area along the gauge length was divided into three zones: small, medium and large. Table 17 shows the maximum elongation (%) which includes elastic and plastic deformation, obtained at the three zones for grade 1200 and 1400. The purpose behind conducting tensile testing using tapered specimen was to obtain higher elongation due to reduced cross-sectional area (as shown in Figure 77). The effect of elongation on the microstructure was further examined using supportive tests such as metallography and microhardness.

Table 17: Tensile testing tapered specimen

	Elongation (%)		Tapered specimen		
	ASTM standards	Standard specimen	Elongation (%)		Standard error
Grade 1200	4	11	Large	2.77	0.03
			Medium	4.27	0.02
			Small	7.50	0.03
Grade 1400	2	9	Large	2.68	0.04
			Medium	4.15	0.30
			Small	7.65	0.02

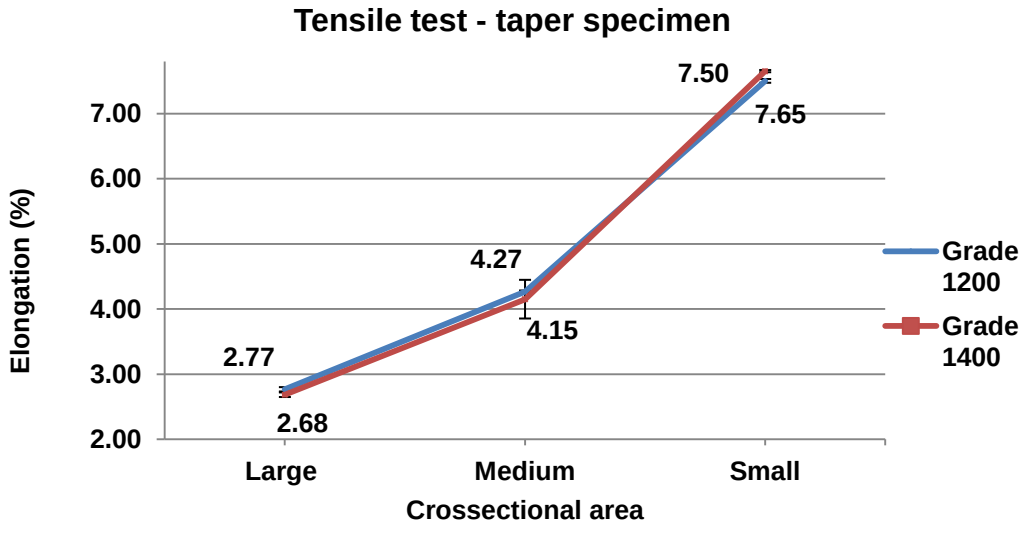

Figure 77: Tensile test tapered specimen - grade 1200 and 1400

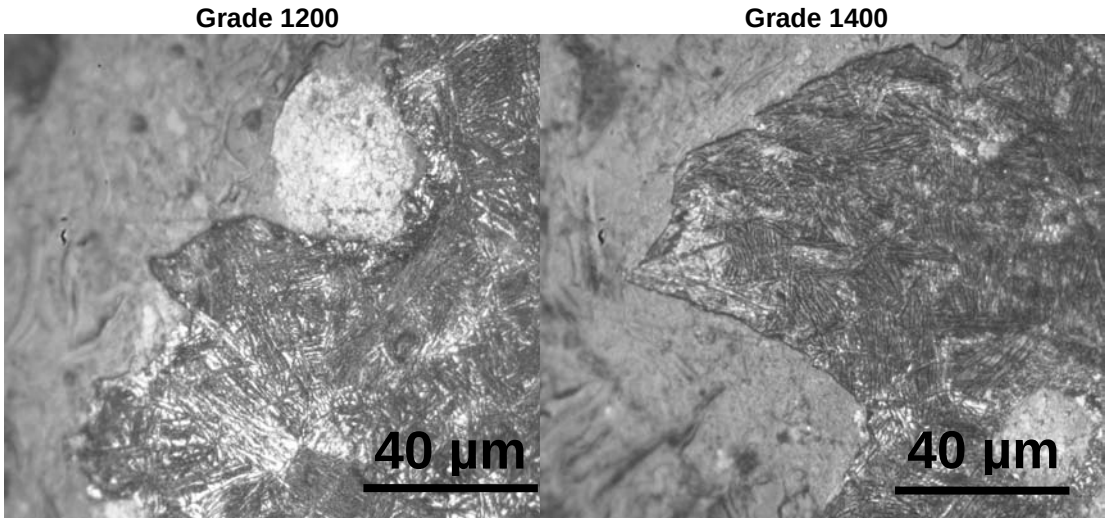

Figure 78: Metallography analysis - tensile tapered samples

Metallographic analysis - tapered specimen

The fractured tapered samples from the tensile test are subjected to metallographic analysis, similar to the technique used for tensile test using standard sample except heat tinting. Figure 78 shows the microstructure at the fracture for grade1200 and 1400. On microstructural examination, it was evident that there was displacement of the ferrite needles leading to ferrite accumulation, exposing the austenite in the areas close to the fracture. Hence, the exposed austenite under the influence of plastic strain has greater tendency for martensite formation due to SIT at the fracture zone. The conversion of nodular graphite to elliptical was a clear indication of the amount of compressive forces involved in the fracture zone (shear zone in machining).

Microhardness analysis - tapered specimen

The fractured samples are subjected to microhardness test in order to verify the extent of SIT. Microhardness test was conducted to confirm the occurrence of SIT as the metallographic technique used, does not include heat tinting to confirm martensite formation. The expected trend of decrease in microhardness values on moving away from fracture zone was observed.

Table 18: Knoop microhardness - away from fracture zone

Distance from fracture (in mm)		0	0.1	0.2	0.3	0.4	0.5	0.6	0.7
Knoop microhardness	Grade 1200	636	573	502	482	459	476	470	410
	Grade 1400	570	554	579	539	527	528	520	485

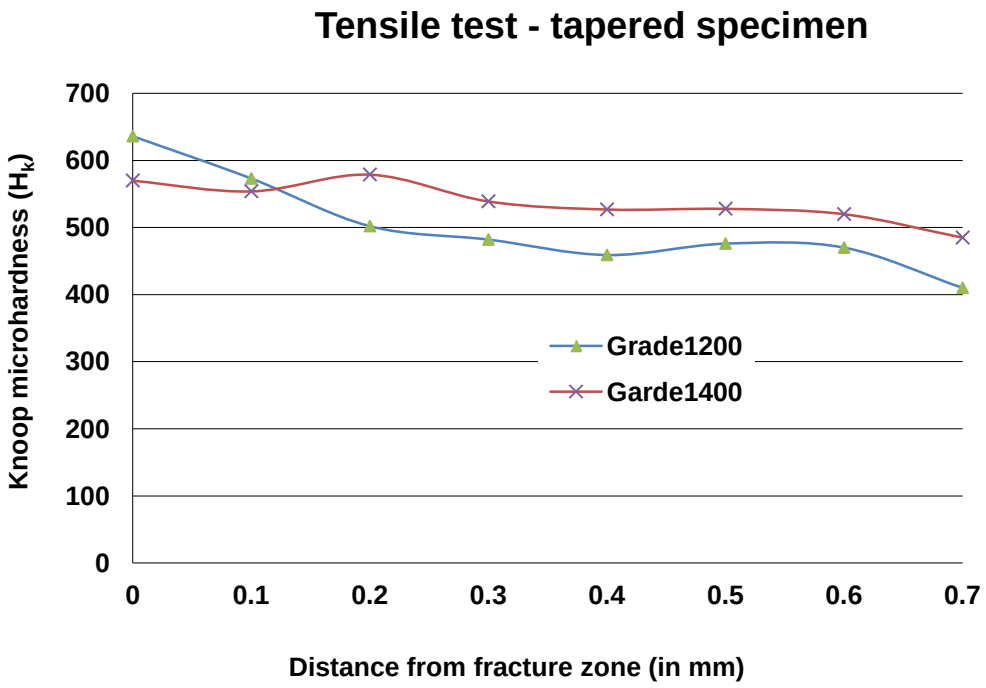

Figure 79: Knoop microhardness - away from fracture zone

Table 18 and Figure 79 show the Knoop microhardness values measured by moving away from the fracture zone. The inferences from these results are discussed in detail in chapter 7.

6.5.4 Modelling of tensile data using ANSYS

The tensile stress-strain data obtained experimentally was validated using FEM. The specimen was subjected to tensile testing using a test setup similar to the experiments by modelling and simulating on ANSYS. The test procedure using ANSYS consist of pre-processing data - specimen modelling and dimensioning, adding constraints and loads; and post processing - data analysis and solution. According to the theoretical explanation given using Hooke's law in section 3.2 and 5.3.4, the material behaviour was linear within the elastic range and becomes non-linear on entering the plastic zone. Hence, in a FEM terminology, non-linear analysis was selected in order to validate the experimental results. Explicit dynamic analysis although feasible was avoided as the inertial loads for a tensile testing scenario was very low. The true strain obtained from the tensile test is sum of the elastic and plastic strain. True strain and UTS were considered as benchmarks for validation of experimental and simulated data using ANSYS. The validation tests are carried out for experimental data obtained using standard specimen for grades 900, 1050, 1200 and 1400.

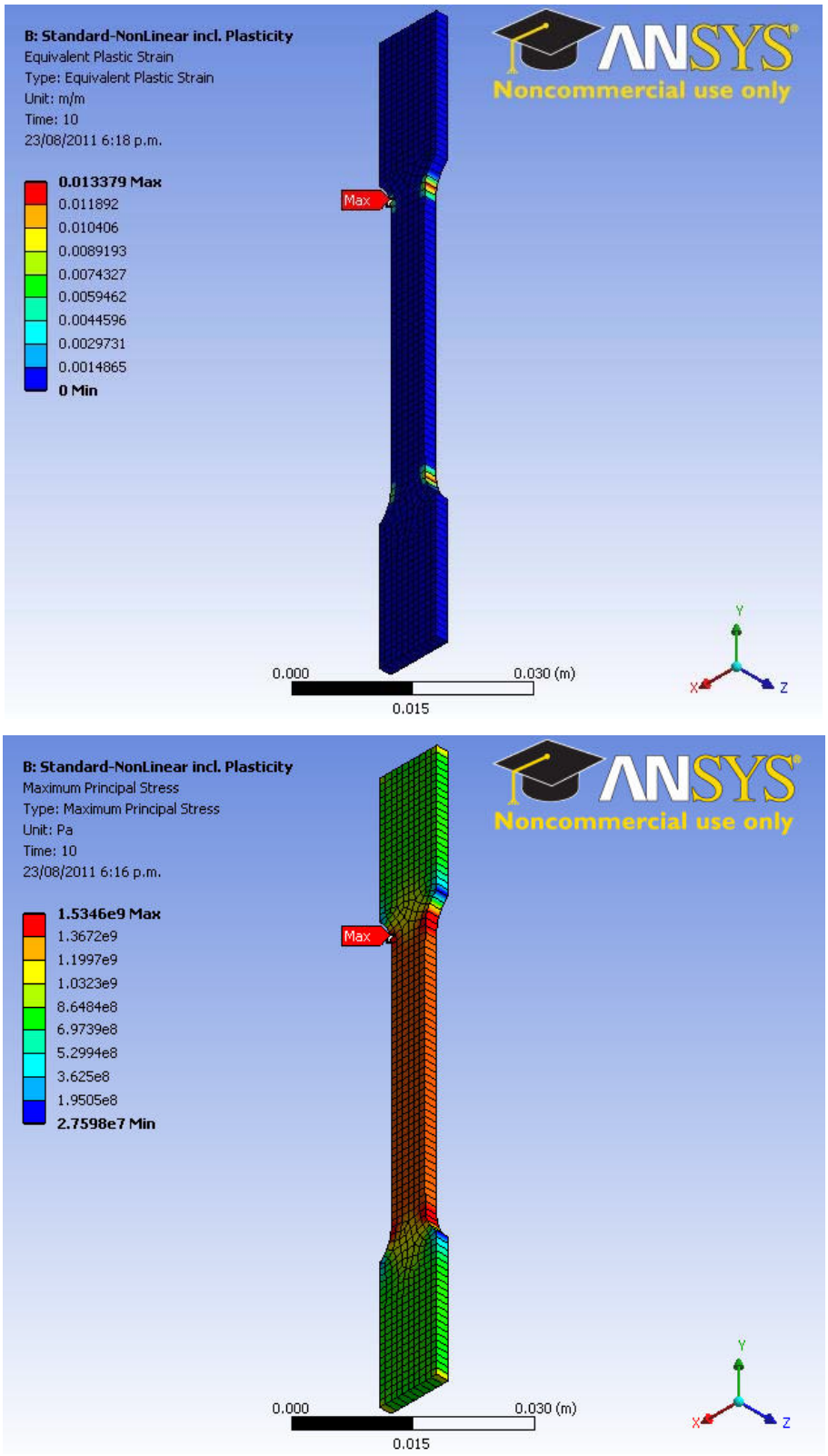

Figure 80: Tensile test using ANSYS - plastic strain & maximum principal stress - grade 1200

Plastic strain and UTS corresponding to a simulated, tensile tested specimen of grade 1200 is shown in Figure 80. Due to limitations in reporting, the results from tensile test simulations for grades 900, 1050 and 1400 are reported under appendix.

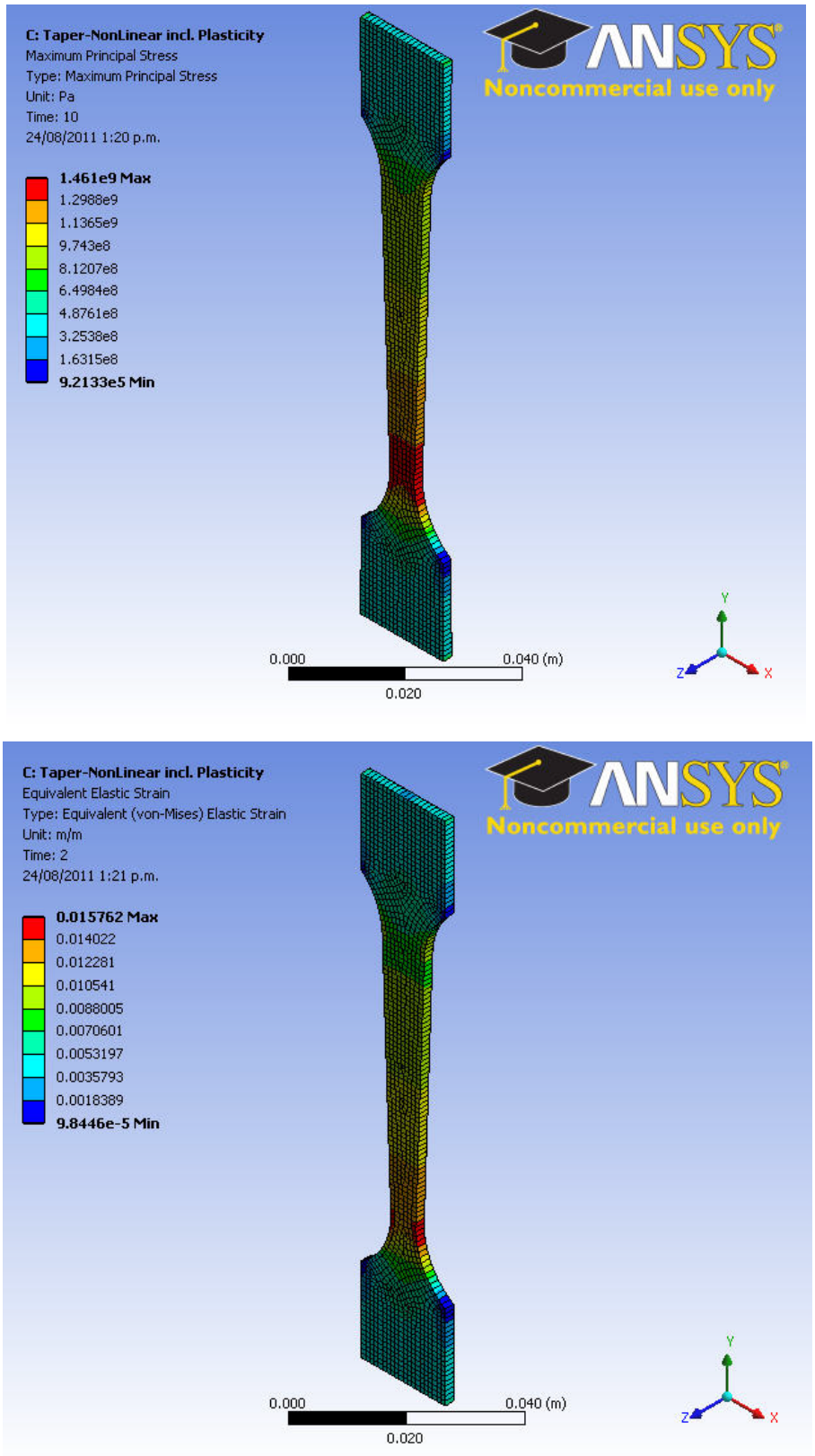

Figure 81: Tensile test-tapered specimen using ANSYS - maximum principal stress & elastic strain - grade 1200

On comparison between a standard and tapered specimen, there was no significant increase in plastic strain when a tapered specimen was used (as shown in Figure 81).

Table 19: Comparison of experimental and simulated results

		Standard specimen		Tapered
		Experimental result	Simulated result - non linear, plastic	Simulated result -non linear, plastic
Grade 900	True stress (Max) MPa	1044	1189	1009
	True strain (Max)	0.018	0.110	0.016
	True plastic strain	0.013	0.04	0.005
Grade 1050	True stress (Max) MPa	1128	1241	1132
	True strain (Max)	0.018	0.128	0.016
	True plastic strain	0.025	0.07	0.031
Grade 1200	True stress (Max) MPa	1509	1613	1452
	True strain (Max)	0.075	0.107	0.016
	True plastic strain	0.013	0.043	0.007
Grade 1400	True stress (Max) MPa	1473	1504	1423
	True strain (Max)	0.018	0.089	0.016
	True plastic strain	0.002	0.008	0.0001

For a tapered sample, as the cross-sectional area is not constant along the gauge length, it was observed that the plastic strains remain almost zero for higher grades such as grade 1400. Due to the tapered nature of the specimen, calculation of strain and UTS at a particular point along the gauge length involves solving complex mathematical equations. Hence, the validation between the experimental and simulated data for a standard specimen was justified. Table 19 shows the experimental and simulated results for standard specimen for grades 900, 1050, 1200 and 1400. The simulated results for a tapered specimen using the true stress-strain data obtained for a standard specimen is also shown in Table 19. The commonality between the results for a standard and tapered specimen lies in the stress-strain curve which shows both the specimens break at almost the same true stress (UTS), for different cross-sectional areas. The units system for FEM simulations was SI, where length was in meters. It was observed that the experimental results are over conservative and lower than the simulated results for all grades. The results confirm the superiority of standard specimen over tapered specimen to be considered for XRD and the assumption of tapered specimen yielding large deformation was not true.

7 Discussion

This research on ADI machining consists of characterisation and machinability evaluation of ADI; and study on phase transformation due to machining. The inferences from the results obtained for the experimental design adopted in this research is explained in this chapter.

7.1 ADI characterisation

ADI characterisation and machinability evaluation was carried out on grades 900, 1050, 1200 and 1400. The material properties of grades vary according to the heat treatment parameters - austempering time and temperature; and alloying elements. As the grade increases from 900 to 1400; the hardness levels, tensile strength and wear resistance increases. The results from the bulk hardness tests (as shown in Table 20) were within the ASTM standard range specified for all grades of ADI. It was observed that the bulk hardness compromises with the evolution of defects during casting and heat treatment process. A common defect such as porosity (as shown in Figure 4) was observed on certain grades of ADI. Because of its high hardness, grade 1200 was selected for milling trials to study phase transformations during machining. XRD analysis was done on all grades of ADI for initial estimation of microstructural constituents (as tabulated in Table 20). XRD data does reveal presence of martensite in small quantities prior to machining.

Metallographic images of all the grades before machining were generated using normal metallographic process of polishing, etching and observing under a high magnification microscope. Metallographic images for all the grades reveal the common microstructural constituents in ADI: ausferrite and graphite nodules. It was also observed that the size and density of the graphite nodules or spacing between the ferrite needles does vary from grade 900 to 1400. For higher grades 1200 and 1400, the size and nodule count of graphite nodules was higher when compared to lower grades 900 and 1050.

Table 20: Initial characterisation data

			Grade 900	Grade 1050	Grade 1200	Grade 1400
Mean Bulk hardness (BHN)			262	366	441	420
Mean Knoop microhardness (H_k)			400	403	493	491
Initial	XRD analysis	Martensite (wt%)	0.4	1.8	0.2	0.1

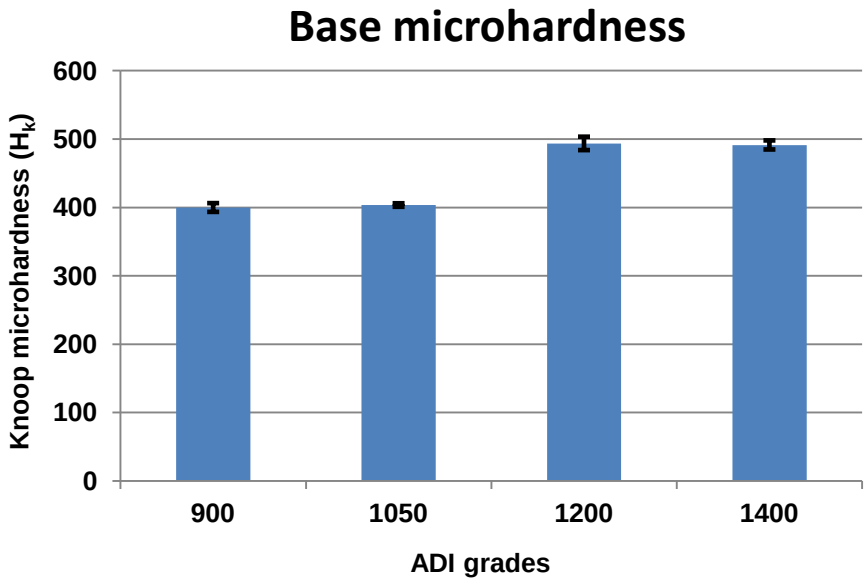

Figure 82: Base microhardness variations from grade 900 to 1400

Using Knoop microhardness test, initial microhardness or base microhardness (as-received condition) was calculated for all grades. The observations along with deviations from the mean value are shown in the form of graph in Figure 82. It was evident that microstructure does effect the microhardness of ADI. Higher grades 1200 and 1400 having high ausferrite content, yield high microhardness values on comparison with lower grades 900 and 1050. The presence of large size graphite nodules for higher grades aids to keep the ausferrite microstructure intact by restricting the movement of the ausferrite on application of external loads.

7.2 Machinability evaluation

The experimental results was divided into two categories for easy evaluation of machinability: numerical or quantitative data such as surface texture (R_a) and microhardness (H_K); and qualitative or image analysis data such as chip morphology and metallography. Machinability evaluation of all grades was done using statistical methods such as value analysis. Each grade was ranked according to the performance based on both numerical and image analysis data. Due to non-availability of extensive machinability data of grades used, pre-defined benchmarks associated with the good machinability characteristics were selected. The chosen benchmark for good machinability consists of lower surface texture (R_a) and microhardness (H_K) values (increase %), consistent chip size and shape; and no signs of white layer formation (work hardening).

Table 21: Machinability evaluation using value analysis

	Grade 900	Grade 1050	Grade 1200	Grade 1400
Surface texture, R_a (Max rating 6)	2	3	6	4
Microhardness, H_k (Max rating 6)	2	3	4	4
Chip Morphology (Max rating 6)	4	4	5	5
Metallography (Max rating 6)	5	4	3	3
Overall rating (Max rating 24)	13	14	18	16
Ranking	4	3	1	2

Grades compliant with selected benchmark were given a high rating (4-6) and non-compliant grades are given a low rating (1-3). The columns representing each grade consisting of individual rating for each category are summed up to give an overall score. Machinability ranking was done based on the overall score. From Table 21, it was evident that grade 900 was having a bottom rank among the grades confirming poor machinability characteristics and vice-versa for grade 1200.

Literature review on ADI material properties suggests good wear resistance for grades 1200 and 1400 and the same was confirmed through the surface roughness result where the grades 1200 and 1400 produced a good finish i.e. lower R_a values. On inspecting ADI microstructure along the hole boundaries, it was evident that grades 1200 and 1400 were showing signs of white layer formation or occurrence of phase transformation. According to previous research works on ADI material characteristics, grade 1200 was regarded to be best grade having balanced and optimised material properties. Machinability evaluation (as shown in Table 21) confirms grade 1200 to be having good machinability with greater signs of work hardening compared to other grades. Hence, grade 1200 was selected for an in-depth analyses i.e. study on phase transformations.

Although tool wear was not part of machinability assessment, the effect of tool material on machinability was researched as TiAlN and PCBN tools were used for drilling and milling trials respectively. The effect of coolant and tool material especially PCBN on cutting action was demonstrated as high cutting forces were obtained for wet (coolant on) milling compared to dry (coolant off) milling. A deeper analysis into the results does confirm the non-compatibility of PCBN and ADI when coolant was used during machining.

7.3 Phase transformations during ADI machining

As part of this research work on ADI machinability, an inquest was carried out on phase transformation during ADI machining and factors affecting it. The factors under consideration are plastic strain (ε_p) and thermal energy (Q). The phase transformation reaction in ADI leads to transformation of retained austenite to martensite. Hence, the martensite content before and after machining was checked using metallography-heat tinting and quantified using XRD analysis. The increase in martensite (wt%) was related to plastic strain and thermal energy.

The relationship between increase in martensite (M) due to phase transformation and factors such as plastic strain (ε_p) and thermal energy (Q) can be expressed as a function given in equation 7-1.

$$M = f(\varepsilon_p , Q) \quad \text{----------} \quad 7\text{-}1$$

As tensile testing was done at room temperature, the effect of thermal energy (Q) on phase transformations was negligible. Hence, the amount of martensite formed at the fracture point in a tensile sample was mainly due to plastic strain (ε_p). The direct relationship between plastic strain (ε_p) and martensite (M) was mathematically written as shown in 7-2

$$M = K\ \varepsilon_p \quad \text{----------} \quad 7\text{-}2$$

where K is a proportionality constant.

The amount of martensite formed during tensile testing was quantified using XRD analysis. The proportionality constant (K) was calculated using the martensite (wt%) and plastic strain (ε_p) as shown in Table 22

Table 22: Calculating proportionality constant (K)

	Plastic strain (ε_p)	Increase in martensite, $M = M_i - M_f$, (wt%)	Proportionality constant (K) = M/ε_p
Grade 900	**0.11**	**4.5**	**40.9**
Grade 1050	**0.13**	**2.7**	**20.8**
Grade 1200	**0.11**	**2.9**	**26.4**
Grade 1400	**0.1**	**1**	**10**

Table 23: Calculating Plastic strain during milling

Wet milling					
	Martensite (wt%)				
DoC (mm)	Before	After	Increase in martensite, $M = M_i - M_f$, (wt%)	Proportionality constant (K)	Plastic strain (ε_p) = M/K
4	0.2	22.1	21.9	26.4	0.83
3	0.2	25	24.8	26.4	0.94
2	0.2	17	16.8	26.4	0.64
1	0.2	12	11.8	26.4	0.44
Dry Milling					
	Martensite (wt%)				
DoC (mm)	Before	After	Increase in martensite, $M = M_i - M_f$, (wt%)	Proportionality constant (K)	Plastic strain (ε_p) = M/K
4	0.2	17.5	17.3	26.4	0.65
3	0.2	24.6	24.4	26.4	0.92
2	0.2	19.4	19.2	26.4	0.73
1	0.2	17.6	17.4	26.4	0.65

Similarly, the amount of martensite formed during milling for grade 1200 under dry and wet conditions was related using equation 7-2. The amount of plastic strain involved during milling was calculated by substituting the value of proportionality constant (K) in equation 7-2, as shown in Table 23.

During a metal cutting operation, most of the mechanical energy consumed is transformed to heat. Therefore, heat generation and dissipation from the cutting zone plays an important role in machining [22]. The role of thermal energy in martensite formation due to phase transformation was explained in section 4.3. Taking into consideration Fe-C equilibrium diagram, it was observed that martensite start temperature (M_s) does depend on carbon (%) in an alloy.

Table 24: Thermal energy effect on martensite formation

Dry milling				
DoC (mm)	Temperature (K)	Thermal energy (J/sec)	Plastic strain (ε_p)	Martensite, M (wt%)
3	576	12319.5	0.92	24.4
1	348	7482	0.65	17.4
Wet milling				
DoC (mm)	Temperature rise (K)	Thermal energy (J/sec)	Plastic strain (ε_p)	Martensite, M (wt%)
3	333	7159.5	0.94	24.8
1	0	0	0.44	11.8

ADI is known to have high carbon (%) and therefore, M_s is reduced appropriately and phase transformation if any, takes place at temperatures lower than expected. The driving force for martensite nucleation (Gibb's free energy, $\Delta G^{\gamma \rightarrow M}$) varies with the temperature and carbon (%) in an alloy. Temperature in the cutting zone effects the phase transformation by acting as a catalyst to SIT. High cutting temperature leads to increase in atomic energy levels, making it easier for the dislocations to cross the grain boundaries and leads to decrease in dislocation density. The temperature in the cutting zone affects the machinability of the workpiece as the shear plane aligns against each other in a parallel pattern due to the excitation of the atoms on absorption of energy.

The procedure used for temperature measurement was a semi-quantitative process. Heat transferred to the chip and tool; heat loss, time lag between the cutting action and thermocouple signal pick-up were some of the errors in the process. Hence, thermal energy calculated using the temperature reading from the thermocouple placed in front of the tool is a value after compensating heat loss and technical errors. The plastic strain (ε_p) and thermal energy (Q) variation for selected DoC (mm) and martensite increase (wt%) under wet and dry milling is given in Figure 83 and Figure 84. The combined effect of plastic strain and thermal energy on martensite formation during wet and dry milling was analysed. It was observed that the amount of martensite formed at DoC-3mm for wet milling was considerably high suggesting prominent role of thermal energy in martensite formation.

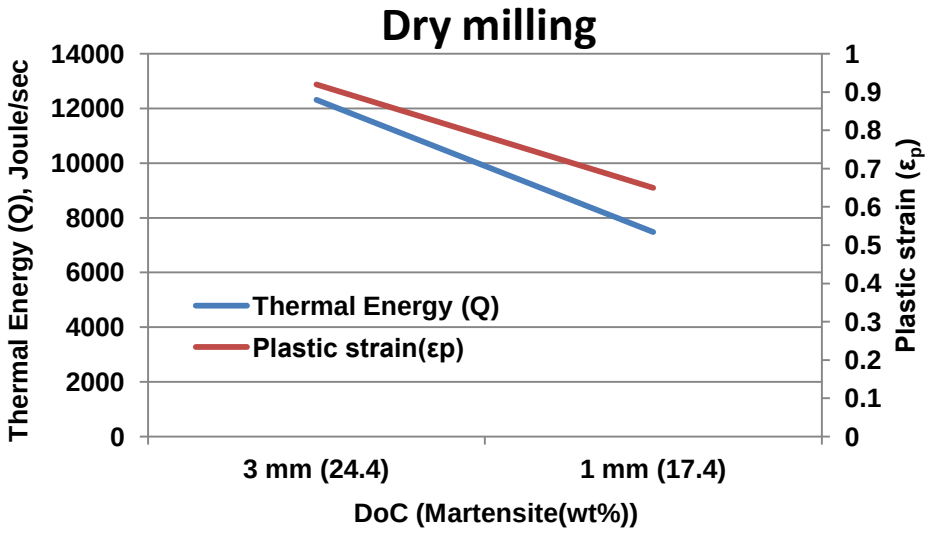

Figure 83: Thermal energy (Q) & plastic strain (ε_p) variation for dry milling

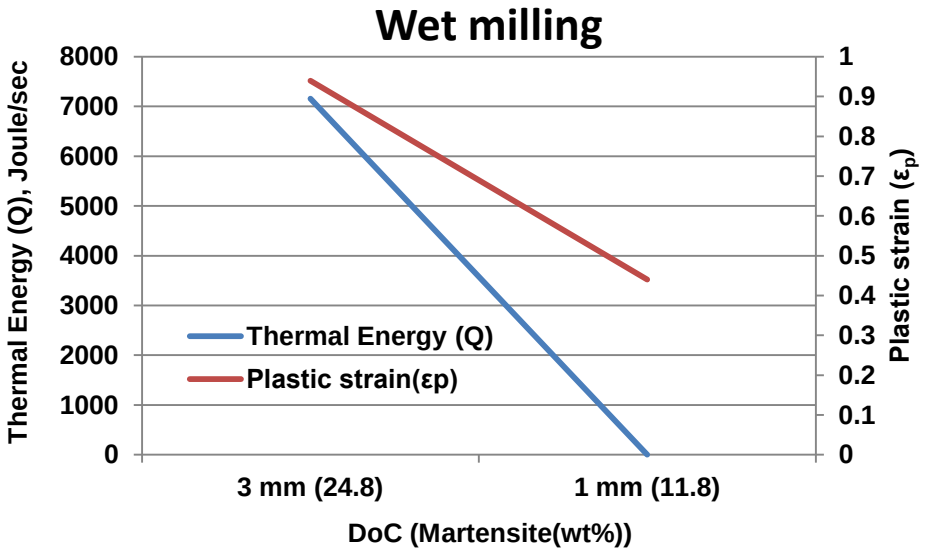

Figure 84: Thermal energy (Q) & plastic strain (ε_p) variation for wet milling

Earlier research studies on ADI machining had suggested machining the material without coolant due to the belief; phase transformation was triggered rapidly due to sudden changes in temperature. The numerical data regards to martensite (wt%), plastic strain and thermal energy were persistent in explaining the phenomenon of phase transformation during ADI machining. The magnitude (numbers) of martensite formation, plastic strain and thermal energy were neglected as the research work approach and aim was to understand the phenomenon of phase transformation.

The tensile test data obtained for all the grades was modelled and validated using ANSYS. The tensile test data validation confirms the amount of plastic strain involved at the fracture point. Simulated results were in convergence with the experimental results. Strain hardening constant was calculated using the tensile test data in order to evaluate the grade sensitivity to SIT during machining. Ferrite needle accumulations, retained austenite exposure, compression of nodular graphite into elliptical shape were some of the metallographic observation from the fractured tensile samples.

8 Conclusion

This chapter concludes the results obtained from the experimentation explained in chapter 6 and discussed in chapter 7. The concluding remarks are categorised into three parts: characterisation, machinability evaluation; and effect of plastic strain (ε_p) and thermal energy (Q) on phase transformations.

8.1 Characterisation of ADI

- From Rockwell hardness tests, it was observed that grade 1200 has the highest and optimum hardness level. Minor aberration such as low hardness was experienced for grades having high porosity. The hardness levels rise as the UTS for each grade increases from 900 to 1400 MPa.

- Heat tinted metallography or colour metallography was conducted for easy identification of the microstructural phases, using colour codes such as retained austenite (light blue), martensite (dark blue), austenite (purple), ferrite (black) and graphite nodule (beige).

- The effect of microstructure on microhardness using Knoop was evident as higher grades 1200 and 1400 having high ausferrite content, have high microhardness on comparison with lower grades 900 and 1050.

- XRD data reveal presence of martensite in small quantities, prior to machining due to casting and heat treatment defects during ADI production.

8.2 Machinability evaluation

- From drilling trials on grades 900, 1050, 1200 and 1400 at constant cutting speed, 693 rpm; feed rate, 0.1 mm/rev, DoC-25 mm with coolant coupled with cutting force measurements, it was observed that there was no significant variation in the thrust force, F_Z (N) and the moment, M_Z (N-m). The results infer that the cutting parameters not effective enough to trigger a phase transformational reaction.

- The effect of feed rate on cutting force and moment on grade 1200 and 1400 at variable feed rate from 0.2 to 0.35 mm/rev, constant depth of cut, 25mm; speed, 45m/min and no coolant shows that the cutting force and moment increase with an increase in feed rate for initial, 0.2 to 0. 25 mm/rev and final feed rates, 0.3 to 0.35 mm/rev. For the middle range i.e. feed rate, 0.25 to 0.3, mm/rev the force and moment almost remain constant.

- The effect of common defects such as porosity was observed in various drilled holes, as they have a higher surface roughness (R_a) values. The effect of tool retraction on surface roughness was ignored as it remains constant for all the samples.

- Grade 1200 sample drilled at high speed, low feed and without coolant has the top finish (low surface roughness, 0.730 μm (R_a)) among all the samples. For all samples drilled without coolant, the surface roughness (R_a) was high compared to the sample drilled with coolant except grade 1200 because of the presence of thermal softening effect, reduced tool wear during dry machining of higher grades of ADI especially grade 1200.

- The drilled holes were subjected to Knoop microhardness test and verified for abrupt increase in microhardness. The data obtained from the microhardness test was divided into three categories which was useful in generating hardness profiles along the hole depth (direction of cut), away from the hole edge and initial microhardness of as received ADI termed as “base”.

- Minor deviation from the regular trend was observed in case of samples having porosity and heat treatment defects. A sudden surge in microhardness was also observed in certain samples, which most probably indicate the occurrence of hardening due to SIT. It was observed that the microhardness value increases as the cutting speeds increases irrespective of the feed rate, grade and coolant condition.

- High value of microhardness was reported in the locations near to the chisel edge which shows that the cold work by the chisel edge also plays an important role in phase transformation apart from SIT due to machining.

- The common observation for almost all samples of grades 900, 1050, 1200 and 1400 was that the microhardness has a lower value for a location away from the hole edge and the microhardness has a high value for a location along the hole depth or direction of cut. Overall, the analysis infers that the microhardness values are higher for dry machining for any grade.

- The type of chips produced while drilling was classified as discontinuous chips except one or two samples having semi-continuous chips. The different types of chip were classified as needle shaped chips, chisel edge chips, fan shaped chips and amorphous chips or flower shaped chips. Chisel edge chips was due to the formation of the chip by the chisel edge which extrudes the material to produce long and narrow chips

- For lower grades 900 and 1050, at low feed rates and speeds, the chip produced was smaller in size on comparison with the chip produced for high feed rate and speed. As the grade increases from 900 to 1400, the hardness levels in the material increase and this leads to increase in the size of the chip and hence, an increase in cutting force and torque to evacuate the large chips was justified.

- Metallographic analysis conducted to examine the microstructural changes along the hole boundaries shows that the chosen speeds and feed rate were ineffective in triggering phase transformation due to SIT for all the samples except in few samples for grade 1200 and 1400.

- The metallographic results confirm that feed rate plays an important role in determining the extent of SIT during machining. Samples drilled at low feed rate irrespective of the cutting speed and coolant, for any grade of ADI did not show any sign of SIT where as sample drilled at high feed rate did reveal at certain location along the hole boundary, the occurrence of SIT. The effect of feed rate was also confirmed through the Tool failure analysis where drilling at high feed rate has led to the failure of the tool. The importance of using the golden rule of machining ADI-using low feed and high speed was evident.

- Overall, machinability analysis was performed using statistical tool such as value analysis in order to find out the best machinable grade. Grades were ranked based on performance on selected benchmarks such as surface texture, microhardness, chip morphology and metallographic analysis. Using value analysis, it was confirmed that grade 1200 has a slightly higher rank compared with other grades and therefore, it was judged as a better machinable grade.

8.3 Effect of plastic strain (ε_p) and thermal energy (Q) on phase transformations

- The tensile test results of grades 900, 1050, 1200 and 1400 implies that the UTS and elongation (%) were consistent with the ASTM standards except for grade 1400. Grade 1050 show the maximum elongation-14% and grade 1200 was the best grade showing optimum values of elongation-11% and UTS-1373 MPa. Tensile test modelling using ANSYS was also done to validate the experimental data.

- The value of strain hardening exponent (n) obtained for grade 1200 was 0.178, which was nearly equal to the strain hardening exponent (n), 0.143 according to the ASTM A897-03 standard. Strain hardening exponent is an important parameter indicating the probable occurrence of SIT during machining.

- For milling, the important parameters under consideration were the forces: thrust force (F_Z) and feed force (F_Y); and moment (M_Z). It was observed that DoC-3 mm was having the highest thrust force (F_Z), feed force (F_Y) and moment (M_Z) for both dry and wet milling. The other significant observation was that the thrust force (F_Z), feed force (F_Y) and moment (M_Z) obtained for wet milling was higher than dry milling.

- Heat-tinted, colour metallographic images confirm martensite formation (dark blue) for higher DoC-4 and 3 mm. Retained austenite (light blue) was seen to maximum extent in DoC-1 and 2 mm, which implies that the machining forces were insufficient for SIT occurrence leading to martensite formation.

- The amount of martensite formed during wet milling justifies the fact that higher forces were obtained for wet milling in addition to the effect of using PCBN tools.

- It was observed that high martensite content obtained for DoC-3 mm under wet and dry milling corroborate with the high cutting forces for DoC-3 mm under wet and dry milling. This can be attributed to the absence of thermal softening effect of the workpiece under wet milling. Hence, dry machining is an ideal way to machine ADI using low feed and high speed.

- The effect of thermal energy on martensite formation due to phase transformation during milling under wet and dry milling at variable DoC was investigated using the temperature measurements. The thermocouple readings taken during milling were used to evaluate the amount of thermal energy involved.

- The martensite (wt%) formed during dry milling of grade 1200, at DoC-3 and 1 mm was estimated to be 24.4 and 17.4 respectively. Influential factors such as the plastic strain for DoC-3 and 1 mm were estimated to be around 0.92 and 0.62; and the thermal energy 12319.5 and 7482 J/sec respectively.

- The martensite (wt%) formed during wet milling of grade 1200, at DoC-3 and 1 mm was estimated to be 24.8 and 11.8 respectively. Influential factors such as the plastic strain for DoC-3 and 1 mm were estimated to be around 0.94 and 0.44; and the thermal energy 0.94 and 0 J/sec respectively.

- Overall, a mathematical relationship was established between the factors responsible for SIT such as plastic strain and thermal energy; and SIT outputs such as increase in martensite (wt%).

9 Future Work

Machining has always been a research area, which still remains unexplored especially for material such as ADI. The task of providing a machinist with a straight forward technique to achieve desirable results on a machined part still remains unknown, due to the constantly changing machining techniques and introduction of new materials such as ADI. The truth lies in the fact that new innovative techniques and approach even though introduced, required to be studied in-depth for practical implementation.

With the introduction multi-axis CNC machines and new machining approaches such as milling interpolation, ADI machinability can be evaluated using these techniques. Milling interpolation is used for generating curve, narrow and deep cavities similar to drilling holes by machining using combination of X, Y, Z and; additional A, B and T-axis. The experimental design needs hard and tough tools (Solid carbide and CBN) to accomplish the task.

The future work of the thesis involves an in-depth study on the new link discovered through this thesis: mathematical model relating the role of plastic strain and thermal energy in martensite formation. Studies on additional factors effecting phase transformations such as tool wear, cutting parameters, machining techniques and metallurgical changes is recommended. Future work plans to extend the experimental trials to other grades 900, 1050 and 1400. Additional work is required to investigate the thermo-mechanical reaction taking place in the tool/workpiece interface. A study can be undertaken to investigate the effect of thermal softening of the workpiece by the tool.

The effect of cutting tool material on machinability of ADI was realised in this research to a limited extent as different tool materials such as TiAlN and PCBN were used. The scope of the research has been limited in considering factors such as tool wear and tool geometries: rake angle, flank, etc. in evaluating machinability of ADI. As part of the future work, the limitation can be overcome by taking up extensive study on the tool geometries and its effect on machinability.

Metallographic examination of the tensile fractured sample has revealed observations such as ferrite accumulation, retained austenite exposure and graphite compression which need further examination.

An extended study can be undertaken on movement of microstructure due to plastic strain and its effect on phase transformations during machining. ADI being a heat-treated material, the amount of residual stress involved on the top layer is quite high. A study on the effect of residual stress on ADI machinability can be undertaken. Study on production process of ADI and its effect on phase transformation can be undertaken. Literature review on ADI has revealed the fact that ADI is machinable provided changes are made in alloying elements and their proportions. The benefits of using High Speed Machining (HSM) on ADI are two-fold both in term of productivity and economics of machining. A research into exploring the idea of using ADI as a material for High Speed Machining (HSM) can be evaluated.

Most of the experimental methods used to estimate the amount on plastic strain and thermal energy, involved the workpiece/tool interface. A direct method of plastic strain measurement during machining can be implemented by freezing the chip using a quick-stop device. The frozen chip gives information on the movement of microstructure from the cut initiation stage to shearing from the parent body. Using metallographic techniques, the plastic strain involved can be estimated by following the microstructure displacement (difference in atomic positions).

The future work of thesis speaks about plans to study the temperature effect in detail using techniques yielding accurate measurements with few errors. New measurements techniques using thermocouple welded to the tip of the cutting tool in order to minimise the time lag and for accuracy can be considered. By setting up a thermal imager or an infra-red camera inside the machine tool, accurate temperature measurements associated with the shear zone can be estimated. The use of statistical analysis was limited to factorial design in this research. Future work can implement better statistical techniques such variance analysis, orthogonal array and other quality control-Taguchi methods.

Finally, the future work in ADI machining and its study on phase transformation can be undertaken provided the researcher understands the economics of ADI machining. ADI being a harder material, this research has shown some setbacks in terms of tool failure, which needs to be considered while planning future trials. The research output can be sustainable provided an analysis is done prior to start of the research on the risk factors as there is a possibility of frequent tool breakdowns due to the high hardness of the material.

References

[1] K. L. Hayrynen, ed. Livonia, Michigan: Applied Process Inc., 2004.

[2] J. R. Keough, K. L. Hayrynen, "Austempered Ductile Iron- The State of the Industry in 2003," in *World ADI Conference*, Louisville, Kentucky, 2003.

[3] D. Y. Li, Z. F. Zhou, and D. Q. Sun, "Morphology and constitution of the phases in as-welded microstructure of austempered ductile iron," *ProQuest Science Journals*, p. 665, 2005.

[4] T. Dorn, J. R. Keough, T. Schroeder, and T. Thoma, "The Current State of Worldwide Standards for Dcutile Iron," in *Keith Mills Symposium On Ductile Cast Iron*, 2003.

[5] *Standard Specification for Austempered Ductile Iron Castings*, A 897/A 897M - 06, 2006.

[6] S. Kesani, "Development of austenite free Austempered Ductile cast Iron (ADI)," Master thesis, Material Science and Engineering, Wayne State University, Detroit, Michigan, 2005.

[7] E. Olivera, M. Jovanovic, L. Sidanin, D. Rajnovic, and S. Zec, "The austempering study of alloyed ductile iron," *Materials and Design*, vol. 27, pp. 617-622, 2006.

[8] Y.-J. Kim, H. Shin, H. Park, and J. D. Lim, "Investigation into mechanical properties of austempered ductile cast iron (ADI) in accordance with austempering temperature," *Materials Letters*, vol. 62, pp. 357-360, 2007.

[9] U. Seker and H. Hasirci, "Evaluation of machinability of austempered ductile irons in terms of cutting forces and surface quality," *Journal of Material Processing Technology*, vol. 173, pp. 260-268, 2006.

[10] K. L Hayrynen, K. R Brandenberg, and J. R. Keough, "Application of Austempered Cast irons," *AFS Transactions*, vol. 02-084, p. 10, 2002.

[11] R. J Warrick, P. Althoff, A. P Druschitz, J. P Lemke, K. Zimmerman, P. H. Mani, and M. L Rackers, "Austempered Ductile Iron Castings for Chassis Application," in *SAE 2000 World Conference*, Detroit, Michigan, 2000.

[12] S. Laino, J. A. Sikora, and R. C. Dommarco, "Development of wear resistant carbidic austempered ductile iron (CADI)," *Wear*, p. 7, 2007.

[13] A. Amirsadeghi Sohi, M. Heydarzadeh, "Comparison of the influence of molybdenum and chromium TIG surface alloying on the microstructure, hardness and wear resistance of ADI," *Journal of Material Processing Technology*, 2007.

[14] C. Brunetti, M. V. Leite, and G. Pintaude, "Effect of specimen preparation on contact fatigue wear resistance of austempered ductile cast iron," *Wear*, vol. 263, pp. 663-668, 2007.

[15] C. M Cakir, B. Ali, I. Yahys, and S. Baris, "The effects of austempering temperature and time onto the machinability of austempered ductile iron," *Material Science Engineering*, vol. 407, pp. 147-153, 2005.

[16] K. R Brandenberg. (2001, May 2002) Machining Austempered Ductile Iron (ADI). *Manufacturing Engineering*.

[17] K. R Brandenberg, J. Ravenscroft, A. Rimmer, Dr., and K. L Hayrynen, "An ADI Crankshaft Designed for High Performance in TVR's Tuscan Speed Six Sports Car," *Society of Automotive Engineers*, 2001.

[18] H. Matsuoka, Y. Tsuda, and H. Ono, "Fundamental Research on Hobbing of Austempered Ductile Iron Gear (Influence of Graphite Particle on Machinability)," *JSME International Journal*, vol. 46, pp. 1160-1170, 2003.

[19] M. Goldberg, G. T. Smith, J. T Berry, and G. Littlefair, "Machinability Assessment and Surface Integrity Characteristics of Austempered Ductile Iron (ADI) Using Ultra-Hard Cutting Tools," in *3rd International Conference on Machining & Grinding*, Cincinati, Ohio, 1999.

[20] A. P Druschitz and D. C Fitzgerald, "MADI: Introducing a New, Machinable, Austempered Ductile Iron," in *2003 SAE World Congress*, Detroit, Michigan, 2003.

[21] C. C. Wang, B. H. Yan, H. M. Chow, and Y. Suzuki, "Cutting austempered ductile iron using an EDM sinker," *Journal of Material Processing Technology*, vol. 88, pp. 83-89, 1997.

[22] Sandvik Coromant, *Modern Metal Cutting*. Sandviken Sweden: A B Sandviken Coromant, 1994.

[23] G. Boothroyd, *Fundamentals of Metal Machining* 1ed. London: Edward Arnold Ltd, 1965.

[24] D. Graham, "Machining cast iron," *Manufacturing Engineering*, vol. 136, pp. 77-83, 2006.

[25] A. Polishetty, T. Wilson, and G. Littlefair, "Characterisation of the machinability of austempered ductile iron using drilling," in *NZ Metals 2008*, Auckland, New Zealand, 2008.

[26] B. O'Rourke. (2003) A look at today's cast iron. *Production-Machining*. 1-5. Available:http://www.lokeymetals.com/Production%20Machining%20magazine%20Dura-Bar%20article.htm

[27] R. D. Griffin, H. J. Li, E. Eleftheriou, and C. E. Bates, "Machinability of Gray Cast Iron," *American Foundary Society*.

[28] S. K. Bhattacharyya, E. O. Ezugwu, and A. Jawaid, "The performance of ceramic tool materials for the machining of cast iron," *Wear*, pp. 147-159, 1989.

[29] R. Komanduri, "Mechanism of Chip Formation in High-Speed Machining " in *Industrial Tooling Conference* Southampton, United Kingdom, 1995.

[30] R. F. Recht, "A dynamic Anlysis of High-Speed Machining," *ASME Journal of Engineering for Industry*, vol. 107, pp. 309-315, 1964.

[31] K. Nakayama, "The Formation of Saw - Totthed Chip," in *International Conference on Procudtion Engineering*, 1974, pp. 572-577.

[32] M. C. Shaw, *Metal Cutting Principles*. New York: Oxford University Press, 1986.

[33] V. P. Astakhov, "Surface integrity - definition and importance in functional performance," *Surface Integrity in Machining*, 2010.

[34] E. P. Degarmo, J. T. Black, and A. R. Kohser, *Materials and Process in Manufacturing*, 9 ed.: Wiley, 2003.

[35] A. K. Ghani, I. A. Choudhury, and Husni, "Study of tool life, surface roughness and vibration in machining nodular cast iron with ceramic tool," *Journal of Materials Processing Technology*, 2002.

[36] F. Klocke, C. Klopper, D. Lung, and C. Essig, "Fundamental Wear Mechanisms when Machining Austempered Ductile Iron," *CIRP*, vol. 56, pp. 73-76, 2007.

[37] E. J. A. Armarego and R. H. Brown, *The Machining of Metals*. Englewood Cliffs, New Jersey: Prentice-Hall Inc, 1969.

[38] S. Kalpakjian and S. R. Schmid, *Manufacturing Engineering and Technology*, Fourth ed.: Prentice-Hall.

[39] R. N. Rai, G. L. Datta, M. Chakraborty, and A. B. Chattopadhyay, "A study on the machinability behaviour of Al-TiC composite prepared by in situ technique," *Science Direct*, vol. 428, pp. 34-40, 25-07-2006 2005.

[40] G. T. Smith, Ed., *Adavcned Machining- The Hadnbook of Cutting Technology*. England: IFS Publications, 1989.

[41] J. P. Davim, Ed., *Surface integrity in machining*. Springer, 2010.

[42] N. Pretorius, "Evaluation of different cutting tool materials for the machining of high strength cast irons," in *Industrial Diamond Conference*, Barcelona, Spain, 2005.

[43] T. Childs, K. Maekawa, T. Obikawa, and Y. Yamane, *Metal Machining - Theory and Applications*. London: Arnold, 2000.

[44] J. Hua and R. Shivpuri, "Prediction of chip morphology and segmentation during the machining of titanium alloys," *Journal of material processing technology,* pp. 124-133, 2004.

[45] N. H. Cook, "Chip formation in machining titanium," in *Symposium on Machine Grind-titanium,* Watertown Arsenal, 1953, pp. 1-7.

[46] R. Komanduri, T. A. Schroeder, D. K. Bandopadhyay, and J. Hazra, "Titanium: a model material for analysis of the high speed machining process, advanced processing methods for titanium," 1982, pp. 241-256.

[47] K. H. W. Seah and X. Li, "Influence of Coolant on Cutting Tool Performance," *Jounral of material science Technology,* vol. 13, pp. 199-205, 1997.

[48] S. A. Batzer, P. D. Rao, D. M. Haan, and W. W. Olson, "An experimental investigation of chip morphology in drilling," *S M Wu Symposium,* vol. 2, 1996.

[49] A. Meena and M. E. Mansoori, "Drilling performance of green austempered ductile iron(ADI) grade produced by novel manufacturing technology," *International journal of advance manufacturing technology,* 2011.

[50] S. A. Batzer, D. M. Haan, P. D. Rao, W. W. Olson, and J. W. Sutherland, "Chip morphology and hole surface texture in the drilling of cast aluminium alloys," *Journal of Material Processing Technology,* 1998.

[51] G. T. Smith, *Industrial Metrology*: Springer, 2002.

[52] M. Pirtini and I. Lazoglu, "Forces and hole quality in drilling," *International Journal of Machine Tools & Manufacture,* vol. 45, pp. 1271-1281, 2005.

[53] Metal Cutting Tool Insitute, *Metal Cutting Tool Handbook*. New York: Metal Cutting Tool Institute, 1965.

[54] I. Bradley, *The Drilling Machine*. London: Model&Allied Publications Ltd, 1973.

[55] B. H. Chambers, *Twist Drills- Their Manufacture Selection & Use*, 1946.

[56] G. T. Smith, "What is Machinability and how can it be assessed," in *Industrial tooling conference,* Southampton, United Kingdom, 1995.

[57] S. Kesani, "Development of austenite free Austempered Ductile cast Iron(ADI)," Master thesis, Material Science and Engineering, Wayne State University, Detroit, Michigan, 2005.

[58] D. A. Porter, K. E. Easterling, and M. Y. Sherif, *Phase Transformations in Metals and Alloys*, Third ed.: CRC Press, 2009.

[59] S. Kiritis. Teach Yourself Phase Diagrams [Online].

[60] R. Abbaschian and R. E. Red-Hill, *Physical Metallurgy Principles*.

[61] Pollack, *Materials Science and Metallurgy*: Prentice-Hall, 1988.

[62] K. Ballentine. Phase Diagram Basics [Online]. Available: http://www.eng.vt.edu/eng/materials/classes/MSE2094_NoteBook/96ClassProj/examples/kimcon.html

[63] J. R. Keough, "Ductile Iron Data for Design Engineers," 1998.

[64] H. Kashani, A. Amdeh, and A. Ohadizadeh, "Effect of temperature on the strain induced $\gamma \rightarrow \varepsilon$ phase transofrmation in Stellite 21 during wear test," *Material Science & Engineering,* pp. 435-436, 2006.

[65] J. Grum, "Residual stresses and microstructural modifications," *Surface Integrity in Machining,* 2010.

[66] J. E. Wyatt and J. T. Berry, "A new technique for the determination of superficial residual stresses associated with machining and other manufacturing processes," *Journal of Material Processing Technology,* vol. 171, pp. 132-140, 2006.

[67] G. A. Chadwick, *Metallography of Phase Transformations*. London: Butterworths, 1972.

[68] G. Vining and S. Kowalski, *Statistical methods for engineers*, Second ed., 2006.

[69] G. F. V. Voort, *Metallography: Principle and Practice*. New York: McGraw-Hill Book Co., 1984.

[70] B. V. S. Kovacs, "A Simple Technique to Identify Various Phases in Austempered Ductile Iron," *Modern Castings,* vol. 77, pp. 34-35, 1987.

[71] J. M. Radzikowska, "Effect of specimen preparation on evolution of cast iron microstructures," 2004.

[72] M. Goldberg, "Machinability research into the mechanics and surface integrity characteristics of Austempered Ductile Iron," PhD Thesis, Faculty of Technology, Southampton Institute, Southampton, 2002.

[73] J. L. Garin and R. L. Mannheim, "Strain-induced martensite in ADI alloys," *Journal of Material Processing Technology,* 2003.

[74] D. Way. (2004) ADI solutions aids vehicle design. *FTJ*.

[75] J. Olofsson, D. Larsson, and I. L. Svensson, "Effect of austempring on plastic behavior of some Austempered Ductile Iron Alloys," *Mettalurgical and material transactions,* 2011.

[76] *Mettalic materials-sheet and strip-Determination of tensile strain hardening exponent*, ISO ISO10275, 1993.

[77] K. Nakayama, "Basic rules on the form of chip in metal cutting," *CIRP,* 1978.

List of publications

1. Conference: ASME conference - International Manufacturing Science and Engineering conference, October 2008, Northwestern University, Illinois, U.S.A.
   Title: A comparative assessment of Austempered Ductile Iron (ADI) as a substitute in weight reduction applications.
   Authors: Ashwin Polishetty, Dr Guy Littlefair and Dr. Sarat Singamneni
   Status: Published

2. Conference: Industrial Tooling 2008, Mississippi State University, Starkville, Mississippi, U.S.A
   Title: Machining characteristics of Austempered Ductile Iron (ADI).
   Authors: Ashwin Polishetty, Dr Guy Littlefair and Dr. Sarat Singamneni
   Status: Published

3. Conference: 4th NZ Metals 2008, October, 2008, Sky City Convention Center, Auckland, New Zealand.
   Title: Characterisation of machinability of Austempered Ductile Iron through drilling.
   Authors: Ashwin Polishetty, Dr Guy Littlefair and Dr. Sarat Singamneni
   Status: Published

4. Published technical article “Why machine Austempered Ductile Iron (ADI)?” in New Zealand, Engineering News, New Zealand

5. Journal: Advanced Materials Research Vols. 97-101 (2010) pp 2036-2039,© (2010) Trans Tech Publications, Switzerland, doi:10.4028/www.scientific.net/AMR.97-101.2036
   Title: Assessment of machining characteristics of Austempered Ductile Iron
   Authors: Ashwin Polishetty and Dr. Guy Littlefair
   Status: Published

6. Journal: International Journal of Mechanical & Mechatronics Engineering
   ISSN: 2077-124X, Manuscript Code: 106101-8787
   Title: Wear Characteristics of Ultra-Hard Cutting Tools when Machining Austempered Ductile Iron
   Authors: Ashwin Polishetty, Dr. Moshe Goldberg, Dr. Guy Littlefair
   Status: Published

7. Conference: ASME International Manufacturing Science and Engineering conference 2010, Penn State University, Eire, Pennsylvania, U.S.A.
   Title: Microstructural Studies on Strain Induced Transformations in Austempered Ductile Iron Using Heat Tinting
   Status: Published

Glossary

Alloy: A metallic alloy is a mixture of a metal with other metals or non-metals.

Cementite: It is chemically known as Iron Carbide (Fe_3C) and has an orthorhombic crystal structure. It is a hard and brittle material and formed due to quenching of austenite in case of steels or iron and from martensite during tempering. It can react with ferrite and austenite to form lamellar structure called pearlite and bainite.

Pearlite: It is a lamellar, two phased structure consisting of alternate layers of Cementite and Ferrite in Steel. It is formed by diffusion of all atoms by a eutectoid reaction when austenite is slowly cooled below 723 ^{o}C. The eutectoid mixture contains 0.83% of carbon at 723 ^{o}C

Bainite: It is generally formed in steel due to displacive transformation of atoms on isothermal cooling of the material or subjected to heat treatment process such as austempering. The structure is similar to lamellar Pearlite structure.

Austenite: It is an interstitial, non-magnetic, metallic solid solution of carbon dissolved in iron above the critical temperature of 723 ^{o}C. It is in the form a face centered cubic crystal and can contain up to 2% carbon in solution. It is also known as gamma (γ) iron. The microstructure on slight lattice distortions leads to the formation of martensite.

Ferrite: It is a body centered cubic form of iron containing small amount of dissolved carbon (a maximum of 0.02% at 723 ^{o}C) It is also known as alpha (α) iron and is responsible for the magnetic properties in steel and iron.

Martensite: It is the hardest form of microstructure formed due to rapid cooling of a material during quenching. The face centered cubic lattice of austenite is transformed to body centered tetragonal on lattice distortion due to rapid cooling rate. Martensite is a ferrite super saturated with carbon.

Enthalpy (H): It is a measure of heat content of the system.

Entropy(S): It is a measure of randomness of the system.

Internal Energy (E): it is the sum of potential energy and kinetic energies in the system.

Kinetic Energy: In Solids and Liquids, it is the energy due to atomic vibrations, in gasses; it is the sum of transitional and rotational energies within the atoms and molecules

Potential Energy: It is the energy due to interactions or bonds between the atoms within the system.

Intensive Property: These properties are independent of the size of the system such as Temperature (T) and Pressure (P).

Extensive Property: These properties depend on the quantity of material in the system such as Volume (V), E, H, S and G (Gibbs free energy)

Avogadro number (n): The number of atoms or molecules within 1 mole of material, $n = 6.023 \times 10^{23}$.

Single component systems: A single component system could be one containing a pure element or one type of molecule that does not dissociate over a range of temperature.

Specific Heat ($C_p = \partial H/\partial T$): It is the quantity of heat (Joules) required raising the temperature of the substance by one degree Kelvin at constant pressure.

Substitutional Diffusion: Diffusion occurs through a vacancy mechanism where smaller atoms occupy an existing vacancy or substitute an existing atom or self diffusion.

Interstitial Diffusion: Diffusion occurs as a result of smaller atoms occupying a vacancy in between larger atoms.

Precipitation transformations: $\alpha' \rightarrow \alpha + \beta$, α' is a meta stable super saturated solid solution; β is a stable or Meta stable precipitate and α is a more stable slid solution with the same crystal structure as α'.

Eutectoid transformations: $\gamma \rightarrow \alpha + \beta$, involve replacement of a meta stable phase (γ) by a more stable mixture of two other phases ($\alpha + \beta$).

Ordering Transformation: α (disordered) $\rightarrow \alpha'$ (ordered)

Massive Transformation: The original phase decomposes into one or more new phases which have the same composition as the parent phase, but different crystal structure. $\beta \rightarrow \alpha$, where the reaction results in only one new phase.

Polymorphic Transformation: It occurs in a single component system when different crystal structures are stable over different temperature ranges.

Appendix: Microhardness analysis

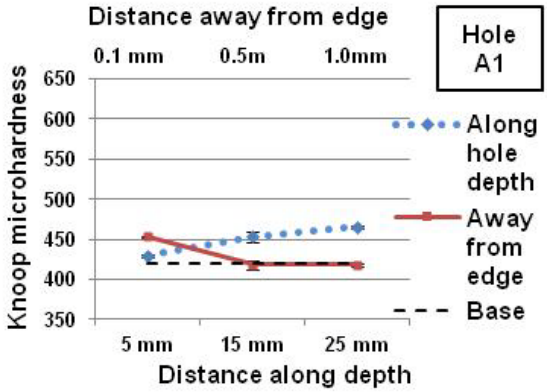

A1-697 rpm, 0.1 mm/rev, coolant on

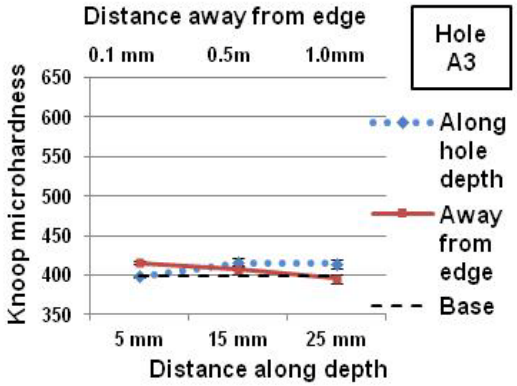

A3-697 rpm, 0.2 mm/rev, coolant on

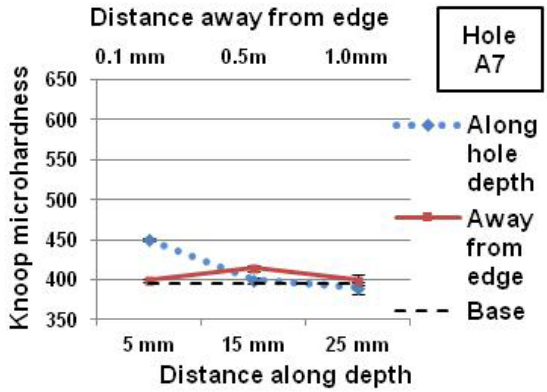

A7-929 rpm, 0.1 mm/rev, coolant on

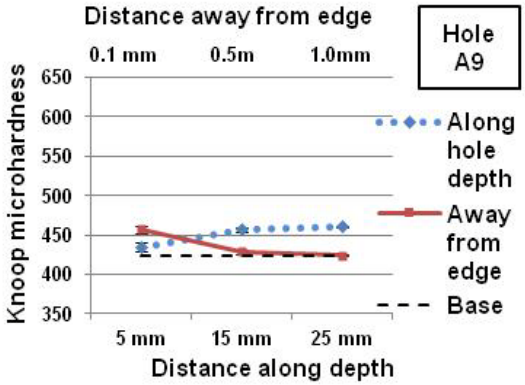

A9-929 rpm, 0.2 mm/rev, coolant on

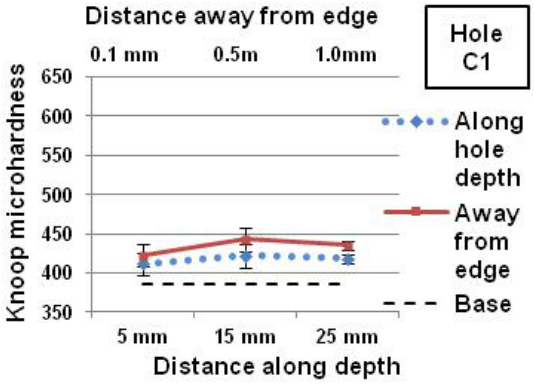

C1-697 rpm, 0.1 mm/rev, coolant off

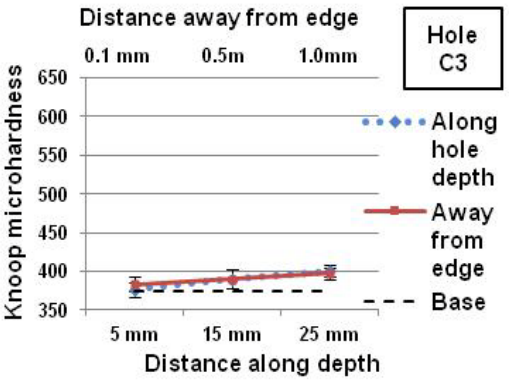

C3-697 rpm, 0.2 mm/rev, coolant off

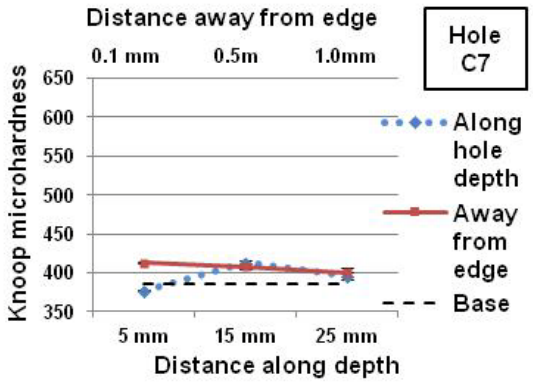

C7-929 rpm, 0.1 mm/rev, coolant off

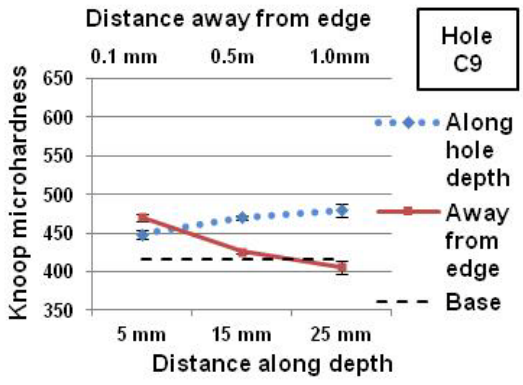

C9-929 rpm, 0.2 mm/rev, coolant off

Figure 85: Knoop microhardness variations along depth and away from edge for grade 900

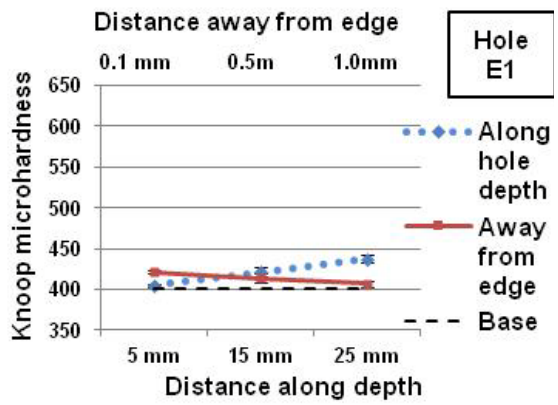

E1-697 rpm, 0.1 mm/rev, coolant on

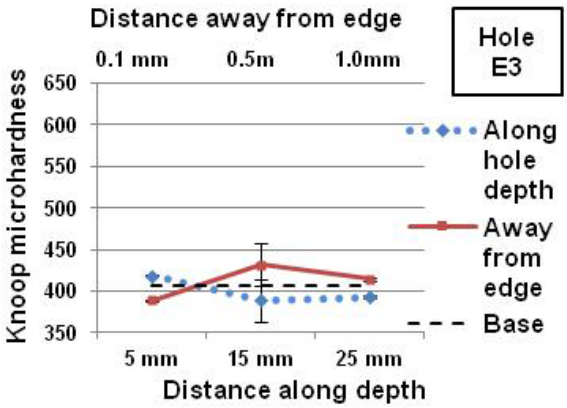

E3-697 rpm, 0.2 mm/rev, coolant on

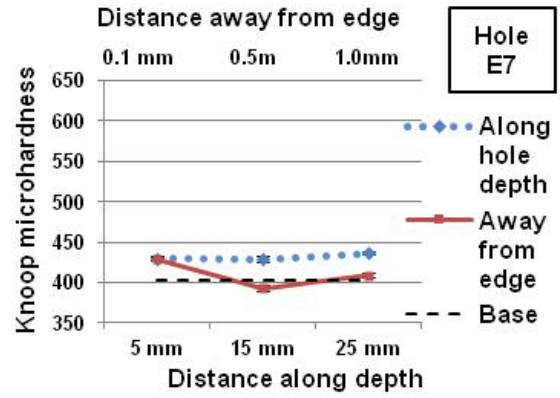

E7-929 rpm, 0.1 mm/rev, coolant on

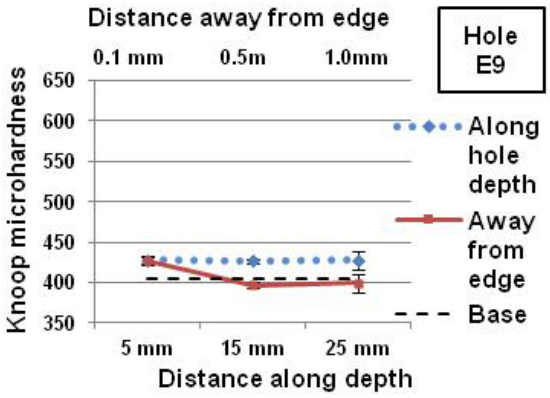

E9-929rpm, 0.2 mm/rev, coolant on

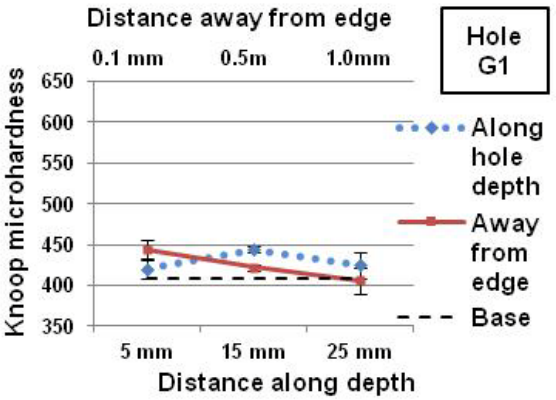

G1-697 rpm, 0.1 mm/rev, coolant off

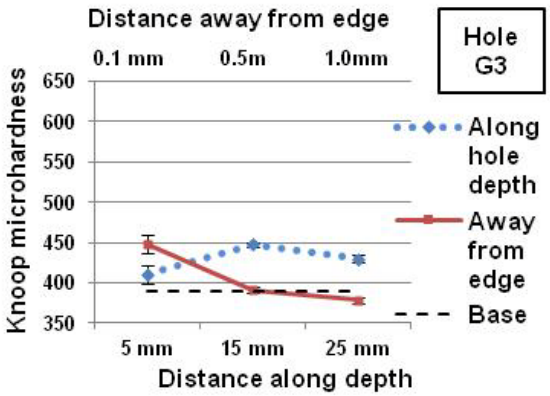

G3-697 rpm, 0.2 mm/rev, coolant off

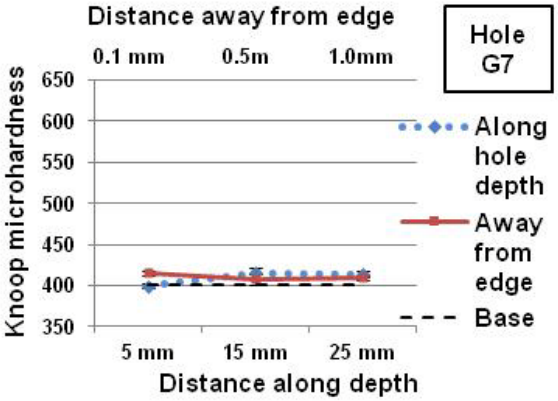

G7-929 rpm, 0.1 mm/rev, coolant off

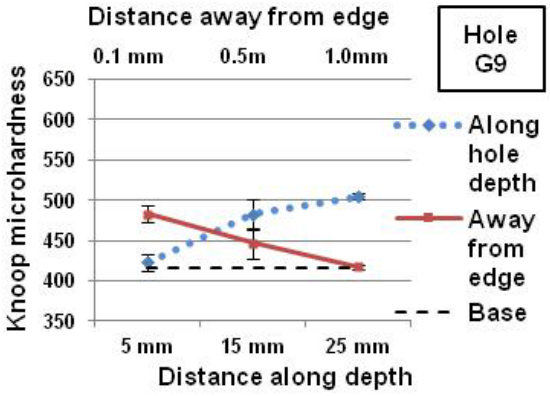

G9-929 rpm, 0.2 mm/rev, coolant off

Figure 86: Knoop microhardness variations along depth and away from edge for grade 1050

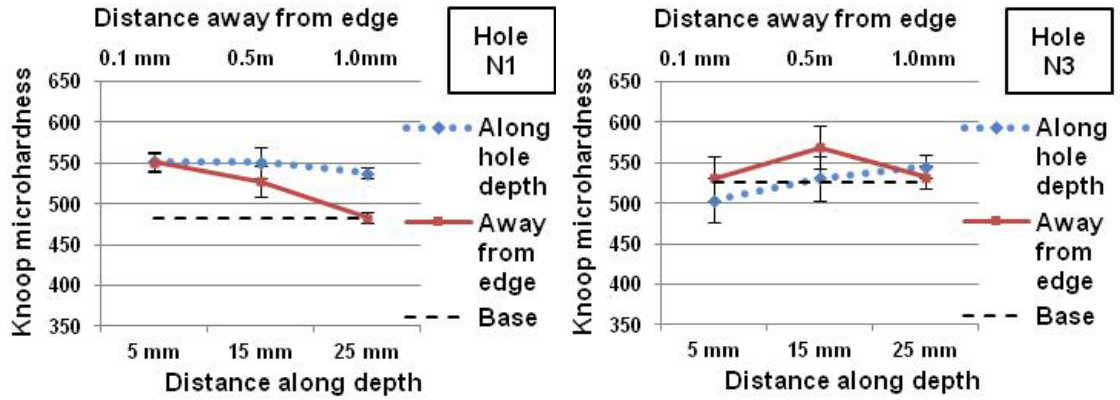

N1-697 rpm, 0.1 mm/rev, coolant on

N3-697 rpm, 0.2 mm/rev, coolant on

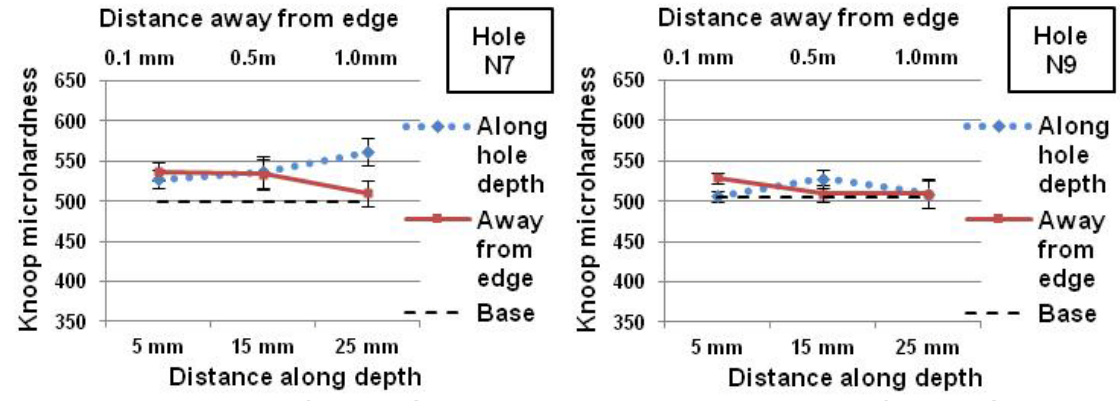

N7-929 rpm, 0.1 mm/rev, coolant on

N9-929 rpm, 0.2 mm/rev, coolant on

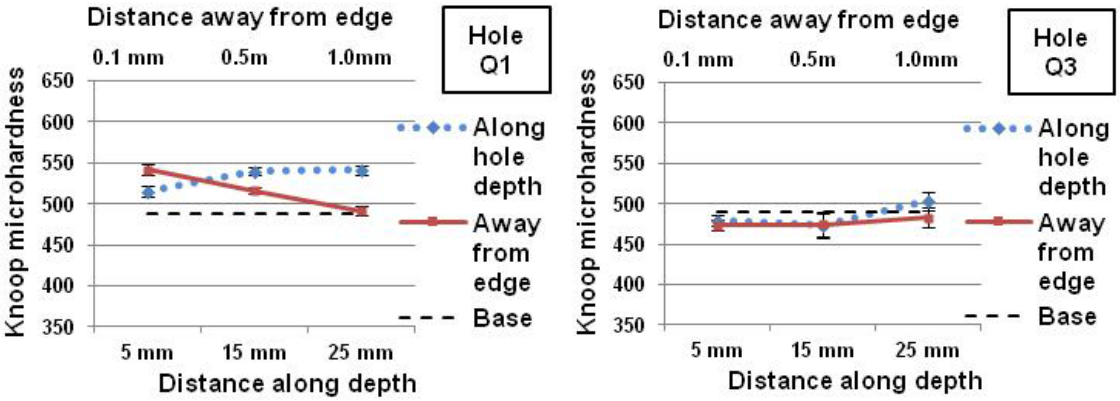

Q1-697 rpm, 0.1 mm/rev, coolant off

Q3-697 rpm, 0.2 mm/rev, coolant off

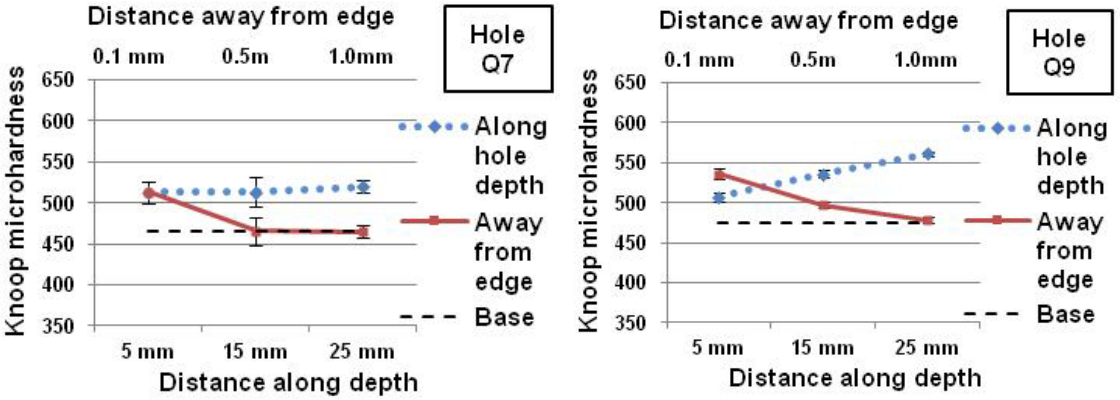

Q7-929 rpm, 0.1 mm/rev, coolant off

Q9-929 rpm, 0.2 mm/rev, coolant off

Figure 87: Knoop microhardness variations along depth and away from edge for grade 1400

Appendix: Chip morphology analysis

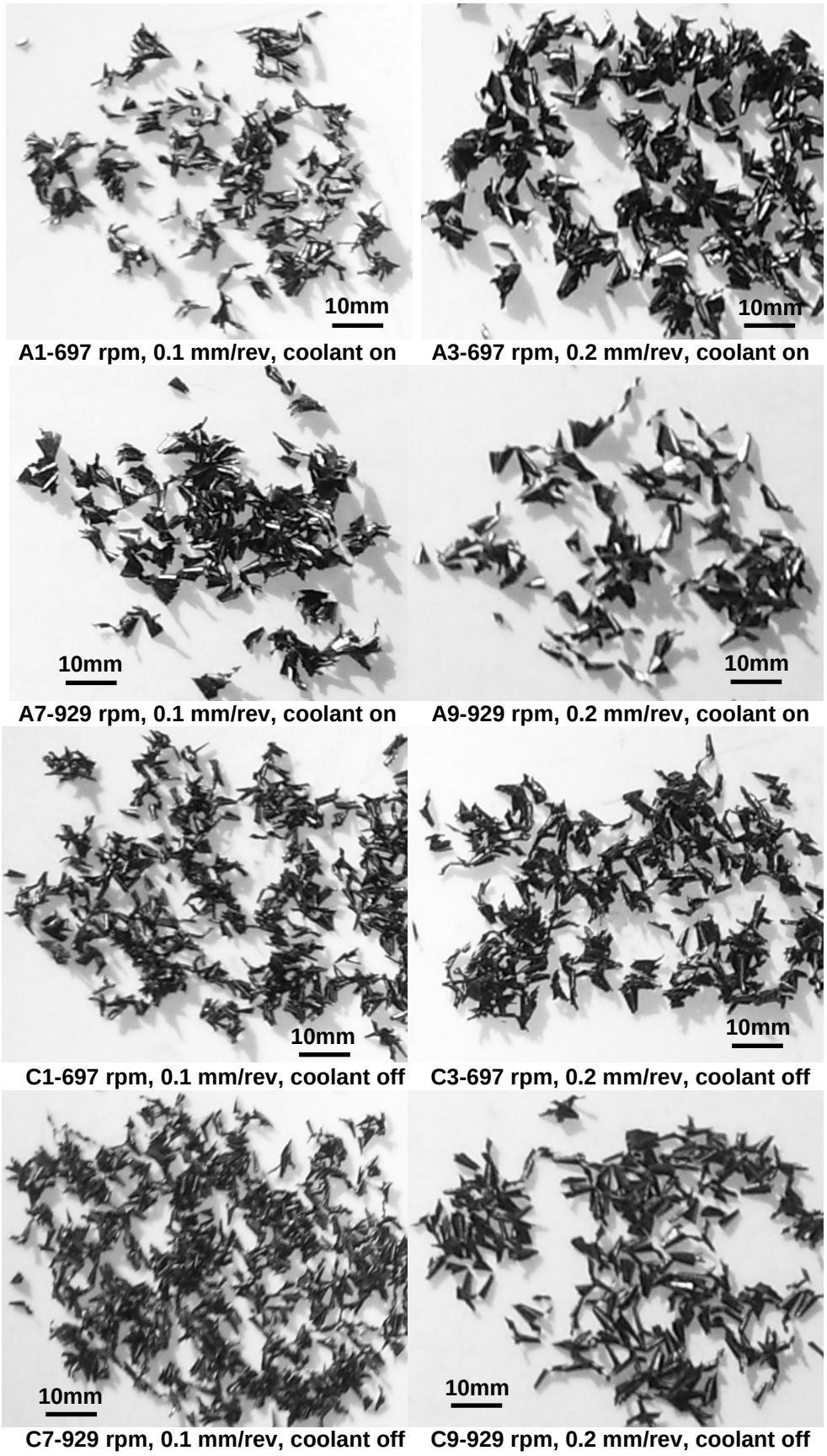

Figure 88: Chip morphology - grade 900

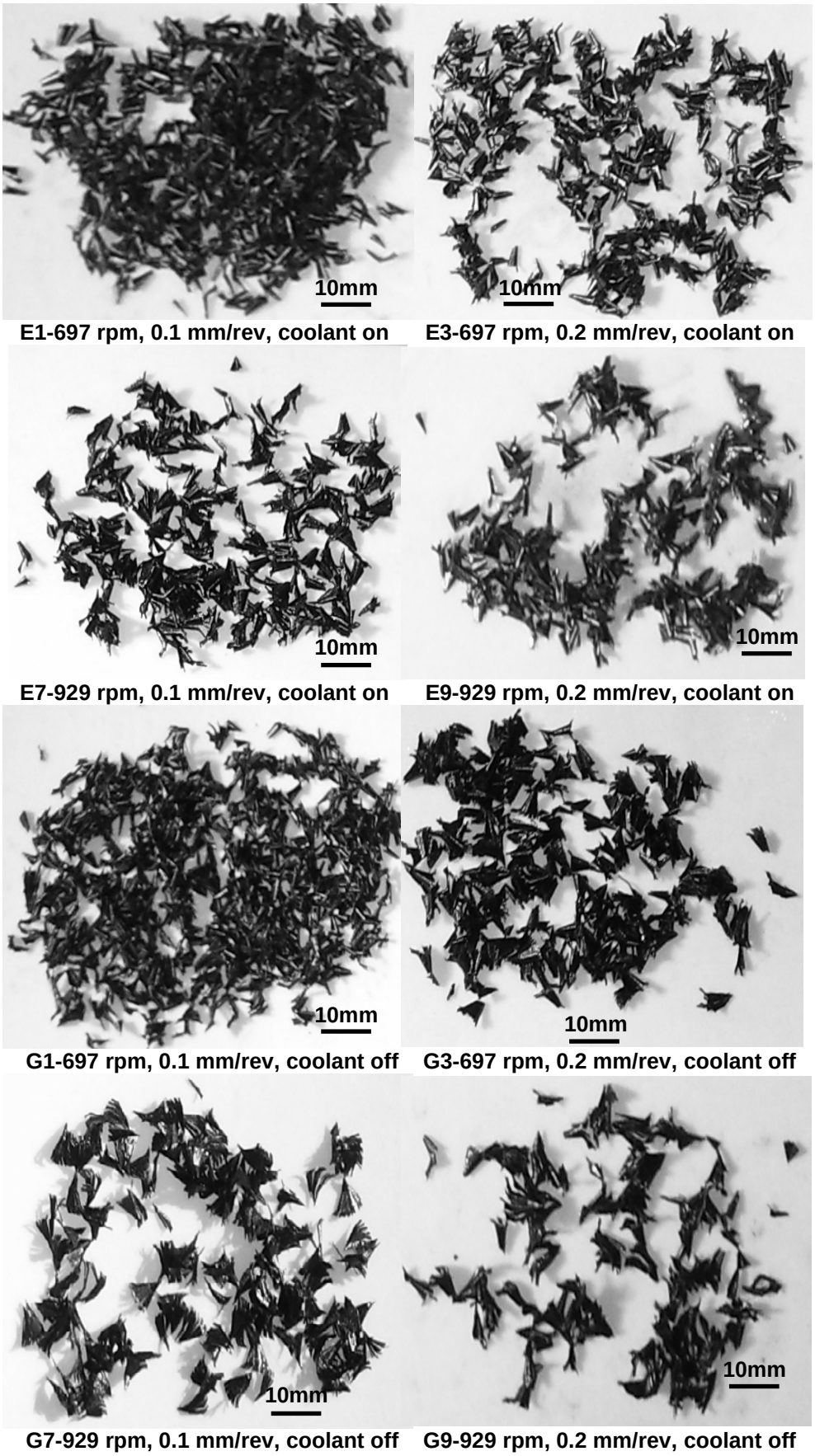

Figure 89: Chip morphology - grade 1050

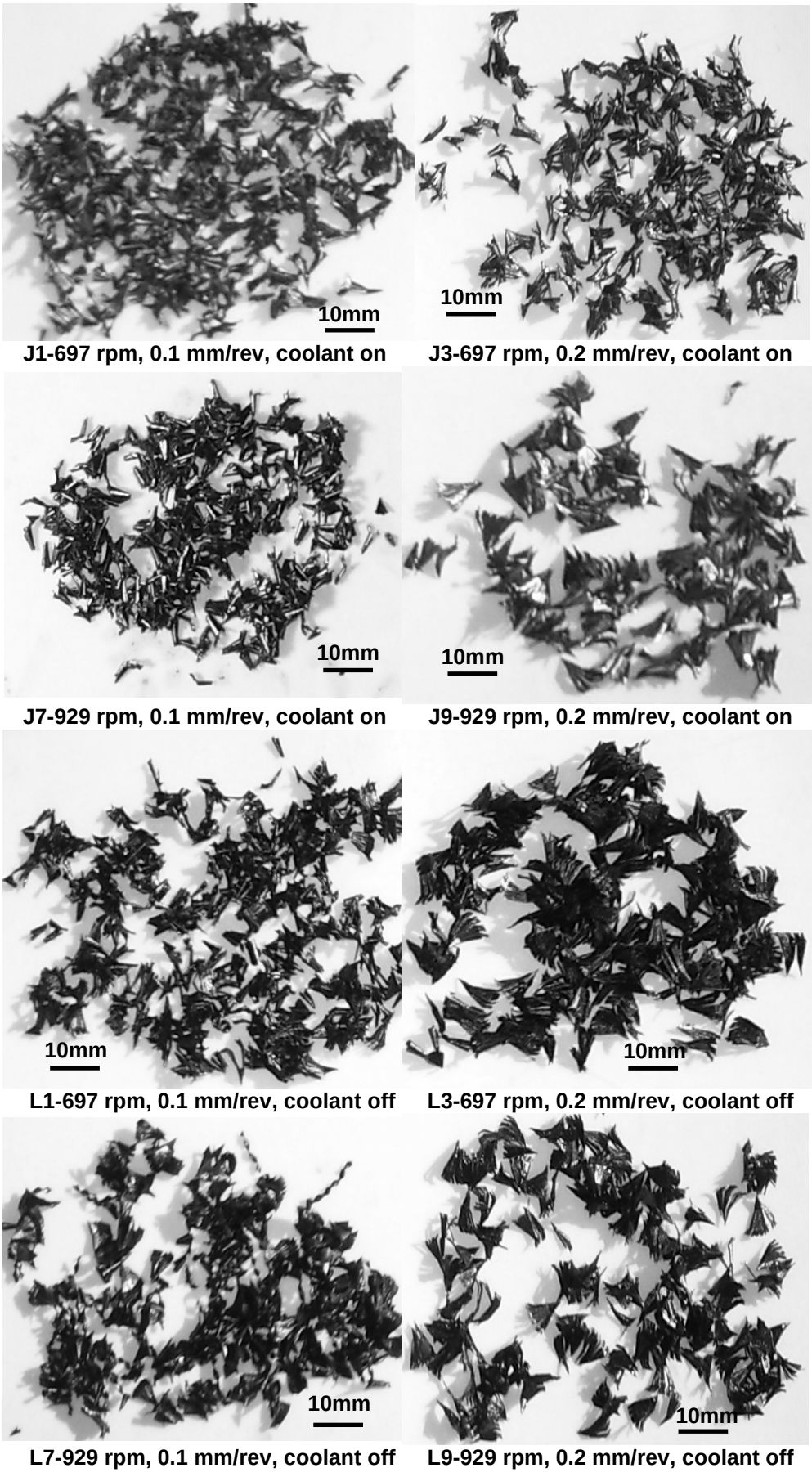

Figure 90: Chip morphology - grade 1200

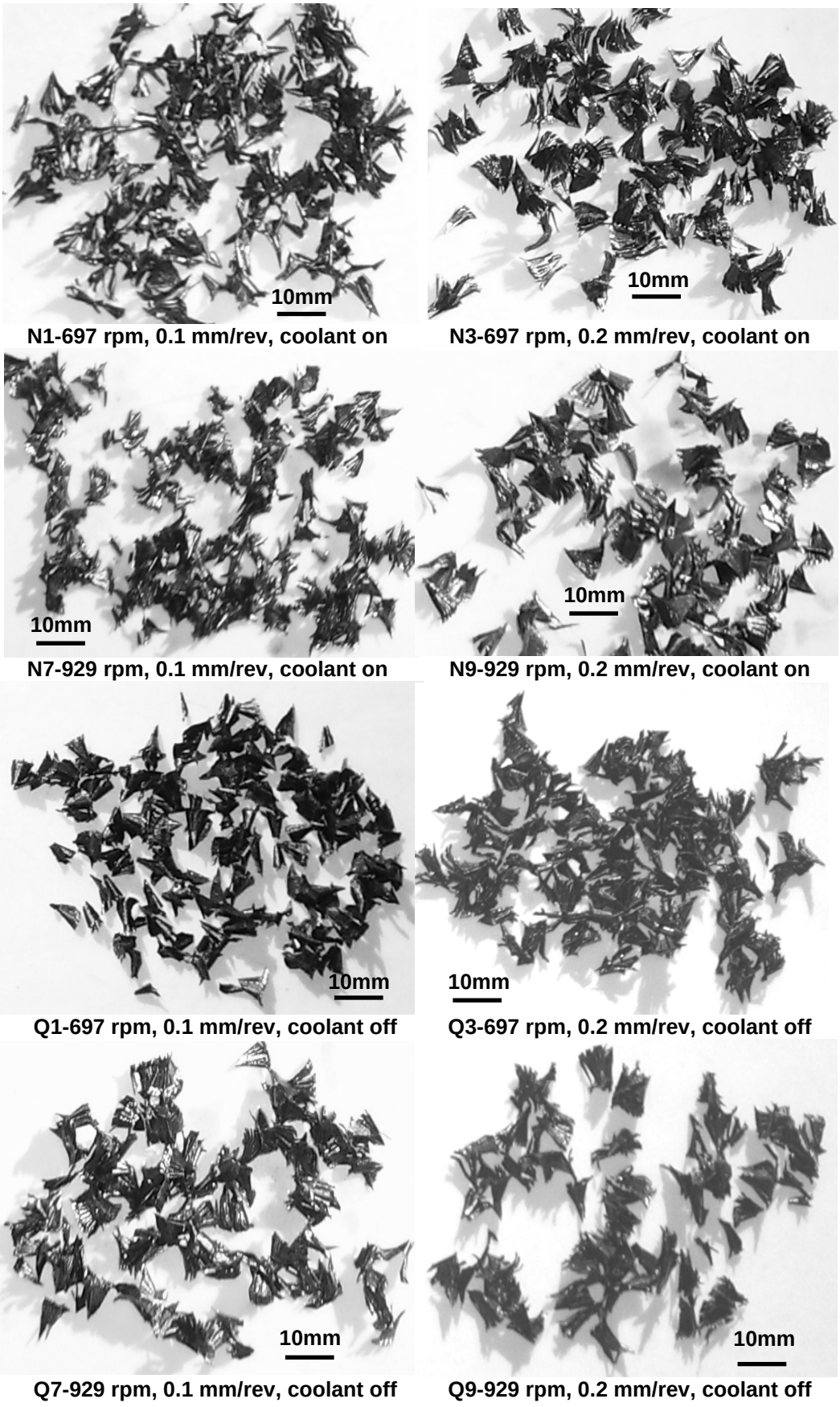

Figure 91: Chip morphology - grade 1400

Appendix: Metallography analysis

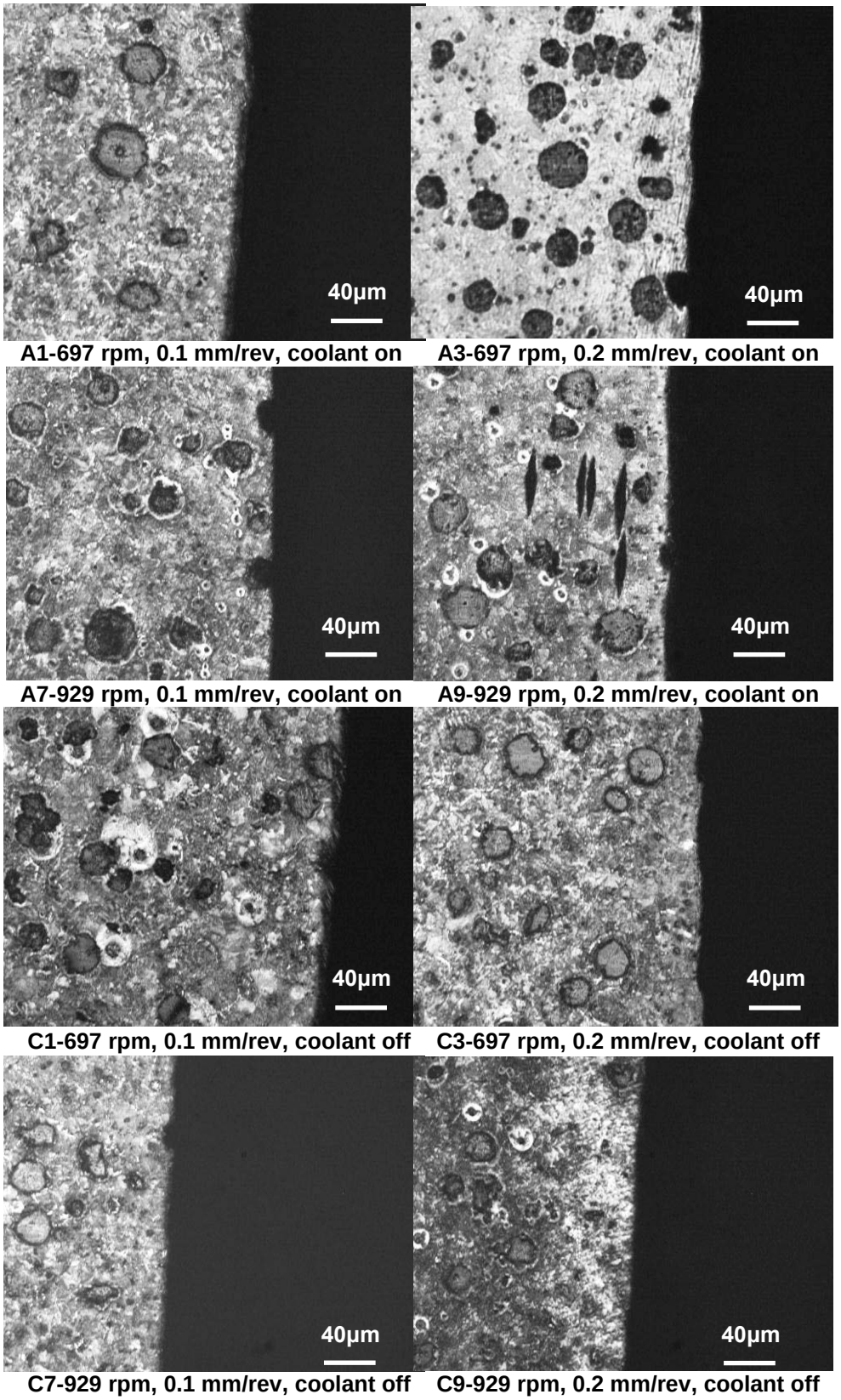

Figure 92: Metallography analysis - grade 900

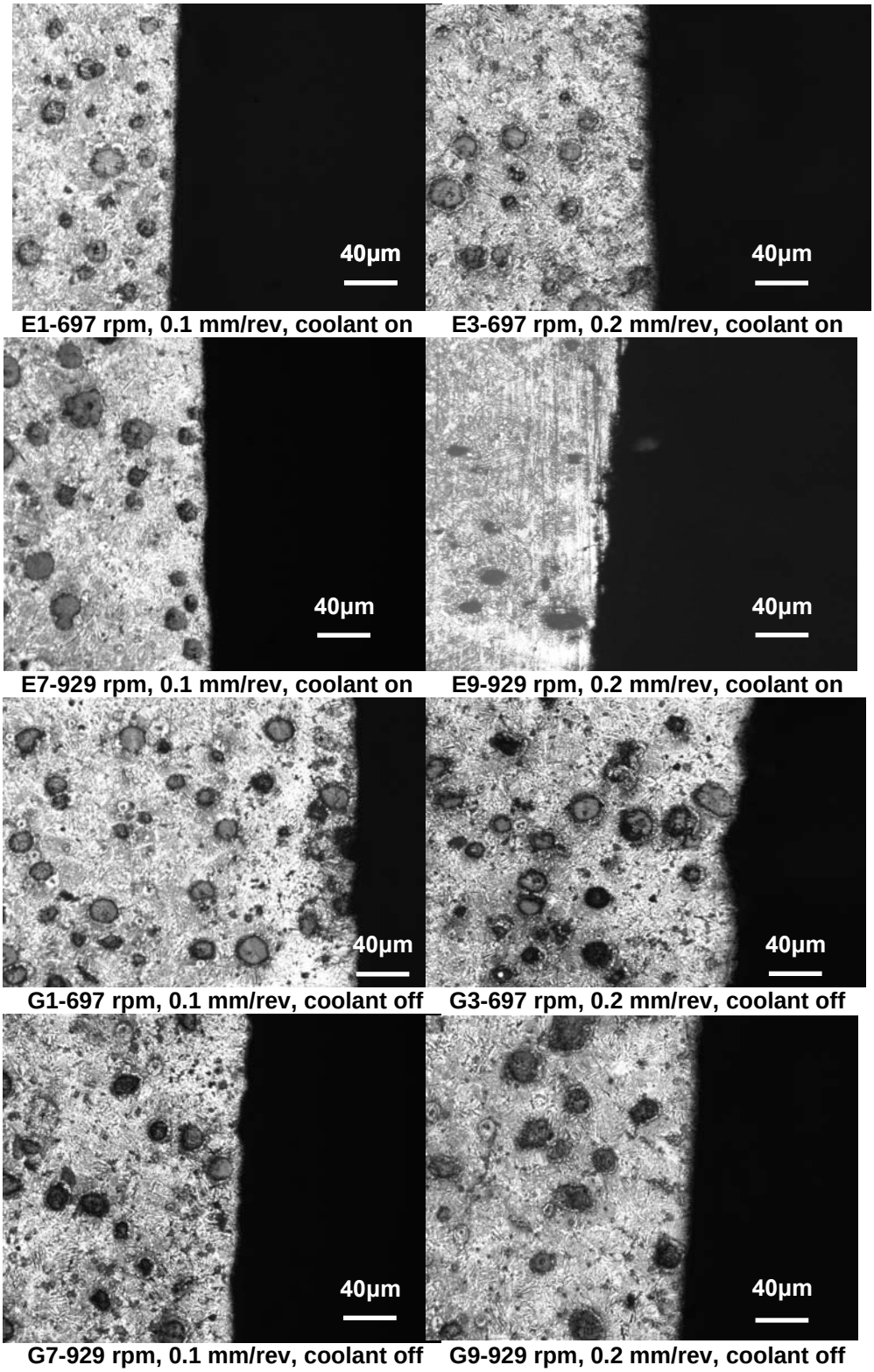

Figure 93: Metallography analysis - grade 1050

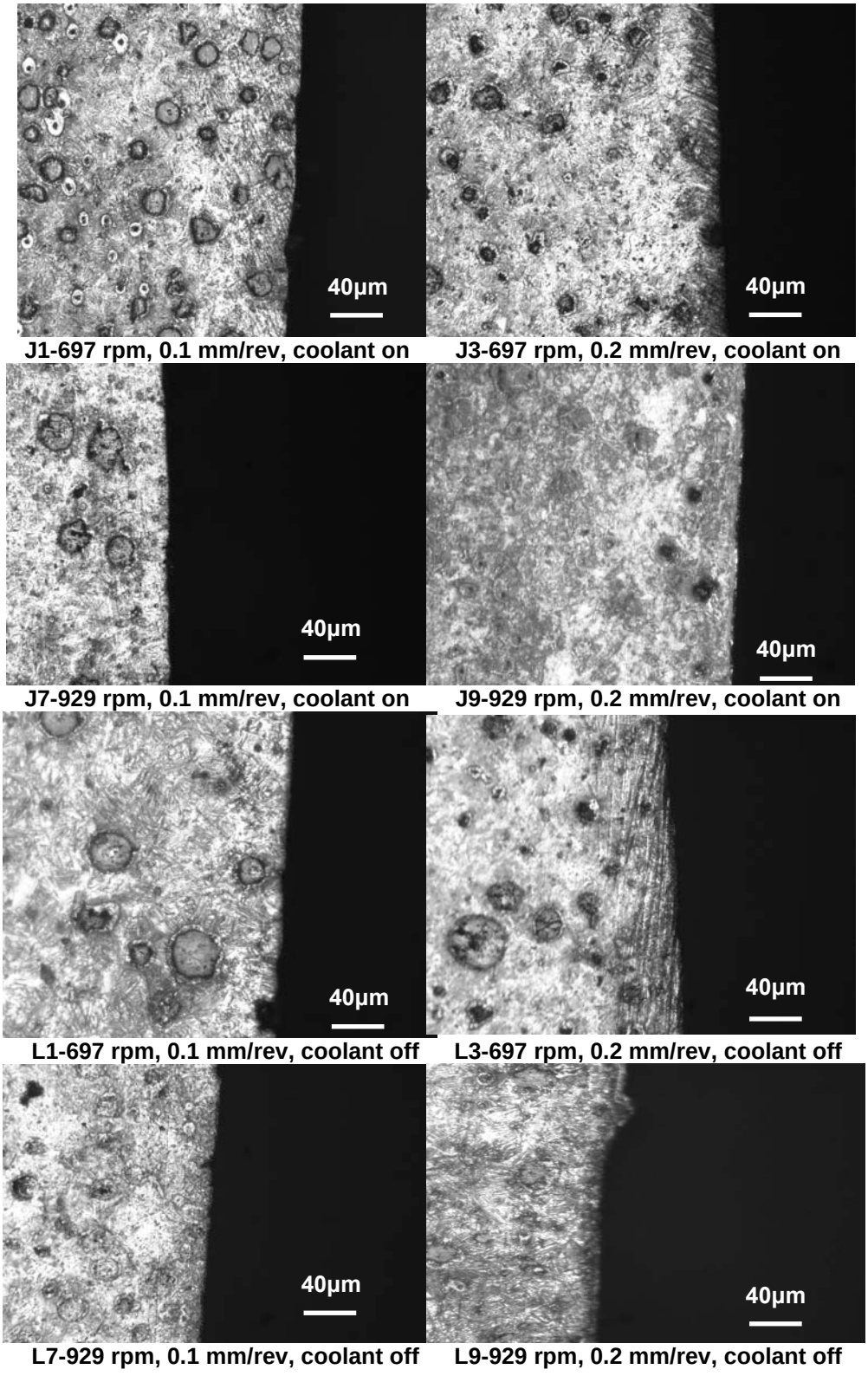

Figure 94: Metallography analysis - grade 1200

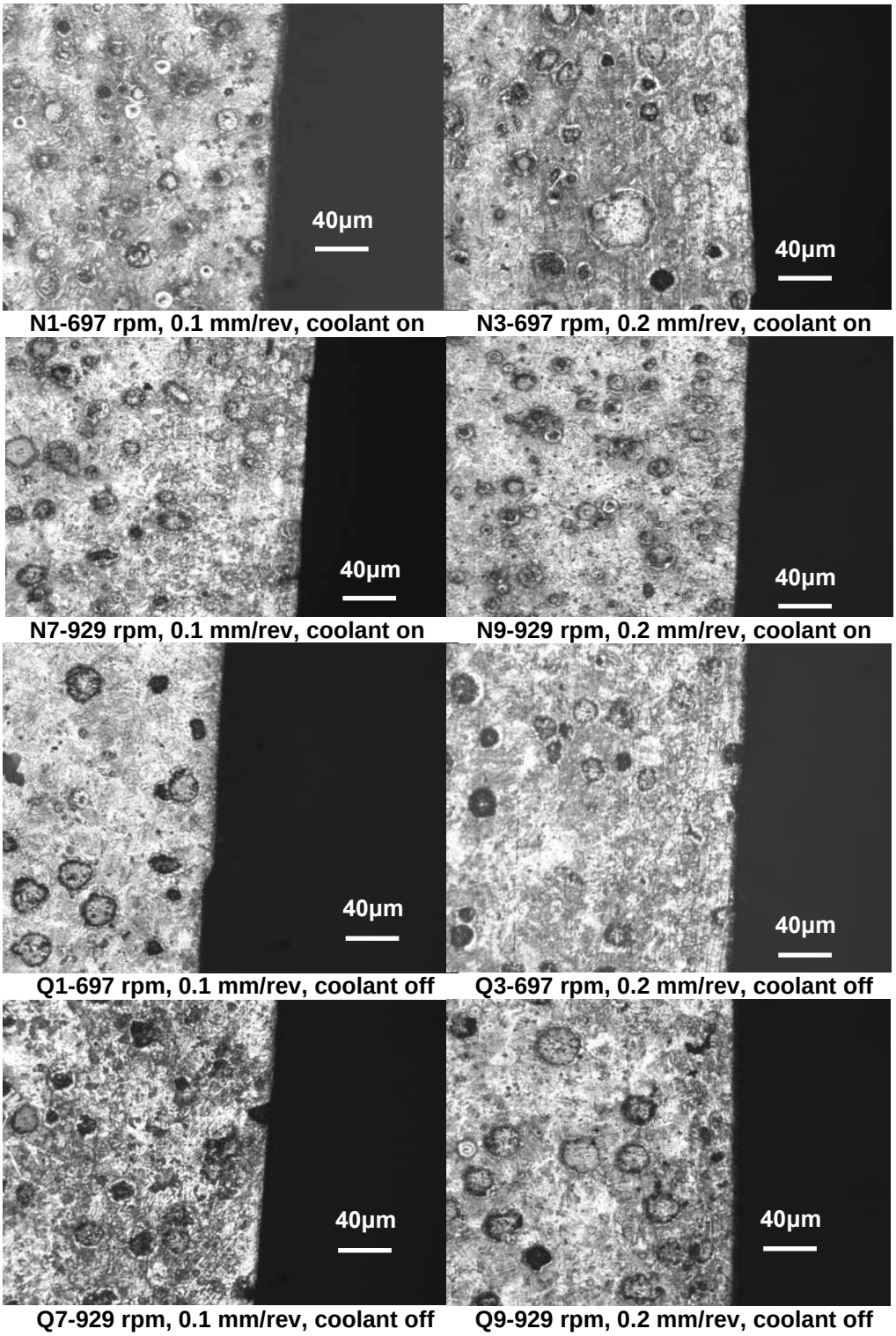

Figure 95: Metallography analysis - grade 1400

Appendix: Tensile testing - standard specimen

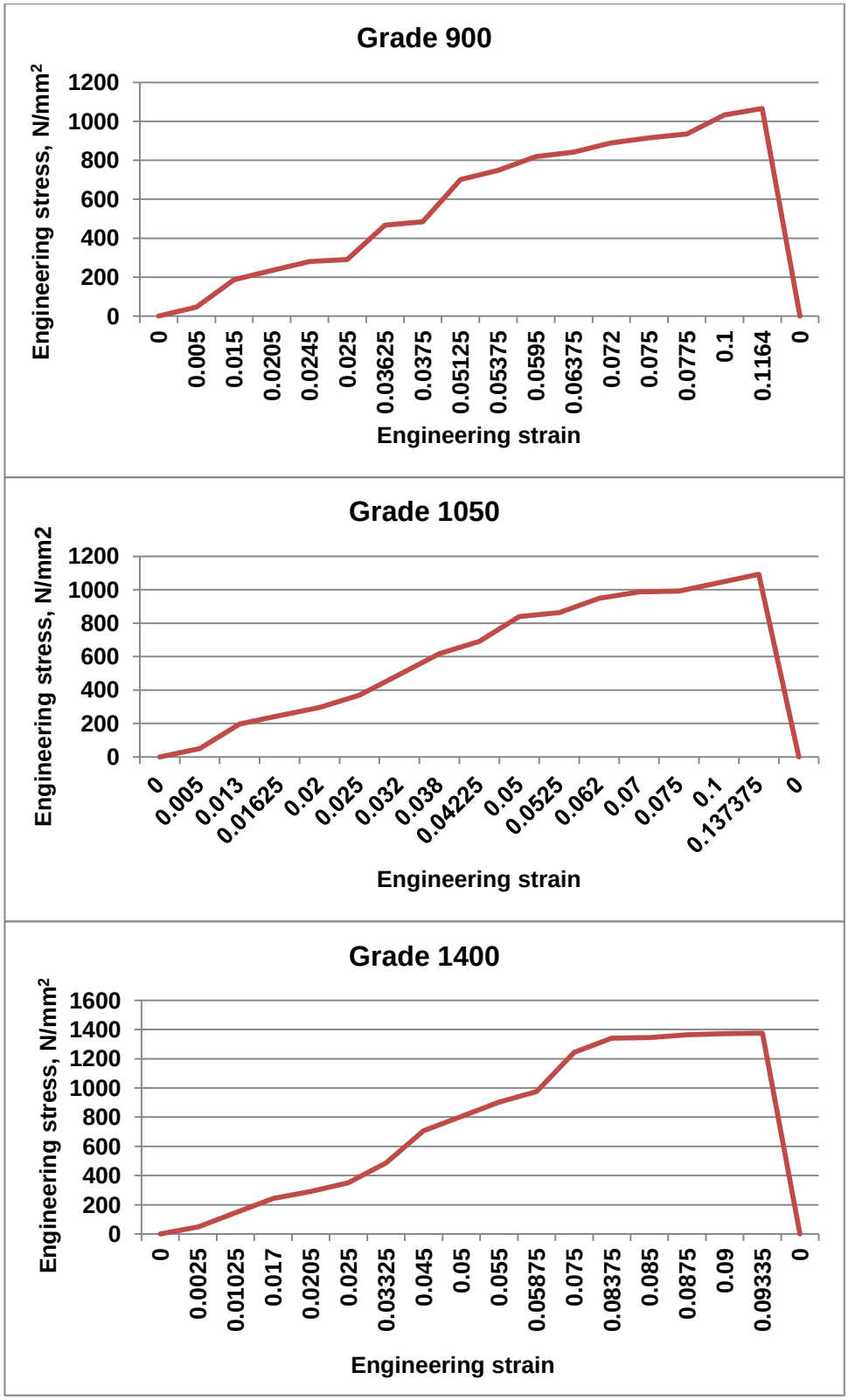

Figure 96: Tensile test results for grade 900, 1050 and 1400 - standard specimen

Appendix: Tensile testing - standard specimen - ANSYS

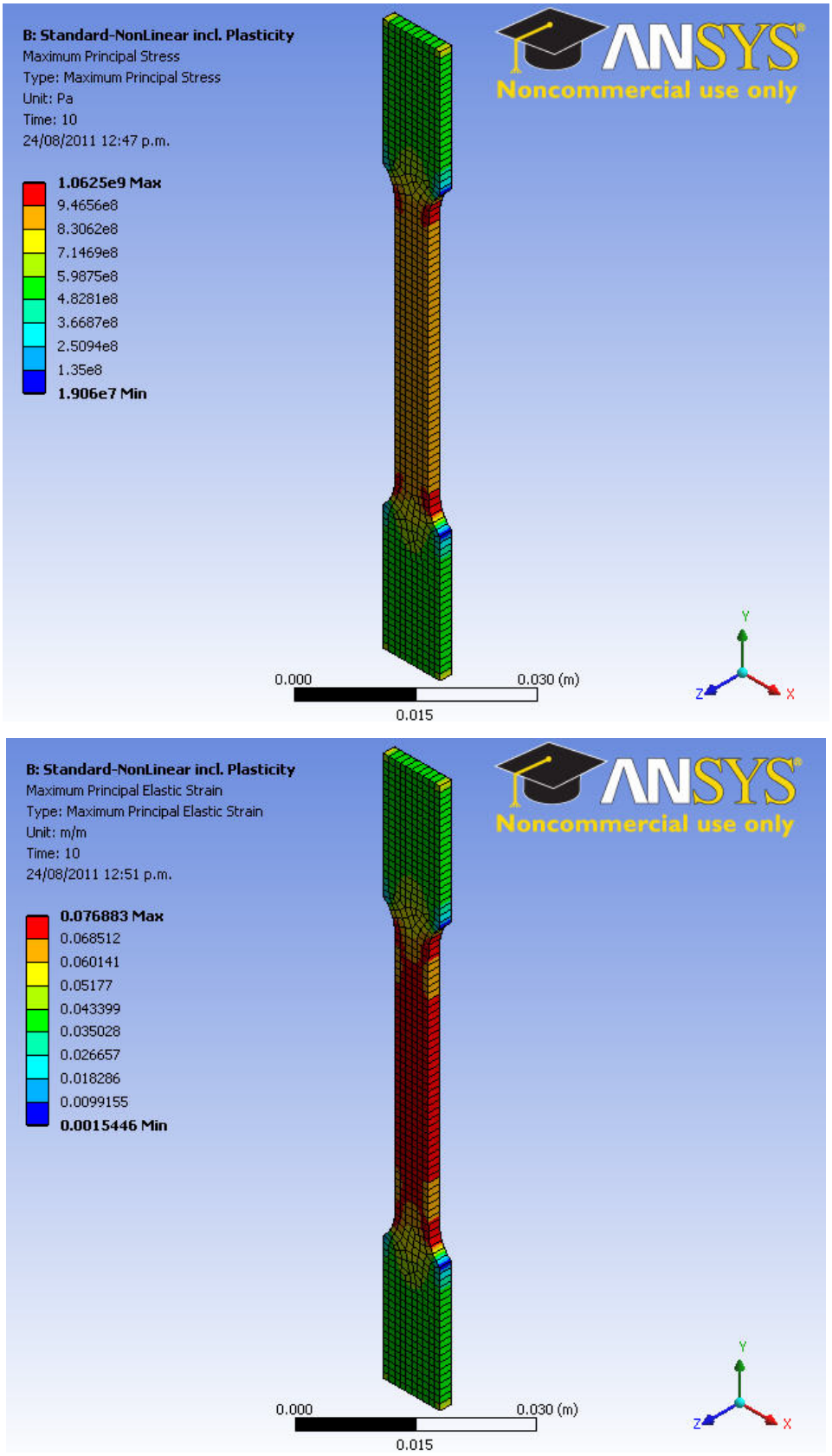

Figure 97: Tensile test using ANSYS - maximum principal stress & elastic strain - grade 900

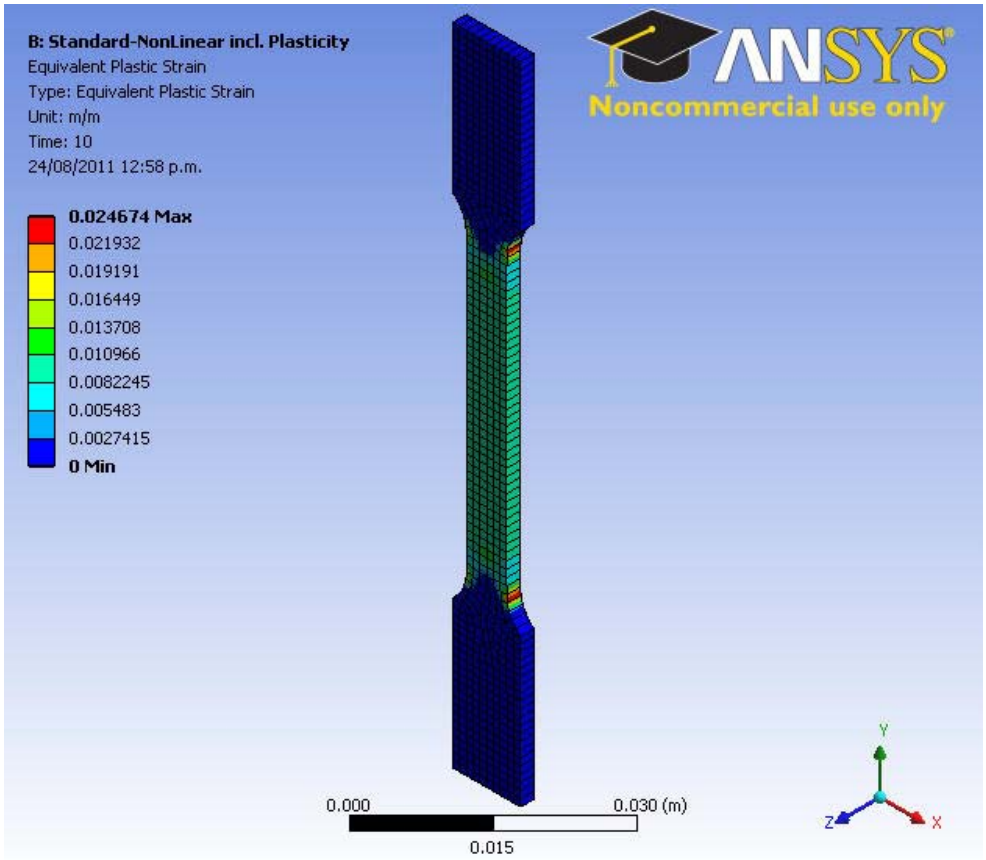

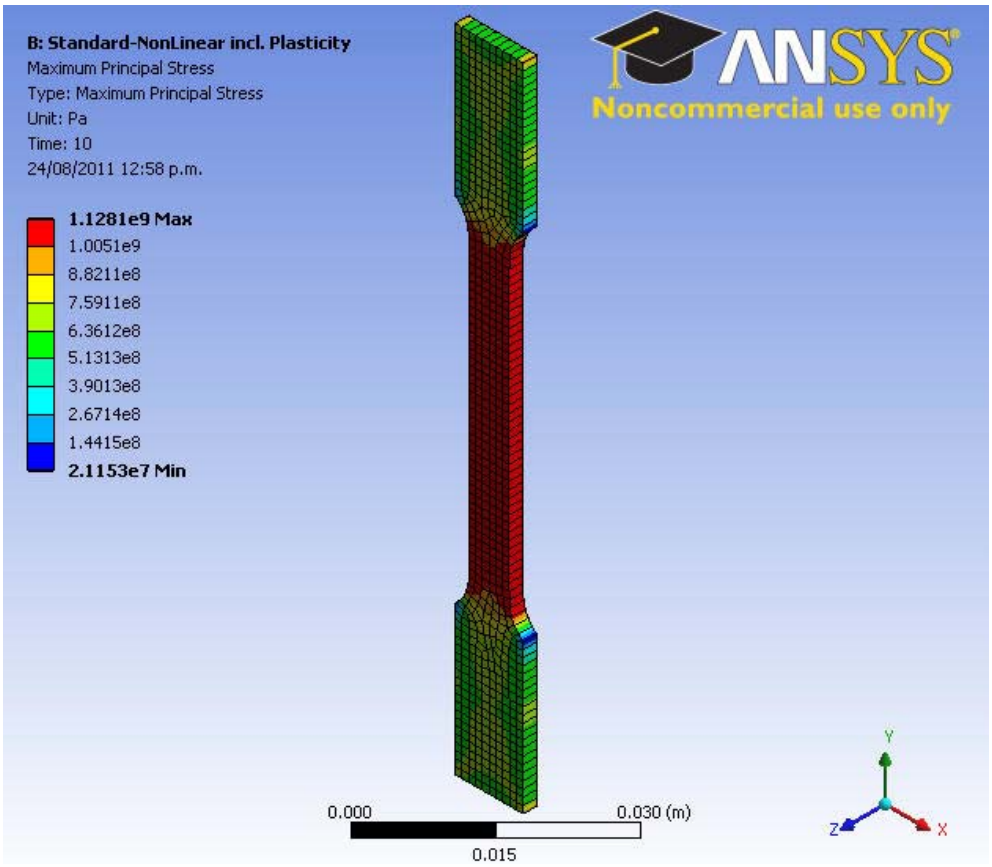

Figure 98: Tensile test using ANSYS - plastic strain & maximum principal stress - grade 1050

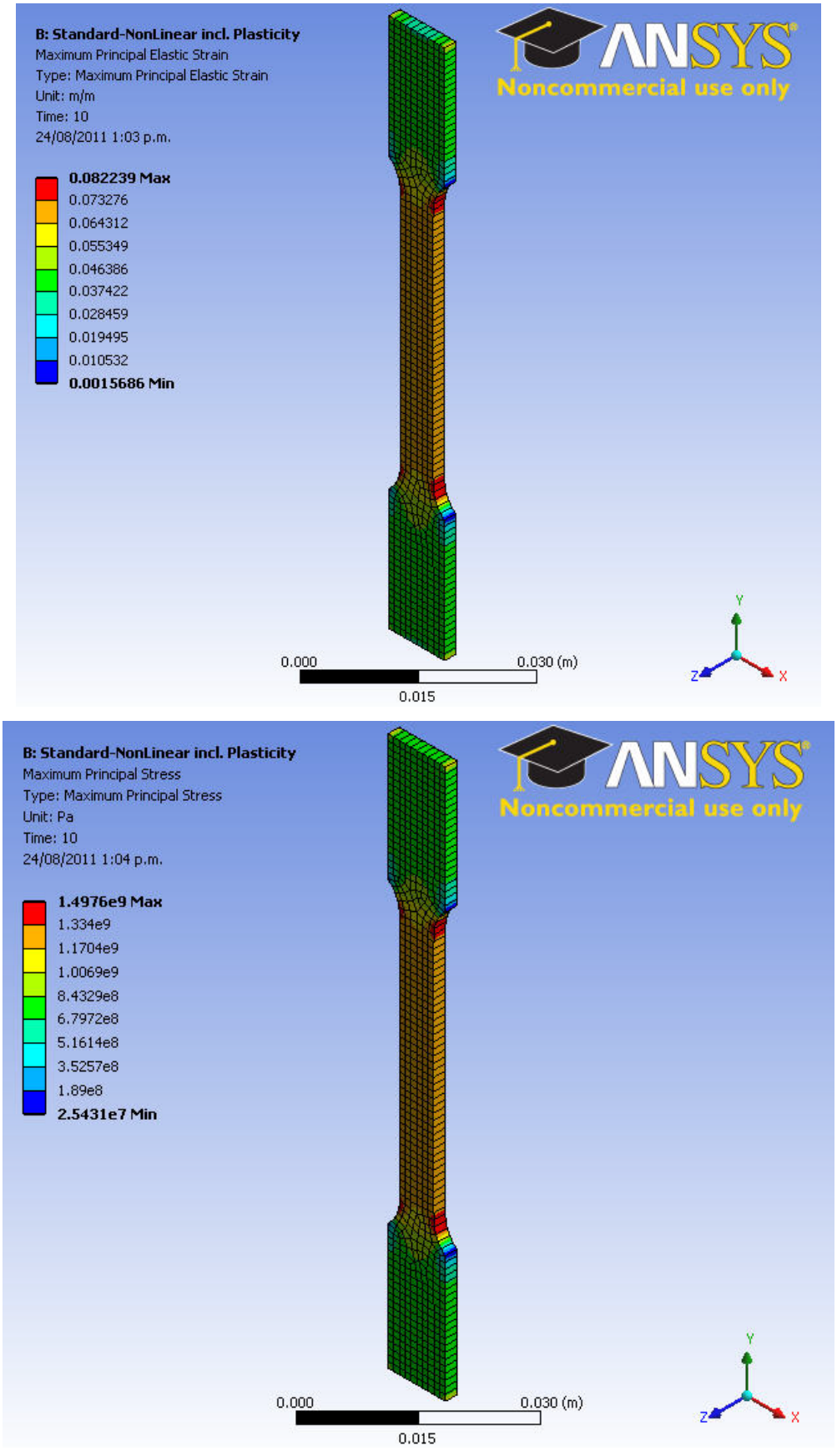

Figure 99: Tensile test using ANSYS - maximum principal elastic strain & stress - grade 1400

Appendix: Tensile testing - tapered specimen - ANSYS

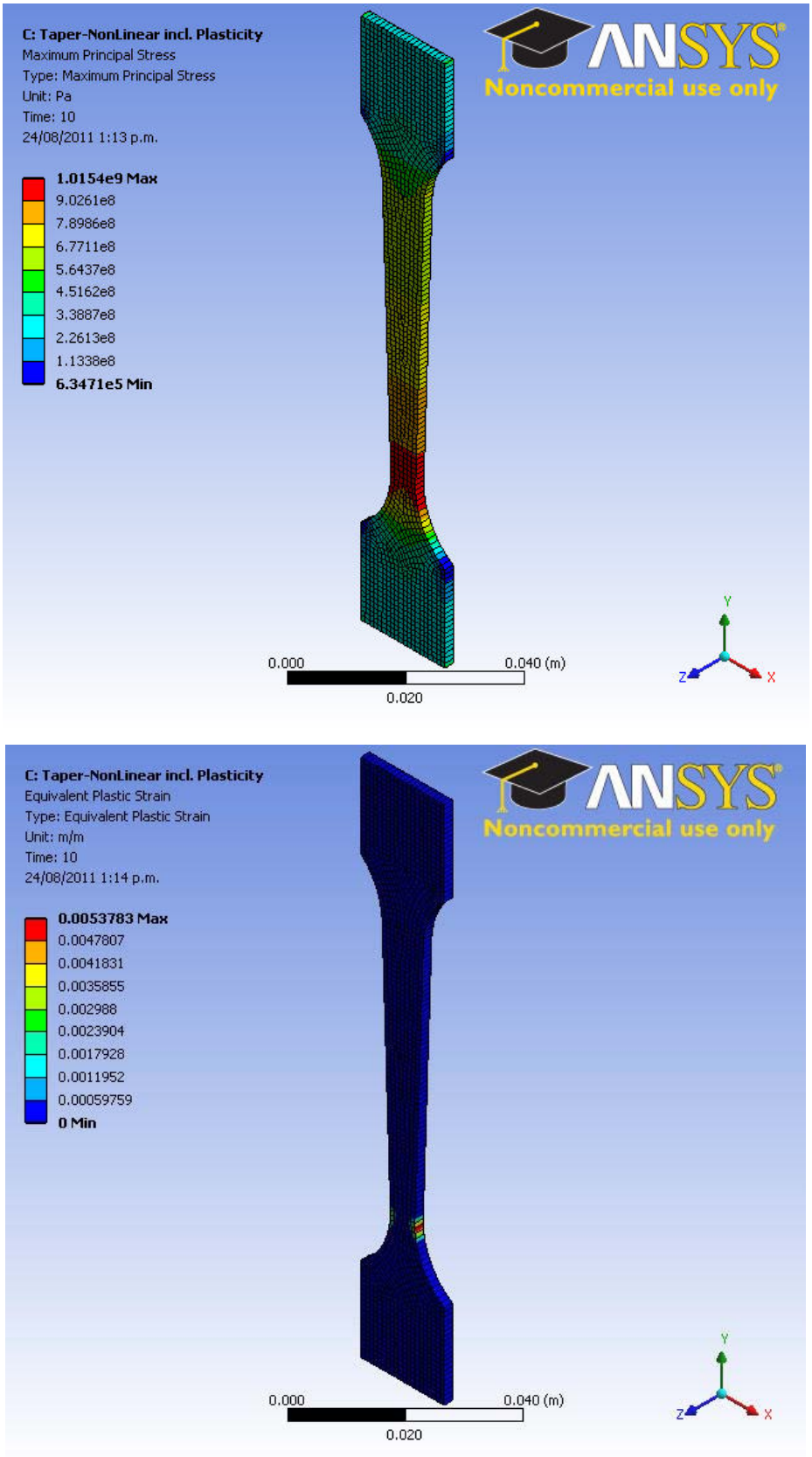

Figure 100: Tensile test using ANSYS - maximum principal stress & plastic strain - grade 900

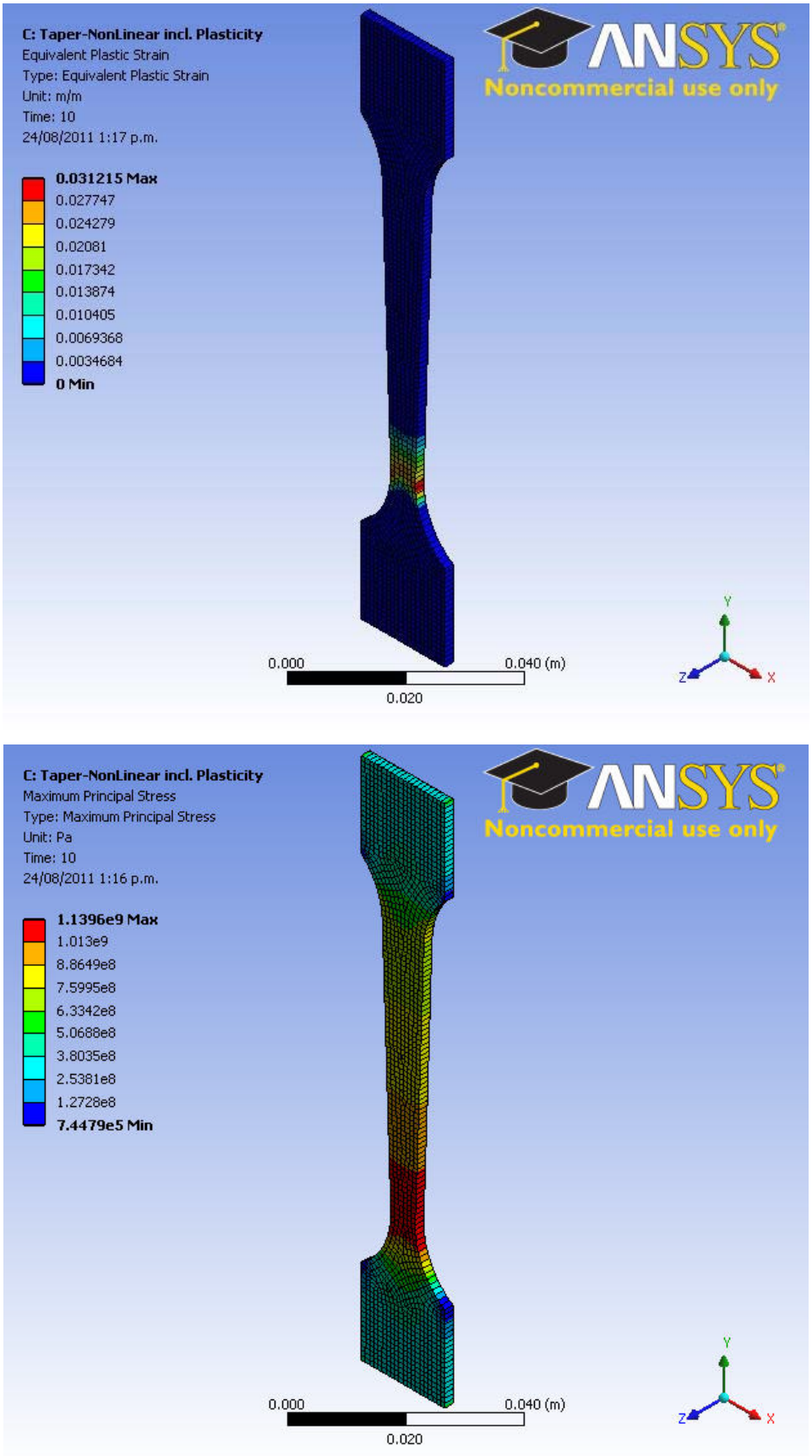

Figure 101: Tensile test using ANSYS - plastic strain & maximum principal stress - grade 1050

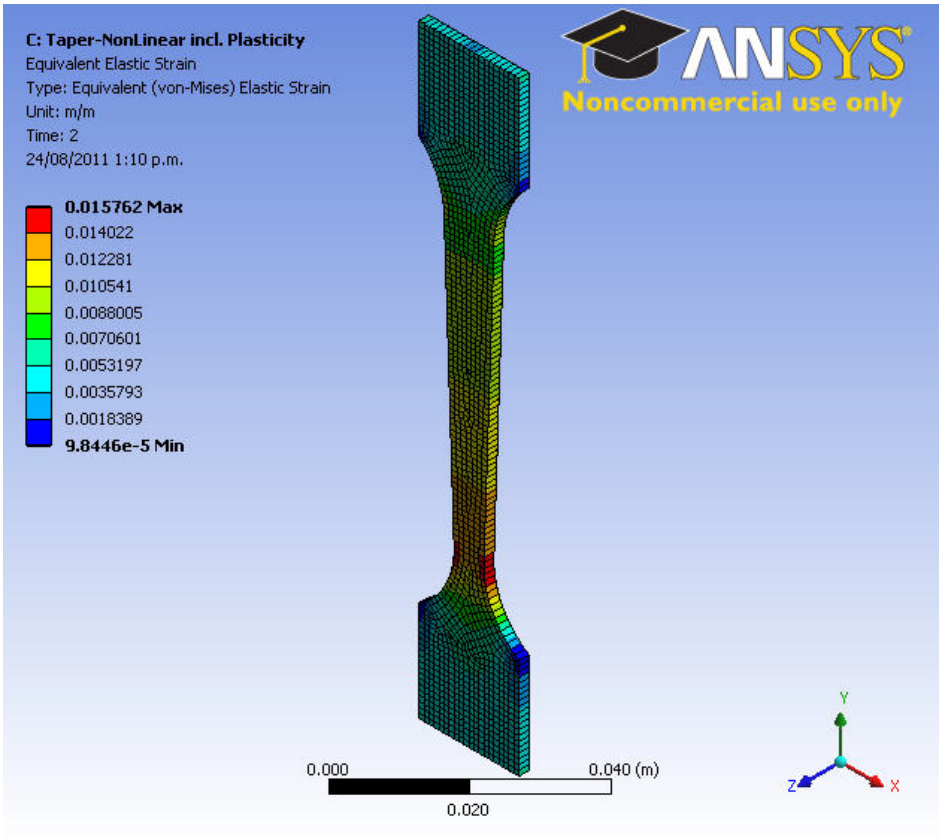

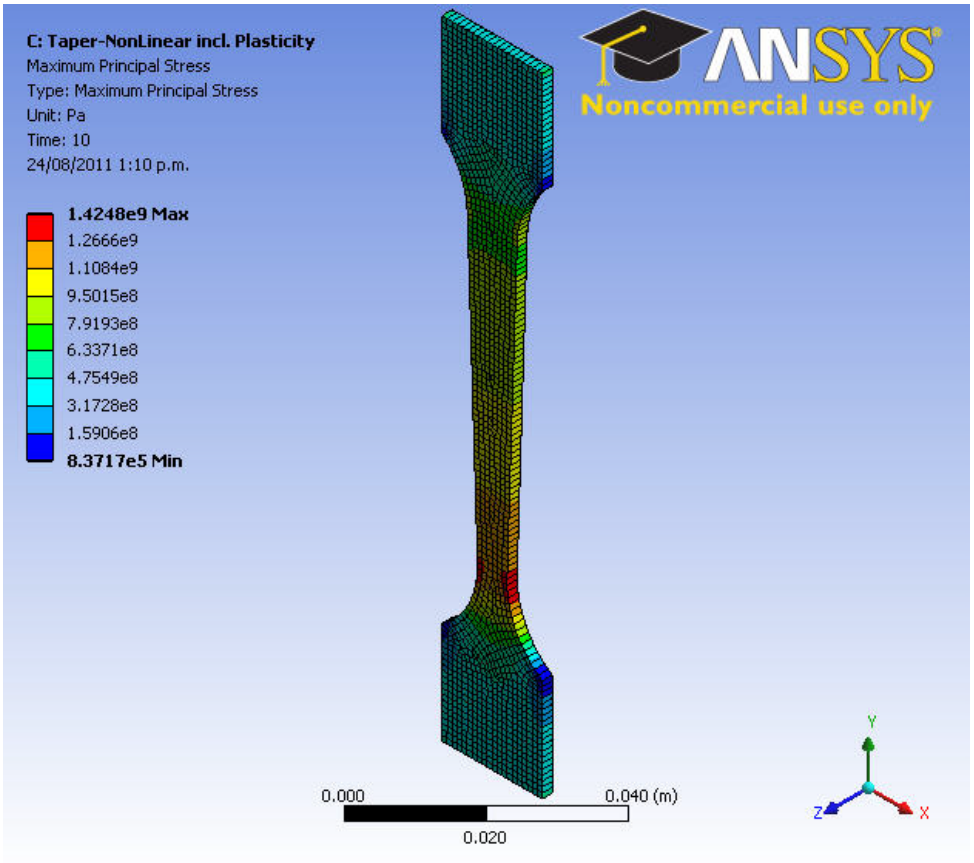

Figure 102: Tensile test using ANSYS - maximum principal elastic strain & stress - grade 1400

Appendix: XRD data for basic samples

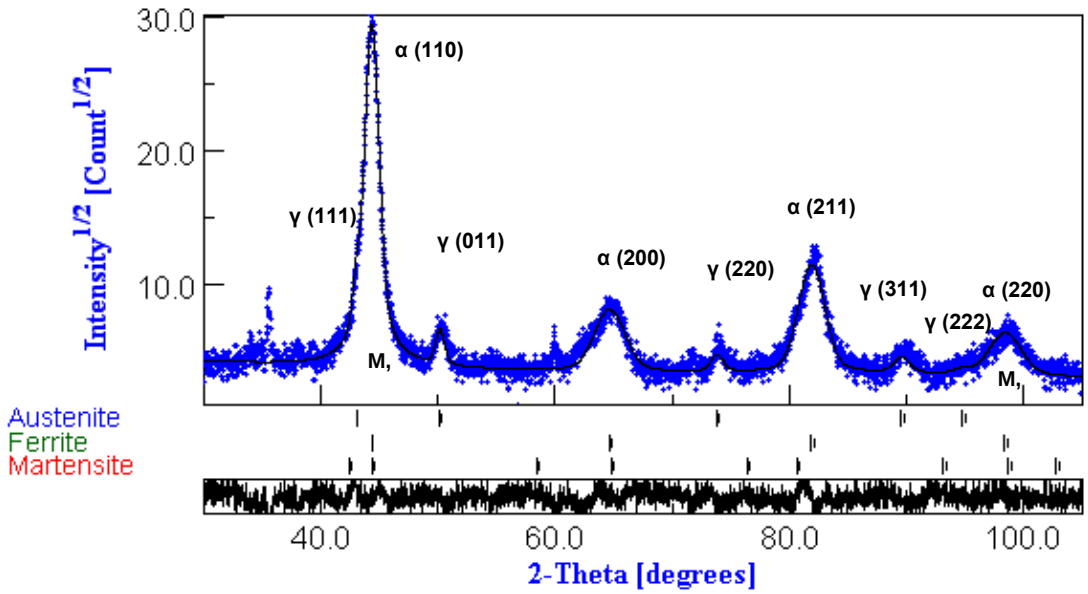

Microstructural phase	Austenite(γ)	Ferrite(α)	Martensite(M)
Weight (%)	6.2 ± 0.2	92 ± 1	1.8 ± 2.3

Grade 1050

Figure 103: XRD data for basic sample - grade 1050

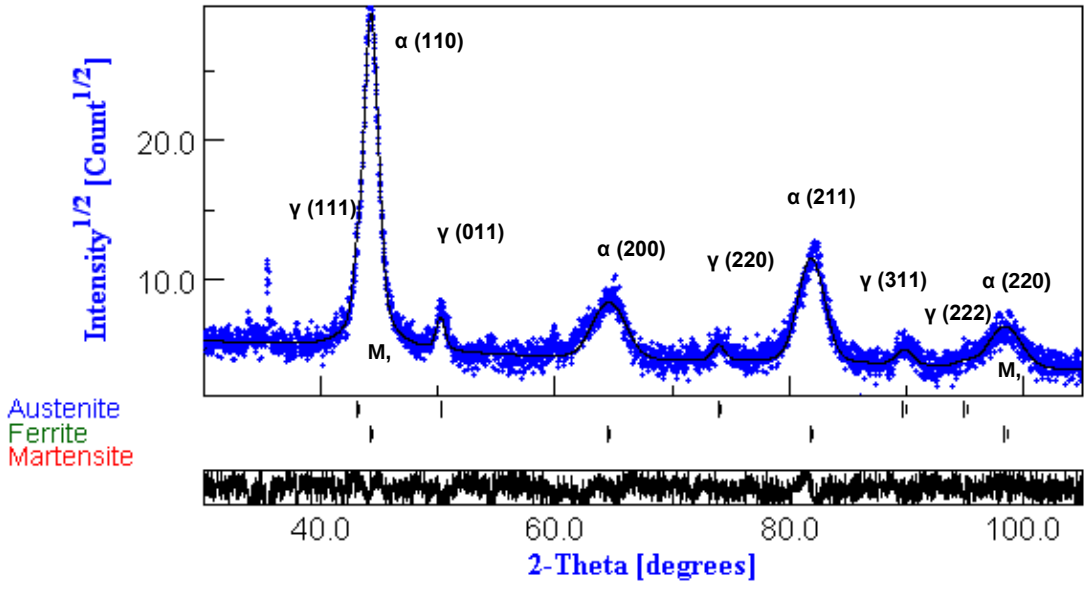

Microstructural phase	Austenite(γ)	Ferrite(α)	Martensite(M)
Weight (%)	6.2 ± 0.2	92 ± 1	0.2 ± 0.1

Grade 1200

Figure 104: XRD data for basic sample - grade 1200

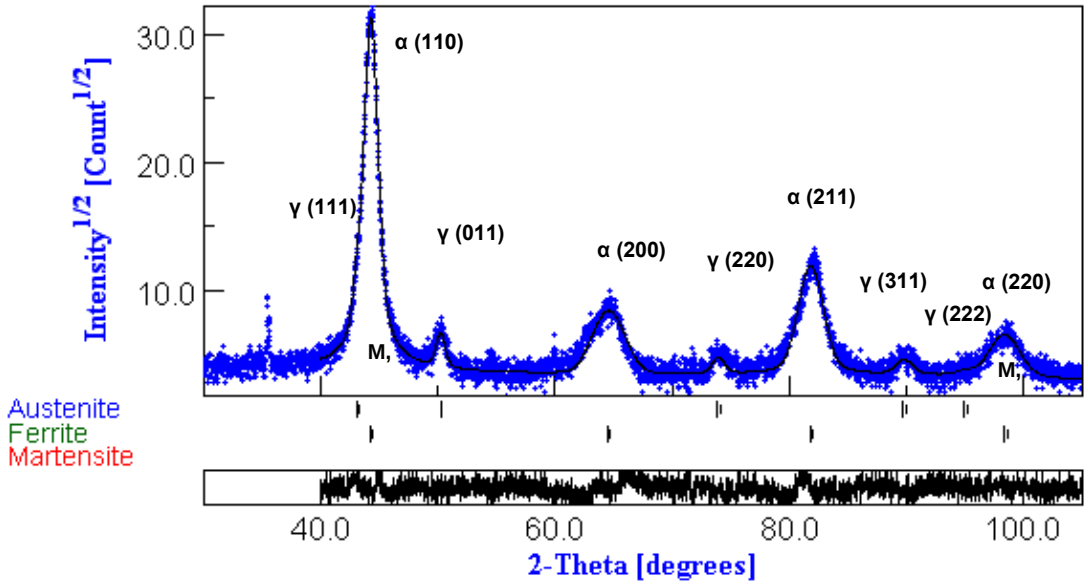

Microstructural phase	Austenite(γ)	Ferrite(α)	Martensite(M)
Weight (%)	6.1 ± 0.2	94 ± 1	0.1 ± 0.1

Grade 1400

Figure 105: XRD data for basic sample - grade 1400

Appendix: XRD data for tensile test - standard specimen

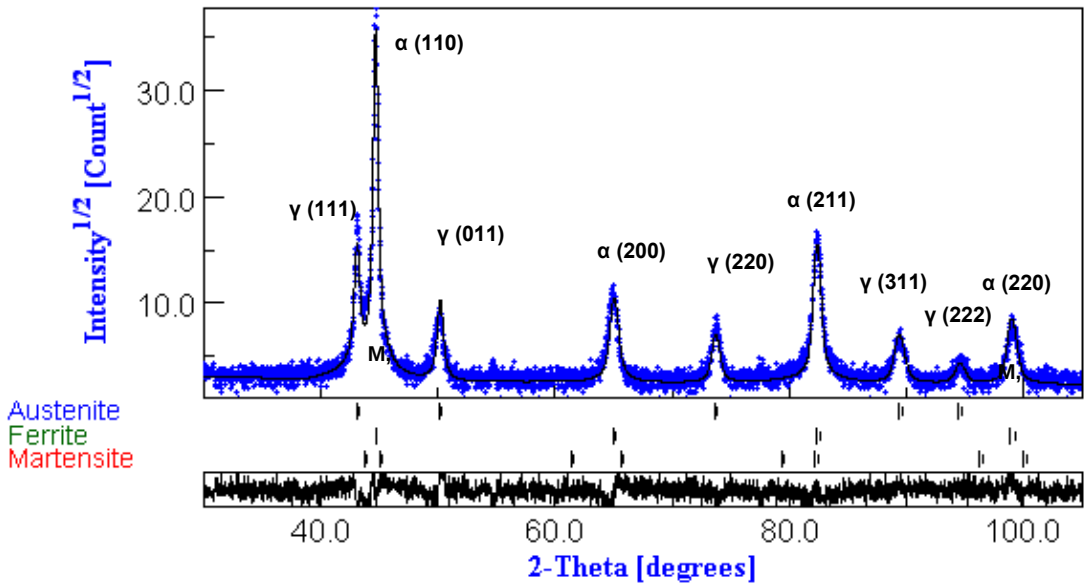

Microstructural phase	Austenite(γ)	Ferrite(α)	Martensite(M)
Weight (%)	22.22 ± 0.4	73.25 ± 1	4.52 ± 0.7

Grade 1050-standard

Figure 106: XRD data for tensile - standard sample - grade 1050

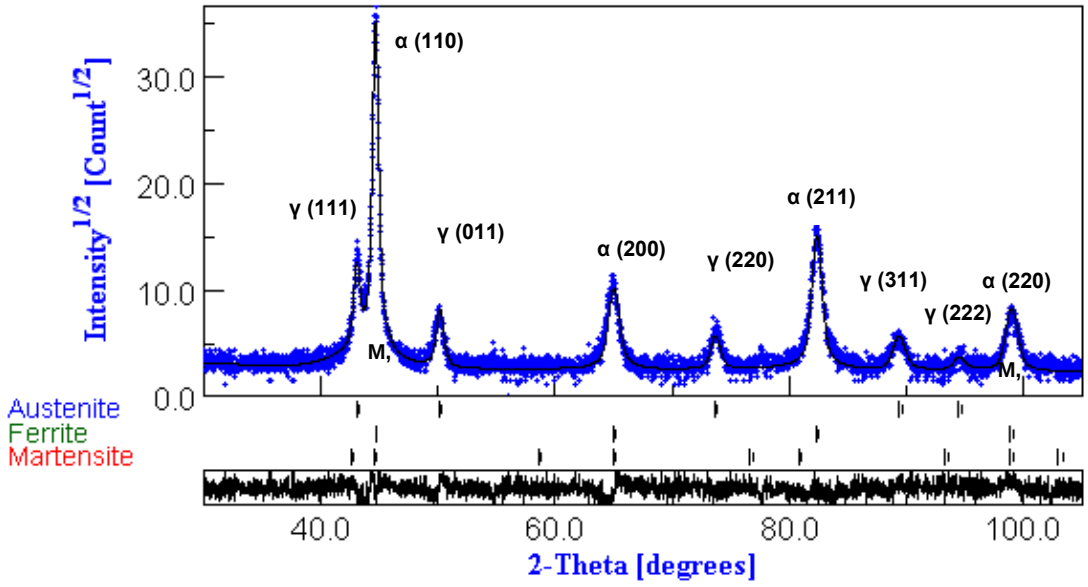

Microstructural phase	Austenite(γ)	Ferrite(α)	Martensite(M)
Weight (%)	15 ± 0.4	82 ± 1	3.1 ± 0.5

Grade 1200-standard

Figure 107: XRD data for tensile - standard sample - grade 1200

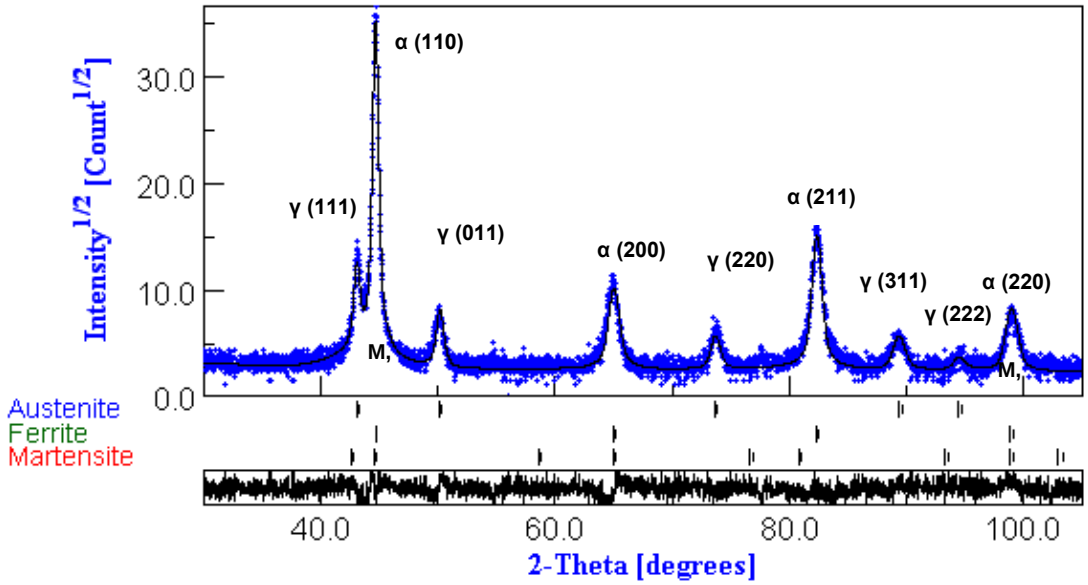

Microstructural phase	Austenite(γ)	Ferrite(α)	Martensite(M)
Weight (%)	20 ± 0.3	80 ± 1	1.2 ± 0.1

Grade 1400-standard

Figure 108: XRD data for tensile - standard sample - grade 1400

Appendix: XRD data for wet milling

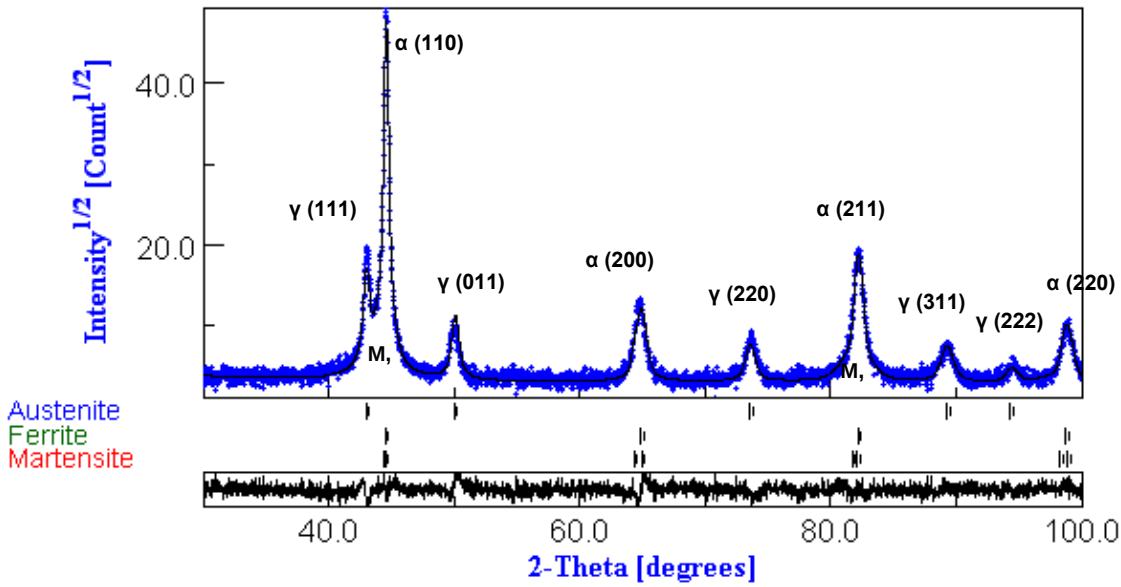

Microstructural phase	Austenite(γ)	Ferrite(α)	Martensite(M)
Weight (%)	18 ± 0.3	60 ± 1	22.1 ± 0.85

DoC-4 mm

Figure 109: XRD data for wet milling - DoC-4 mm

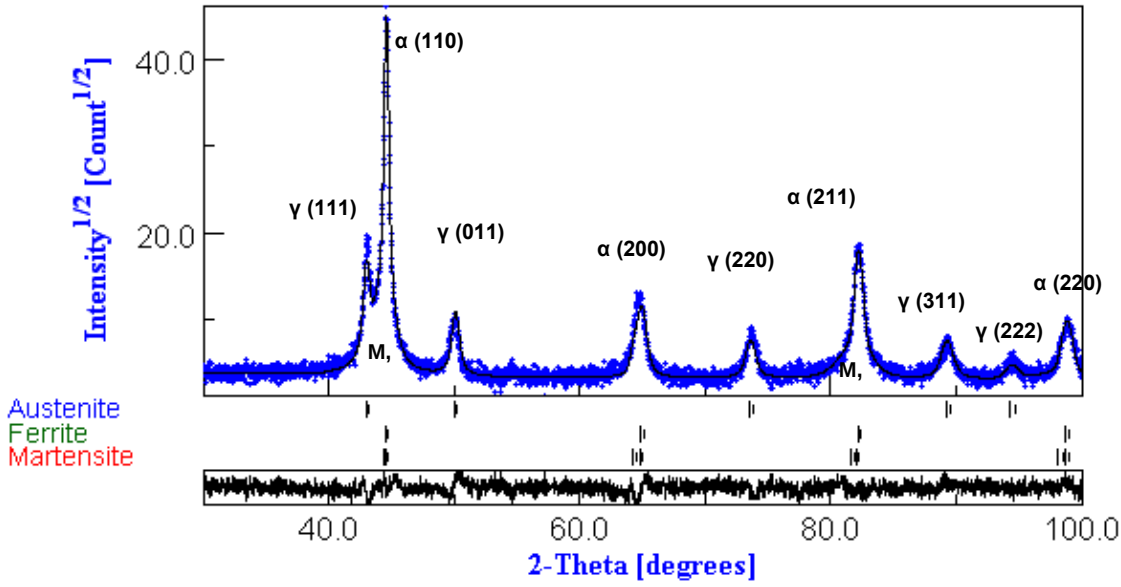

Microstructural phase	Austenite(γ)	Ferrite(α)	Martensite(M)
Weight (%)	18.2 ± 0.3	57 ± 1.2	25 ± 1

DoC-3 mm

Figure 110: XRD data for wet milling - DoC-3 mm

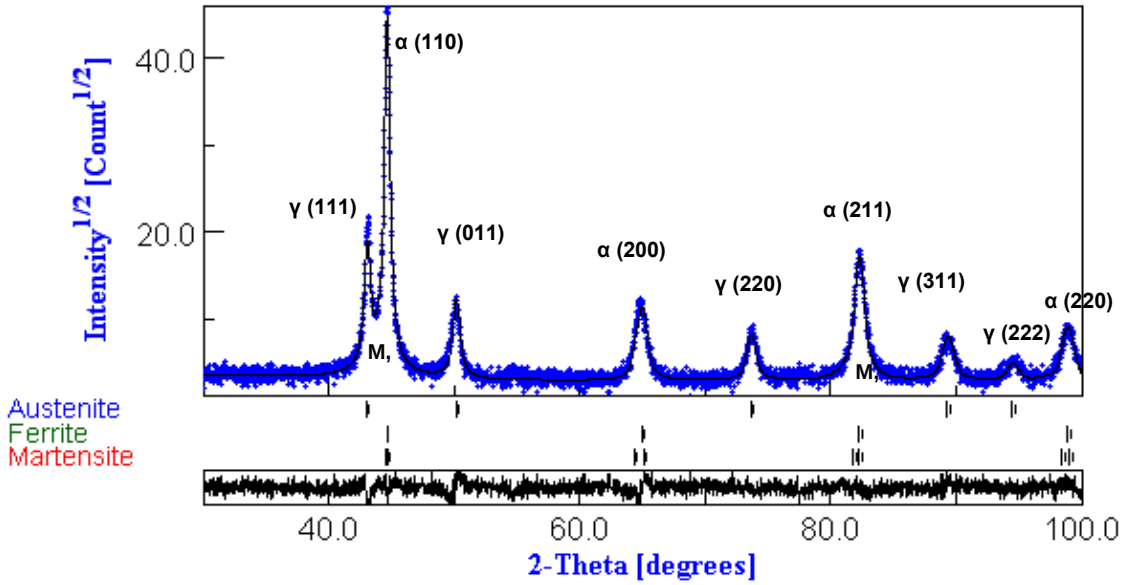

Microstructural phase	Austenite(γ)	Ferrite(α)	Martensite(M)
Weight (%)	23 ± 0.3	60.4 ± 1	17 ± 1

DoC-2 mm

Figure 111: XRD data for wet milling - DoC-2 mm

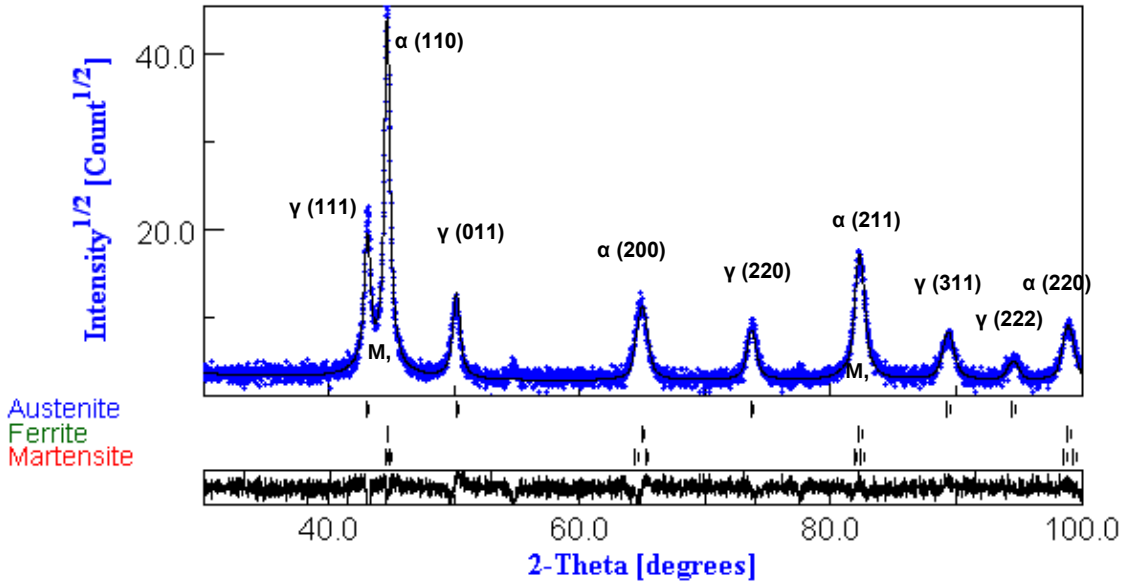

Microstructural phase	Austenite(γ)	Ferrite(α)	Martensite(M)
Weight (%)	25.4 ± 0.3	63 ± 1.3	12 ± 1.1

DoC-1 mm

Figure 112: XRD data for wet milling - DoC-1 mm

Appendix: XRD data for dry milling

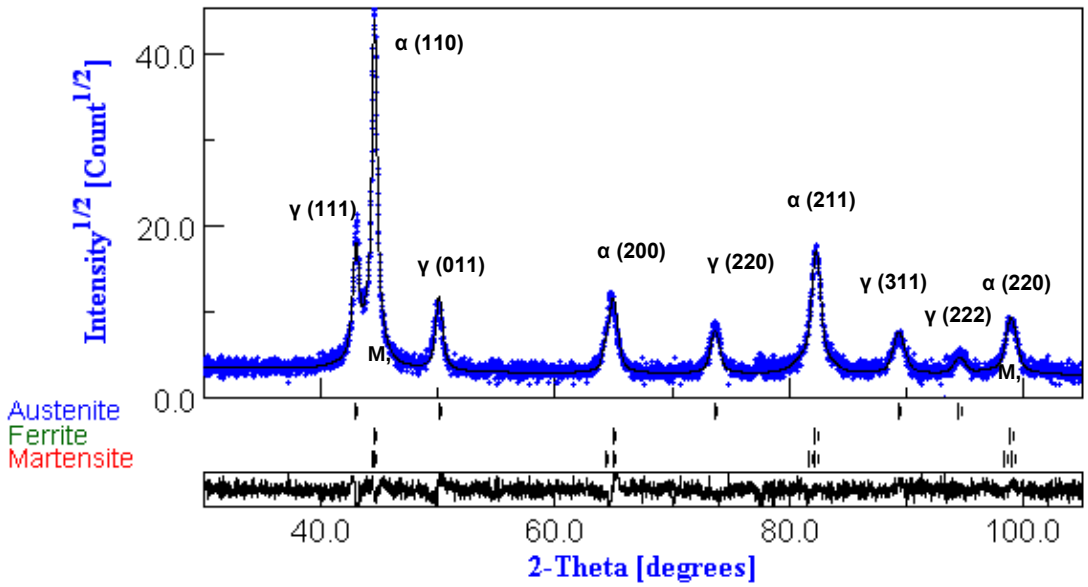

Microstructural phase	Austenite(γ)	Ferrite(α)	Martensite(M)
Weight (%)	21.4 ± 0.3	61.1 ± 1.4	17.5 ± 1.2

DoC-4 mm

Figure 113: XRD data for dry milling - DoC-4 mm

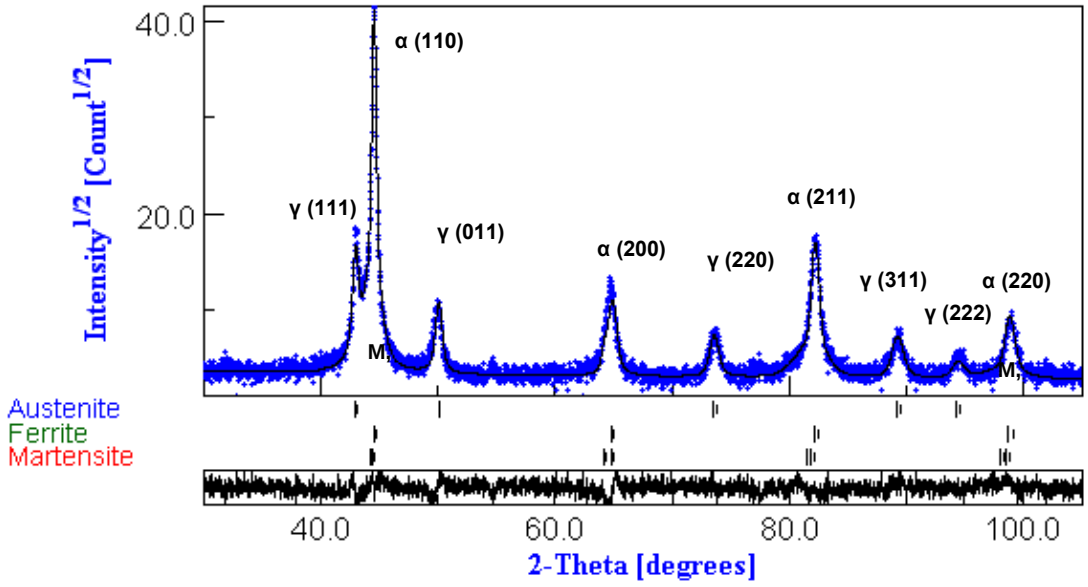

Microstructural phase	Austenite(γ)	Ferrite(α)	Martensite(M)
Weight (%)	19.3 ± 0.3	56 ± 1.3	24.6 ± 1.1

DoC-3 mm

Figure 114: XRD data for dry milling - DoC-3 mm

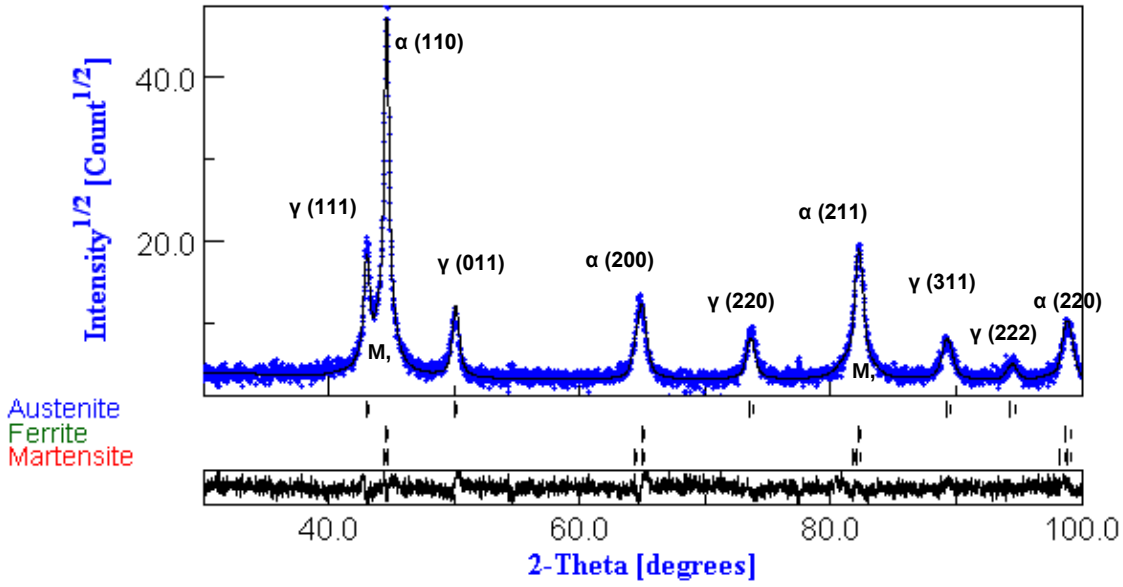

Microstructural phase	Austenite(γ)	Ferrite(α)	Martensite(M)
Weight (%)	19.3 ± 0.3	61.3 ± 1.2	19.4 ± 1

DoC-2 mm

Figure 115: XRD data for dry milling - DoC-2 mm

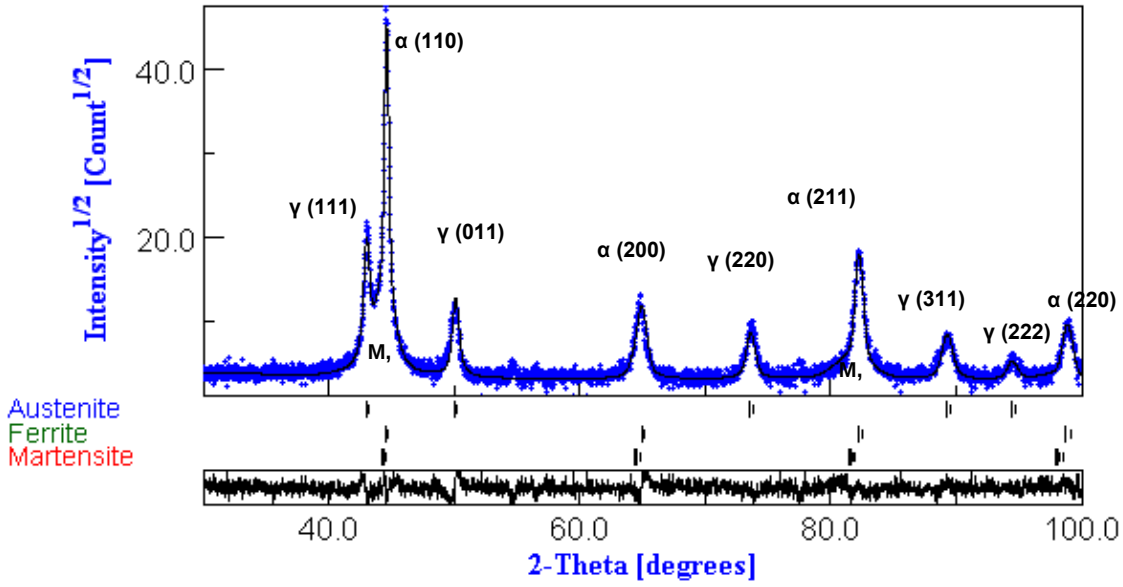

Microstructural phase	Austenite(γ)	Ferrite(α)	Martensite(M)
Weight (%)	22.4 ± 0.4	60 ± 1.3	17.6 ± 1

DoC-1 mm

Figure 116: XRD data for dry milling - DoC-1 mm